Rutherford
Appleton
Laboratory

RAL-85-110
Volume II

Proceedings of the Eighth Meeting of the International Collaboration
on Advanced Neutron Sources 8 — 12 July 1985

ICANS - VIII

Volume II
Neutron-scattering instruments

Rutherford
Appleton
Laboratory

RAL-85-110
Volume II

Proceedings of the Eighth Meeting of the International Collaboration
on Advanced Neutron Sources 8 — 12 July 1985

ICANS - VIII

Volume II
Neutron-scattering instruments

RAL-85-110

ICANS-VIII

Proceedings of the Eighth Meeting of the International Collaboration on Advanced Neutron Sources

8-12 July 1985

VOLUME II

Neutron-scattering instruments

Rutherford Appleton Laboratory
Chilton
DIDCOT
Oxfordshire

November 1985

Cover: Neutron-scattering instruments (LOQ, IRIS, TFXA and HET) on north side of SNS experimental hall (see pp 523 - 545)

PREFACE

The eighth meeting of the International Collaboration on Advanced Neutron Sources was hosted by the Rutherford Appleton Laboratory and held at Keble College Oxford, from the 8th to 12th July 1985. The timing, and venue in the UK, were particularly appropriate in view of the contemporaneous start-up of RAL's spallation neutron source.

Following the traditional cycle of programming, ICANS-VIII concentrated on target and moderator systems for accelerator-based sources, and on neutron-scattering instrumentation. Continuing the trend of recent meetings, there was an increasing emphasis on data and results from operating facilities, but amidst the success stories came the announcement of the demise of the SNQ project. The achievements of the Jülich team have been quite remarkable, and other ICANS laboratories will continue to benefit from their work for many years to come.

The meeting also noted with regret the recent passing of Rex Fluharty, formerly of Los Alamos. Rex had been involved with ICANS since its inception, and with his breadth of experience had been a stalwart of the Collaboration, and a valued colleague at numerous international meetings and workshops.

These ICANS-VIII proceedings follow a familiar format, opening with status reports from the participating laboratories. The presentation of subsequent papers adheres more or less to the organisation of the meeting; there has been minimal editing of individual papers in order to facilitate reproduction procedures. Two *ad hoc* workshop sessions held during the meeting, on "Boosters and Delayed Neutrons" and "The Second User Revolution" led by John Carpenter and Peter Egelstaff respectively, have not been recorded here. These sessions highlighted two important issues facing the neutron-scattering community at this time. With many of the new generation sources now becoming operational alongside the more conventional reactor sources, it is timely to ask how we proceed towards the next generation of advanced facilities, while at the same time reappraising the optimal means of exploiting their potential. It was appropriate that the present meeting chose to address these problems, which are certain to feature even more prominantly in future ICANS programmes.

GEORGE C STIRLING
Rutherford Appleton Laboratory
November 1985

Eighth Meeting of the International Collaboration on Advanced Neutron Sources (ICANS-VIII), Oxford, 8-12 July 1985

REGISTERED PARTICIPANTS

B Alefeld	Jülich	M Kohgi	Tohoku
C Andreani	Rome	J Laakmann	Jülich
T W Armstrong	La Jolla	A J Leadbetter	RAL
F Atchison	SIN	G Manning	RAL
J R J Bennett	RAL	F A Morse	LANL
S Biggin	Bristol	R O Nelson	LANL
D E Bohringer	ANL	K Neumann	IKE Stuttgart
T A Broome	RAL	R J Newport	RAL
F Brumwell	ANL	T G Perring	Cambridge
C J Carlile	RAL	G E Ostrowski	ANL
J M Carpenter	ANL	M Paoli	Oxford
B G Chidley	CRNL	J Penfold	RAL
F Cilloco	Frascati	C Petrillo	Perugia
P Cloth	Jülich	D J Picton	Birmingham
H Conrad	Jülich	B H Poulten	RAL
R Cywinski	RAL	V T Pugh	RAL
W I F David	RAL	A V Rauchas	ANL
M Davidovic	Vinca	R A Robinson	LANL
V Drüke	Jülich	H Robinson	LANL
P A Egelstaff	Guelph	G J Russell	LANL
D Filges	Jülich	F Sacchetti	Perugia
W E Fischer	SIN	A W Schulke Jr	ANL
J B Forsyth	RAL	P A Seeger	LANL
R Geick	Würzburg	R N Silver	LANL
P S Goyal	BARC Bombay	H Stechemesser	Jülich
D A Gray	RAL	H Stiller	Jülich
R K Heenan	RAL	G C Stirling	RAL
A W Hewat	ILL	Y Takeda	SIN
W S Howells	RAL	A D Taylor	RAL
Y Ishikawa	Tohoku	I M Thorson	TRIUMF
M W Johnson	RAL	Ch Tschalär	SIN
T J L Jones	RAL	H Tietze	Würzburg
M Kimura	Sendai	R C Ward	RAL
W Kley	JRC Ispra	W G Williams	RAL
K J Knowles	RAL	C G Windsor	AERE
A Kollmar	Jülich	H Wroe	RAL

TABLE OF CONTENTS

VOLUME 1

STATUS REPORTS, NEW CONCEPTS

TARGET SYSTEMS

VOLUME III

SHIELDING, BEAM DEFINITION

CHOPPER SYSTEMS

DETECTORS

DATA ACQUISITION

ANCILLARY DEVICES AND EQUIPMENT

Proceedings of the Eighth Meeting of the International Collaboration on Advanced Neutron Sources (ICANS-VIII)
8-12 July 1985, Rutherford Appleton Laboratory Report RAL-85-110

NEUTRON SCATTERING RESEARCH RESULTS FROM THE LOS ALAMOS NEUTRON SCATTERING CENTER

Richard N. Silver
Physics Division, MS H805
Los Alamos National Laboratory
Los Alamos, New Mexico 87545

ABSTRACT

The Los Alamos Neutron Scattering Center (LANSCE) is a new high intensity pulsed spallation neutron source for research in the structure and dynamics of condensed matter. With first operation in 1985, LANSCE is expected to produce the world's highest peak thermal flux of 1.7 X 10^{16} n/cm^2-sec by 1987. A description of the LANSCE facility and source characteristics is presented. Some experimental highlights of research at the low intensity (peak thermal flux of 6 X 10^{13} n/cm^2-sec) WNR predecessor to LANSCE are described which illustrate the scientific potential and instrumentation of LANSCE. Future plans for the LANSCE facility and research program are discussed.

I. INTRODUCTION:

The Los Alamos Neutron Scattering Center (LANSCE), which is just beginning operation at the Los Alamos National Laboratory, is a pulsed spallation neutron source for research in condensed matter science (solid state physics, chemistry, materials science, and biology).[1] The peak thermal flux of LANSCE is expected to reach 1.7 X 10^{16} n/cm^2-sec by 1987. This is a factor of forty increase beyond present pulsed source capabilities in the United States. It will be competitive with the new Spallation Neutron Source beginning operation at the Rutherford Appleton Laboratory in the United Kingdom. Based at the world's highest current proton accelerator, the Los Alamos Meson Physics Facility (LAMPF), LANSCE has the potential for significant further upgrades at a small fraction of the costs for constructing a new facility of comparable capability. This can keep the U.S. at the forefront of pulsed neutron scattering research through the remainder of this century. The accelerator, instrumentation, and research

experience developed at LANSCE should also lead to a proposal for a next-generation[2] neutron source (peak thermal flux of 10^{17}-10^{18} n/cm^2-sec) for condensed matter research in the 21st century.

This paper describes the characteristics of the LANSCE facility. Neutron scattering research highlights are presented from the past three years of operation of the low intensity (peak thermal flux of 6 X 10^{13} n/cm^2-sec) Weapons Neutron Research (WNR) predecessor to LANSCE, with a discussion of implications for LANSCE research. Long range plans are described for LANSCE facility development, instrumentation, and research programs.

II. LANSCE FACILITY DESCRIPTION:

Pulsed neutron scattering research began at Los Alamos in 1977 with the first operation of the Weapons Neutron Research (WNR) facility.[3] LAMPF produces protons at 120 Hz in "macropulses" of approximately 750 μsecs pulse width. The requirement for short pulse widths for time-of-flight neutron scattering allowed only a small fraction of each macropulse to be used. The characteristics of the WNR facility were 3.5 μA time average proton current, 120 Hz repetition rate, 5 μsecs proton pulse width, and 6 X 10^{13} n/cm^2-sec peak thermal neutron flux. Compared with an optimal pulsed neutron source, the proton current was too low, the repetition rate was too high, and the proton pulse width was too long. In addition, beam time had to be split between neutron scattering and the other competing uses of the WNR facility for nuclear physics, neutrinos, and defense programs. Nevertheless, the operation of the WNR facility from 1978 to 1984 provided valuable experience in pulsed neutron scattering research, to be described later in this report.

The WNR also led to the development of the world class LANSCE facility which is beginning operation in 1985. The Los Alamos Neutron Scattering Center, LANSCE, is the name given to the materials science research program at the facility created by the combination of the WNR facility with a new $22M Proton Storage Ring (PSR),[4] which acts as a pulse compressor of LAMPF macropulses. By compressing one in ten of every macropulse, a much improved pulsed neutron source is created with 100 μA time average proton current, 12 Hz repetition rate, 0.27 μsec proton pulse width and 1.7 x 10^{16} n/cm^2-sec peak thermal flux. The PSR first accepted proton beam on April 26, 1985, and the testing of this facility is proceeding on schedule with the design characteristics expected to be reached in October, 1986. The upgrade of the facility includes a proton beam multiplexing scheme and the construction of new target areas to allow simultaneous use by the four major research programs in neutron scattering, nuclear physics, neutrinos,

and defense. The neutron scattering target/moderator assembly is also being rebuilt to improve shielding to handle the much higher proton current, increase the number of possible flight paths to 17, and install a 20 K H_2 moderator for long wavelength neutron experiments. The new LANSCE facility is approximately a two orders of magnitude improvement over the WNR facility which preceeded it.

III. NEUTRON SCATTERING RESEARCH RESULTS FROM THE WNR:

This section reviews some highlights of condensed matter research and instrument development during the operation of the low intensity WNR facility. This will illustrate the characteristics of time of flight instrumentation and some of the possible research areas with the new LANSCE facility. Prototype neutron scattering instruments first became operational at the WNR in 1981, so the results discussed below were obtained in the three-year period from 1981 to 1984. Unfortunately, for many of the experiments in the 1984 run cycle, the data analysis is not yet complete or the papers have not yet been accepted for publication. Therefore, many interesting results from the WNR could not be included in this review.

Of course, the increase of 300 in peak neutron flux made possible by the PSR should open up qualitatively new research areas, such as the study of dispersive elementary excitations (e.g., phonons and magnons) at high energy transfers. Similarly, the factor of ten lower repetition rate and the installation of a cold H_2 moderator should make possible experiments with long wavelength neutrons. So the following represents only a glimpse into the future of LANSCE.

Single Crystal Diffraction

Fig. 1 shows a schematic drawing of the Single Crystal Diffractometer (SCD) at the WNR facility. A white beam of neutrons travels 7.5 m from the moderator to the sample mounted on a displex refrigerator, and then Bragg scatters into a ^3He multiwire position sensitive neutron detector. Data are recorded in a three dimensional histogramming memory corresponding to X and Y on the detector and the total time-of-flight. This allows the scattering angles and wavelengths to be reconstructed. The instrument may be thought of as a wavelength resolved Laue camera. The sample is mounted on a two-axis (ω and ϕ drive) goniometer, which is sufficient to cover the majority of the reciprocal space sphere.

The SCD was used to determine the hydrogen positions in the first example[5] of molecular hydrogen reversibly bound to the central metal of an organometallic transition metal complex. Fig. 2 shows the core atoms of $W(CO)_3(P\text{-}Pr^i_3)_2(\eta^2\text{-}H_2)$, where the circled P represents a phosphine ligand.

The hydrogen-hydrogen distance (0.82 Å) is significantly larger than that obtained in free hydrogen (0.74 Å). This type of binding had been proposed to explain some types of catalytic reactions and these structural results clearly demonstrate the existence of such a bonding mode.

A new technique[6] for performing room temperature high-pressure single crystal neutron diffraction (up to 20 kbar) has been developed for the SCD. This uses a cylindrically symmetric pressure cell mounted on the incident collimation with rotation axis coincident with the neutron beam and a specific crystal orientation chosen with beam passing midway between major lattice vectors. For a crystal of orthorhombic or higher symmetry, it is possible to refine a three-dimensional structure with only one pressure loading. Presence of an area detector allows easy identification of superlattice reflections which occur as a result of phase transitions, and the multiwavelength neutron source provides considerably more information for a single setting of the crystal than conventional single wavelength sources. This technique was used[7] to study the structural phase transition above 5.2 kbar in ReO_3, where the high pressure structure (Fig. 3) has ten times the compressibility of the normal phase (termed a "compressibility collapse" transition). At the transition, the $Re-O_6$ octahedron begin to rotate causing an apparent hinging of the linear Re-O-Re chains rather than a shortening of the Re-O distances, which doubles the unit cell giving rise to superlattice reflections easily visible with an area detector.

Powder and Liquids Diffraction

A large number of powder diffraction studies have been conducted at the WNR using the Rietveld powder profile refinement method. One should note that good resolution at high d-spacing is a major advantage of time-of-flight diffraction. Most of the research has involved actinide compounds which are important to the Laboratory's applied programs or to basic research on f-electron phenomena.

Fig. 4 shows the room temperature structure of $BaPuO_3$ determined[8] using the Neutron Powder Diffractometer on a 10 m flight path at the WNR. $BaPuO_3$ is an important material in the technology of nuclear waste recovery. This experiment required the use of special sample environments to handle extremely radioactive materials. The structure is found to be a distorted perovskite structure ($GdFeO_3$ type), with nearly regular PuO_6 octahedra but 1.46 degree hinging of the O-Pu-O angles, in excellent agreement with expectations based on crystal chemical models.

PGa_3 has the cubic Cu_3Au - type structure and exhibits a very small glitch in its magnetic susceptibility curve at ~ 65 K. Previous studies of this compound suggested that it was paramagnetic down to 4.2 K. Reactor neutron powder diffraction studies later suggested an antiferromagnetic

structure, though harmonic contamination of the incident beam obscured the superlattice reflections. A reinvestigation of this material by neutron time-of-flight techniques[9] eliminated the contamination problem and allowed unambiguous confirmation of the existence of a simple antiferromagnetic structure with a Neel temperature of 70 K. Also studied was UGa_2, a low-temperature ferromagnet with the hexagonal AlB_2 structure. Values of the moments obtained as a function of temperature are shown in Fig. 5. The value of the moment in UGa_2 is 3.0 μ_B indicating some delocalization of the moment. The value for UGa_3 is 0.95 μ_B indicating considerable delocalization. These observations are consistent with the observed U-U distances of 4.02 Å and 3.01 Å for UGa_2 and UGa_3 respectively.

Pulsed neutron sources are particularly advantageous for studies of the structures of liquids and amorphous materials because of the very high epithermal neutron flux. Using high incident energies at low scattering angles to achieve a desired momentum transfer Q greatly reduces the inelasticity, or Placzek, corrections required to convert a cross section to a structure factor. In practice, such corrections introduce unwanted model dependent assumptions into the data analysis. The high energies also allow one to reach very large Q values (50 $Å^{-1}$ is easily attained) which is especially important for molecular liquids. This allows fourier transform of the data to obtain radial distribution functions without introducing model dependent assumptions about the large Q scattering. Fig. 6 shows the hydrogen-hydrogen partial structure factor for liquid water measured[10] in a hydrogen/deuterium isotope substitution experiment at the WNR, as compared with two molecular dynamics simulations based on differing intermolecular water potentials. While agreement with the simulations is very good, the data reveal a water structure with stronger short range order (closer to the structure of ice) than either simulation.

Inelastic Scattering

The Be-BeO Filter Difference Spectrometer[11] (FDS) at the WNR facility is used for vibrational spectroscopy on non-dispersive excitations up to energies of several hundred meV. The FDS uses the low pass Bragg cutoffs of Be at 5.2 meV and BeO at 3.6 meV to fix a final neutron energy bandpass, with the incident energy determined by the total time-of-flight.

Fig. 7 shows measurements[12] using the FDS of the vibrational spectra of hydrogen chemisorbed on Raney nickel (top) and coprecipitated nickel (bottom), both materials that are closely related to commercial catalysts. The spectra give information about the strength of the bonding of hydrogen to the substrate (namely, the energy of the transition) as well as the geometry of the adsorption site. By a straightforward calculation the

peaks at 120 and 140 meV can be associated with the vibrations parallel and perpendicular (respectively) to a hydrogen atom adsorbed over the center of a triangular, or (111)-like, site. The pair of peaks at 80 and 200 meV would then correspond to hydrogen over the center of a fourfold, or (100)-like, site. The relative number of (100) sites in the coprecipitated nickel appears to be larger than in Raney nickel. The next step toward understanding catalysis of these systems would be to coadsorb oxygen and hydrogen to see which sites are more reactive.

The normal modes of H in metals cannot be studied by any other technique but neutron scattering, and they are of high enough energy to often require the unique spectral characteristics of a pulsed neutron source. In a bcc hydride such as TaH_x and NbH_x, the hydrogen vibrations can be described in terms of a localized, slightly anharmonic potential in a tetragonal ($\bar{4}2m$) site. Fig. 8 shows the vibrational spectra of $TaH_{0.46}$ measured[13] with the FDS at very high energy transfers up to 400 meV. These measurements of the positions of the higher harmonics of the singlet (out-of-plane) and doublet (in-plane) fundamentals have been used to determine the independent terms in the third and fourth order anharmonic perturbation expansion of the hydrogen potential, to compare with theoretical calculations and with other measurements such as the activation energy for hydrogen diffusion.

The Constant-$\underline{Q}$ Spectrometer[14] (CQS) shown in Fig. 9 is a pulsed neutron source instrument for studies of $\vec{Q}$-dependent collective excitations such as phonons and magnons in single crystal samples, which are studied with triple axis spectrometers (TAS) at reactor neutron sources. The CQS uses Bragg reflection of scattered neutrons from an array of analyzer crystals to fix the perpendicular momentum transfer and to determine the final neutron energy. Then, the total time-of-flight to the detectors fixes the remaining parameters ($\vec{Q}$, ω). Compared with a TAS, the CQS will allow a broad region of $\vec{Q},\omega$ space to be measured simultaneously, will reach higher energy transfers, and will have complementary focusing conditions. This was a development instrument at the WNR, poised to exploit the increased flux provided by the PSR. WNR research demonstrated the viability of the CQS method. Background levels are comparable to current reactor practice, both dispersive and non-dispersive phonon branches have been measured in aluminum in good agreement with the literature, and the exploitation of reciprocal space focusing has been demonstrated.

The prospect of using high energy neutrons has also stimulated some theoretical work. In the high Q limit, the scattering is thought to approach the impulse approximation limit in which the scattering function $S(\vec{Q},\omega)$ becomes related to the ground state momentum distribution $n(\vec{p})$. Los Alamos work has shown[15] that the relationship between these two functions

is mathematically equivalent to a Radon transform, in which the matrix relating the polynomial expansions of both functions is diagonal. Further, in the case of ions in solids, these polynomial expansions will be rapidly converging for realistic potentials, even in the case of strong anharmonicity as in double well hydrogen bonds. Thus, a polynomial fit to $S(\vec{Q},\omega)$ in the impulse approximation limit will yield the terms in the polynomial expansion of $n(\vec{p})$. Planning for experiments on hydrogen bonded systems to test these ideas are in progress at LANSCE.

IV. THE FUTURE OF LANSCE:

The approximately two orders of magnitude improvement in source characteristics to be provided by the Proton Storage Ring should open up many areas for neutron scattering research at LANSCE which were impossible or marginal with WNR. The kinds of neutron scattering experiments which would benefit from more intensity are well documented,[16] including higher resolution, smaller cross section, differential scattering, and polarization analysis experiments. The new field of neutron scattering experiments on high energy excitations[16] in condensed matter made possible by pulsed neutron sources requires the improvement in peak flux as well as the better time-of-flight resolution provided by the decreased proton pulse width of the PSR. Because of the much lower repetition rate which eliminates "frame overlap" and the installation of a 20 K liquid H_2 moderator, cold neutron science (such as small angle neutron scattering studies of structural biology, polymers, and metallurgy) will become possible for the first time at Los Alamos.

To take optimal advantage of LANSCE intensities to perform high resolution experiments and to provide the conveniences and services required to operate LANSCE as a national user facility to attract the condensed matter science community to pulsed neutron scattering, an expansion beyond the existing WNR experimental hall is essential.[17] The present hall has a maximum flight path length of 13 m, so that higher resolution experiments requiring longer flight paths must be carried out in sheds built in a time-of-flight yard, and there are no ancillary support facilities for users. An $18M proposal[18,19] to the Department of Energy would provide for a new experimental hall with up to 50 m flight paths, as well as sample preparation laboratories, computers, office space and additional instrumentation. Provided initial funding in FY86, this expansion should by completed by the end of 1988.

Current instrument construction projects at LANSCE include two instruments scheduled for initial operation in 1986, a Low Q Diffractometer for small angle neutron scattering experiments and a Chopper Spectrometer for studies of high energy excitations. Three additional

instruments are in the early conceptual design stage to be constructed as part of the new experimental halls project: a High Resolution, High Throughput Powder Diffractometer (HRPD); a 10 μeV resolution Quasielastic Neutron Spectrometer (QENS) for studies of chemical spectroscopy, diffusion, tunneling, etc.; and a Polarization Analysis Instrument[20] (PAN) using a supermirror guide, neutron chopper, and the neutron spin echo technique to achieve very high resolution for the study of high energy excitations.

These projects require advances in neutron scattering technology. Los Alamos has active development efforts in very high rate (10 MHz) data acquisition systems (FASTBUS μVAX), target/moderator optimization including fission boosted targets and cold moderators, high speed position sensitive scintillator detectors, new plastic neutron scintillator materials, 600 Hz magnetic bearing neutron choppers, pressed Ge and Cu crystal monochromators, etc. Other technologies needed for instrument development (such as neutron guides and supermirrors) will be acquired through collaborations or purchase.

Provided Congressional approval for FY86 funding of the Neutron Scattering Experimental Halls project and adequate operations and research support from the Department of Energy, one can speculate on a possible timetable for LANSCE and U.S. pulsed neutron scattering development:

1985 - PSR reaches 20 μA at 24 Hz, W target installed (peak thermal flux of 1×10^{15} n/cm^2-sec)

1986 - Begin architectural design for new halls, PSR reaches 100 μA at 12 Hz (1×10^{16} n/cm^2-sec), LQD and CS begin operation

1987 - Install depleted uranium target (1.7×10^{16} n/cm^2-sec), construction of experimental halls

1988 - Occupy new halls, initiate formal National User Program, HRPD and QENS begin operation, bring PSR operation up to 200 μA at 24 Hz

1989 - Occupy remainder of construction project, PAN begins operation, install fission boosted target (peak thermal flux of 5×10^{16} n/cm^2-sec)

1990-2000 - Routine operation of LANSCE with continuing instrument development, begin to develop proposal for an advanced pulsed neutron source based on LANSCE experience (peak thermal flux 10^{17} - 10^{18} n/cm^2-sec)

1996 - Begin construction of an advanced U. S. pulsed neutron source for the 21st century.

One can see that the beginning of operation of the Los Alamos Neutron Scattering Center is an exciting and challenging opportunity to advance the state of the art in condensed matter research.

V. ACKNOWLEDGEMENTS

This is a report on the work of the many individuals who have participated in the development of the LANSCE facility and research programs. In particular, we thank: R. Woods and his WNR operations team; G. Lawrence, G. Sawyer, and R. Hardekopf who have led the team which made the PSR possible; the staff of the neutron scattering research group P-8, and the staff of other Los Alamos divisions, who have performed the research reported in this article; and J. Browne and F. Morse for the support and encouragement of Laboratory management. We also thank our colleagues at the Intense Pulsed Neutron Source at the Argonne National Laboratory, the Spallation Neutron Source at the Rutherford Appleton Laboratory, the AERE Harwell, and the KENS facility in Tsukuba, Japan, who, as members of the International Collaboration on Advanced Neutron Sources, have pioneered so much of pulsed neutron scattering research. This work was performed under the auspices of the U.S. Department of Energy, with partial support from the Office of Basic Energy Sciences/Division of Materials Science.

REFERENCES

1. See companion article by F. Morse in these proceedings.

2. For a scientific justification for advanced neutron sources, see the proceedings of the "Workshop on Scientific Opportunities with Advanced Facilities for Neutron Scattering," Shelter Island, October 23-26, 1984. Available from the National Technical Information Center, U.S. Department of Commerce, CONF-8410256.

3. G. J. Russell, P. W. Lisowski, S. D. Howe, N. S. P. King, M. M. Meier, "Characteristics of the WNR - A Pulsed Spallation Neutron Source," Nuclear Data for Science and Technology, p. 831 (1983)

4. G. Lawrence, R. Cooper, D. Hudgings, G. Spalek, A. Jason, E. Higgins, R. Gillis, "LASL High Current Proton Storage Ring," Proceedings of the XI International Conference on High Energy Accelerators, Geneva, July, 1980, Published in Experimentia: Supplement 40, 103 (1981); G. P. Lawrence, R. A. Hardekopf, A. J. Jason, P. N. Clout, G. A. Sawyer, "Los Alamos High Current Proton Storage Ring Status Report," Proceedings of the 1985 Particle Accelerator Conference, LA-UR 85-1613.

5. G. J. Kubas, R. R. Ryan, B. I. Swanson, P. J. Vergamini, and H. J. Wasserman, Journal of the American Chemical Society 106, 451 (1984), and unpublished.

6. R. W. Alkire, A. C. Larson, P. J. Vergamini, J. E. Schirber, and B. Morosin, Journal of Applied Crystallography 18, 145 (1985).

7. J. E. Schirber, B. Morosin, R. W. Alkire, A. C. Larson and P. J. Vergamini, Physical Review B29, 4150 (1984)

8. G. G. Christoph, P. G. Eller, J. D. Purson, R. A. Penneman, and G. H. Rinehard, "Crystal Structure Determination of Barium Plutonate by TOF Neutron Powder Diffraction," Submitted to the International Conference on Neutron Scattering, Santa Fe, New Mexico, Aug 19-23, 1985.

9. A. C. Lawson, A. Williams, J. L. Smith, P. A. Seeger, J. A. Goldstone, J. A. O'Rourke, Z. Fisk, Journal of Magnetism and Magnetic Materials ,in press (1985)

10. A. K. Soper, R. N. Silver, Physical Review Letters 49, 471 (1982)

11. A. D. Taylor, E. J. Wood, J. A. Goldstone, J. Eckert, Nuclear Instruments and Methods 221, 408 (1984)

12. J. Eckert, C. J. Wright, unpublished

13. J. Eckert, J. A. Goldstone, D. Tonks, D. Richter, Physical Review B27, 1980 (1983), and same authors unpublished.

14. R. A. Robinson, R. Pynn, and J. Eckert, "An Improved Constant-Q Spectrometer for Pulsed Neutron Sources," LA-UR 85-1900, submitted to Nuclear Instruments and Methods in Physics Research

15. G. Reiter, R. N. Silver, Physical Review Letters 54, 1047 (1985)

16. R. N. Silver, "Proceedings of the 1984 Workshop on High-Energy Excitations in Condensed Matter," Los Alamos, New Mexico, February 13-15, 1984. LA-10227-C, V. 1 & 2

17. Report of the Pulsed Neutron Sources Review Panel, W. Brinkman, chairman, 1982; Report of the Neutron Scattering Experimental Halls Review Panel, J. M. Rowe, chairman, 1983

18. Major Facilities for Materials Research and Related Disciplines, National Academy Press, Washington, D.C., 1984, p. 455

19. A. Robinson, "Los Alamos Neutron Source Meets First Test", Science 228, 1417 (1985)

20. F. Mezei, unpublished

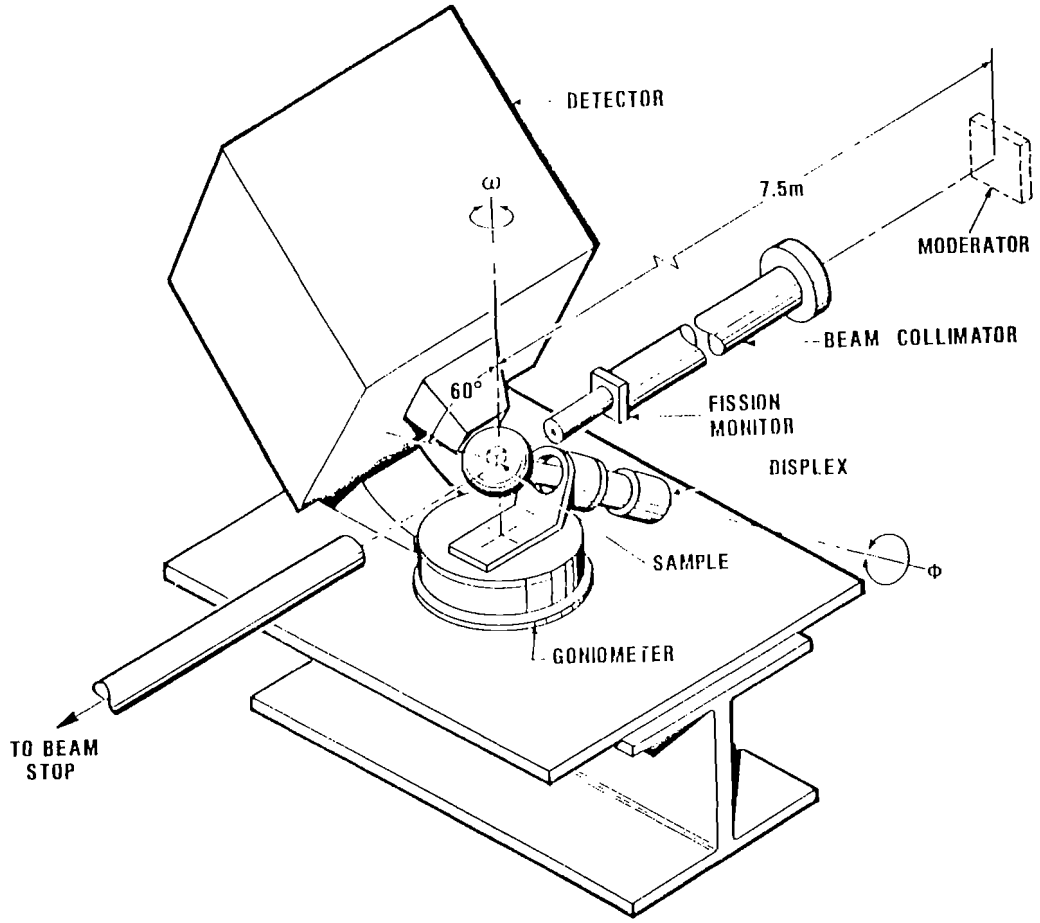

Fig. 1 Schematic drawing of the Single Crystal Diffractometer at LANSCE.

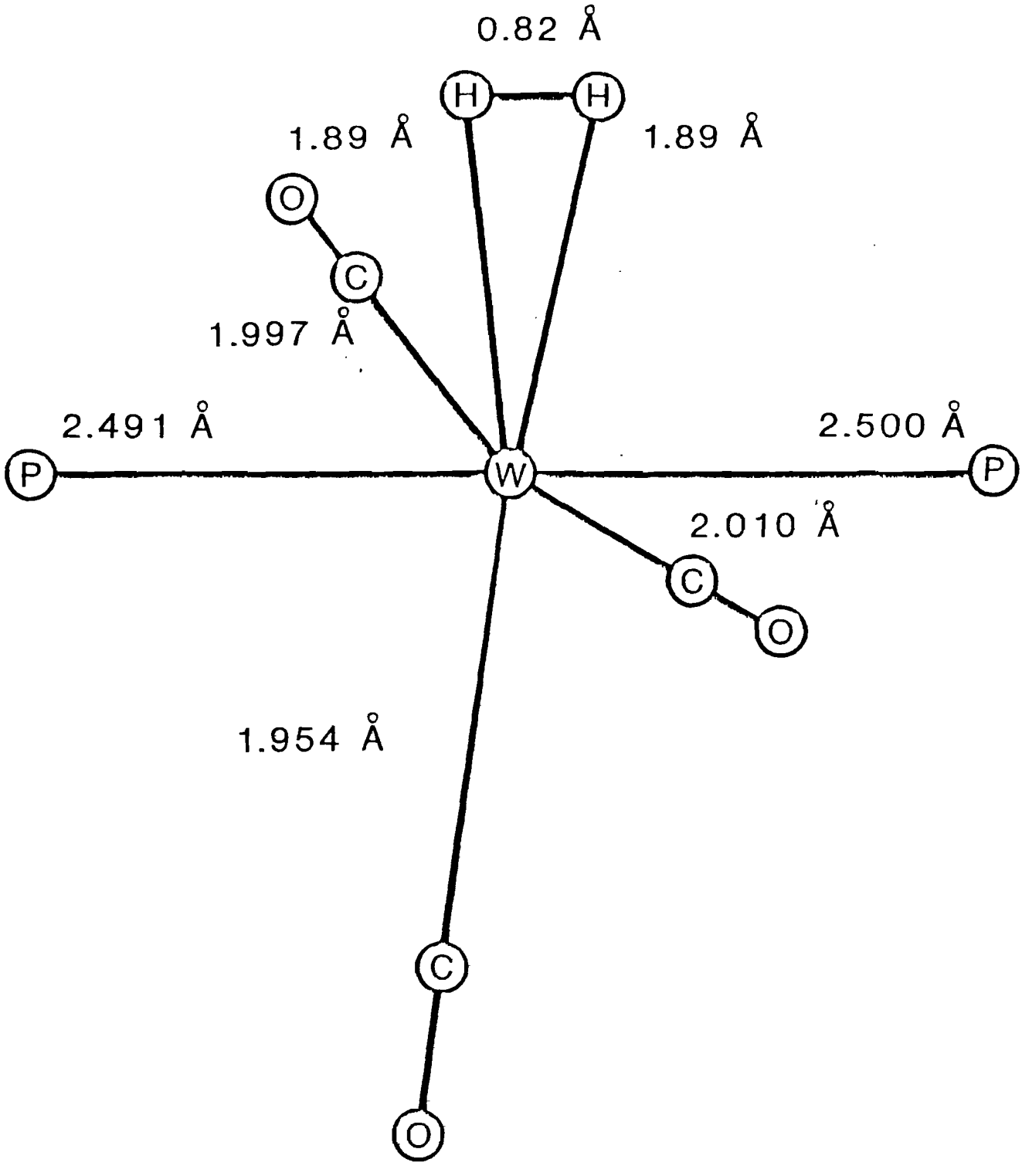

Fig. 2 Core atoms of $W(CO)_3(P\text{-}Pr^i_3)_2(\eta^2\text{-}H_2)$. This first example of an organometallic complex which reversibly binds molecular hydrogen was initially observed at the WNR facility. The circled P's represent phosphine ligands.

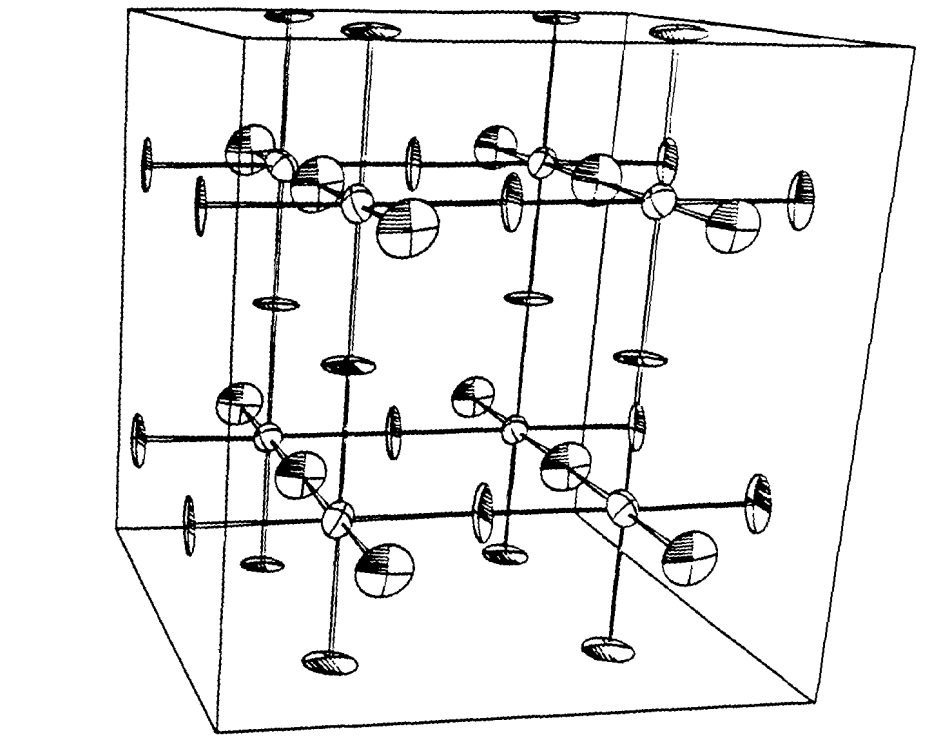

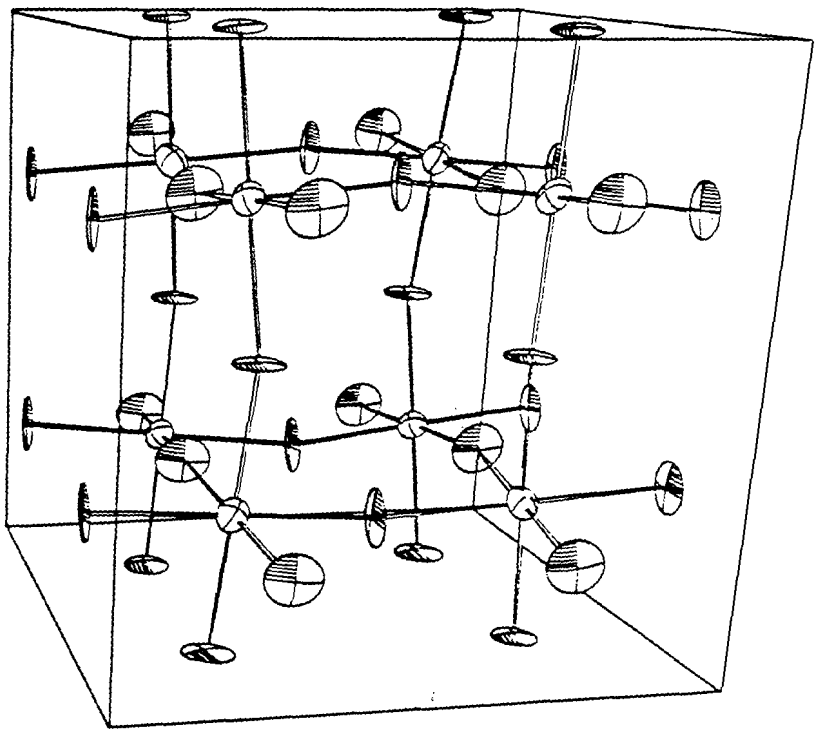

Fig. 3 The structure of ReO_3 at zero pressure (top - eight unit cells) and at 15 kbar (bottom - single unit cell) as measured on the Single Crystal Diffractometer at the WNR.

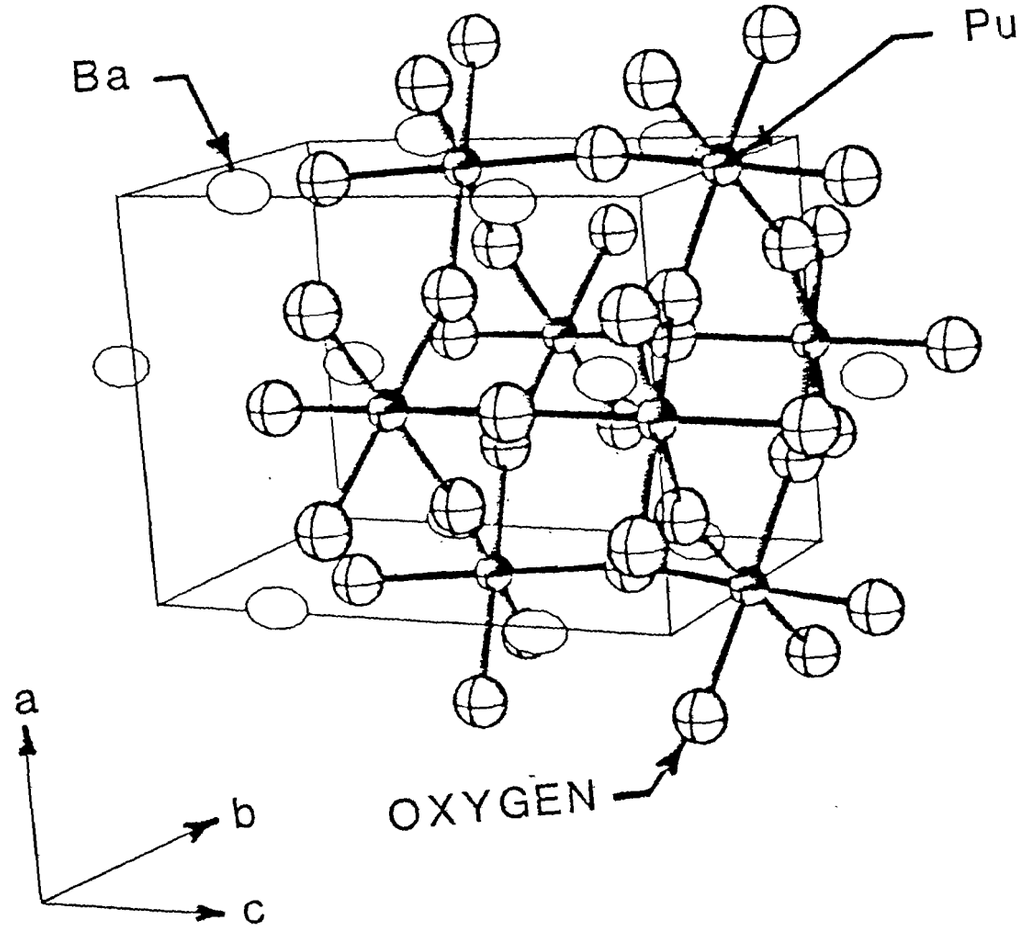

Fig. 4 The structure of $BaPuO_3$ as measured by time of flight powder diffraction at the WNR.

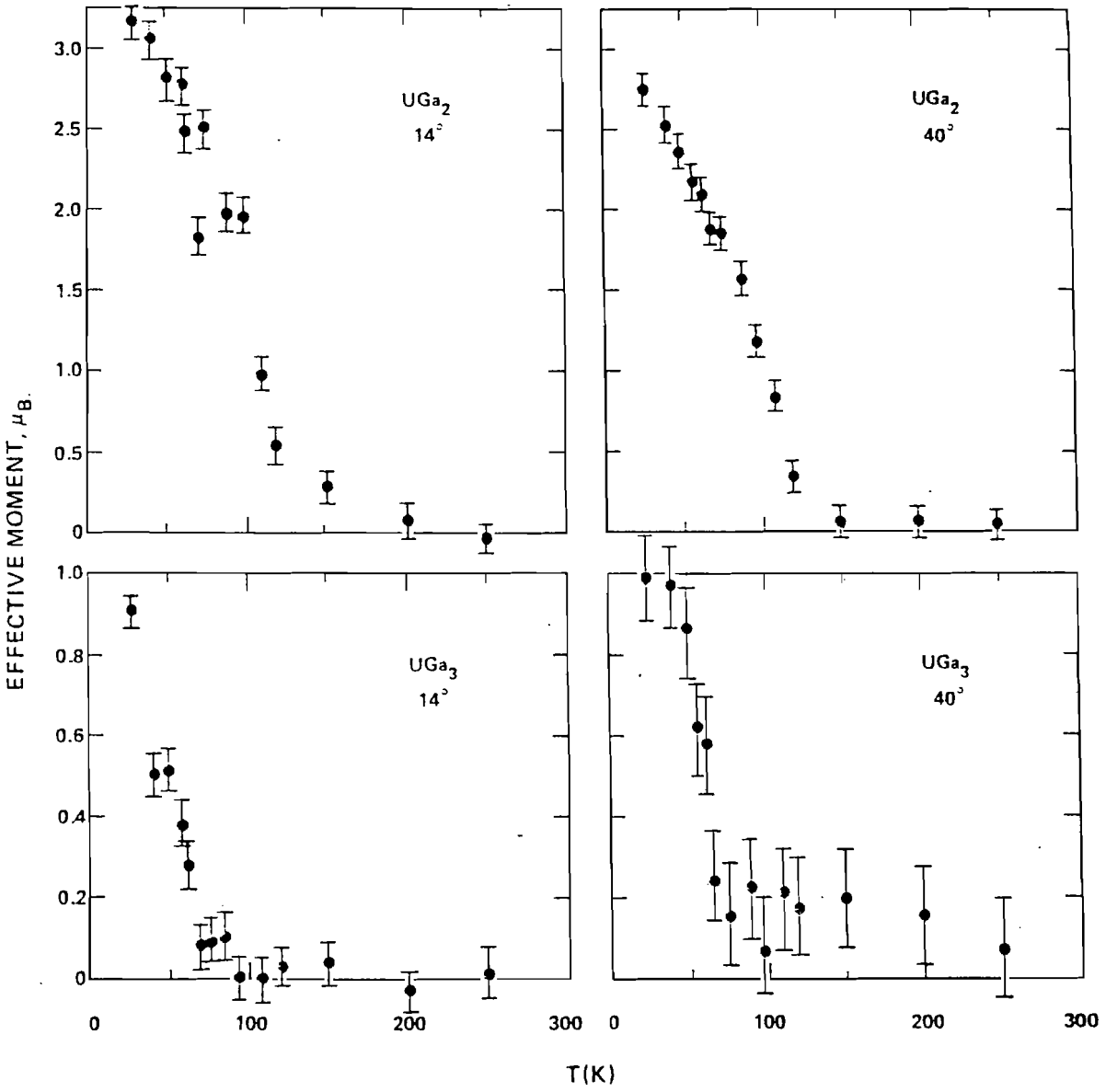

Fig. 5 Uranium magnetic moments as a function of temperature measured by time-of-flight neutron powder diffraction in the ferromagnet UGa_2 amd the antiferromagnet UGa_3.

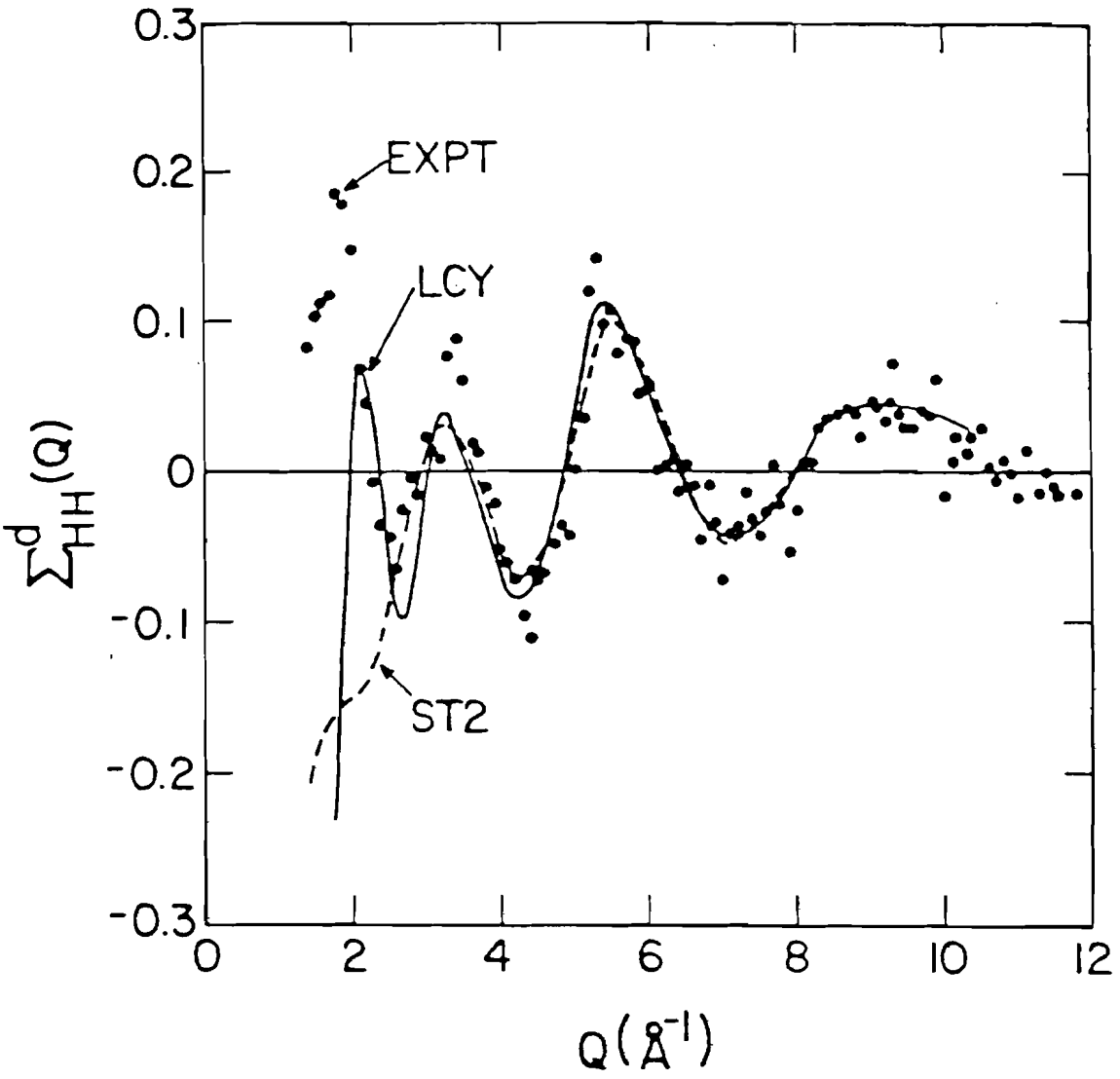

Fig. 6 Hydrogen-hydrogen partial structure factor for liquid water (dots) as measured in an hydrogen/deuterium isotope substitution experiment at the WNR, compared with two theoretical simulations LCY (Lee, Clementi, and Yoshimini) and ST2 (Stillinger and Raman) based on model intermolecular water potentials. Water has stronger short range order (more ice-like) than either simulation.

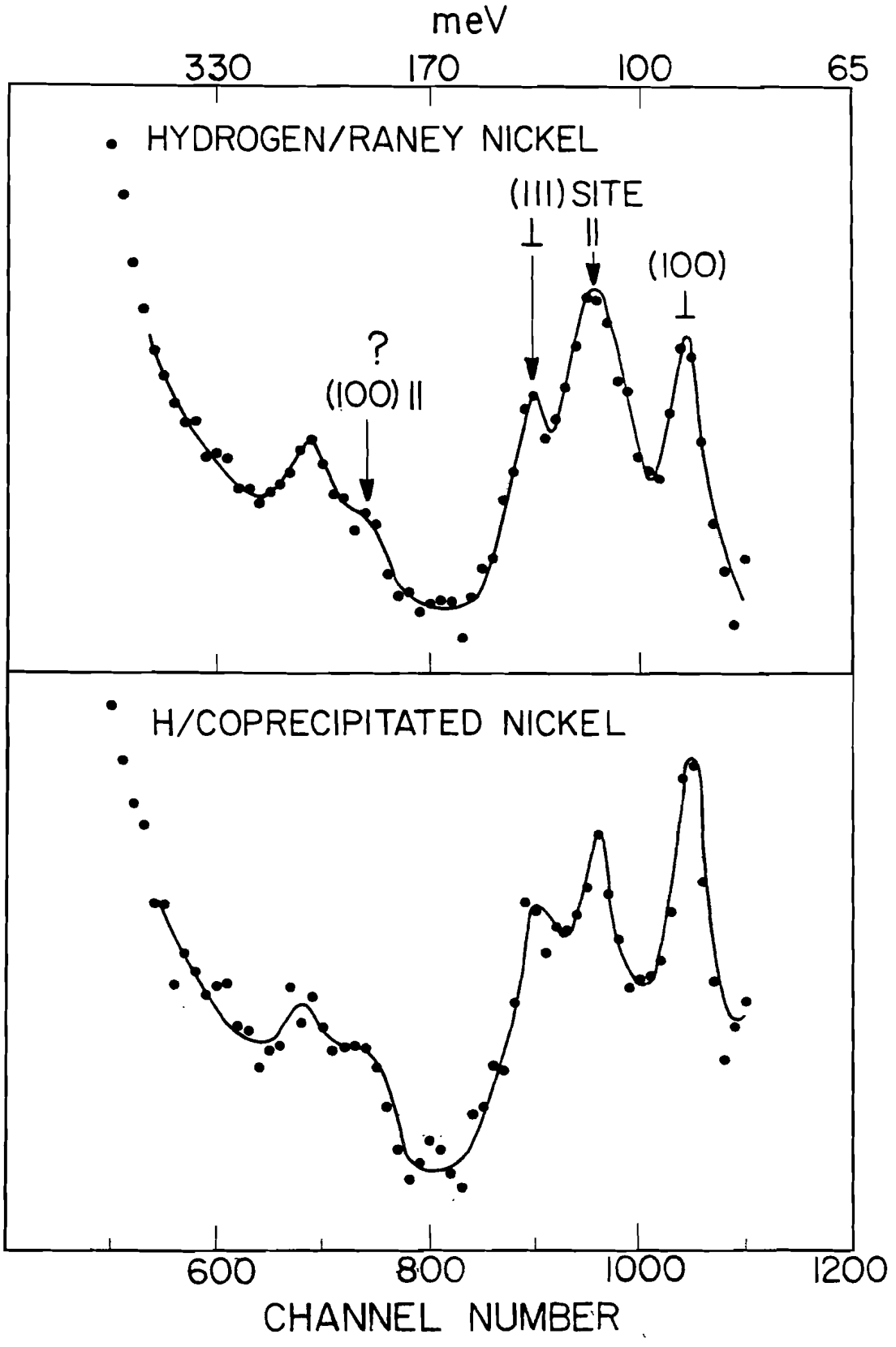

Fig. 7 Inelastic neutron scattering spectra of hydrogen chemisorbed on Raney nickel and coprecipitated nickel, as measured on the Be-BeO Filter Difference Spectrometer at the WNR facility.

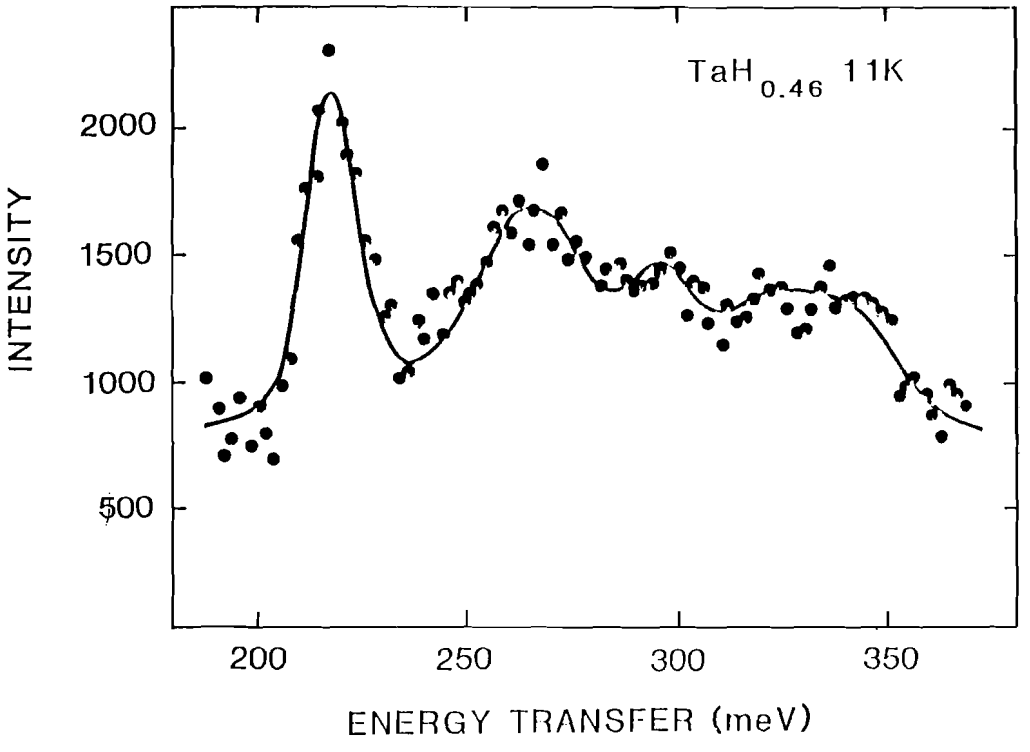

Fig. 8 High energy transfer part of the vibrational spectrum of $TaH_{0.46}$ as measured on the Be-BeO Filter Difference Spectrometer at the WNR facility.

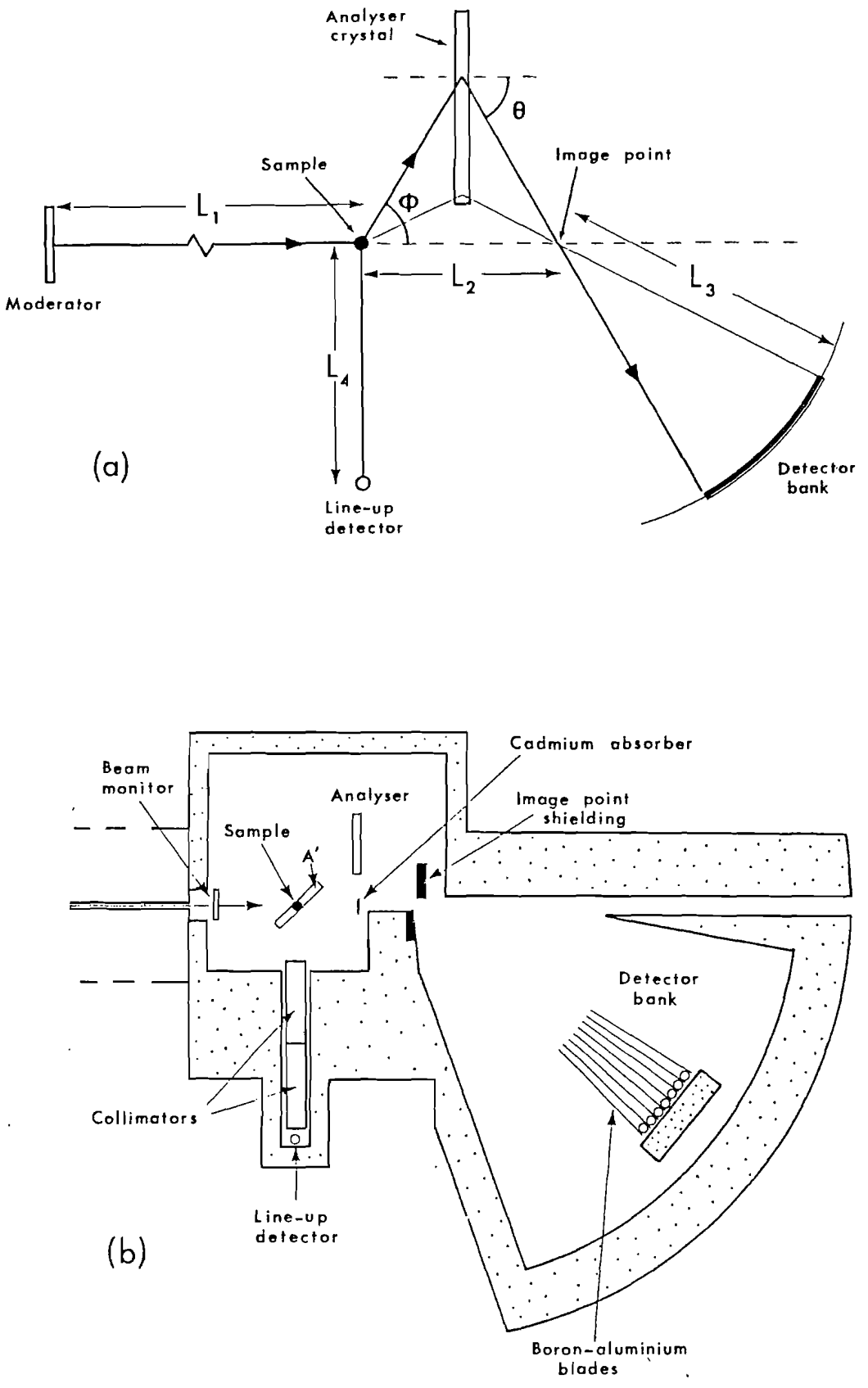

Fig. 9 Schematic diagrams of the Constant-Q Spectrometer at LANSCE, an instrument for the measurement of elementary excitations in single crystal samples.

Proceedings of the Eighth Meeting of the International Collaboration on Advanced Neutron Sources (ICANS-VIII)
8-12 July 1985, Rutherford Appleton Laboratory Report RAL-85-110

Phase Space and Phase Space Transformations

B. Alefeld, A. Kollmar

Kernforschungsanlage Jülich, D 5170 Jülich, BRD

Abstract

The large advantage of a pulsed neutron flux consists in the applicability of time dependent phase space transformations. A large number of neutrons are wasted, if the same transformations are applied at a steady state source. Three typical examples of phase space transformations at a pulsed neutron source will be discussed. The first example is the well known time of flight technique. Neutron bunching is an example of a phase space transformation performed by time and by forces (moving crystal). In the last example, the Doppler instrument, only a force is used to transform a phase space volume. The shape is time independent. The last two techniques have not been used on steady state sources, however, they may become very attractive on pulsed sources because in addition to the gain of the peak flux an extra gain of about 10 for the bunching spectrometer and 20 for the Doppler instrument have been estimated as compared to conventional techniques like chopper and rotating crystal instruments (IN5 and IN4 at the ILL in Grenoble).

Introduction

The phase space concept was first applied by Maier-Leibnitz to intensity and resolution considerations of neutron scattering instruments and experiments /1/. One advantage is the fact that the natural quantity "momentum", which plays a superior role in neutron scattering theory, is used in this formalism. In contrast, intensity and resolution considerations with quantities like wavelength, energy and solid angle are very cumbersome. As has been pointed out by Maier-Leibnitz and Springer, another great advantage of the phase space concept is the direct application of Liouville's theorem to a "neutron gas" /2/. This theorem tells us, that the phase space density remains unchanged during the free propagation of a neutron beam or in a transformation of the coordinate system (e.g. Bragg reflection,

mirror reflection) and under the influence of conservative forces (such as gravity, magnetic field gradients or moving crystals). The behaviour of a phase space volume can be compared with an incompressible liquid /3/. This means that the shape of the phase space volume can easily by changed, but not the density. For neutron scattering instrumentation Liouville's theorem plays a similar role as the second law of thermodynamics at least in the sense that from time to time "ingenious" devices are discussed seriously, which are meant to increase the phase space density, these devices are analogous to a perpetuum mobile of the second kind.

Phase Space and Neutron Intensity

The phase space density is defined as

$$\frac{\Delta^6 n}{\Delta V_p} = \frac{\Delta^6 n}{\Delta k_x \Delta k_y \Delta k_z \Delta x \Delta y \Delta z \hbar^3}$$

n is the number of neutrons in the phase space volume.

For a Maxwellian distribution one obtains

$$\frac{\Delta^6 n}{\Delta V_p} = \frac{\Phi m}{2\pi \hbar^4 k_T^4} e^{-k^2/k_T^2}$$

$$\text{with } k_T = \sqrt{2mk_B T}/\hbar$$

It is important to note that for a fixed k there is one moderator temperature for which the phase space density has a maximum. The intensity of a neutron beam in z-direction through an area ΔF(sample area) is proportional to the phase space density in the moderator

$$\Delta^5 J = \frac{\Phi k_z}{2\pi k_T^4} e^{-k_z^2/k_T^2} \Delta k_x \Delta k_y \Delta k_z \Delta F$$

The most important task for a neutron scattering experiment is the optimization of the intensity and the resolution. With respect to k, the best what has been achieved up to now is the installation of three different moderators, a hot, a thermal and a cold moderator (ILL). What remains to be done is the selection and shaping of the momentum space volume $\Delta k_x \Delta k_y \Delta k_z$. In the following it will be shown that the phase space concept is very useful to treat this problem, expecially for a pulsed neutron source.

Phase Space Transformations

a) Time dependence of the phase space volume of a short neutron pulse

We consider the most important case of a phase space transformation at a pulsed neutron source, the development in time of the phase space volume of a short polychromatic neutron pulse. To simplify the discussion, it is assumed that the neutron pulse is propagating within a neutron guide tube in z-direction. In this case the time dependent phase space volume is two-dimensional, because the x- and y-componets and their conjugate components are conserved.The abscissa in Fig. 1 represents the z-coordinate on the ordinate the conjugate variable k_z is shown. The phase space volume at

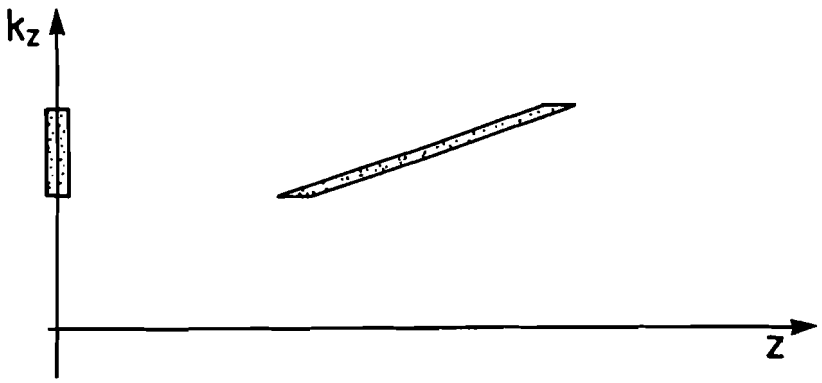

Fig. 1: The time dependence of a twodimensional phase space volume of a short neutron pulse propagating in a neutron guide tube. In this case the four other dimensions of the phase space volume are time independent.

t = 0 is represented by a rectangular area at z = 0. This area is homogeniously filled with neutrons. Due to the fact that the neutrons in the upper part of the area move faster than the neutrons in the lower part, the area will be elongated in z-direction after a time t_1. The area and hence the phase space density is conserved. The elongation of the area in z-direction is proportional to the flight path. This kind of phase space transformation serves to separate neutrons of different velocities in space or at a fixed point z in time. This is the fundamental technique in all time of flight methods to separate neutron velocities. It is obvious that this technique is especially useful for pulsed sources, because all the neutrons, which are produced in the moderator, are contained in th phase space volume (at

least in the ideal case), whereas on a steady state source short pulses have to be cut out of the continous beam, leading to a loss factor of neutrons given by t_n/T, where t_n is the pulse length and T is the repetition rate.

b) Neutron bunching

A high resolution time focussing spectrometer, also called bunching spectrometer, was proposed by Maier-Leibnitz fifteen years ago /4/. This type of instrument never was built on a continous source. But on a pulsed source, this instrument may become very attractive. Its principle is based on a phase space transformation inverse to the one described in section a. In Fig. 2 again a twodimensional phase space is shown. At z = 0 a space volume of which $\Delta z = v_o t_n$ is produced in the moderator. The width Δk_z can be produced with choppers. One special transformation is shown for a distance far outside the shielding of the neutron source. From now on we consider only those neutrons which are contained in the dashed perpendicular stripe. After an additional length L_B (bunching length) the elongated dashed stripe is selected and transformed into the stripe below. After the distance L_B backwards on the z-axis this phase space volume is focused in space and time. The realization of this phase space transformation can be performed with a moving crystal which slows down the neutrons which are faster and speeds up those neutrons which are slower than the mean velocity v_o. The time dependence of the neutron velocity in the dashed area at L_B is given by

$$v(t) = v_o - \frac{v_o^2}{L_B} t$$

(Neutrons with the velocity v_o arrive at the crystal at t = 0). If the crystal at rest reflects a velocity v_o then it has to be moved with a velocity

$$v_D(t) = -\frac{v_o^2}{L_B} t$$

because the relative velocity between the neutrons and the moving crystal has to be v_o. First the crystal has to be moved in the direction of the neutron beam (away from the source), at the arrival time of v_o the direction is turned (v_D = 0) and then it moves against the beam. It follows that the neutron velocity are shifted from

$$v(t) = v_o + \frac{v_o^2}{L_B}t \quad \text{to} \quad -v_o - \frac{v_o^2}{L_B}t$$

which gives the transformation shown in Fig. 2. After this velocity transformation the phase space volume is transformed by time of flight into the perpendicular stripe. It should be mentioned that this bunching technique is very similar to that applied in accelerators /5/. A rather detailed

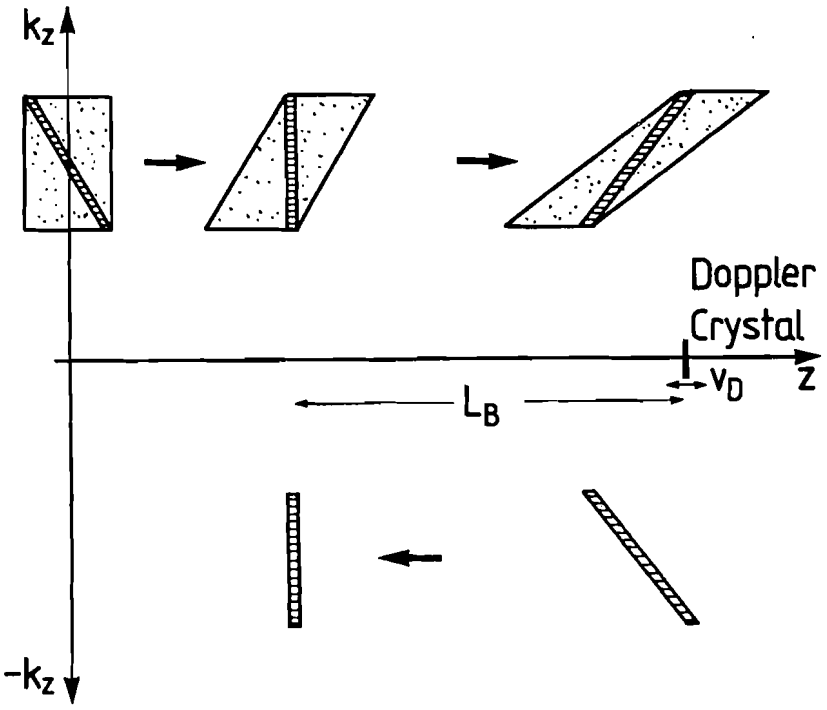

Fig. 2: Phase space transformation of the bunching instrument. The hatched part of the whole neutron pulse near the moderator (z = 0) is first transformed by time of flight, then it is backscattered by a moving crystal and transformed into the lower part of the (k_z, z)-plane. This phase space volume is refocussed after the distance L_B^z.

discussion on the realization of a bunching spectrometer at a pulsed source has been given by RICHTER and ALEFELD /6/. It was shown that in addition to the gain of the peak flux of a pulsed source a factor of about 10 is gained as compared to a nonfocusing spectrometer with the same resolution of about $\Delta E/E = 10^3$.

c) The increase of the phase space density by a fast moving crystal at thermal energies.

It has been shown above that the phase space density of a neutron spectrum in thermal equilibrium with the moderator is given by

$$\frac{\Delta^6 n}{\Delta V_p} = \frac{\Phi m}{2\pi \hbar^4 k_T^4} e^{-k_z^2/k_T^2}$$

Fig. 3 shows the phase space density of a cold moderator with a temperature of 50 K and of a thermal moderator with a temperatur of 350 K. If it is possible to shift the phase space density of the cold moderator to a higher k_z value one obtains a phase space density which is higher than available from the source. In Fig. 3 it was assumed that the phase space density for a wave vector k_z can be shifted to a wave vector $(k_z + 1.59)$ Å^{-1} which is equivalent to a shift from the velocity v_z to the velocity $(v_z + 1000)$ m/s. The highest gain factor of 28 is obtained by shifting neutrons with $k = 1.4$ Å^{-1} to a wave vector $k = 3$ Å^{-1}. This corresponds to a shift from 889 m/s to 1889 m/s. In Fig. 4 this phase space transformation is again shown in the twodimensional phase space of a neutron guide tube. We assume that the pulse length of the source is 350 µs for all velocities. The twodimensional phase space volume of the neutron pulse near to the moderator is shown at z = 0. A nearly monochromatic region around the velocity 889 m/s is labeled with the letter a. The whole phase space volume moves to the right and at a distance of about 20 m a crystal in back reflection is moved with a velocity of 500 m/s against the neutron beam. The lattice spacing of the crystal is chosen in such a way that it would reflect neutrons with a velocity of 1389 m/s if it were at rest. The moving crystal picks up the neutrons around the velocity 889 m/s (labeled with b) and after the reflection the neutrons are transformed to the velocity $-(889 + 2v_D) = -1889$ m/s, this part is labeled with c. First of all we see that the pulse length of the original neutrons of 350 µs is compressed to a pulse length of 164 µs. For most applications, this pulse length still is too long. A simple possibility to shorten the pulse length is to rotate the crystal during the reflection time. In this case the condition for back reflections is time dependent. If the crystal is out of back reflection by an angle α the angle of the reflected neutrons relative to the neutron guide is changed by 2α. A pulse length of $t_n = \Delta\alpha/\omega$ is expected, where $\Delta\alpha$ is the divergence for neutrons with the velocity 1389 m/s. This value is 10^{-2} rad for a nickel

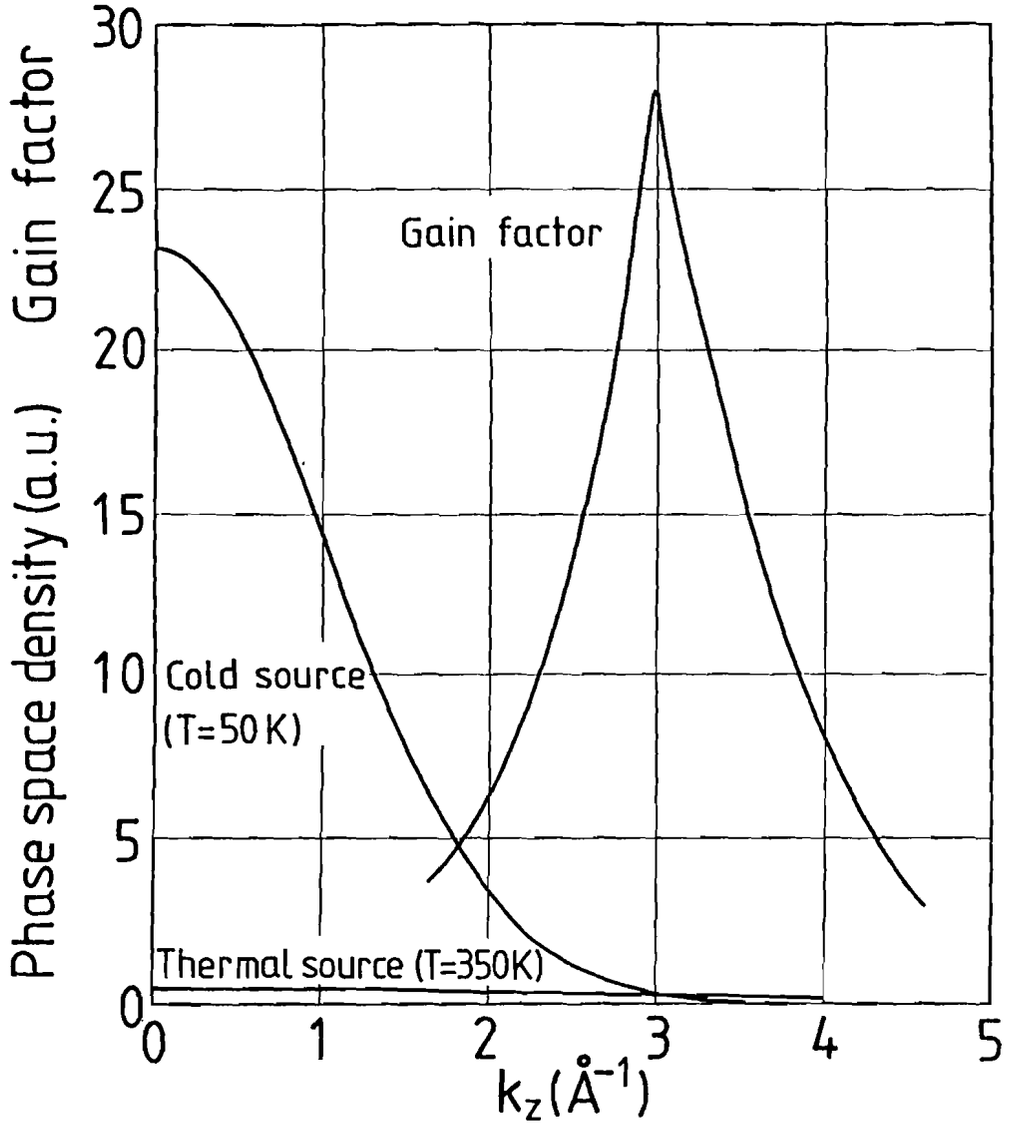

Fig. 3: The phase space density $\Delta^6 n/\Delta^6 V_p$ of a cold moderator (T = 50 K) and a thermal moderator (T = 350 K). The gain is obtained by shifting neutrons from k_z to $(k_z + 1.59)$ Å^{-1} which is equivalent to a shift from v_z to $(v_z + 1000)$ m/s. For $k_z < 3$ Å^{-1} the gain factor is defined as the ration between $\exp-(k_z-1.59)^2/k^2_{T=50}$ and $\exp-k_z^2/k^2_{T=50}$. For $4.59 > k_z > 3$ the gain is defined as the ratio between $k^{-4}_{T=50}\exp-(k_z-1.59)^2/k^2_{T=50}$ and $k^{-4}_{T=350}\exp-k_z^2/k^2_{T=350}$.

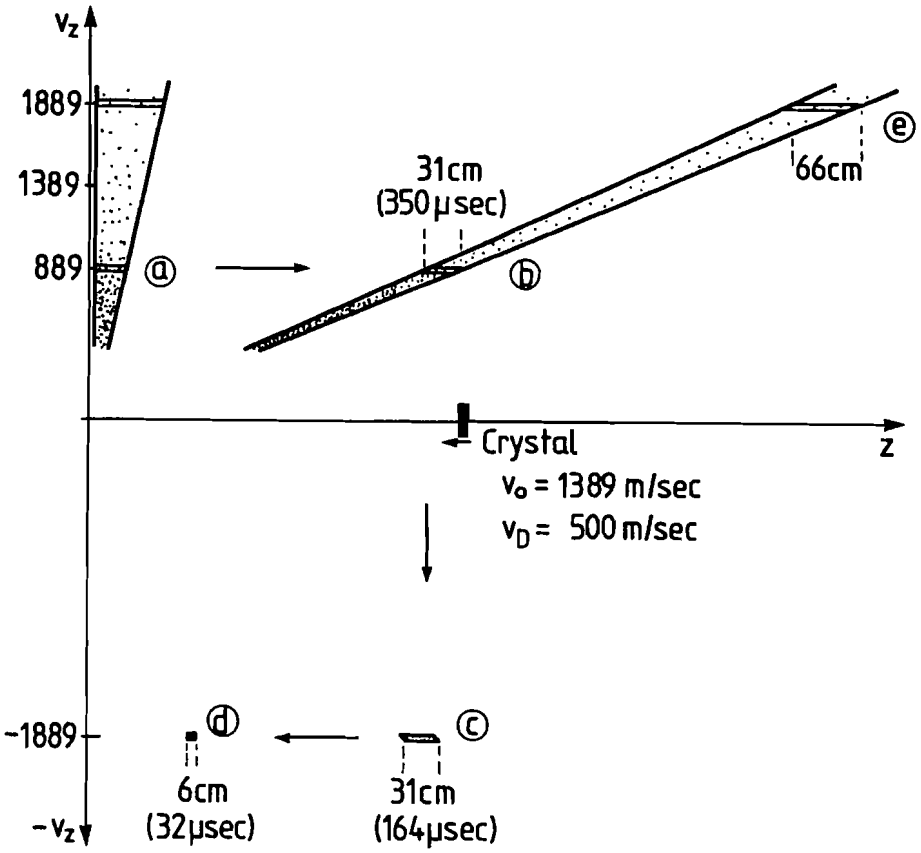

Fig. 4: Phase space transformation of a Doppler instrument. The phase space volume at z = 0 (near to the moderator) moves for some time, till the hatched nearly monochromatic region around 889 m/s, (labeled by a) is impinging onto a crystal which is moved against the neutron beam. The phase space volume labeled by b is only slightly deformed. After the reflection the phase space volume is shifted to a region where the original phase space density was much lower. Compare region c with region e. The cutting down of the pulse length of 156μs to 32μs is achieved by a simultanious rotation of the Doppler crystal.

coated neutron guide tube. Putting $\omega = 314\ s^{-1}$ we finally obtain for the pulse length the value $t_n = 32\ \mu s$. This part of the phase space volume in Fig. 4 is labeled with d. The most important point however is the fact that the phase space density in the part d is by a factor of 28 (see Fig. 3) larger than in the conventional case by taking the original phase space volume at v = 1889 m/s (labeled with e in figure 4) and cutting it down with choppers to the length of 32 μs. It should be noted, that the peak flux at the cold source of the SNQ is expected to be about a factor of 2 lower than at the thermal source /7/. From Fig. 3 it can be seen that in this case a maximum gain factor of about 10 is obtained for $k = 2.8\ \text{Å}^{-1}$.

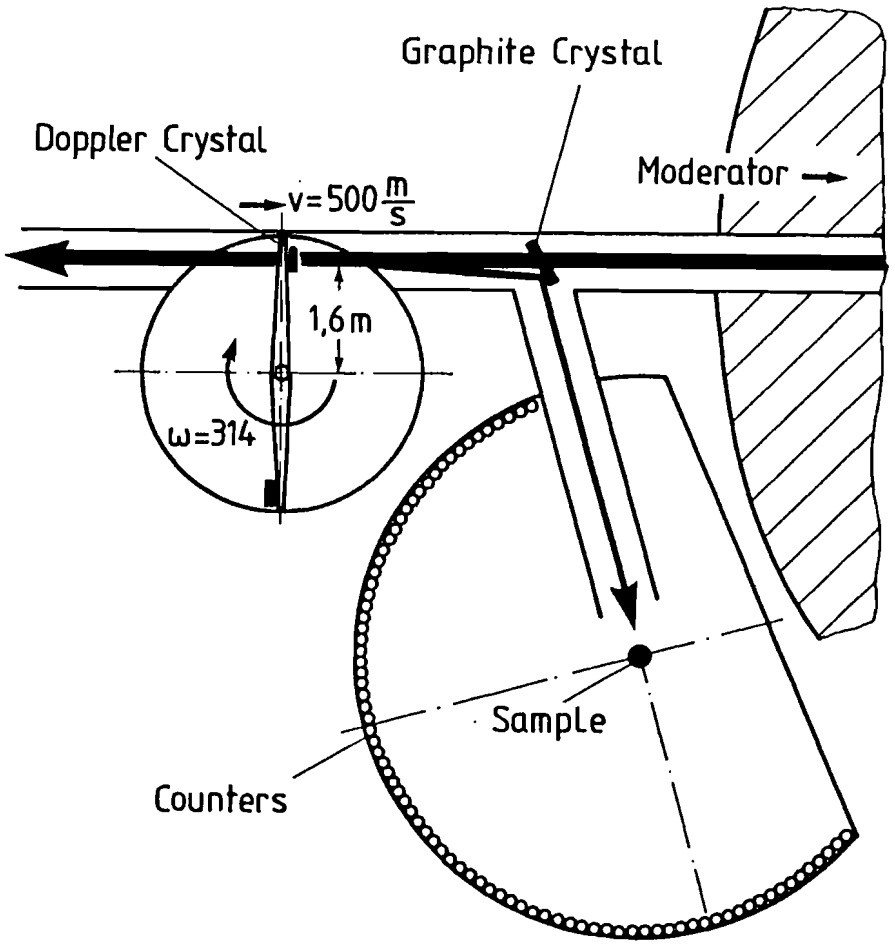

Fig. 5 Schematic drawing of a Doppler instrument. A white neutron beam passes the graphite crystal and hits the Doppler crystal which is mounted on a two-armed wheel. The wheel rotates with a frequency of 50 Hz and is synchronized to the source. The back reflected neutrons are deflected by the graphite crystal to the sample. The rest of the spectrometer is conventional.

Fig. 5 shows a schematic drawing of the Doppler instrument (BALDI). A white neutron beam passes the graphite crystal and hits the Doppler crystal which is mounted on a wheel with two arms. The wheel is synchronized to the pulsed source and rotates with $\omega = 314\ s^{-1}$. The reflected neutrons are deflected by the graphite crystal to the sample. The rest of the spectrometer is conventional.

Finally it should be mentioned that there are a number of other techniques of phase space transformations, which have been proposed to utilize the neutron flux of a pulsed source in a more efficient way than is possible on a steady state source /7,8,9/.

Acknowledgement

The authors like to thank Prof. H.H. Stiller for many stimulating discussions.

References

/1/ H. Maier-Leibnitz, Nukleonik 8, 61 (1966)

/2/ H. Maier-Leibnitz, T. Springer, Ann. Rev. Nuc. Science 16, 207 (1966)

/3/ A. Sommerfeld, Thermodynamik und Statistik, Akademische Verlagsanstalt Geest u. Portig K.-G., Leipzig 1962, page 178

/4/ H. Maier-Leibnitz, Verlag der Bayr. Akad. Wiss., München 1967, Sonderdruck 16

/5/ J. Schelten, private communication

/6/ D. Richter, B. Alefeld, JÜL-1954 ed. by R. Scherm and H.H. Stiller, KFA Jülich 1984, page 409.

/7/ B. Farnoux, A. Steyerl, J. Deutz, B. Alefeld, JÜL-1954 ed. by R. Scherm and H.H. Stiller, KFA Jülich (1984), page 108.

/8/ J. Schelten, B. Alefeld, ibid., page 157.

/9/ J. Schelten, B. Alefeld, ibid., page 378.

Proceedings of the Eighth Meeting of the International Collaboration on Advanced Neutron Sources (ICANS-VIII)
8-12 July 1985, Rutherford Appleton Laboratory Report RAL-85-110

PERFORMANCE FEATURE OF CRYSTAL ANALYSER MIRROR TYPE SPECTROMETERS USING COLD AND THERMAL PULSED NEUTRON SOURCES

Kazuhiko INOUE

Department of Nuclear Engineering,
Hokkaido University, Sapporo,
060 Hokkaido, Japan

Abstract

We have been engaged in developing the crystal analyser mirror type spectrometers combined with the KENS cold and thermal neutron sources. Our studies have revealed that the crystal analyser mirror(LAM type mirror) is the simplest but most suitable device for the spectrometers using pulsed sources. Performance feature of the LAM type quasielastic and inelastic spectrometers is described.

In order to carry out neutron spectroscopy using the pulsed source, it is most desirable that the neutron pulse emitted from the source be utilized directly for energy analysis using the time-of-flight technique without any auxiliary device for narrowing the pulse width. As to accompanying secondary energy analysing devices, there are several options. Our crystal analyser mirror is the most suitable one. Therefore, we adopted the arrangement of devices shown in Fig. 1.

In the case of time-of-flight measurements, the energy resolution required is attained by selecting an appropriate length of neutron flight path to the width of the neutron pulse. Of course, in the case of cold neutron scattering for a long flight path, the neutron guide tube must be used. Next, a wide range energy resolution of the crystal analyser is

appropriately selected by adjusting the Bragg angle. This combination of devices enabled us to design a set of quasielastic and inelastic spectrometers with large flexibility of performance.

If the design parameters of the spectrometers are appropriately selected, the time spectrum of the scattered neutrons from the sample at a scattering angle θ is simply expressed as follows [1].

$$\eta(t;\theta)=\text{const.}\int\int\phi(E_1,t-t_2)\sigma(E_1\rightarrow E_2,\theta)R(E_2)dE_1dE_2, \tag{1}$$

where $\phi(E_1,t_1)$ is the incident neutron flux at time t_1 into the sample, $\sigma(E_1\rightarrow E_2,\theta)$ is the incoherenet differential scattering cross section, $R(E_2)$ is the energy resolution function of the crystal analyser mirrors, m is the neutron mass, ℓ_1 and ℓ_2 are the average flight path lengths of the incident and scattered neutrons, t_1 and t_2 are given by the followings,

$$t_1=\ell_1/\sqrt{2E_1/m}\ , \tag{2}$$

$$t_2=\ell_2/\sqrt{2E_2/m}\ . \tag{3}$$

The quantities measured is the energy transfer, ε, defined by

$$\varepsilon=E_1-E_2\ . \tag{4}$$

The overall energy resolution of the spectrometers, $\Delta\varepsilon$, is approximately given by the following expression,

$$\Delta\varepsilon=(\Delta E_1^{\,2}+\Delta E_2^{\,2})^{1/2}. \tag{5}$$

The energy resolution, ΔE_1, in the time-of-flight experiments is given by

$$\Delta E_1=2E_1(\Delta t_z^{\,2}+\Delta t_1^{\,2}+\Delta t_2^{\,2})^{1/2}/t_1\ , \tag{6}$$

where Δt_z is the pulse width of the neutrons emitted from the source, Δt_1 is the variance of the flight time due to the variance of ℓ_1, and Δt_2 is the variance of the flight time due to the scattered neutrons from the sample to the counters.

To decide the dimensions of the analyser mirror, many factors are involved. We designated the position inside the medium of the sample as $\mathbf{r}$, the position on the mirror as Σ and the position on the assumed plane of the diaphragm of the counter as S. The Bragg angle spread of the analyser mirror is calculated by the following equation [1].

$$\hat{R}(\theta_B)=\iiint p(\mathbf{r},\Sigma,S)|\mathbf{r}-\Sigma|^{-2}|\Sigma-S|^{-2}\delta[\theta_B-\hat{\theta}_B(\mathbf{r},\Sigma,S)]d\mathbf{r}d\Sigma dS \ , \qquad (7)$$

where $\theta_B(\mathbf{r},\Sigma,S)$ is the Bragg angle determined by the positions $\mathbf{r}$, Σ and S, and $p(\mathbf{r},\Sigma,S)$ is a factor representing efficiency due to the projection of each plane and the mosaicness of the crystals.

The energy resolution of the analyser mirror is estimated by the following expression,

$$\Delta E_2=2E_2[(\cot\theta_B\Delta\theta_B)^2+(\Delta\tau/\tau)^2]^{1/2} \ . \qquad (8)$$

Here $\Delta\tau$ is the variance of the reciprocal lattice vector, τ, due to the limitation of the number of lattice planes contributing to the reflection. In our case, the second term in the brackets in the right hand side of Eq. (8) may be small enough to neglect as compared with the first term.

Quasielastic spectrometers (LAM-40 and LAM-80)

To attain the optimum condition for quasielastic measurements, that is, the desired resolution and high efficiency, it is necessary to match the energy resolution in time-of-flight measurement, ΔE_1, for the energy resolution of the analyser mirror, ΔE_2, according to Eqs. (1) and (4).

For the case of flight path lengths 6, 30 and 150 m, the variances of incident and scattered neutron energies, ΔE_1 and ΔE_2, as functions of the Bragg angle calculated by Eqs. (6) and (8) are depicted in Fig. 2. Of course, ΔE_1 depends on the Bragg angle, but ΔE_2 does not depend on the flight path length. An optimal condition is achieved by matching ΔE_1 to ΔE_2. Thus, the optimal condition for the desired performance can be found around the points where the two curves cross, as shown in Fig. 2.

The two spectrometers, the LAM-40 and the LAM-80 (Fig. 3-a,b), utilize two sets of LAM-type analyser mirrors(lattice-$\frac{d}{\Lambda}$-crystal analyser mirror), of which the structural frames supporting the crystal pieces were fabricated according to the same design method described in the previous chapter. The main difference between them is in the Bragg angles, 39° for the LAM-40, and 80° for the LAM-80, respectively. Next, for the LAM-40, small beryllium filters of 6 cm thickness were used. The average distance from the sample to the counter diaphragm via the mirror crystals is 120 cm for both sets of mirrors.

Currently we are working on the design of a LAM-type analyser mirror having a Bragg angle of 86° to 88° in the hope of developing a quasielastic spectrometer having a few μeV resolution.

The energy resolution of the LAM-40 has a special feature in its shape, that is, it shows a sudden steep rise on only one side of the resolution function, and this shape enebles clear observation of a faint spectrum existing in the energy transfer range about 0.3 meV to 1 meV. Then, the LAM-40 has been used to investigate the non-Markovian random process in the motion of polymer chains. A typical example of the measured spectra is shown in Fig. 4. The central peaks of spectra in the figure are the elastically scattered components, which are broadened by the resolution function of the spectrometer. The down-scattering

quasielastic spectrum exists in the time-of-flight region from about 160 channel to 230 channel. We do not utilize the up-scattering quasielastic spectrum existing in the channels above 230 channel because it was distorted by the undesirable tail of the resolution function. Expanded quasielastic spectra on the scattering angle of 88° at various temperatures are shown in the figure.

The LAM-80 is an intermediate resolution spectrometer with a wide energy window. Fig. 5 shows some preliminary data obtained by using the LAM-80. In this case the sample was poly(butadiene) at a temperature between melting and glass-transition points. The wide energy window covered by the LAM-80 is shown in the insert in Fig. 5. The upper limit of energy transfer is due to the transmission of the guide tube.

Down-scattering spectrometer (LAM-D)

Arrangement of the LAM-D is illustrated in Fig. 3-c. A beryllium filter, which has a length of 20 cm, is used at liquid nitrogen temperature. Fig. 6 shows the energy transfer resolution devided by the incident neutron energy for several cases of the incident flight path length. This figure reveals that the LAM-type mirror is also very useful for the inelastic scattering. The resolution in the range 100-3000 cm^{-1} is estimated to be 2-3 % for 10 m incident path length. In this region, the resolution is approximately proportional to the reciprocal of incident path length. Then, better resolution (1 % or less) will be easily attained by using longer incident path length, if we use more intense source.

Fig. 7 is the observed spectra for PMMA(h_8), in which S/N is excellent. But present LAM-D has only one analyser mirror and data acquisition rate is not high. We have begun a design of new improved

version of present LAM-D, which has four analyser mirrors.

Reference

[1] K. Inoue, et al.: Nucl. Instr. and Meth., 178(1980)459.

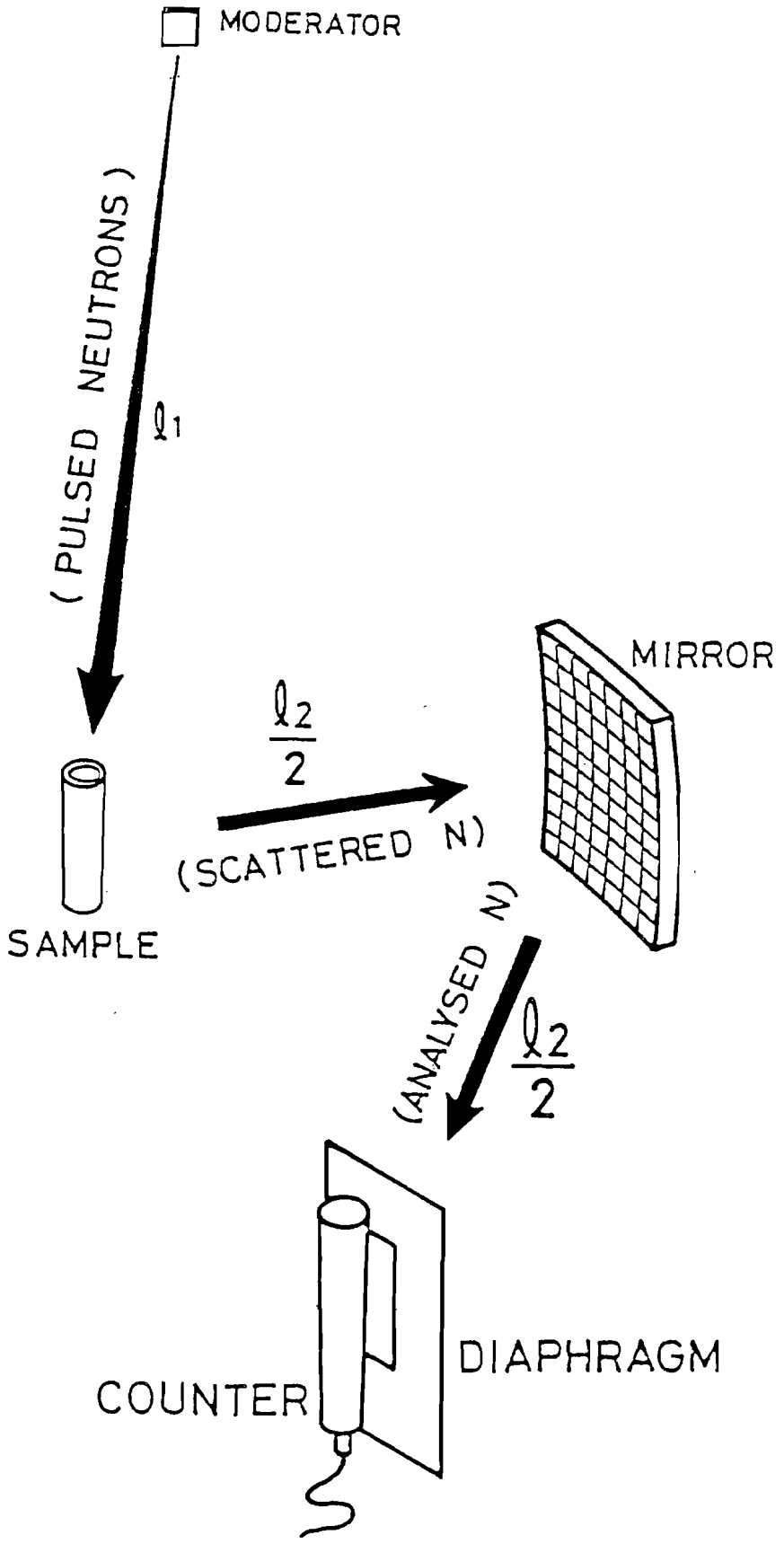

Fig. 1 General layout of the inverted geometry spectrometer using a pulsed neutron source and the LAM-type analyser mirror.

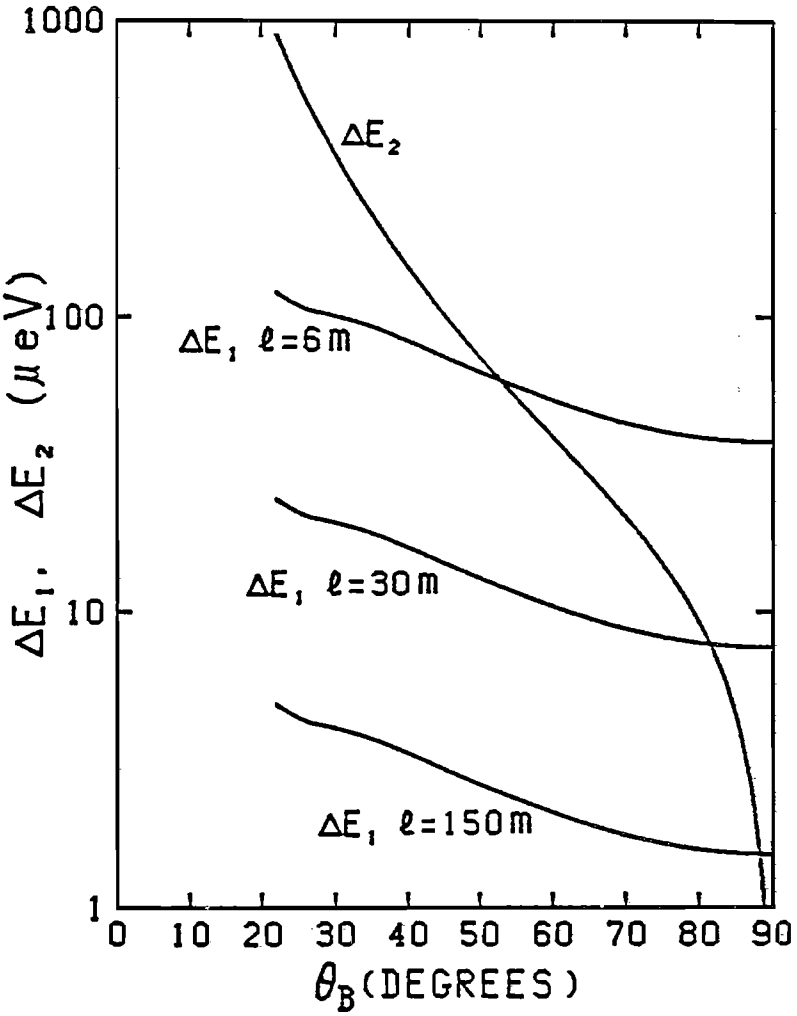

Fig. 2 Partical energy resolutions, ΔE_1 and ΔE_2, plotted as functions of the Bragg angle for three cases of flight path length in the time-of-flight measurement using the pulsed cold source.

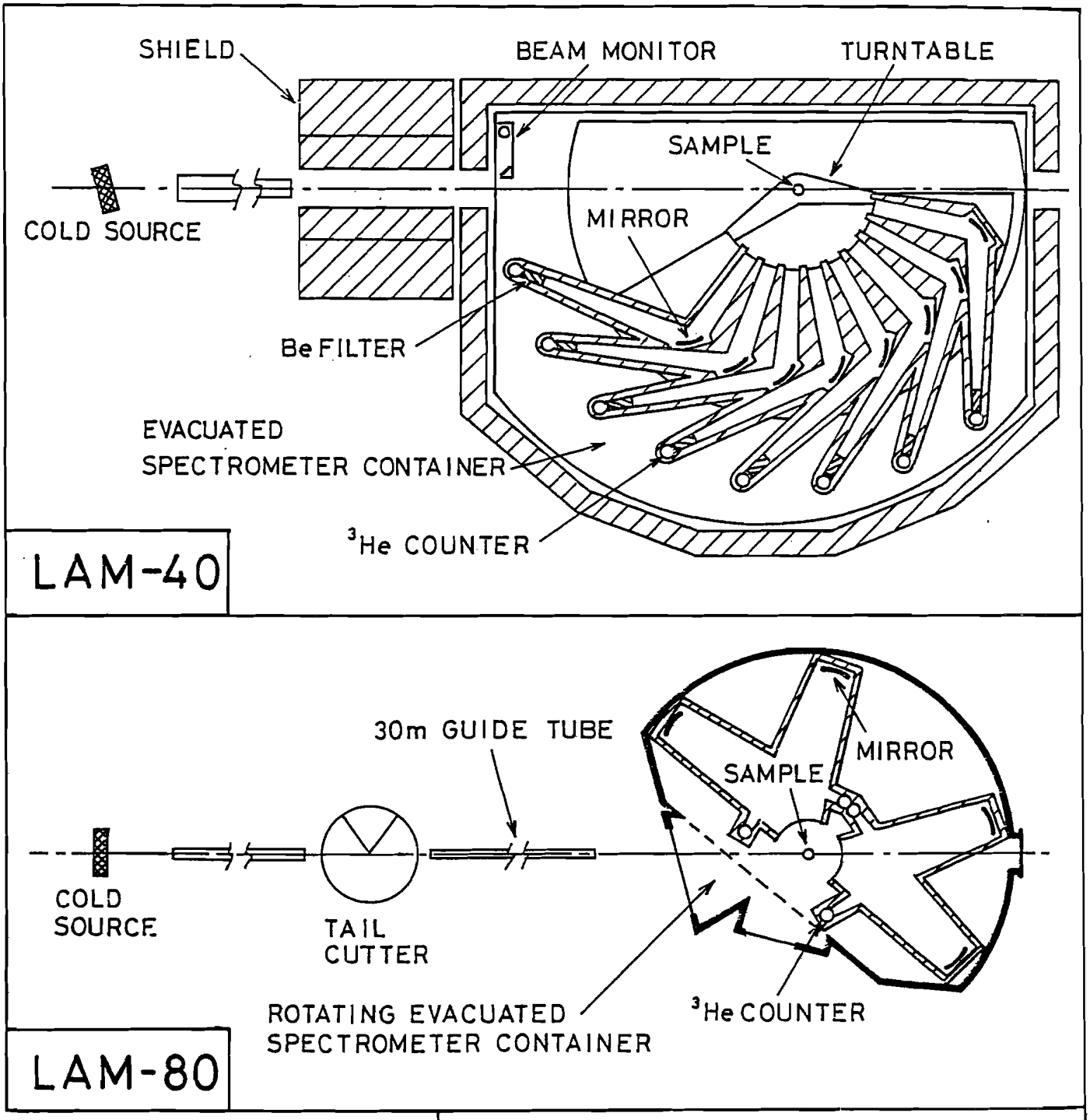

Fig. 3

Layout of three spectrometers, LAM-40, LAM-80 and LAM-D.

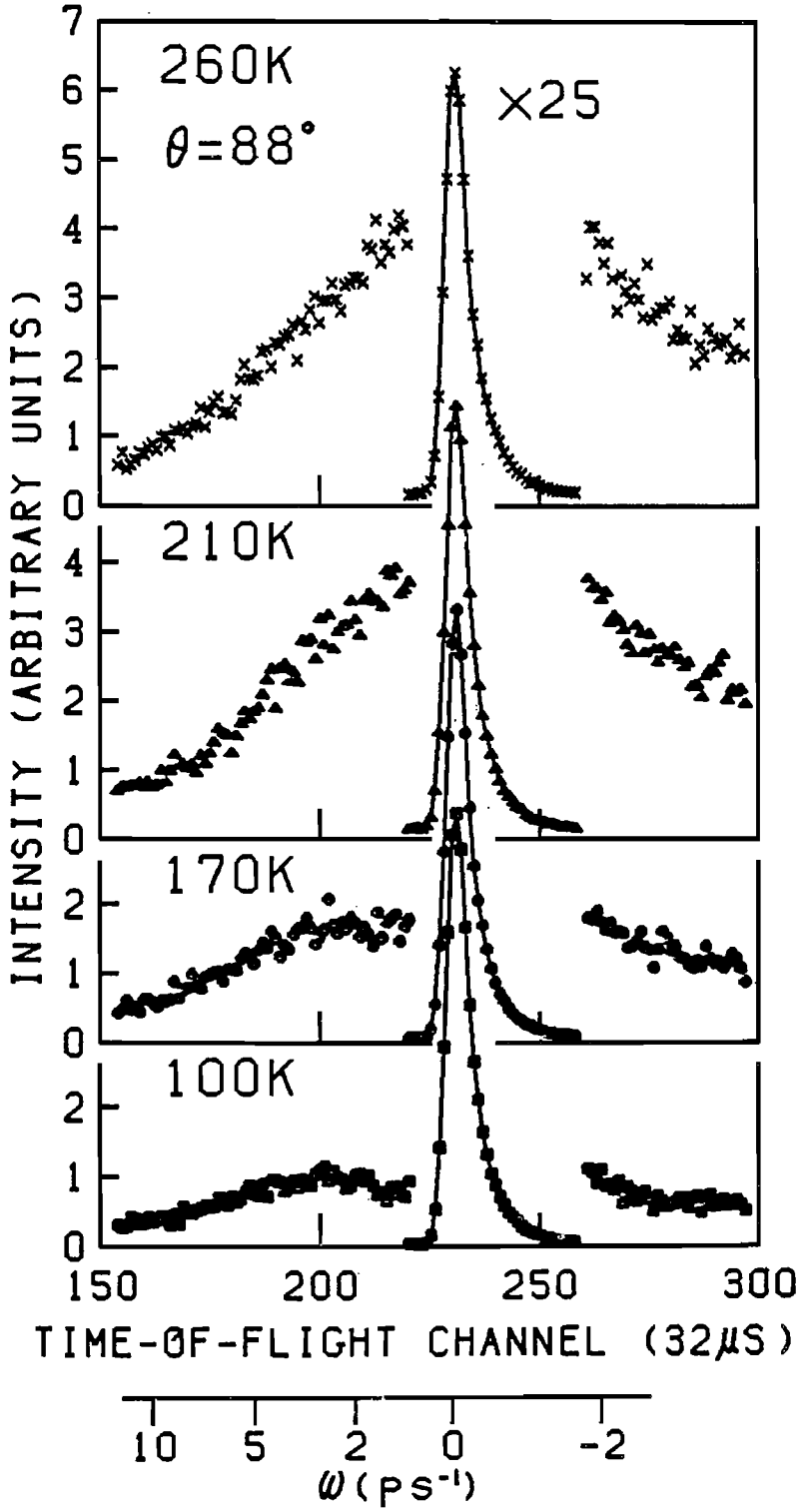

Fig. 4 Time-of-flight spectra from poly(butadiene) at various temperatures, measured by the LAM-40.

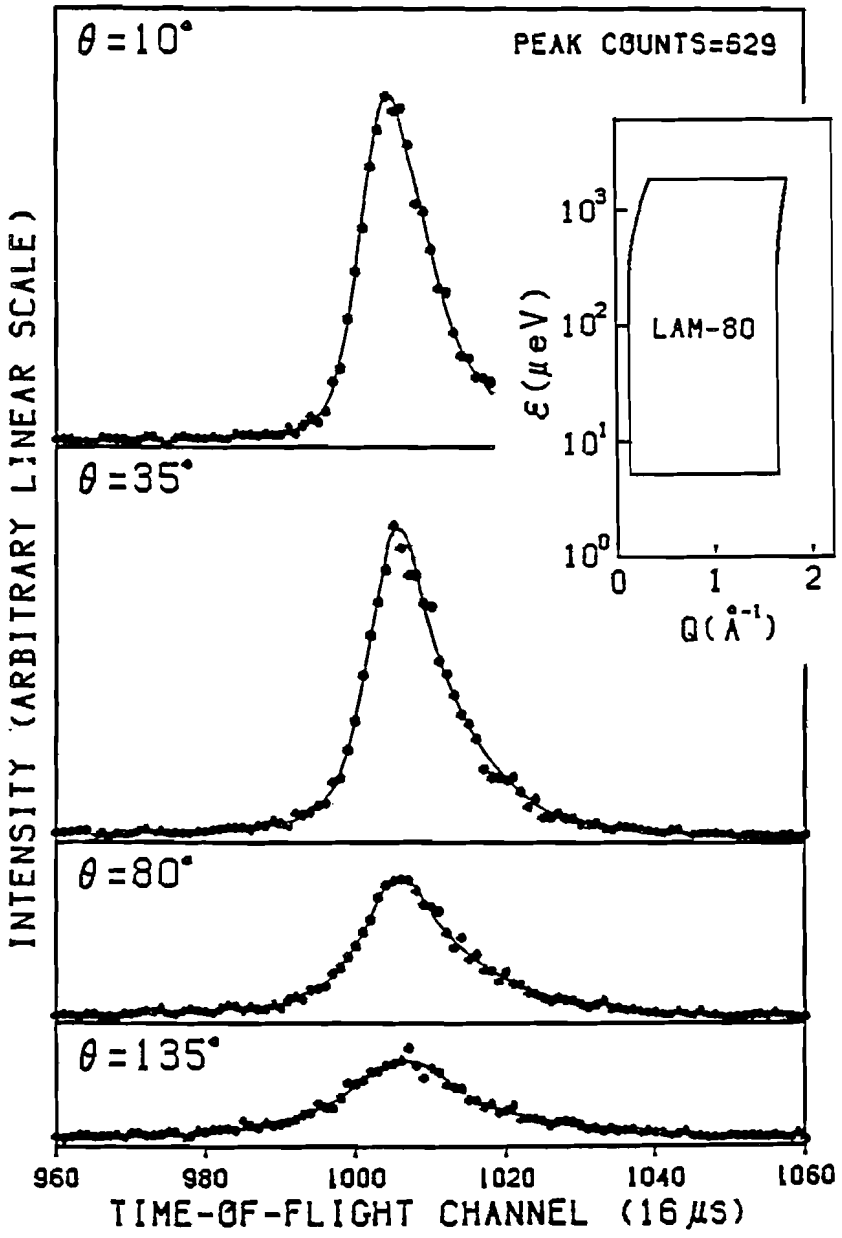

Fig. 5 Time-of-flight spectra from poly(butadiene) at a temperature below melting point, measured by the LAM-80.

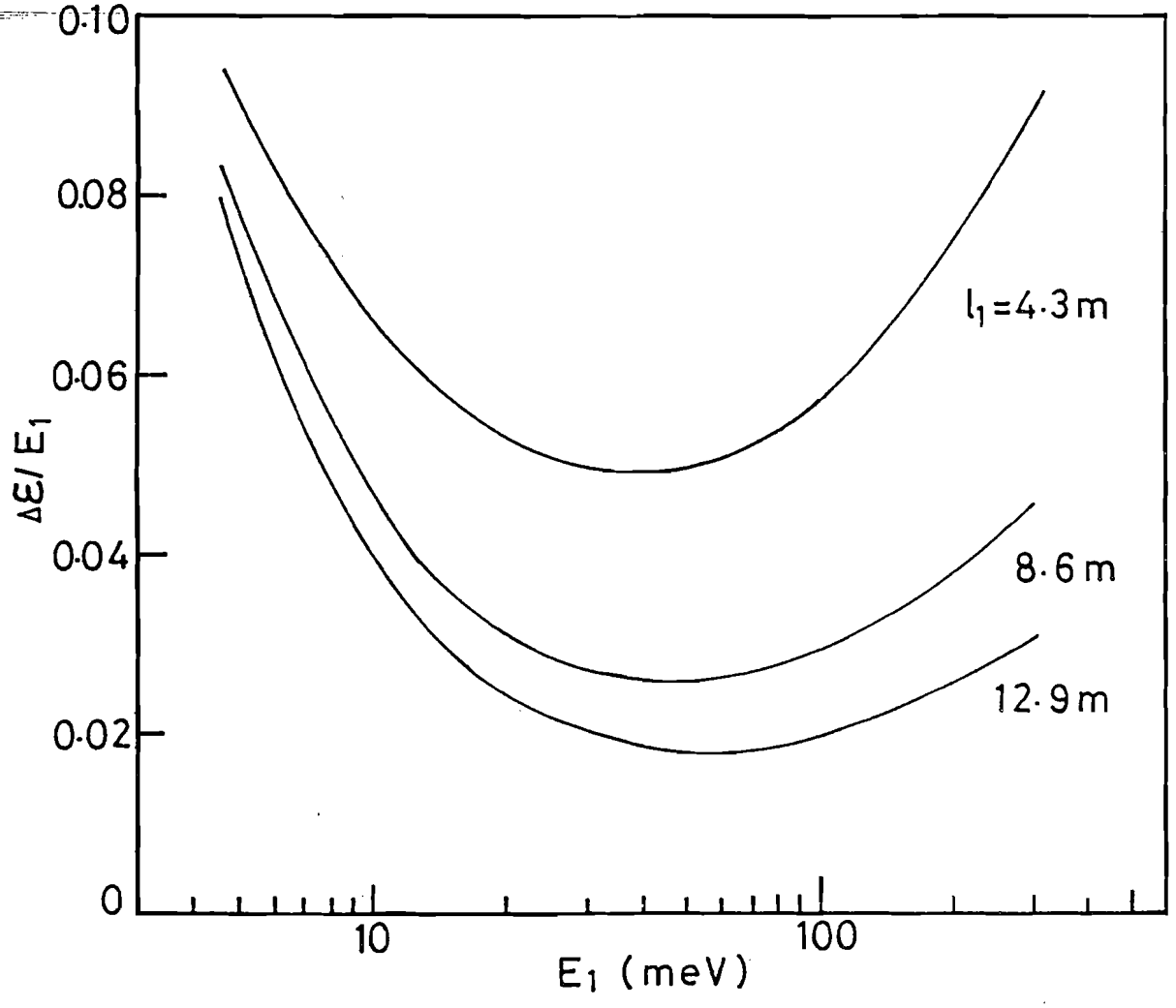

Fig. 6 Overall energy resolution devided by the incident neutron energy, E_1, as a function of E_1 for three cases of incident flight path length in the time-of-flight measurement using the pulsed thermal source.

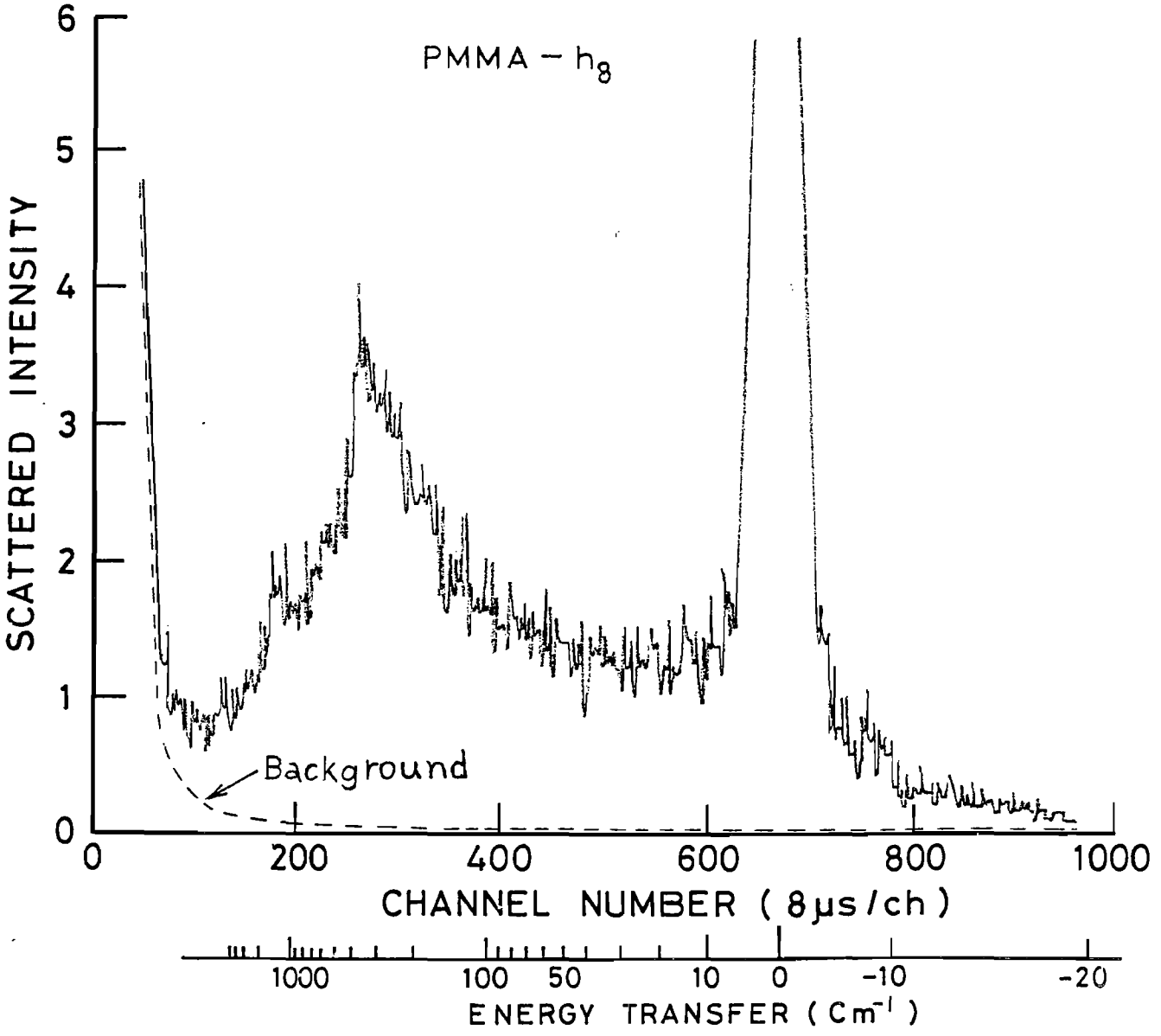

Fig. 7 Time-of-flight spectra from poly(methyl methacrylate) measured by the LAM-D.

Proceedings of the Eighth Meeting of the International Collaboration on Advanced Neutron Sources (ICANS-VIII)
8-12 July 1985, Rutherford Appleton Laboratory Report RAL-85-110

DEVELOPMENTS IN LIQUID DIFFRACTION ON THE SNS

W S Howells
Neutron Division
Rutherford Appleton Laboratory

1. Results from LAD on SNS

First results have just been obtained on the Liquids and Amorphous Diffractometer (LAD) on the SNS. The instrument was constructed several years ago and spent 2 years operating on the Harwell Linac before returning to RAL for installation on the SNS. A brief run was carried out in December 1984 and commissioning of the instrument started in July 1985. The instrument views the 90K liquid methane moderator and the incident spectrum as measured by the scintillator monitor is shown in figure 1 (not corrected for monitor efficiency). Small discontinuities due to the Bragg edges from the aluminium windows are just visible. Calibration will be carried out using a standard nickel powder and resonance foils. The raw nickel powder pattern for the 150° backward angle bank is shown in figure 2. The resolution has been calculated to be ~ 0.5% (standard deviation). The pattern for the lower angles (90° down to 5°) are shown in figure 3. Resolution in the short time region (around 1 eV) is better than on the Harwell Linac and this is most obvious in the low angles where the main peaks are at short times. The fast neutron background from the power pulse decays away by about 100 μs, so there are encouraging signs that energies up to 50 eV may be usable.

2. New Design for SANDALS

The original design for the SANDALS instrument was presented at the ICANS-IV meeting[1]. Since then experience gained on existing pulsed sources has shown that the use of short wavelengths and low scattering angles can dramatically reduce the need for corrections for inelastic scattering. Although large scattering angle (150°) detector banks provide high count rates, interpretation of the data is often difficult. Results on silica using reactor and pulsed source instruments show that the corrections are unreliable above about 90°; for samples containing elements of lower mass the upper limit in angle

could be as low as 20°. The solution is therefore to concentrate the detectors into forward scattering to reduce the inelastic correction and extend the Q range at a particular angle by using higher energy neutrons (up to 100 eV, say).

The instrument is designed for the Q range from 0.05Å^{-1} to at least 50Å^{-1}. The upper limit ensures adequate resolution in real space when Fourier Transforming the data. Maximum scattering angle is to be 50° and Q-resolution at around 30° scattering angle should be $\leq$ 1%. The sample position will be at 14m from a cold methane moderator and maximum sample size of the order 20 mm diameter. The detectors will be of Li^6 glass scintillator - a 5 mm thick scintillator has an efficiency of 30% at 10 eV and 10% at 100 eV. A schematic layout of the instrument is shown in figure 4.

3. Resolution Corrections

The effects of instrument resolution are not often considered in liquid structure calculations whether on reactor or pulsed source instruments. Problems analysing recent data taken on the Harwell Linac instruments, TSS and LAD, prompted a study of the resolution on pulsed souce diffractometers. The resolution function can be considered as the convolution of a Gaussian representing the geometrical effects and a decaying exponential to describe the source emission time distribution within the pulse. The shape of the Bragg peaks are then asymmetric and its centry of gravity is shifted from the nominal position. The effect this has on liquid structure has been investigated by calculating a hard sphere S(Q) and folding it with the resolution function to give an 'experimental' curve. The result shown in figure 5 shows that the main peak is shifted and reduced in height. In real experimental data this shows up as a decrease in peak height as the scattering angle decreases. One method of correcting for resolution uses the moments method and in a recent paper[2] it has been shown that the technique is successful.

References

1. W S Howells, Proceedings of ICANS-IV, Kens Report, II, 1981
2. W S Howells, Nucl Inst & Methods, A235, 553, (1985)

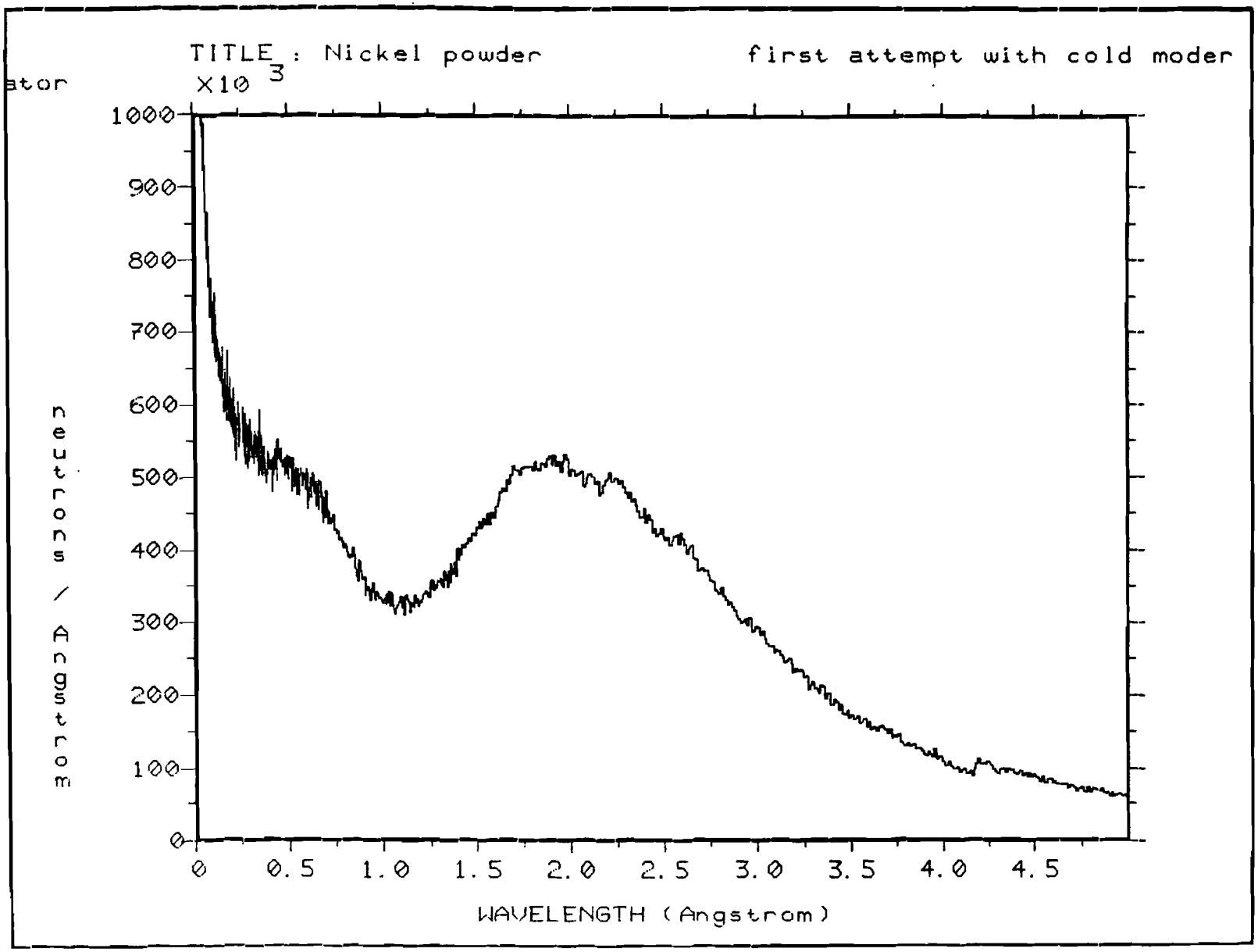
TITLE : Nickel powder
first attempt with cold moder
ator
X10 3
1000
900
800
700
600
500
400
300
200
100
0
0
0.5
1.0
1.5
2.0
2.5
3.0
3.5
4.0
4.5
WAVELENGTH (Angstrom)

FIGURE 1

INSTRUMENT: LAD
RUN NUMBER: 57
SPECTRUM : 1
LOCATION: DQA0: [LADMGR.DATA]LAD00057.RAW

USER: WSH
RUN START TIME: 2-JUL-1985 08:09:00
PLOT DATE: FRI 5-JUL-1985 14:52:39
NO GROUPING OF BINS

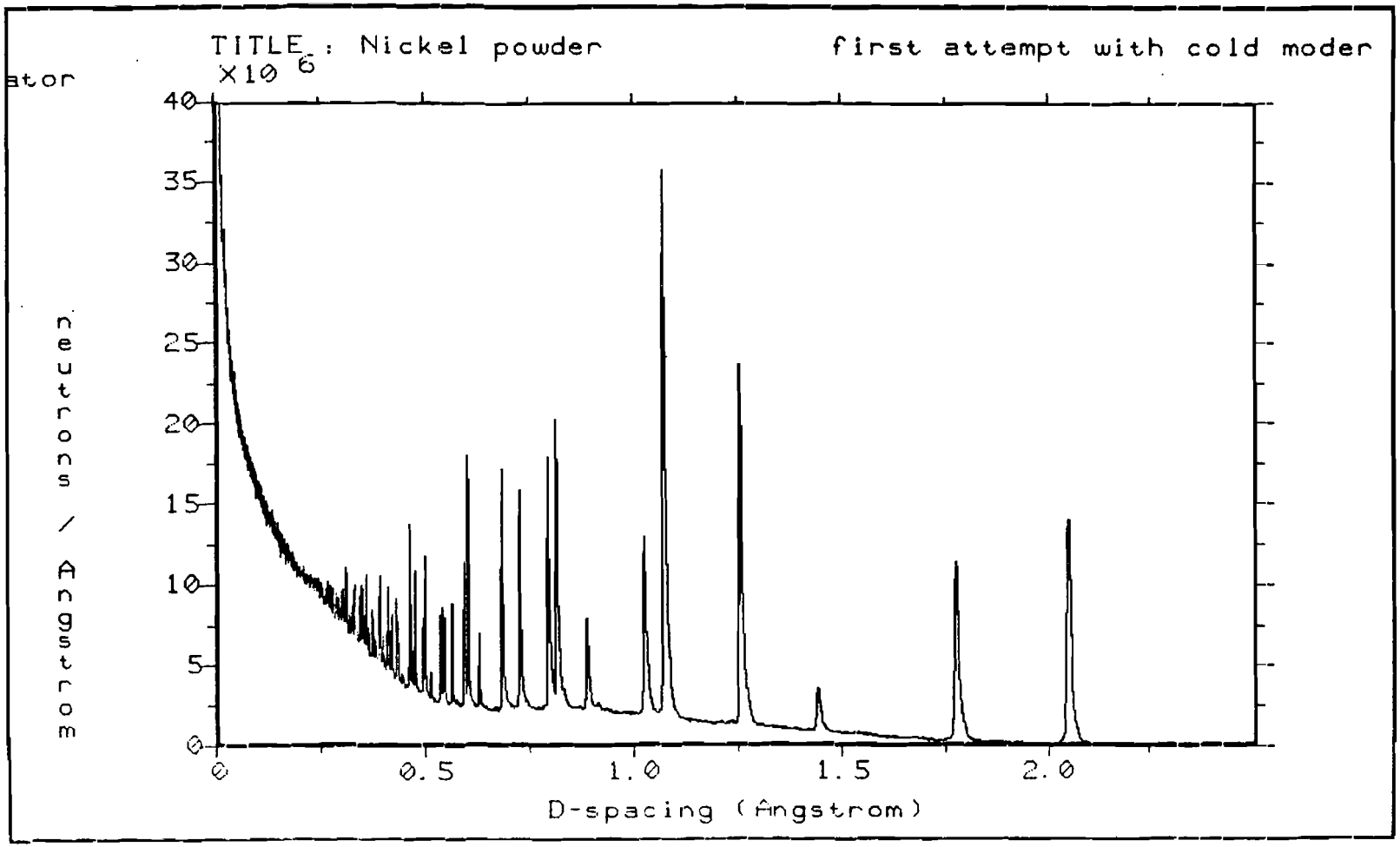

FIGURE 2

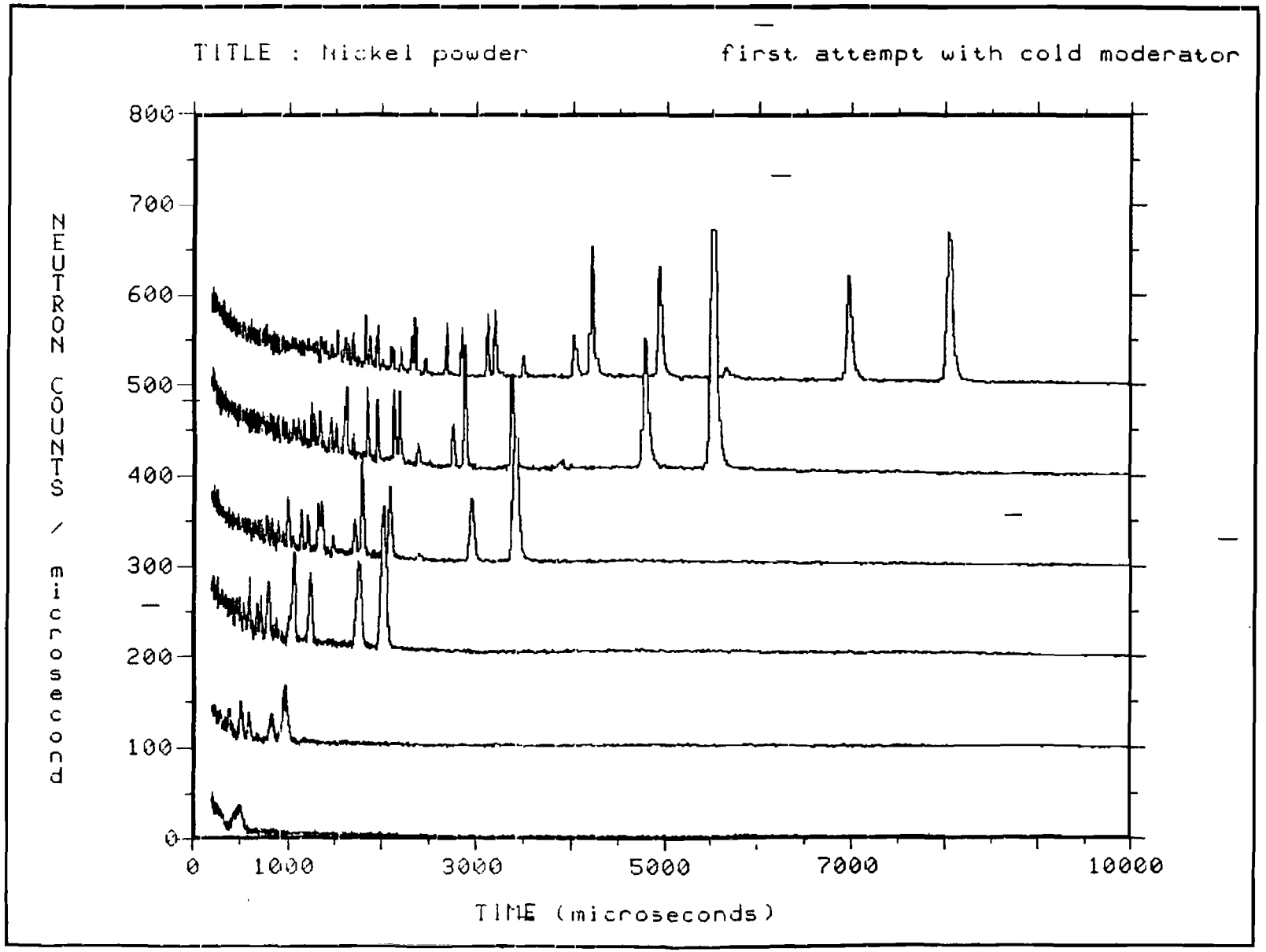
TITLE : Nickel powder
first attempt with cold moderator
NEUTRON COUNTS / microsecond
800
700
600
500
400
300
200
100
0
0
1000
3000
5000
7000
10000
TIME (microseconds)

FIGURE 3

SCHEMATIC LAYOUT OF SANDALS

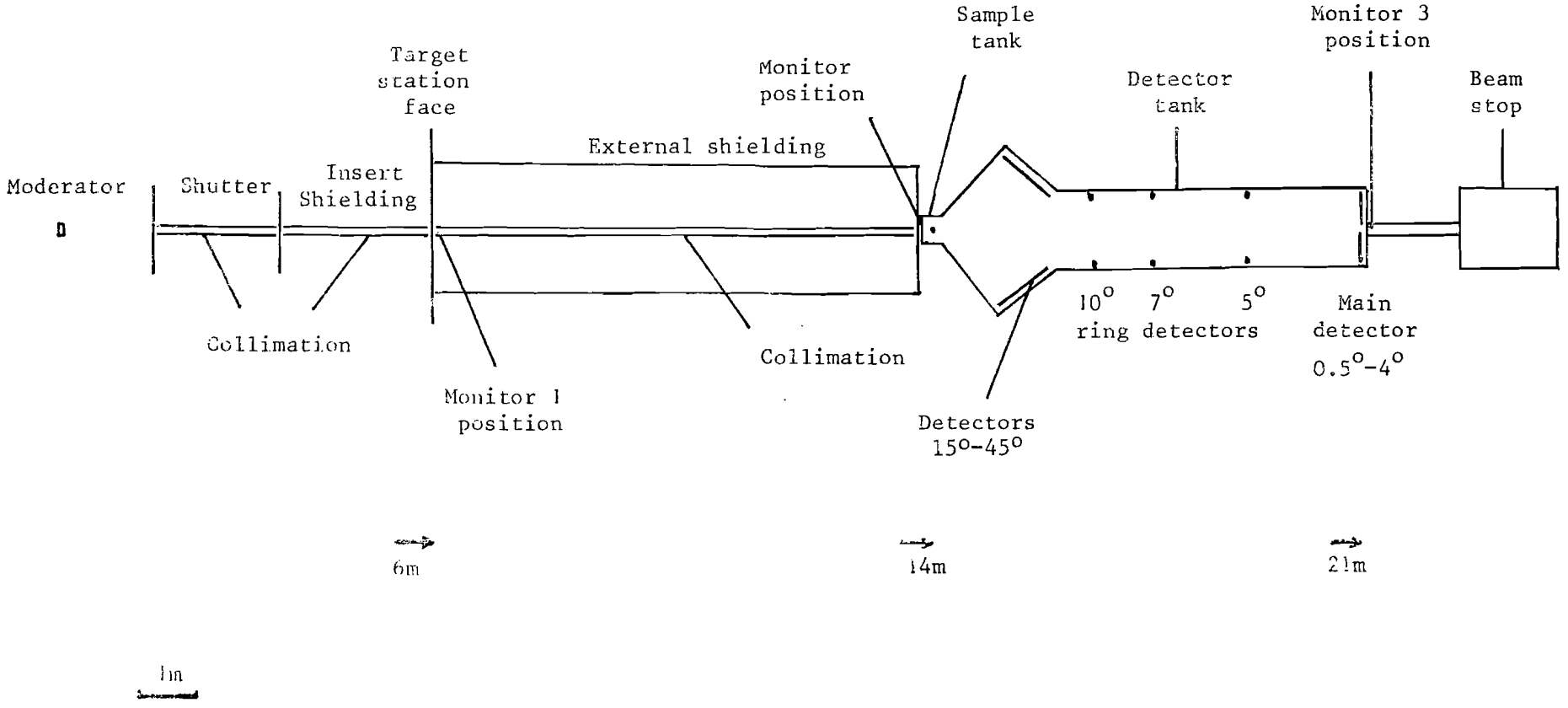

FIGURE 4

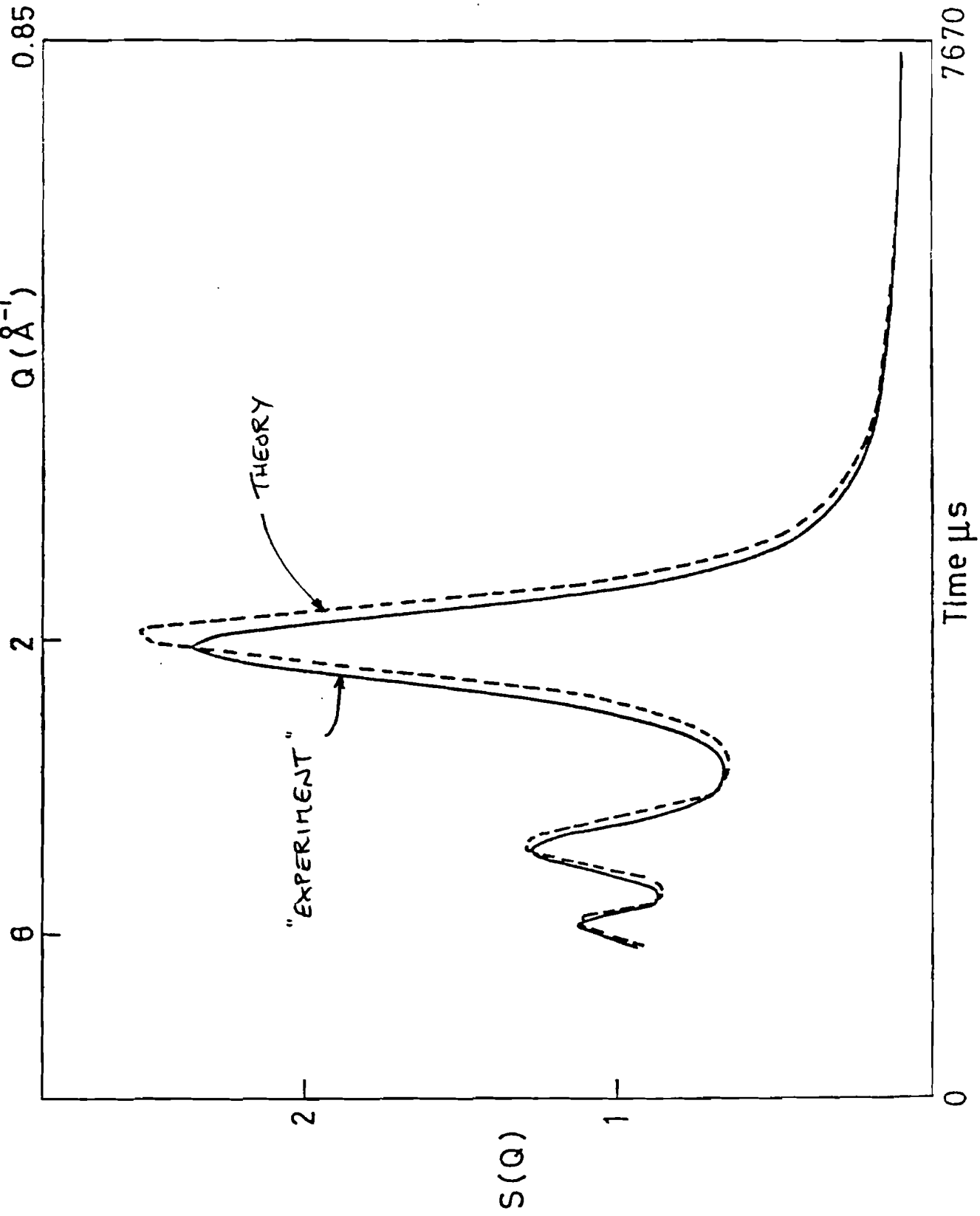

FIGURE 5

Proceedings of the Eighth Meeting of the International Collaboration on Advanced Neutron Sources (ICANS-VIII)
8-12 July 1985, Rutherford Appleton Laboratory Report RAL-85-110

DIFFRACTION STUDIES OF LIQUID AND AMORPHOUS MATERIALS AT SPALLATION NEUTRON SOURCES

M Davidovic and Dj Jovic
"Boris Kidric" Institute of Nuclear Sciences
Vinca, 11001 Belgrade, Yugoslavia

W S Howells
Neutron Division, Rutherford Appleton Laboratory
Chilton, Didcot, Oxon, OX11 0QX, UK

J Rhyne
National Bureau of Standards, Reactor Radiation Division
Gaithersburg, Maryland 20899, USA

ABSTRACT

The static properties of liquid and amorphous metals have been explored very extensively over the last thirty years. The studies have usually been performed by neutron scattering at steady state reactors and only recently at advanced spallation neutron sources. From such mesurements one determines the static structure factor S(Q) in a wide Q-region which then gives information on the structure of the metal, i.e. the spatial arrangement of atoms or magnetic moments. The structure factor S(Q) is now more easily determined at spallation neutron sources, where the effective flux of neutrons, particularly at higher energies, is much greater than that previously available at steady state reactors. The two limiting values of S(Q) for Q small and Q large are difficult to measure with good accuracy. In the case of liquid metals and small Q-values, the difficulty stems from the low cross-section. In the case of amorphous materials a lot of structure still remains at large Q-values between 20-30 $Å^{-1}$. For example in the metal-metaloid amorphous alloys it is necessary to measure the scattered intensity up to 25-30 $Å^{-1}$, which can easily be done at the neutron spallation sources such as the SNS, IPNS-1 etc.

1. INTRODUCTION

Before presenting some recent results on the structural investigations of liquid and amorphous materials, we shall outline some advantages of spallation sources (pulsed neutron techniques) over the steady state reactors (the continuous neutron source) [1-6]. First of all, the neutron flux that can be obtained at the pulsed source is biassed towards higher

energies, say 8 to 0.08 eV, i.e. 0.1 and 1Å [7]. This makes spallation sources preferable for the investigation of large energy and large Q transfer experiments. In the case of liquid metals this energy change is associated with the existence of collective excitations [8] and in the case of amorphous materials, short range order [9]. The major problems in the study of collective excitations in liquid metals are associated with the limited resolution of the spectrometers and with the need for different corrections which have to be applied to the experimental data. One additional limitation of such measurements is that the velocity of the incoming neutrons has to be of the order of twice the velocity of sound in liquid metals, corresponding to neutron wavelengths less than or equal to 1.1Å for liquid lead and 0.35Å for liquid aluminium. Such neutrons are best provided at sufficient intensity at the pulsed spallation sources. The epithermal neutrons from the spallation sources can be moderated to wavelengths similar to those in conventional reactors, but with fluxes of higher intensity. Proper utilisation of the pulse structure of the flux requires the use of time-of-flight techniques.

One further advantage of the pulsed technique in the study of the static properties of liquid metals at high temperatures is the possibility of performing the experiments at fixed scattering angle. This method eliminates many difficulties associated with shielding and screens around the sample.

2. STRUCTURE STUDIES

In the pulsed neutron technique a white pulsed beam impinges on the sample and the scattered neutrons are collected into a fixed angle θ_{Sc}, figure 1a, where their distribution is resolved by the time-of-flight technique. In the case of continuous neutron sources the scattered neutrons are counted at different angles θ_{Sc}, at fixed wavelength, figure 1b. The neutron time of flight t serves to identify neutron wavelength or wavevector Q as [10]

$$Q[\text{Å}^{-1}] = 31.75 * \frac{L[m]}{t[\mu sec]} * \sin\frac{\theta Sc}{2} \qquad (1)$$

L is the flight path between the moderator and the sample. To demonstrate the accuracy of the SNS diffractometer for liquid and amorphous materials [11] we show in figure 1c $\frac{dQ}{Q}$ vs θ_{Sc}. At relatively small scattering angles θ_{Sc}, the values of $\frac{dQ}{Q}$ takes high values of around a few percent. This means that the demand for measuring the structure factor S(Q) at small Q values with the accuracy round 1% cannot be easily realised at the spallation sources. In order to increase the resolution $\frac{dQ}{Q}$ at small values of the scattering angles θ_{Sc}, it is useful to insert a guide tube (rectangular shape, figure 2) between the neutron source and the furnace-sample as well as between the furnace and the detector. Divergency of such guide tubes is smaller than 90 minutes [12]. In general it is easier to use guide tubes and run experiments at fixed scattering angles on pulsed neutron sources than the corresponding experiment on continuous neutron sources.

As already mentioned, to determine the spatial arrangement of atoms in a sample it is necessary to measure precisely the structure factor in a wide Q-region. On the other hand, studies of short range order in amorphous materials require higher resolution than shown in figure 1c. This is achieved by placing, between the moderator and furnace, one or more guide tubes, and in that case the resolution $\frac{dQ}{Q}$ at figure 1c drops below 1% at 10-15°.

3. CORRELATIONS

It is found that for high density liquid metals, for example Al, Pb, Bi..., short wavelength density oscillations are overdamped especially near the position of the main peak in S(Q). Thus if one measured S(Q) up to 12-15 $Å^{-1}$ one will be able to determine the shape of the repulsive part of the interatomic potential X(r). In the case of amorphous materials density oscillations are less overdamped which means that one has to measure S(Q) in a much higher Q domain, even up to 20-30 $Å^{-1}$. In figure 3 we show the Fourier transform of S(Q), i.e. the pair correlation function g(r) for a liquid metal and the radial distribution function RDF(r) for amorphous alloys [13] :

$$g(r) = 1 + (2\pi^2 nr)^{-1} \int_0^\infty Q\,[S(Q)-1]\,\sin(Qr)dQ$$

$$RDF(r) = 4\pi.r^2.n.g(r) = \frac{2}{\pi} \int_0^\infty rQ\,[S(Q)-1]\,\sin(Qr)dQ \qquad (2)$$

where n is the number of atoms per unit volume. It is obvious from figure 3 that a difference is noticeable not only in the number of peaks but also in the height. Such differences in height are a consequence of the different stuctural order in the liquid and amorphous phase, there being obviously more structural ordering in the amorphous phase than in the liquid. From a previous study of amorphous alloys it is known that two kinds of short range ordering exist [13], topological and compositional (chemical). Structural ordering is caused by the existence of different structural defects, such as the vacancies corresponding to the free volume in liquids and amorphous metals [14-15]. The atomic structure of liquid and amorphous materials is shown schematically in figure 4. One should notice the redistribution of the first and second neighbours around the structural defect (V-vacancy) which is manifested by shifts in the RDF(r) [16] before and after annealing [13]. On annealing, the metastable phase of amorphous metals changes to a more stable phase. To follow this change one has to study the atomic mechanism of structure relaxation. From the RDF(r) analysis one only obtains averaged local one-dimensional information about the three-dimensional structures of the amorphous metals varied locally. By time-of-flight neutron diffraction the changes of RDF(r) caused by structural relaxation can be seen up to 20-30 Å, figure 3. Srolovitz et al [16] have shown that the so-called reduced radial distribution function G(r) expressed by

$$G(r) = \frac{RDF(r)}{r} - 4\pi nr$$

$$= \frac{2}{\pi}\int_0^\infty Q[S(Q)-1]\,\sin(Qr)dQ - 4\pi nr \qquad (3)$$

This is accompanied by the relation to the hydrostatic isothermal stress tensor p. For this case $G_p(r)$ can be related to the second moment of $\langle p^2 \rangle$ [16]

$$G_p(r) = G_o(r + \xi p)$$

$$\cong G_o(r) + \frac{\xi^2}{2}\frac{\partial^2 G_o(r)}{\partial r^2}\langle p^2\rangle + \ldots. \qquad (4)$$

where $G_o(r)$ is the RDF(r) from atoms with p=0 and ξ is constant beyond the first peak in G(r).

In order to probe the structure relaxation before and after thermal annealing one needs relations between the changes in the ΔRDF(r) and the second moment of hydrostatic internal stress distribution $\langle p^2 \rangle$ which can be written as

$$\Delta RDF(r) \sim -\frac{\xi^2}{2}\frac{\partial^2 G_o(r)}{\partial r^2}\left[\langle p^2\rangle_{annealed} - \langle p^2\rangle_{quenched}\right] \qquad (5)$$

Using a spallation source to provide thermal neutrons one can study precisely the change of ΔRDF(r), i.e. the parameter ξ, the proportionality coefficient $\frac{\partial^2 G_o(r)}{\partial r^2}$ and the distribution $\langle p^2 \rangle$. The last describes the fluctuation in the local density which is proportional to the gradient of interatomic potential $\psi(r)$. This study is now in progress.

In the case of liquid metals the relaxation phenomena can be studied by the full space and time correlation function G(r,t) which also of course can be measured at the SNS.

REFERENCES

1. G H Lander and J M Carpenter, *Neutron Scattering in the Nineties*, p17 (IAEA Vienna 1985)

2. A J Leadbetter, *Neutron Scattering in the Nineties*, p219 (IAEA Vienna 1985)

3. J M White and C G Windsor, Rept Prog Phys, 47, 707 (1984)

4. J M Carpenter, G H Lander and C G Windsor, Rev Sci Inst, 55, 101 (1984)

5. S W Lovesey and R Scherm, Condensed Matter Research Using Neutrons, Vol 112, (Plenum Publ Co London 1985)

6. J Rhyne, *Scientific Opportunities with Advanced Facilities for Neutron Scattering*, Shelter Island Workshop, New York October 1984 CONF-84 10256 (1985)

7. P Ageron, *Neutron Scattering in the Nineties*, p135 (IAEA Vienna 1985)

8. R Scherm, *Proceedings of the Workshop on the Neutron Scattering Instrumentation for SNQ*, Maria Laach 3-5 September 1984, eds R Scherm and H Stiller (1984)

9. P Chieux and H Ruppersberg, J de Physique LAM4, C8-145 (1980)

10. J M Carpenter, Nucl Inst and Meth, 145, 91 (1977)

11. *Neutron Scattering Instruments at the SNS*, Neutron Division, Rutherford Appleton Laboratory, Chilton, Didcot, Oxon, OX11 0QX, UK (February 1985)

12. J Konstantinovic, Private communication

13. M Davidovic, B Djordjevic, Dj Jovic and J Rhyne, *Proceedings of the Seminar on Scientific Cooperation between NBS and IBK in the 1980-1984 Period* 1 May 1985, Belgrade (1985)

14. M Davidovic, M Stojic and Dj Jovic, J of Non-Crystalline Solids, 61 and 62, 517 (1984)

15. N March, R A Street and M Tosi, *Amorphous Solids and the Liquid State*,Physics of Solids and Liquids, (Plenum Press 1985)

16. D Srolovitz, T Egami and V Vitek, Phys Rev, B24, 6936 (1981)

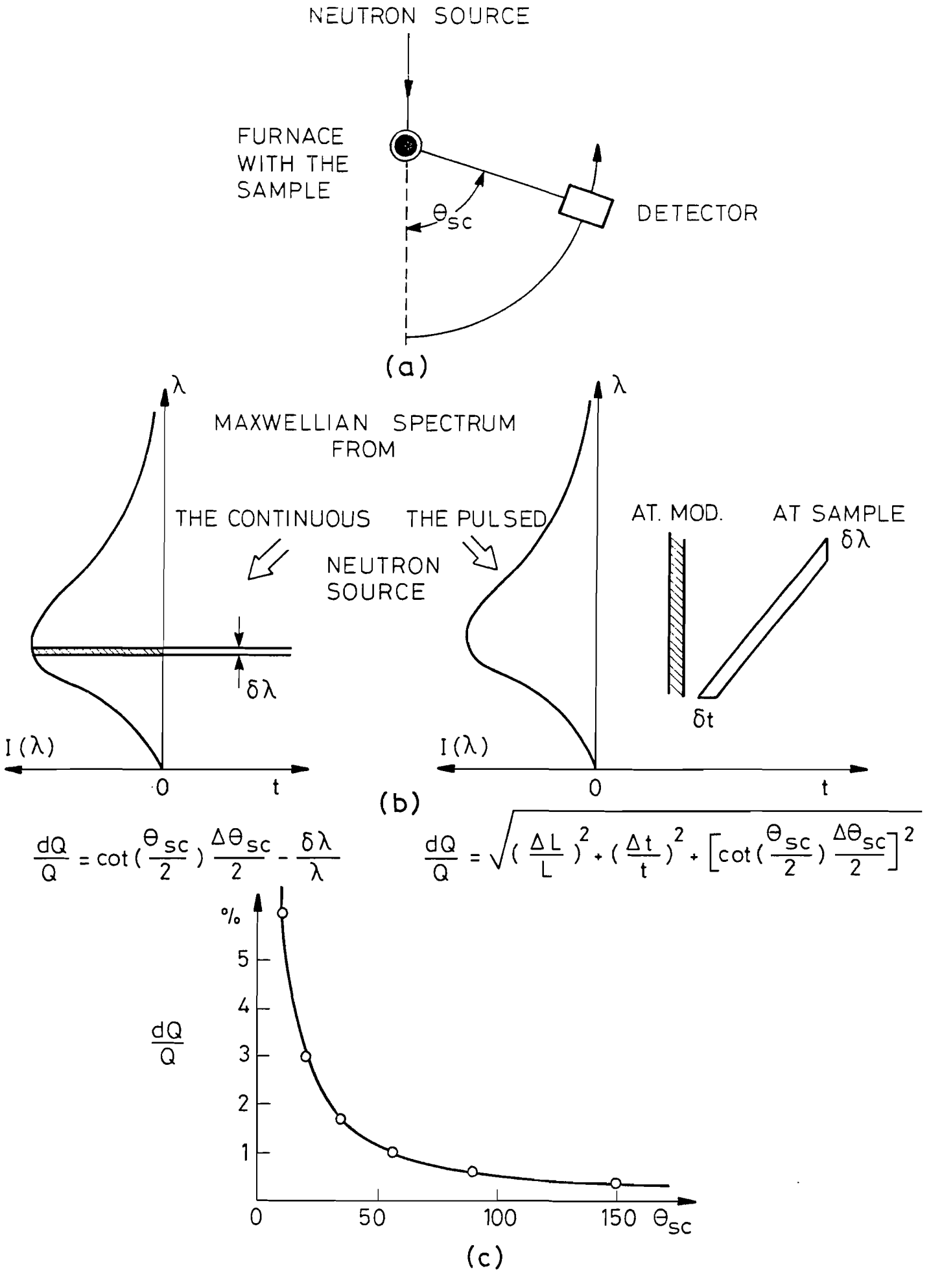
NEUTRON SOURCE
FURNACE WITH THE SAMPLE
θ_{sc}
DETECTOR
(a)
λ
MAXWELLIAN SPECTRUM FROM
THE CONTINUOUS NEUTRON SOURCE
THE PULSED
δλ
I(λ)
0
t
AT. MOD.
AT SAMPLE
δλ
δt
(b)
$\frac{dQ}{Q} = \cot\left(\frac{\theta_{sc}}{2}\right)\frac{\Delta\theta_{sc}}{2} - \frac{\delta\lambda}{\lambda}$
$\frac{dQ}{Q} = \sqrt{\left(\frac{\Delta L}{L}\right)^2 + \left(\frac{\Delta t}{t}\right)^2 + \left[\cot\left(\frac{\theta_{sc}}{2}\right)\frac{\Delta\theta_{sc}}{2}\right]^2}$
%
$\frac{dQ}{Q}$
5
4
3
2
1
0
50
100
150
θ_{sc}
(c)

Figure 1

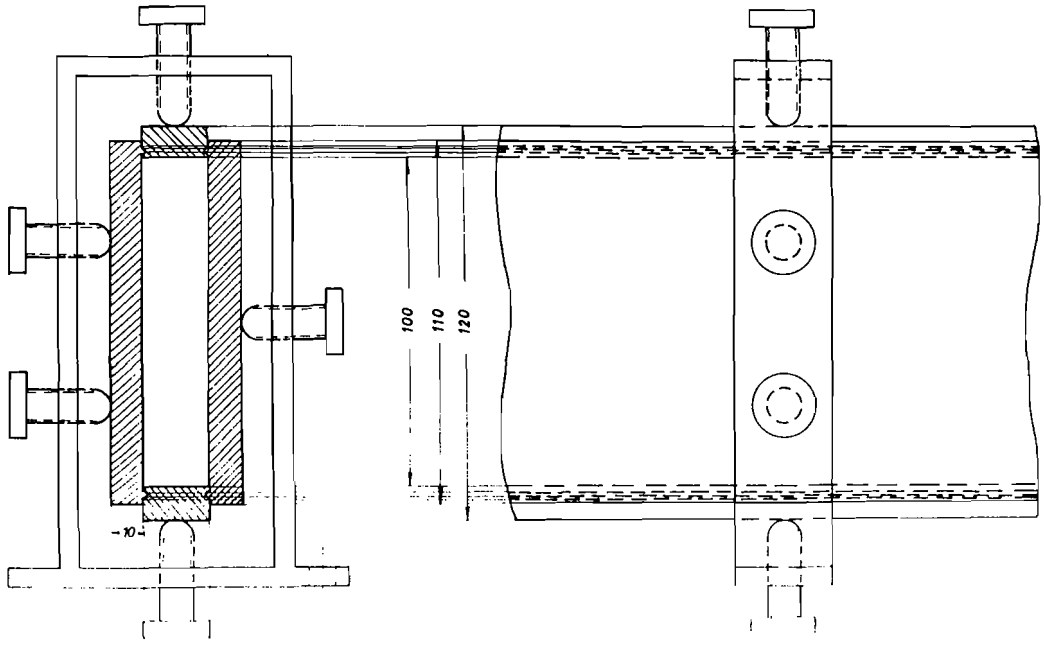

FIGURE 2

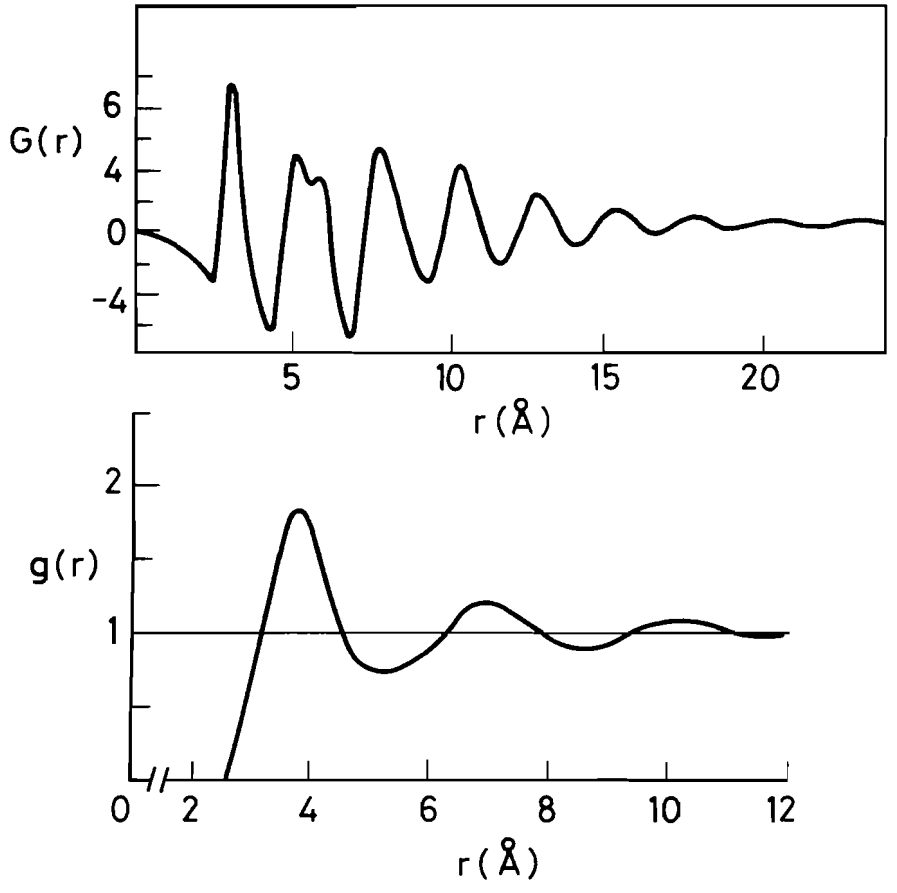

Figure 3

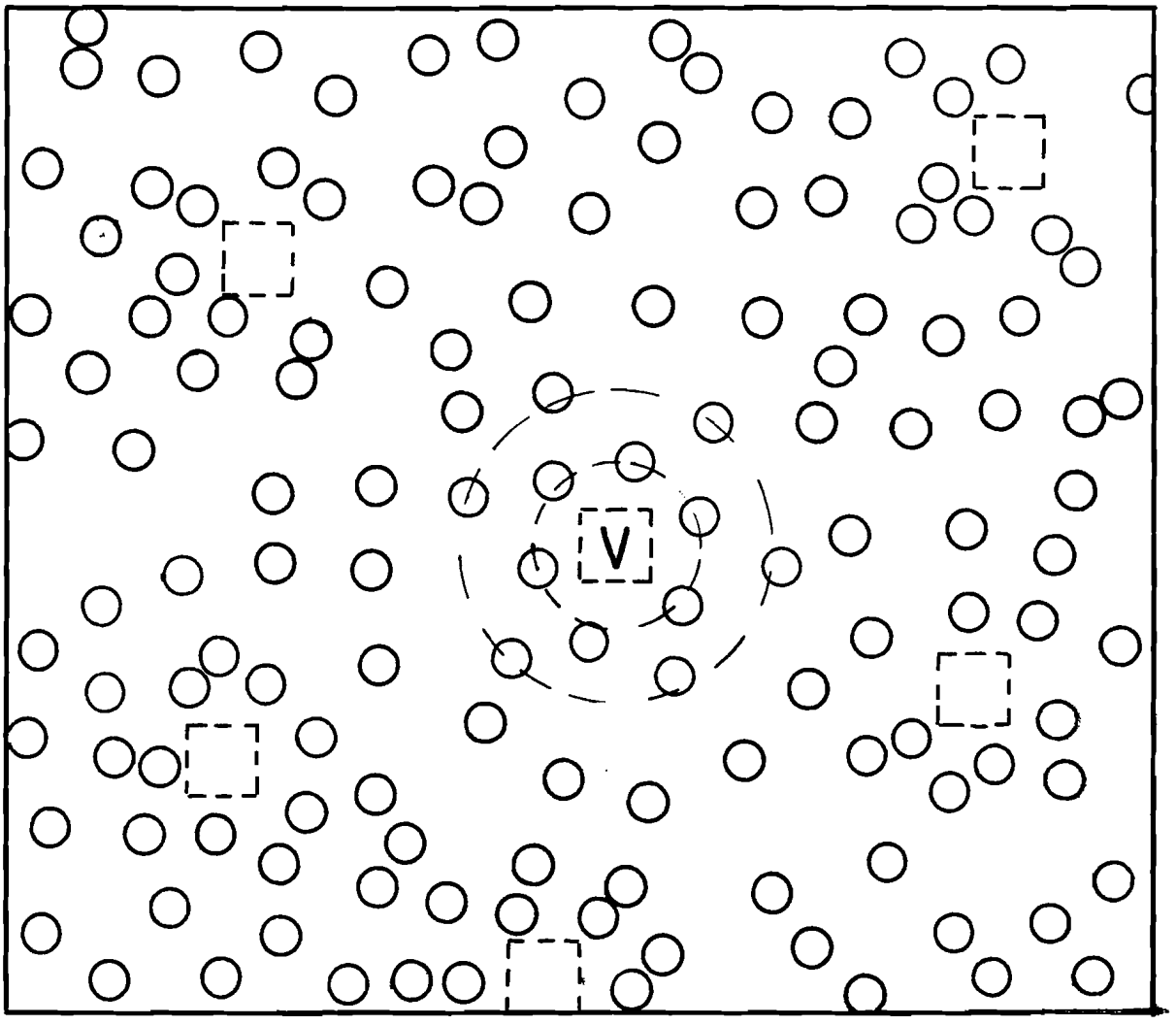

FIGURE 4

Proceedings of the Eighth Meeting of the International Collaboration on Advanced Neutron Sources (ICANS-VIII)
8-12 July 1985, Rutherford Appleton Laboratory Report RAL-85-110

FIRST RESULTS FROM THE HIGH RESOLUTION POWDER DIFFRACTOMETER HRPD AT THE SNS

W I F David and M W Johnson

Neutron Division
Rutherford Appleton Laboratory
Chilton, Didcot, Oxon, OX11 0QX, UK

INTRODUCTION

The High Resolution Powder Diffractometer (HRPD) at the SNS is the first of a new generation of high-flux neutron powder diffractometers to exploit resolutions of under 10^{-3}. The first results, after two weeks of commissioning, have been very promising and have confirmed the major aspects of the instrument. Data have been collected at high ($\Delta d/d \simeq 4 \times 10^{-4}$) and (comparatively) low ($\Delta d/d \simeq 10^{-3}$) resolution positions from samples of Ni, NiO and Si powders. Several new observations have been obtained, as a consequence of the uniquely high resolution of HRPD, from preliminary analysis of the six data sets.

In order to achieve ($\Delta d/d$) resolutions of the order of 4×10^{-4} the primary flight path of the diffractometer must be of the order of 100 m. At the SNS design pulse repetition frequency of 50 Hz this introduces problems of frame overlap that have been circumvented by using two beam choppers. However, in the initial commissioning period the lower repetition rates of between 50/16 Hz and 50/64 Hz have produced no severe frame overlap problems.

The primary flight path of HRPD has been enclosed within a curved nickel glass guide tube of cross-section 8 cm x 2.5 cm to attenuate the γ-rays and fast neutrons associated with the initial neutron burst. The curved section of the guide tube, which extends from 6 m to 60 m from the moderator, has a radius of curvature of 18 km. These parameters represent

the optimised configuration for a 50 Hz source in which no line of sight neutrons reach the sample yet the radius of curvature is sufficiently shallow to allow transmission of sub-angstrom neutrons. The 60 m - 96 m straight section of the guide is necessary to smooth out beam intensity inhomogeneities in the guide. Figure 1 shows the observed and calculated fluxes (curve A) at the sample extrapolated to full SNS intensity. No neutrons are transmitted with $\lambda \lesssim 0.5$ Å whilst for $\lambda \gtrsim 5$ Å the flux varies as $\sim \lambda^{-5}$. Curve B gives the expected flux at 100 m in the absence of a guide. It is evident from comparison of curves A and B that the use of a guide has produced a substantial increase in flux at the sample by allowing neutrons to be carried over the long flight path without the usual inverse square loss of intensity. Indeed at 1 Å and 2 Å the flux expected for HRPD are roughly equivalent to 30 m and 15 m machines respectively.

A schematic drawing of HRPD is given in Figure 2. Two sample positions are available, at 1 m and 2 m from the backscattering bank of detectors, with vertical access to both positions for sample environment instrumentation. The backscattering detector at present consists of two of a final eight octants that form a series of 20 concentric detector rings. This fibre-optic encoded position sensitive detector, constructed at the Rutherford Appleton Laboratory, detects neutrons by scintillation within a Li-doped cerium glass. The concentric geometry of detector matches that of the Debye-Scherror cones thereby eliminating geometrical contributions to the profile line shape. Further details are summarised in Table 1.

The resolution of HRPD results from a combination of different physical variables and a detailed discussion of the matching of different instrument parameters will be given elsewhere (1). A simplified account of the resolution contributions to $(\Delta d/d)$ begins with the assumption that all variables are independent and that

$$\left(\frac{\Delta d}{d}\right)^2 = \left(\frac{\Delta t}{t}\right)^2 + \left(\frac{\Delta \ell}{\ell}\right)^2 + (\Delta\Theta \cot\Theta)^2 + \left(\frac{d}{p}\right)^2$$

$(\Delta t/t)$ arises from the time distribution of the neutron pulse resulting from the moderator. Moderator optimisation studies (eg. (2)) has led to the decision to use a 10 x 10 cm 95 K poisoned methane moderator. Δt (μsec) is of the order of 8λ(Å) giving a resolution contribution $(\Delta t/t) \sim 0.03\%$ for a 98 m instrument. $\Delta \ell$ is the uncertainty in the flight path ℓ and results from finite sample (1.0 cm) and detector (0.5 cm)

widths. For ℓ = 98 m this is of the order of $(\Delta\ell/\ell) = 0.01\%$. The angular uncertainty $\Delta\Theta \cot\Theta$ resulting from sample and detector size is only small for $\Theta \geq 85°$ thus necessitating a high angle backscattering bank. At the 1 m position the angular resolution of the 10th detector ring is 0.06% while for the 2 m position $(\Delta\Theta \cot\Theta) \sim 0.015\%$. Thus neglecting particle size effects (d/p where d = d spacing of reflection and p = particle diameter)

$(\Delta d/d)^2 \sim 0.1\%$ 1 m position

$(\Delta d/d)^2 \sim 0.04\%$ 2 m position

There is thus a significant geometrical contribution to the 1 m but not the 2 m position. This gives the experimenter a choice between a higher resolution (2 m position) or higher intensity configuration (1 m position). The backscattered flux intercepted by the detector with the 1 m sample position is roughly 4 times that at 2 m.

INITIAL COMMISSIONING EXPERIMENTS

In the initial commissioning period (2nd - 28th July 1985) calibration experiments have been performed using 3 samples (Ni, NiO and Si) at both high and low resolution positions on HRPD. A selection of the results obtained so far are presented in the following sections:

Nickel

Figure 3 shows the Ni 111 reflection individually plotted for each of the 20 concentric rings of one detector octant. The differing times of arrival of the 111 reflection arise because of the differing 2θ values ($160° \leq 2\theta \leq 176°$) for the detector rings. Figure 3b highlights the expected exponentially-decaying trailing edge: Figure 3a, however, shows a pronounced leading edge unanticipated from instrumental considerations. Subsequent analysis at the higher resolution 2 m position (Figures 4a and b) revealed that the leading edge has a Lorentzian character. The convolution of exponential and Lorentzian functions gave a significantly improved fit over the conventional exponential/Gaussian convolution. The Lorentzian character may be attributed to particle-size effects: a straightforward calculation yields a domain size of 1710(70) Å.

Nickel Oxide

Antiferromagnetic NiO was chosen since, at room temperature, cubic rocksalt symmetry is lost and the structure appears to be rhombohedral. High resolution x-ray diffraction has established that the rhombohedral unit cell constants are a = 4.1758 Å, α = 90.058(2)°. To observe the resultant splitting of Bragg peaks requires a resolution of less than 0.001. The profiles presented in Figures 5 and 6 clearly indicate that this resolution has been achieved. The splittings of 75 μs and 82 μs in Figures 6a and b correspond respectively to unit cell angles of 90.0591° and 90.0588° that are in excellent agreement with the literature value.

Silicon

The silicon standard material (NBS Si640a : a = 5.430825(11) Å), Hubbard (1983)) has been used as a calibrant of the overall flight path of HRPD at the 1 m and 2 m positions. Surprisingly in common with the Ni diffraction patterns discussed above, the convolution of exponential and Lorentzian functions gives a fit that is significantly superior than the exponential/ Gaussian convolution (Figure 7) for all diffraction peaks. The linear variation with time (d-spacing) (Figure 8) of the full width at half maximum of the Lorentzian component of the fitted peak shape precludes particle-size effects suggesting rather that the Si standard sample suffers from Lorentzian strain broadening of the order of 10^{-4}. These results highlight the fact that the high instrumental resolution of HRPD will not only prove advantageous for structure refinement but, additionally, will yield further information about the strain and size distributions of crystallites.

INITIAL CONCLUSIONS

The initial commissioning experiments have proved extremely fruitful and have allowed the following aspects of the machine to be validated:

- Verification of poisoned moderator characteristics: 35 μs decay constant observed in peak shape.

- Satisfactory alignment of neutron guide: wavelength cutoff = 0.48 Å.

- No observable cross-talk and acceptable quiet counts (~ 1 count cm^{-2} min^{-1}) in encoded scintillator detectors.

- Observation of NiO rhombohedral splitting ($\Delta d/d$ full-width at half maximum of 4×10^{-4} measured).

- No observed splitting of NiO 200 reflection implying that NiO monoclinic splitting corresponds to a strain of less than 2×10^{-4}.

- Line broadening in Ni and Si diffraction patterns. (Exponential/Lorentzian convolution gives excellent least-squares fit of peak shapes).

ACKNOWLEDGEMENTS

The authors wish to acknowledge the help of numerous members of staff at the Rutherford Appleton Laboratory. Additionally, the authors wish to thank Dr A K Cheetham (University of Oxford) for suggesting NiO as a test material and providing the sample and M M Eddy (University of Oxford) for assistance with a number of the initial experiments.

REFERENCES

Hubbard, C. R., (1983) J. Appl. Cryst. 16 285-288.

TABLE 1 HRPD parameters

MODERATOR	10 x 10 cm CH_4 @ 95K.
PRIMARY FLIGHT-PATH	96 m evacuated curved neutron guide.
GUIDE PARAMETERS	width 2.5 cm height 8.0 cm length of sections = 1 m 4 m - 6.5 m straight 6.5 m - 60 m curved: r = 18 km 60 m - 100 m straight λ^* = 0.98 Å
DISC CHOPPERS	At 6 m and 9 m. 3 apertures corresponding to 1, 2 or 5 frame apertures.
DETECTOR TANK	Evacuated (10^{-1} torr normal, 10^{-6} available) light shielding. 2 sample positions at 1 m and 2 m from back-scattering detector.
DETECTOR (eight octants)	1. Back-scattering: 160 elements, 20 rings. r_{min} = 3 cm r_{max} = 37 cm

	1 m	2 m
Ω	0.37	0.1
$2\theta_{min}$	160°	170°
$2\theta_{max}$	176°	178°

MONITORS	2 monitors at - 250 cm and 105 cm from 2 m position.
TIME SORTING	$n_t \leq$ 64K channel time boundaries software set.

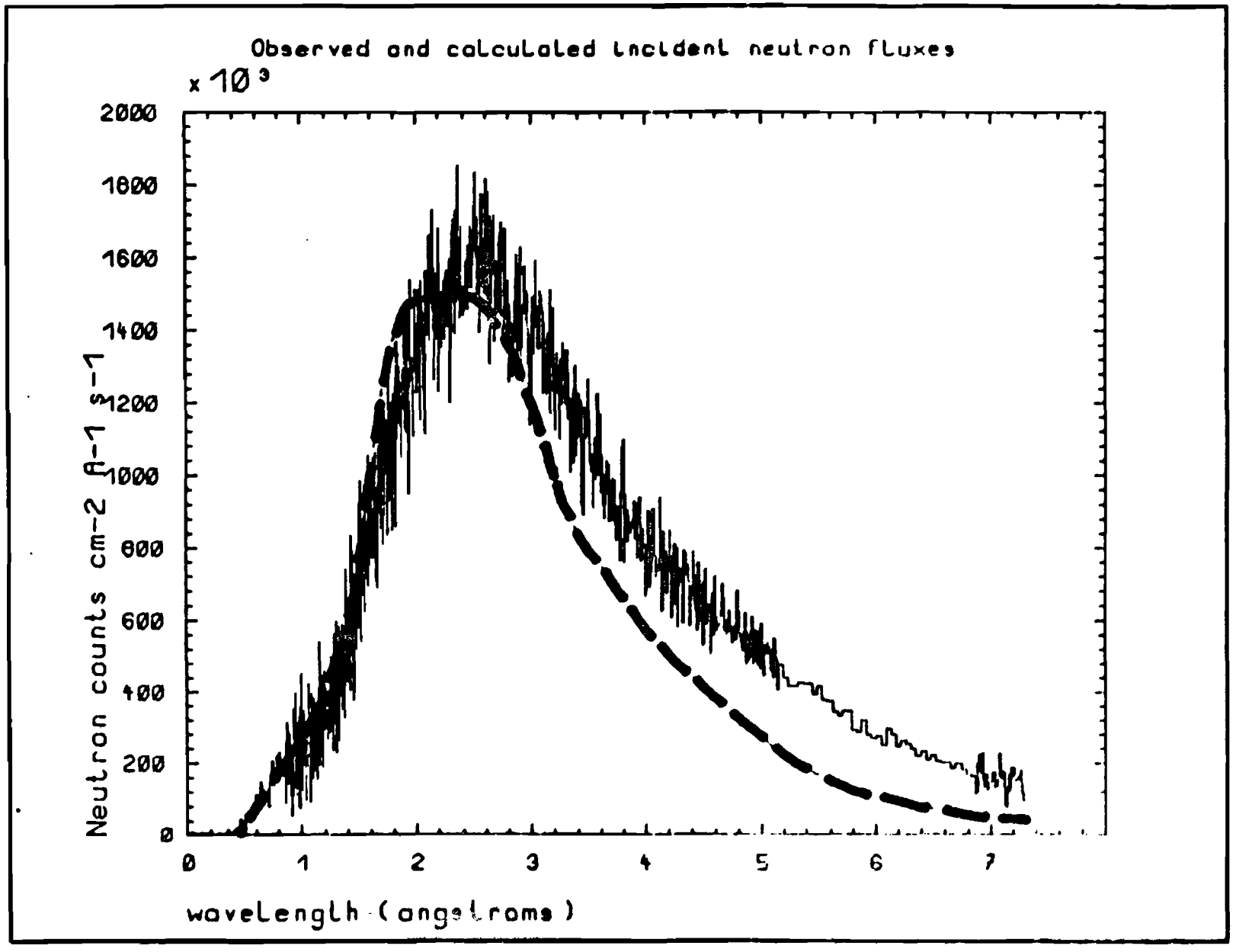

Figure 1: Observed and calculated neutron fluxes (extrapolated to full SNS intensity) for HRPD. Note the absence of epithermal neutrons below $\lambda = 0.5$Å.

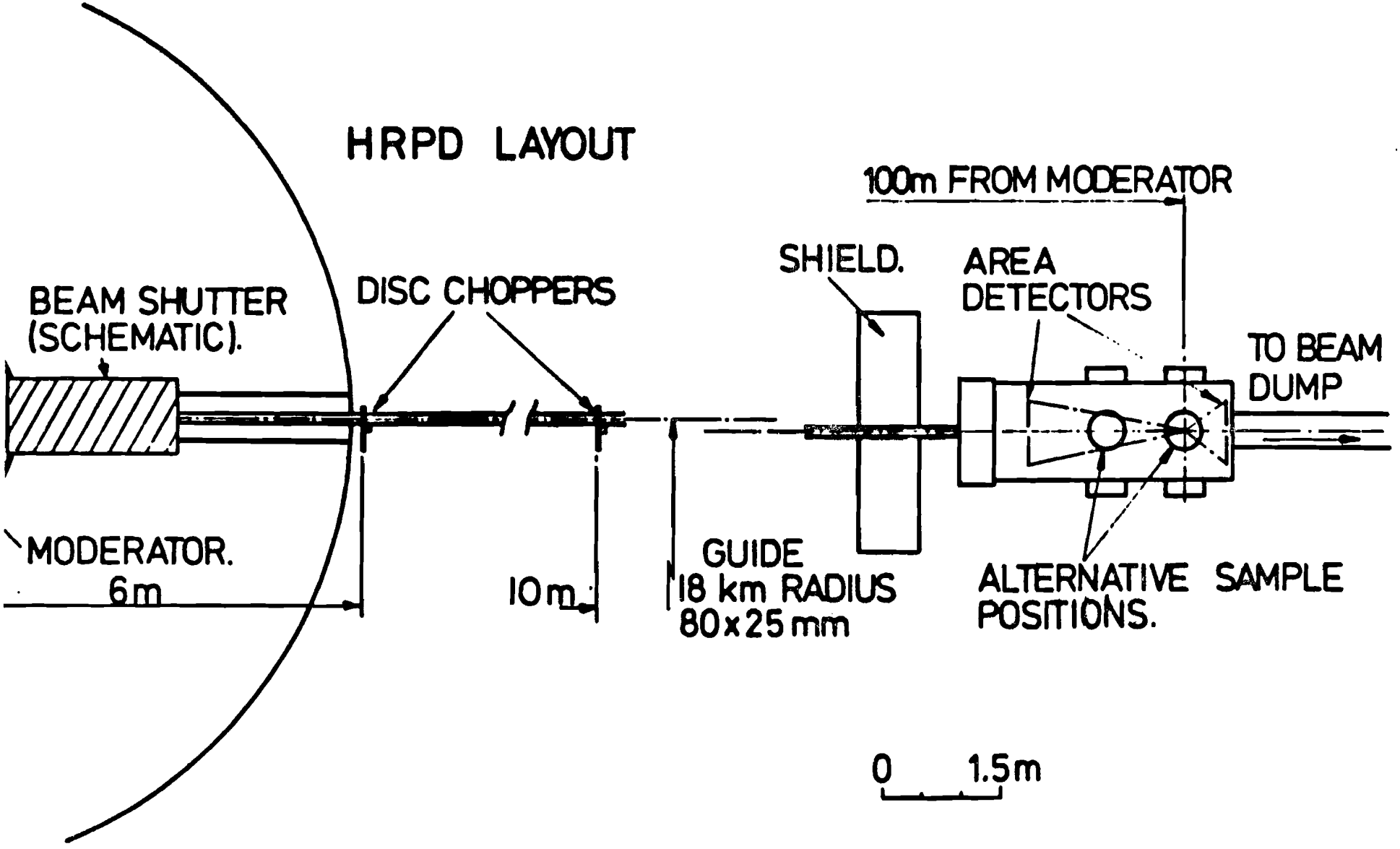

Figure 2: HRPD instrument configuration.

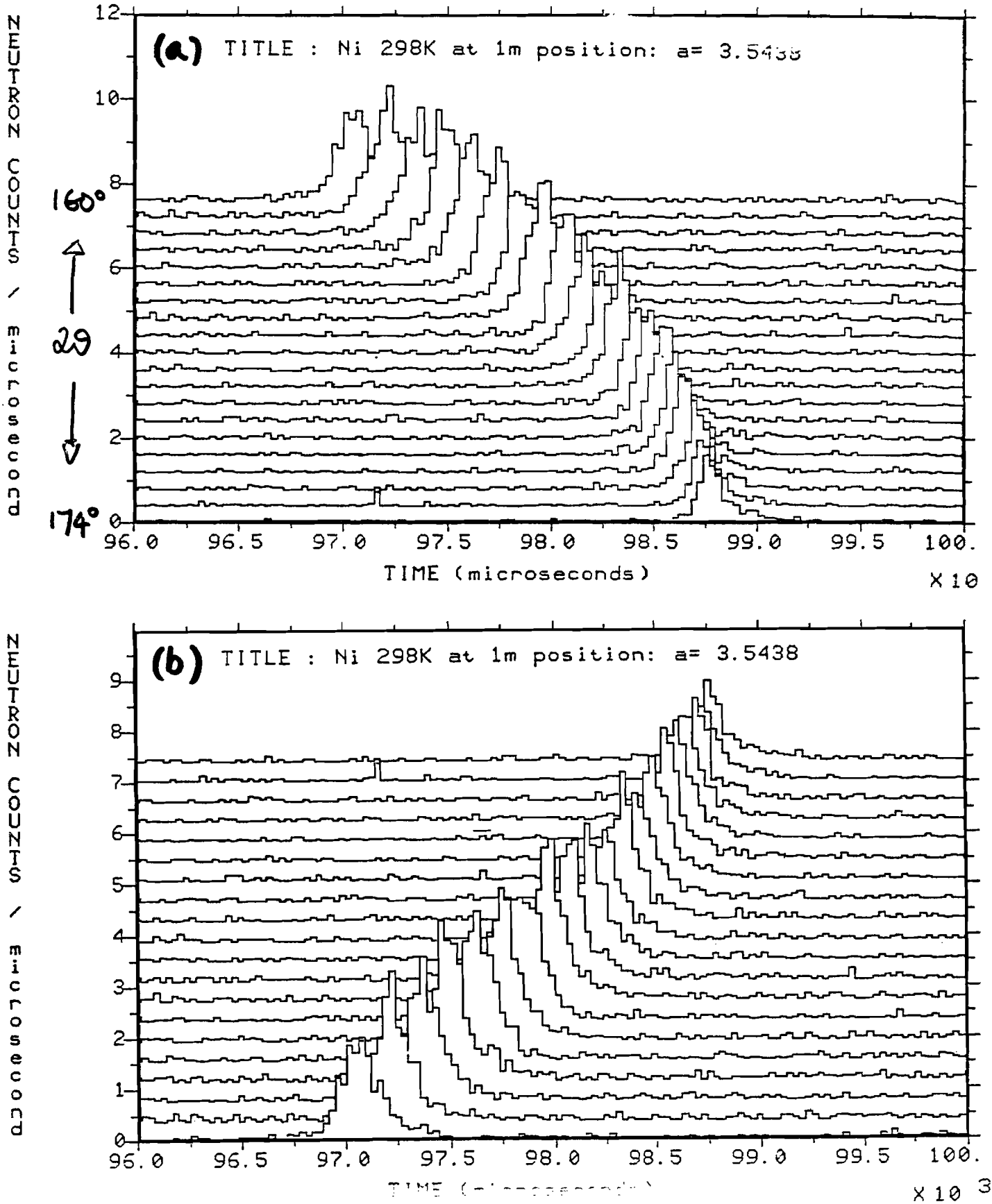

Figure 3: Multispectral plot of the Ni 111 reflection for one detector octant showing (a) the Lorentzian leading edge and (b) the exponential trailing edge. Crosstalk between detector rings is not observed.

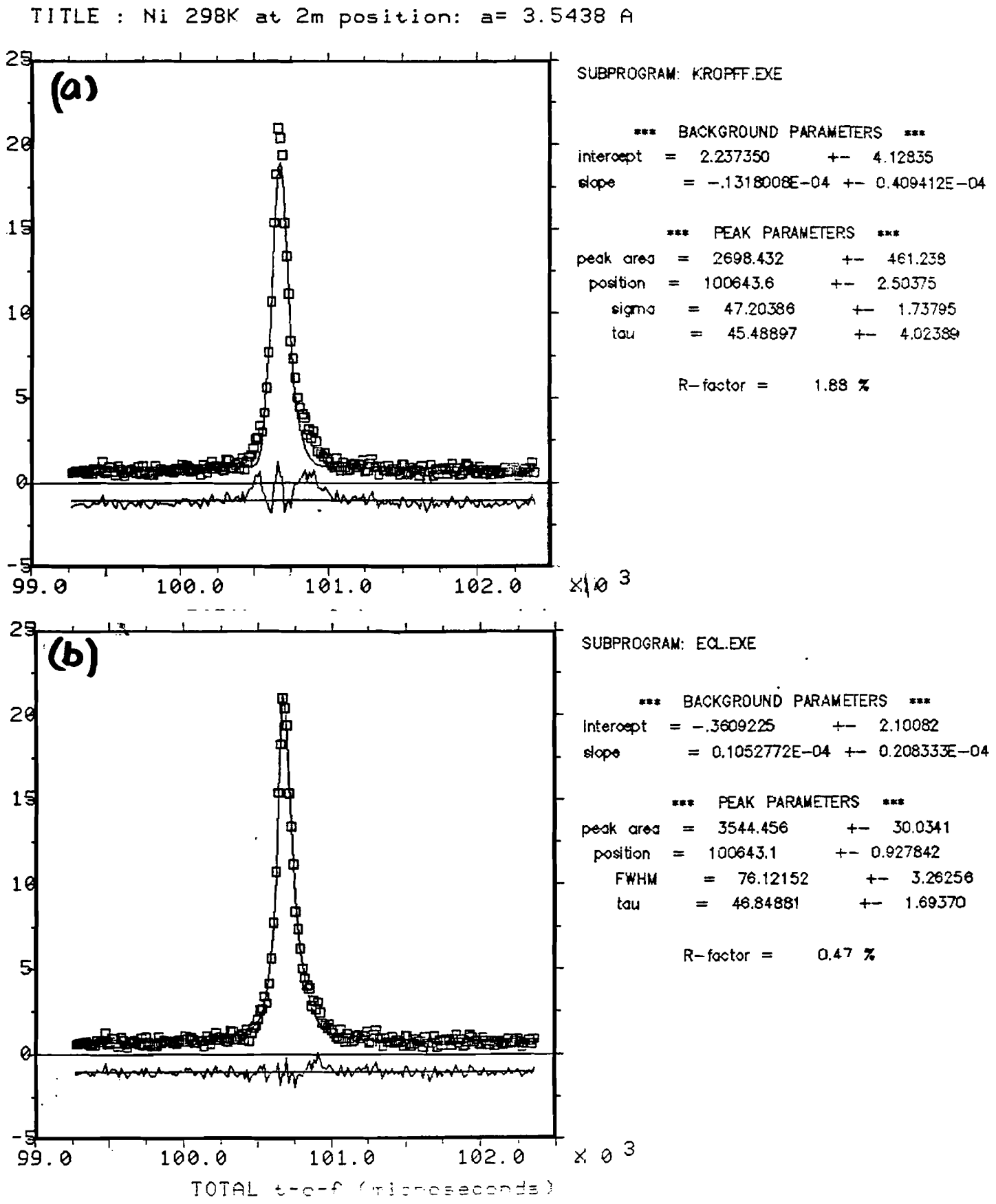

Figure 4: (a) Exponential/Gaussian and (b) Exponential/Lorentzian convolution fits of the 111 Ni diffraction peak. The significantly superior fit of the latter peak shape may be attributed to particle size effects (average = 1710(70) Å).

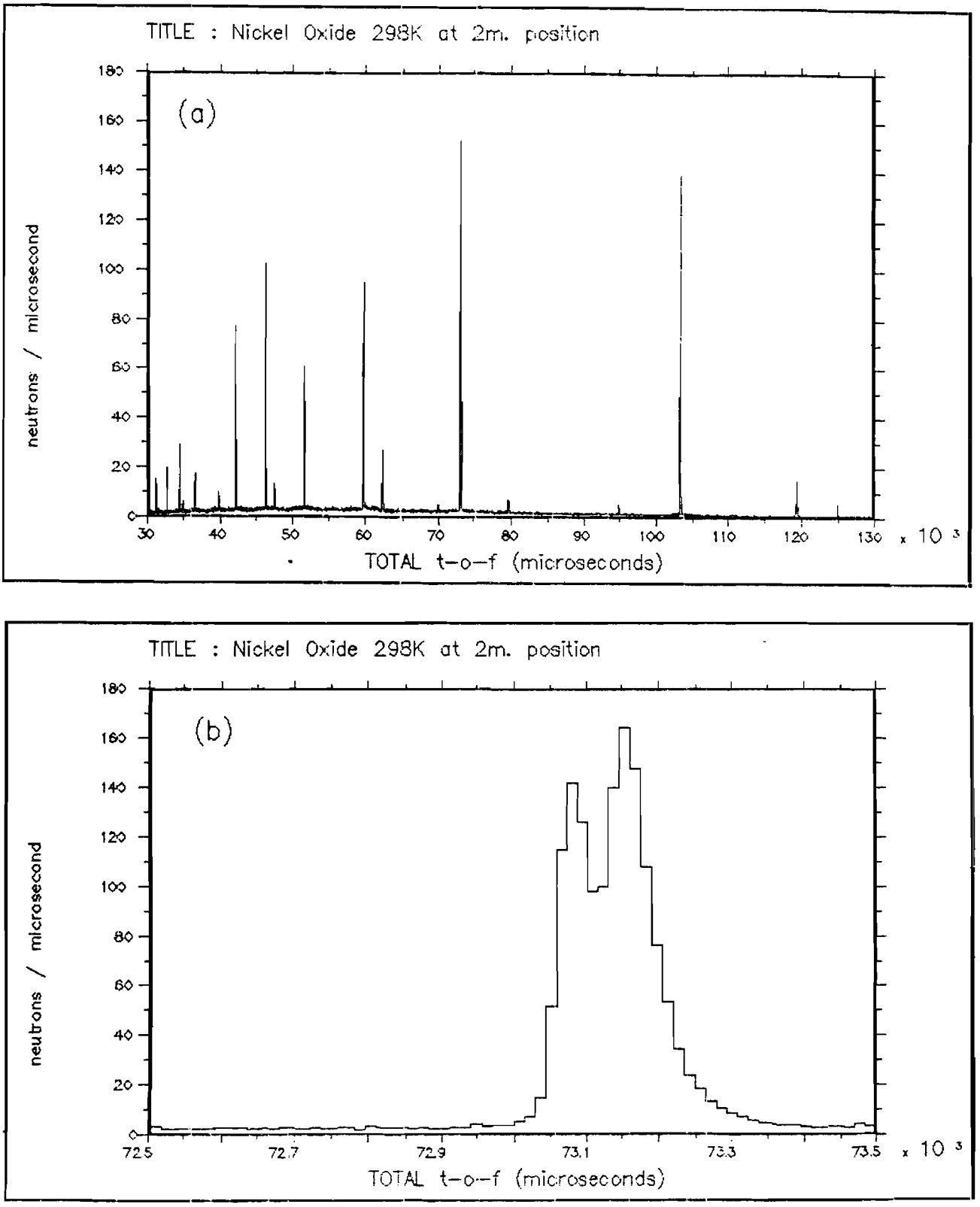

Figure 5: NiO diffraction pattern. (a) The large time range (30000 μs ≤ t ≤ 130000 μs) clearly illustrates the good signal-to-noise levels and high resolution of HRPD. (b) The expanded region between 72500 μs and 73500 μs highlights the ultra-high resolution of HRPD. (The time bin-widths are given by the equation $\Delta t = 0.0002\ t$).

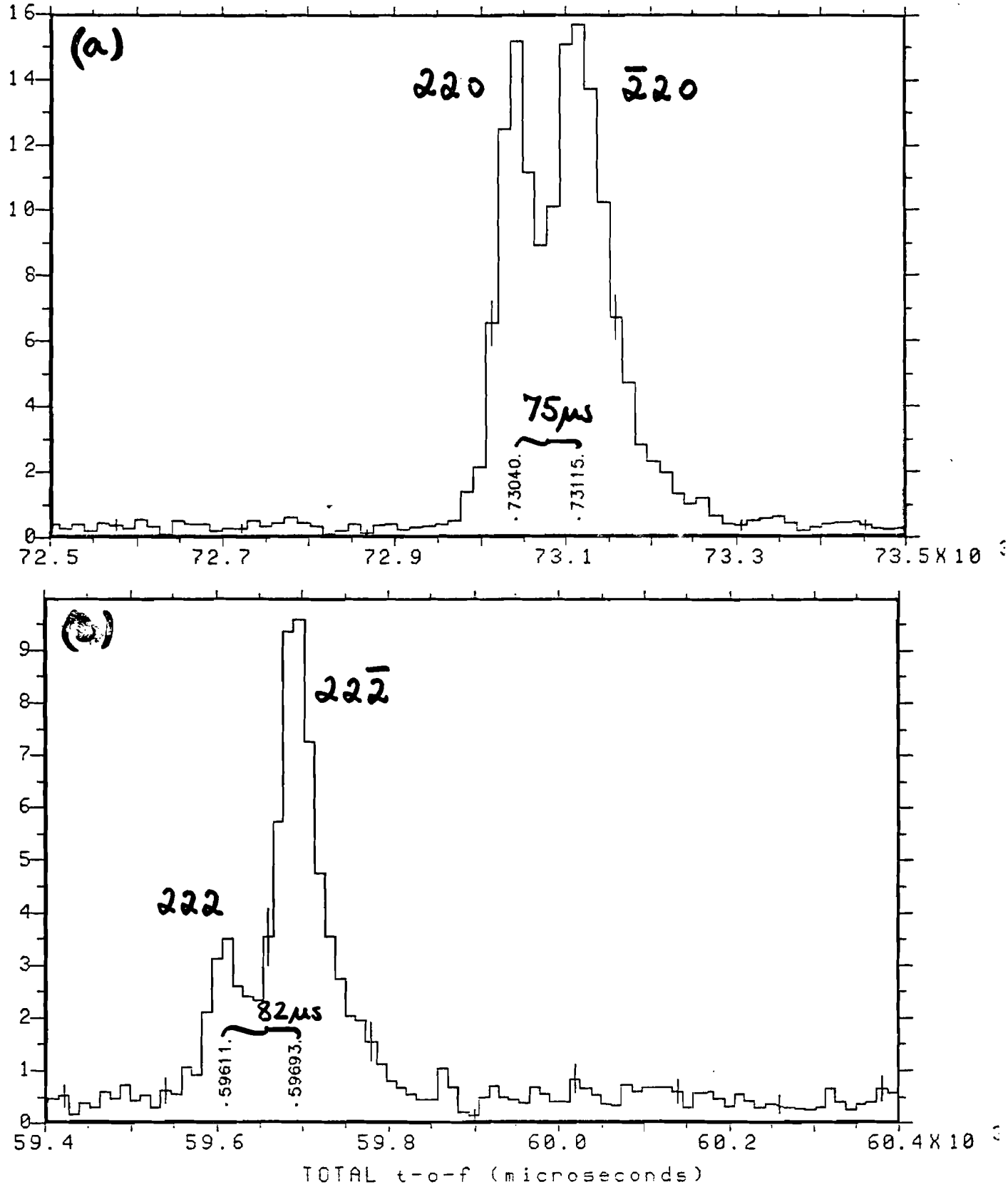

Figure 6: NiO diffraction patterns of (a) 220 splitting and (b) 222 splitting.

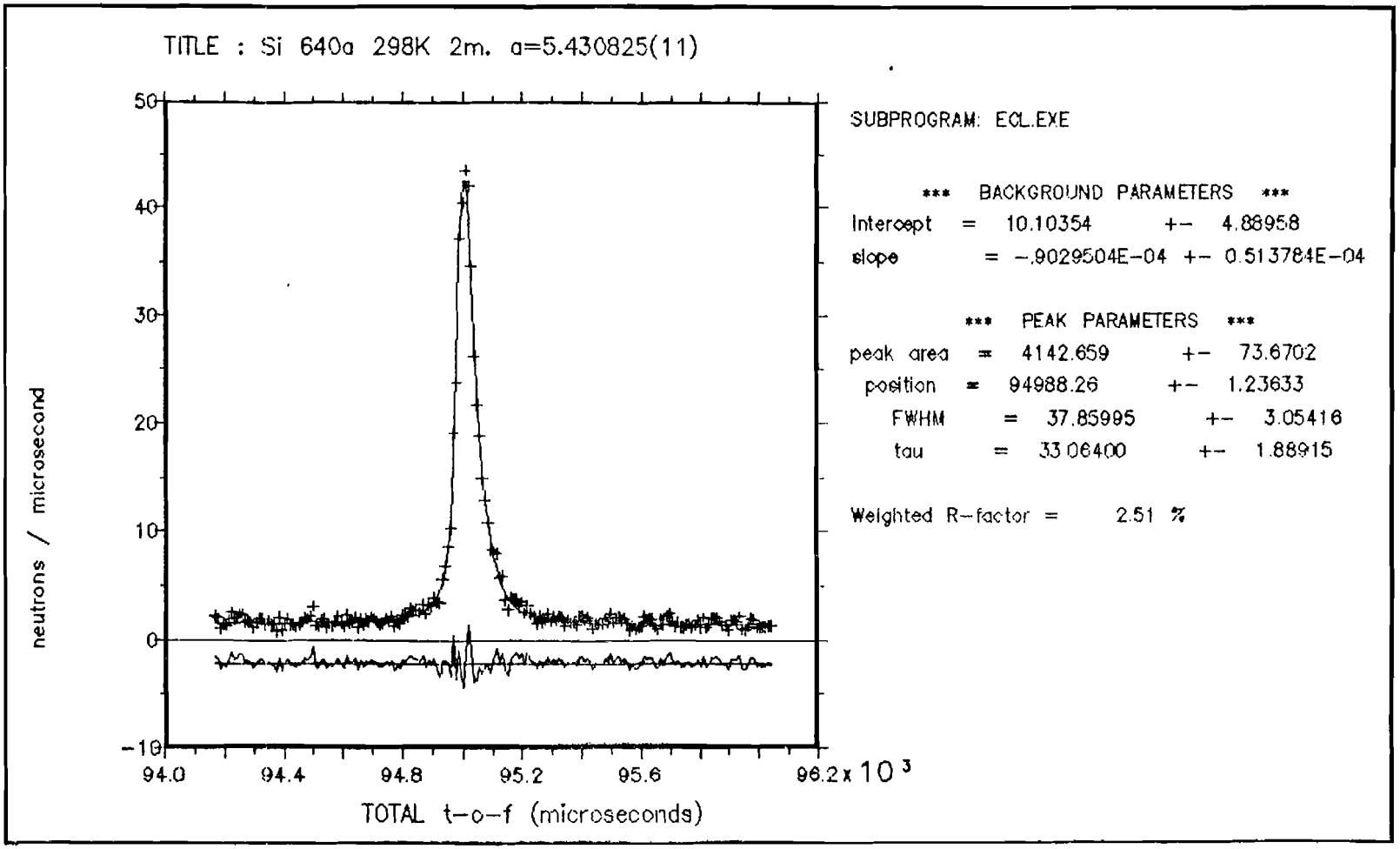

Figure 7: Exponential/Lorentzian fit of the 311 Si peak.

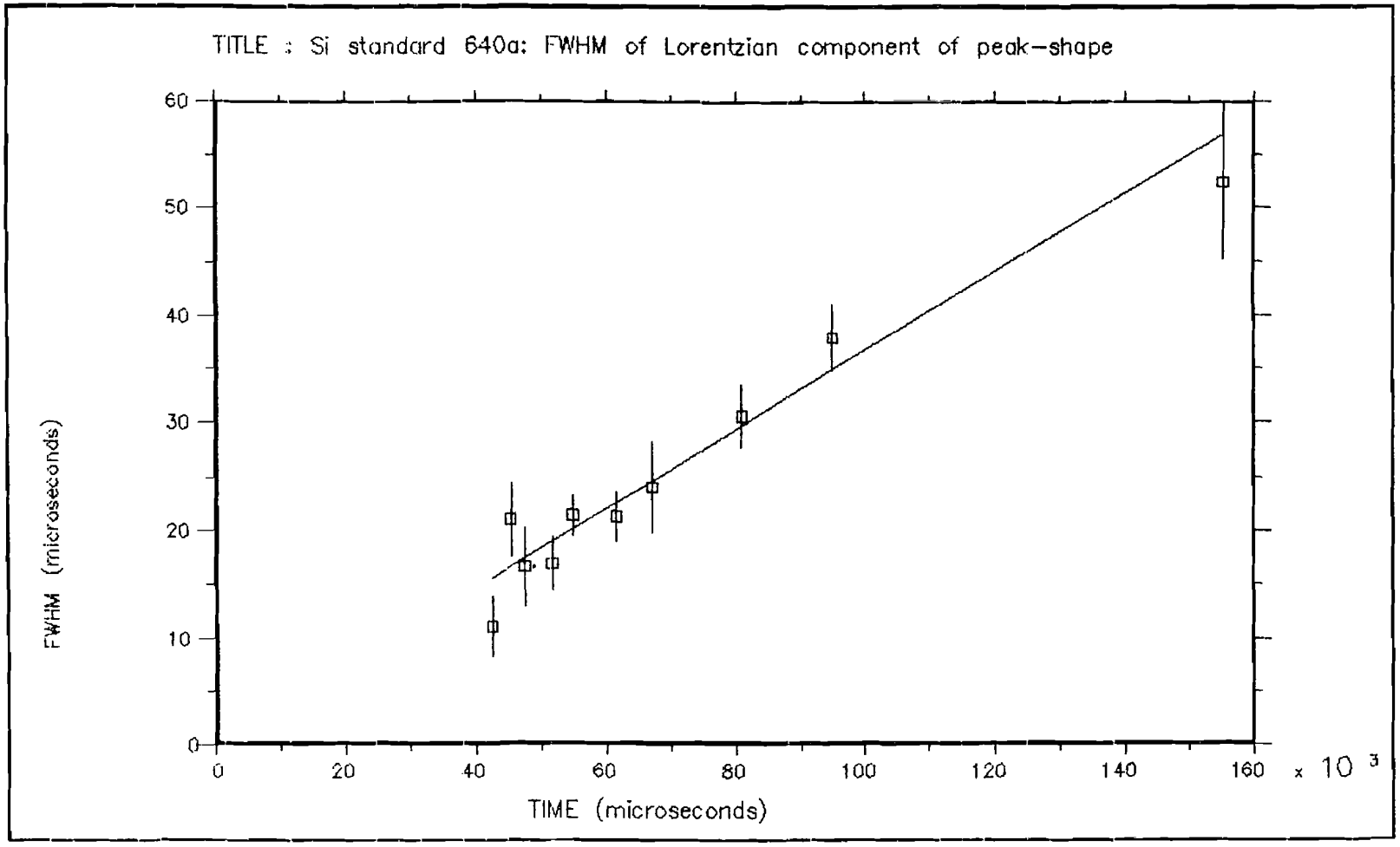

Figure 8: The variation of full width at half maximum of the Lorentzian component of the Exponential/Lorentzian convolution peak shape as a function of time-of-flight.

Proceedings of the Eighth Meeting of the International Collaboration on Advanced Neutron Sources (ICANS-VIII)
8-12 July 1985, Rutherford Appleton Laboratory Report RAL-85-110

DESIGN OF THE LOW-Q DIFFRACTOMETER AT LOS ALAMOS

P. A. Seeger, A. Williams, and J. Trewhella
Los Alamos National Laboratory, Los Alamos, NM 87545, U.S.A.

Abstract

Instrument criteria are presented for the Low-Q Diffractometer (LQD) at the Los Alamos Neutron Scattering Center (LANSCE), and a design is developed to meet these criteria. The collimator consists of multiple-aperture pinhole plates, and incorporates "dynamic gravity focusing" to center all wavelengths on the detector. Monte-Carlo simulations are used to test and optimize the design. Analysis of these simulations required development of some of the data-reduction software which will be used to convert experimental histograms vs. radius and time to I(Q) data.

1. Introduction

The Low-Q Diffractometer (LQD) for the Los Alamos Neutron Scattering Center (LANSCE) will be installed on flight path 10 (the northeast corner) in the existing Weapons Neutron Research (WNR) experimental hall. With the Proton Storage Ring (PSR) operating at 24 Hz, the proposed total flight path of 12.5 m allows use of neutron wavelengths out to 13 Å before frame overlap, without the need for choppers or filters. The general floor plan is shown in fig. 1.

This flight path views a liquid hydrogen moderator which should produce the same neutron spectrum as the SNS liquid hydrogen moderator. The measured spectrum [1] is shown in an equal-area plot (i.e., number of neutrons proportional to area anywhere on the plot) in fig. 2 (solid line). There is a peak at 14 meV (2.4 Å wavelength) due to the transparency of para-hydrogen, and the long-wavelength data (measured to 10 Å or 0.8 meV) fit a Maxwellian of effective temperature 2.1 meV. We have arbitrarily

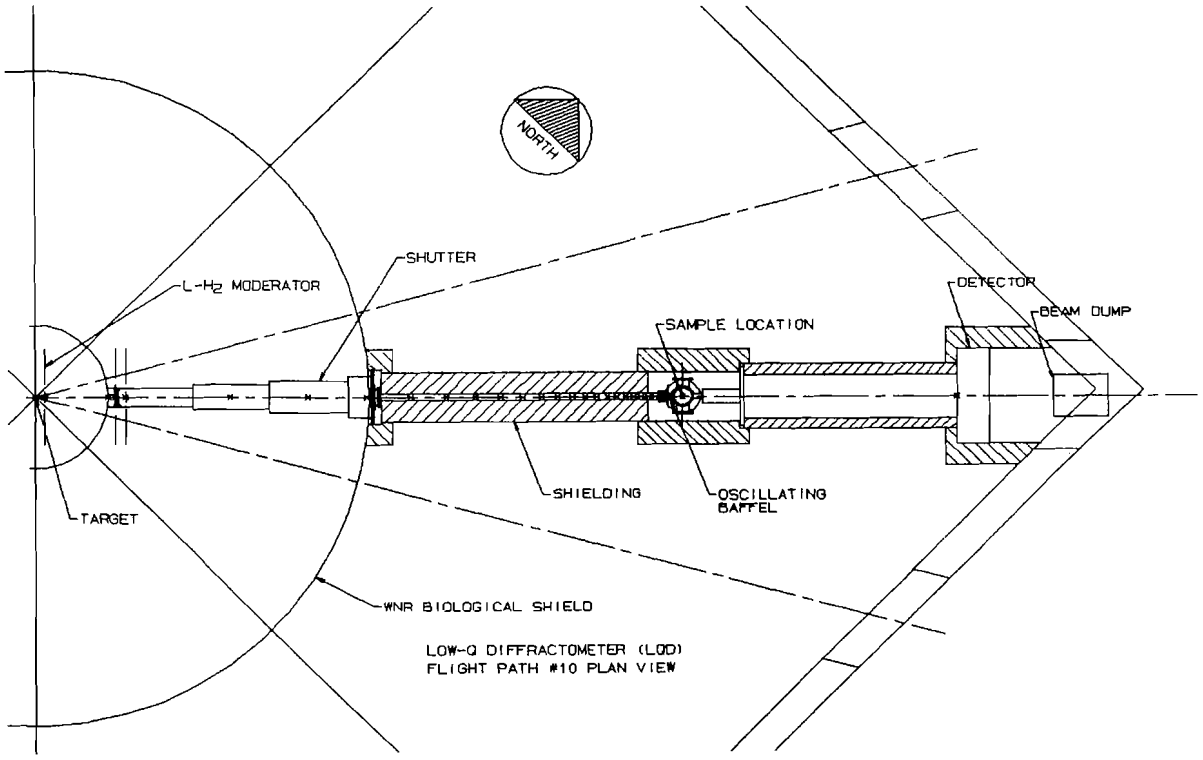

Fig. 1. Floor plan of the proposed LQD, at flight path 10 of LANSCE.

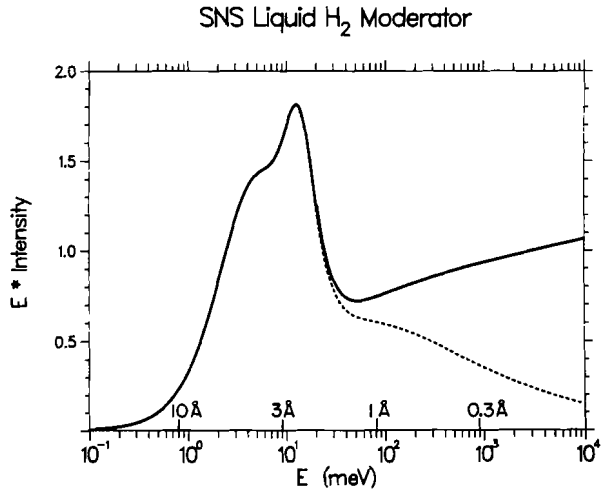

Fig. 2. Measured spectrum from the liquid hydrogen moderator at SNS.

chosen λ = 8 Å, at which the intensity is about a quarter maximum, to represent the maximum wavelength for obtaining statistically significant results when estimating the low-Q limit of the instrument.

The detector resolution and efficiency are assumed to be good enough not to affect optimization. For instance, the Anger camera [2,3] is recorded in bins 2.3 mm square, and it has an rms resolution better than 1.5 mm. This will not contribute significantly to the resolution if the sample-to-detector distance L_2 > 2.5 m. Efficiency affects the short-wavelength/high-Q end of the spectrum; the dashed line in fig. 2 illustrates the effective spectrum for a 1/v detector equivalent to a 2-mm thickness of ^{6}Li glass scintillator. At 0.3 Å, the efficiency is 39%.

2. Design Criteria

The primary requirement of the instrument is to be able to take statistically significant data at a minimum momentum transfer $Q_{min} = 0.003\ \text{Å}^{-1}$. With $\lambda_{max} = 8$ Å,

$$\theta_{min} = \frac{\lambda_{max} Q_{min}}{2\pi} = 3.8 \text{ mrad} \qquad (1)$$

We also require an rms resolution at least as good as 30% at Q_{min}, so that the standard deviation of θ must be

$$\sigma_\theta < 1.15 \text{ mrad.} \qquad (2)$$

These angular criteria will establish the relative sizes of the collimator apertures, and will be developed more fully in the next section.

An obvious design goal is to maximize the counting rate of an experiment. Once the angular parameters are determined, however, there is very little which can be done to affect the flux on sample [4]; for instance, if the instrument is shortened to gain flux by the $1/R^2$ increase of solid angle, then the area of moderator seen at any point on the sample must be decreased by exactly the same factor to maintain resolution. For a given moderator surface brightness ($n/cm^2/ster/s$), the only way to increase intensity is by increasing the sample size, up to the limit that the full moderator surface is being used. Since frame overlap (as well as the available space in the experimental hall) limits the scale factor by which the design can be multiplied, the only way to increase sample size is through use of multiple-aperture collimators.

The third criterion is to allow an extended dynamic range in Q, up to at least $1.0\ \text{Å}^{-1}$. This is readily accomplished by utilizing a wide band of the wavelength range of the pulsed source, and by using an area detector covering a reasonably large angular range. Since we wish to record all wavelengths longer than 0.3 Å, a chopper to block the power pulse is impractical. If located 4.5 m from the source, it would have to be fully open within 320 μs after the proton pulse. Since the beam diameter is about 80 mm at that location, the linear velocity would be 250 m/s and the diameter would be 3.3 m. We will rely on time of flight to eliminate the power pulse; the detector and associated electronics must recover fully within a few hundreds of μs.

3. Collimator Aperture Sizes

The variance of the scattering angle, θ, due to moderator and sample collimation is [5]

$$V[\theta] = \frac{1}{2L_1^2}\,\overline{r_1^2} + \frac{1}{2}\left(\frac{1}{L_1} + \frac{1}{L_2}\right)^2 \overline{r_2^2}\ , \qquad (3)$$

where r_1 and r_2 are axial displacements on the moderator and sample, respectively, and the path lengths are as shown in fig. 3. In all previous studies [5-7], the distances ℓ_1 and ℓ_2 were assumed to be small, and the radii of the moderator and sample were assumed to be equal to the aperture radii, R_1 and R_2. At the recommendation of our design review committee [8], we now propose that ℓ_1 be relatively large so that we will have the versatility of changing the collimator system without changing anything inside the biological shield. The effect of ℓ_1 and ℓ_2 on aperture optimization must be re-examined.

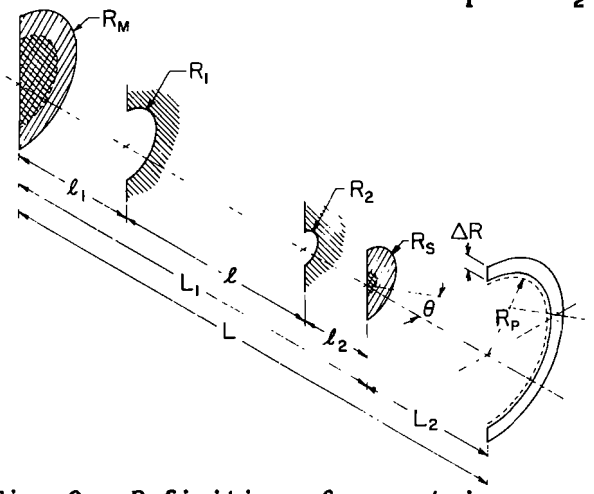

Fig. 3. Definition of geometric parameters.

From the development of either [5] or [6], the two terms in eq. (3) should be made equal. Thus

$$\overline{r_1^2} \,/\, \overline{r_2^2} = \left(\frac{L_1 + L_2}{L_2}\right)^2 , \qquad (4)$$

or the root-mean-square radii are proportional to distances from the detector. The distribution of r_1^2 is constant out to the radius of the umbra, $R_1 + (R_1 - R_2)\ell_1/\ell$, and falls to zero at the penumbra radius, $R_M = R_1 + (R_1 + R_2)\ell_1/\ell$. Thus r_1^2 depends on both R_1 and R_2 (as does r_2^2), but the arithmetic average of the umbra and penumbra radii is $R_1(1+\ell_1/2\ell)$.

We now choose path lengths based on practical considerations, and hunt for aperture sizes which satisfy eqns. (1), (2), and (4). If necessary, we can then modify the path lengths and iterate. For L_1 = 8.75 m and L_2 = 3.75 m, we require

$$\overline{r_2^2} \,/\, \overline{r_1^2} = (0.30)^2 \qquad (5)$$

Assuming ℓ_1 = 4.75 m, ℓ_2 = 0.25 m, and ℓ = 3.75 m, a simple Monte-Carlo code was run and the radii adjusted until the ratio converged at

$$R_2/R_1 = 0.55, \tag{6}$$

which is about 8% larger than it would be if the aperture radii (instead of the rms radii) converged to the detector. The penumbra radius at the detector,

$$R_P = R_2 + \frac{R_1+R_2}{\ell}(L_2+\ell_2) = 3.99\ R_2\ , \tag{7}$$

must be chosen to satisfy eq. (1). Allowing a 1 mm safety margin, and taking ΔR = 2.3 mm,

$$\theta_{min} = (R_P + 1\ \text{mm} + \Delta R/2)/L_2 \tag{8}$$

$$R_P < 12.1\ \text{mm} \tag{9}$$

$$R_1 = 5.47\ \text{mm}, \quad R_2 = 3.03\ \text{mm} \tag{10}$$

The standard deviation of θ (square root of eq. (3)) is then 0.81 mrad, well within eq. (2). The penumbra radii at the moderator and sample are

$$R_M = 16.2\ \text{mm}, \quad R_S = 3.6\ \text{mm} \tag{11}$$

4. Multiple Apertures

The moderator and sample sizes in eq. (11) do not take good advantage of the available source. Multiple aperture sets, all converging to the same point at the detector, increase the intensity without affecting the resolution. The pattern of 19 holes shown in fig. 4 matches the size of the moderator (120 mm x 120 mm) and illuminates a sample 36 mm in diameter.

Intermediate beam scraping baffles are required to prevent neutrons crossing from one imaginary tube to another in the multiaperture system. The holes in these baffles should be large enough not to intercept the actual beam, and must be further enlarged to account for the different parabolic trajectories followed through the collimator by neutrons of different velocities (because of gravity, the neutrons do not follow straight lines; see the following section). Twelve baffles will be required, with variable spacing; they become quite close as the size of holes relative to their spacing increases.

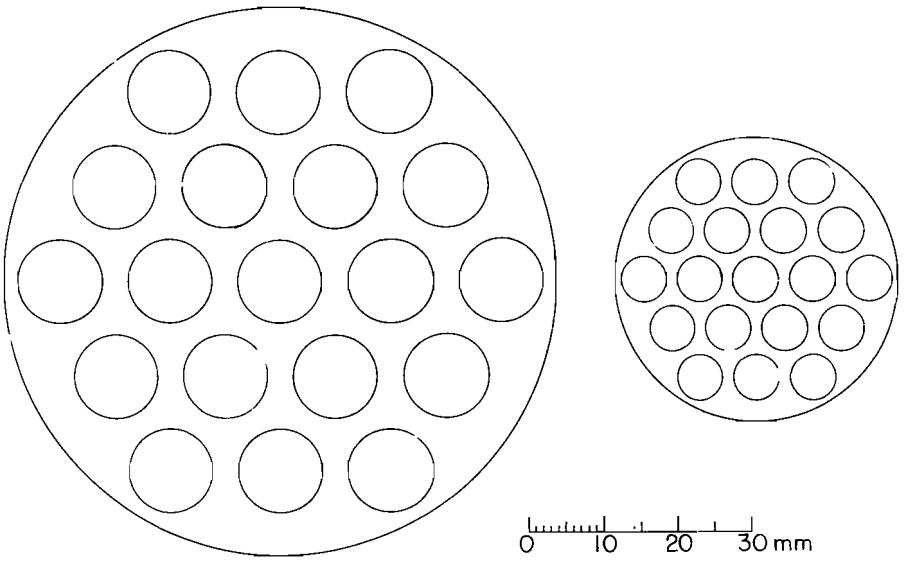

Fig. 4. Entrance and exit aperture plates for the LQD collimator. Each corresponding pair of holes defines a beam with appropriate divergence, and all converge to the same point at the detector. Intermediate baffles prevent crosstalk between beams.

In the limit that the holes cover the entire area of the baffles, the collimators are continuous and take the form of converging Sollers. We considered three possible geometries: concentric converging cones, an array of converging hexagonal pyramids, and conventional alternating horizontal and vertical Soller slits. However all systems involving extended surfaces were rejected because of "mirror reflection" of long wavelength neutrons from any surface [9]. In fig. 5 we show the reflection probability for 8-Å neutrons as a function of glancing angle, from three different substances. For absorbing surfaces, the effective index of refraction is complex and there is no critical reflection angle (as there is for Cu). But the probability always goes to unity as the angle goes to zero, and reflection at angles comparable to our required collimation is far from negligible. The situation is improved if the surfaces are rough, but there will always be some halo always be some halo on the beam, requiring a larger beam stop and hence larger θ_{min}. Also note that the reflection probability is proportional to λ^2, so the effect is most damaging at the smallest values of Q.

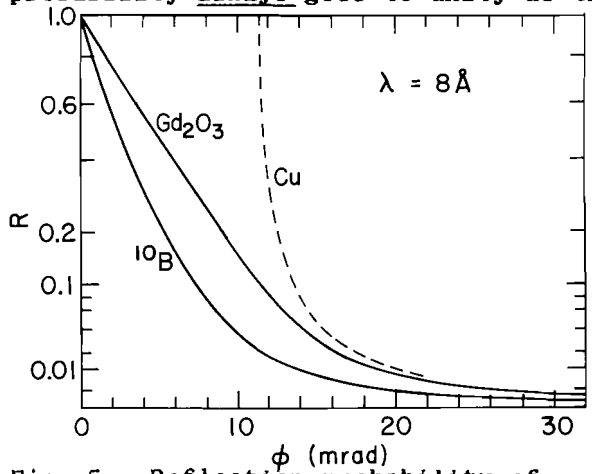

Fig. 5. Reflection probability of 8 Å neutrons.

5. Dynamic Gravity Focusing

At 24 Hz, neutrons recorded at the end of the frame will have fallen 8.50 mm under the influence of gravity, compared to where they were pointed when they left the moderator. (Gravity is smaller at LANSCE than at any other source represented in ICANS, because of our lower latitude and higher altitude.) To minimize the size of the beam stop we want to choose neutrons whose trajectories strike the detector at its center; fig. 6 shows the parabolic trajectories of two neutrons with different horizontal velocity. If we replace the horizontal velocity by $h/m\lambda$, and use y_o and v_o to represent the initial position and vertical velocity of the neutron, then

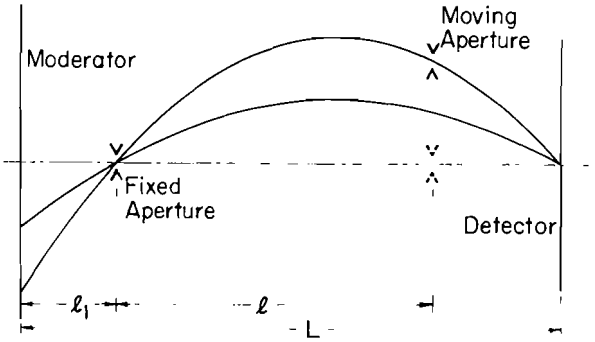

Fig. 6. Dynamic gravity focusing.

$$y = y_o + \frac{m}{h}\lambda\, v_o\, x - \frac{1}{2} g \left(\frac{m}{h}\lambda\right)^2 x^2 \quad . \tag{12}$$

If the entrance aperture and the detector center are taken as fixed points, so that $y = 0$ at $x = \ell_1$ and at $x = L$, then

$$y = \frac{1}{2} g \left(\frac{m}{h}\lambda\right)^2 [-\ell_1 L + (\ell_1 + L)\, x - x^2] \tag{13}$$

The exit aperture of the collimator, at $x = (\ell_1 + \ell)$, must move vertically in phase with the beam. Neutrons of wavelength λ arrive at the moving aperture at $t = (\ell_1 + \ell)m\lambda/h$, and the required motion is

$$y = \frac{1}{2} g \left(\frac{L}{\ell_1 + \ell} - 1\right) \left(1 - \frac{\ell_1}{\ell_1 + \ell}\right) t^2 \tag{14}$$

For the flight paths chosen for the LQD, this becomes

$$y = (1.016\ \text{m-s}^{-2})\, t^2 \quad , \tag{15}$$

and the maximum excursion (for 13 Å neutrons) is 0.82 mm. Without correction, the droop at the detector would be 1.69 mm. This correction has become much smaller than our original estimates, because ℓ_1 is much larger. If we return to the design with $\ell_1 = 1.00$ m, the maximum excursion is

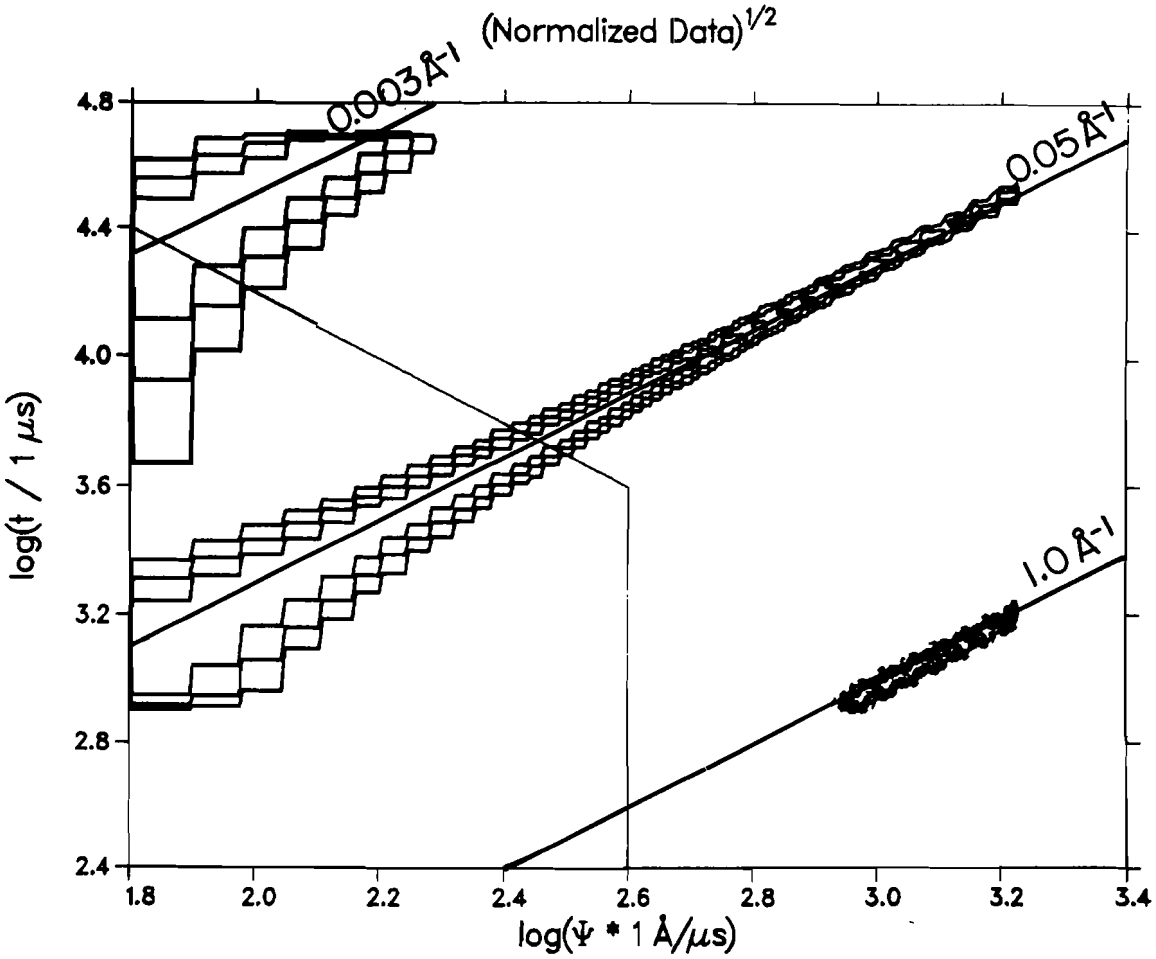

Fig. 7. Simulated data for scattering at three values of Q. Ψ represents the radial coordinate on the detector, and t is a measure of neutron wavelength. Data have been normalized to the incident spectrum.

1.63 mm, to correct for a droop of 2.50 mm. Whether or not the dynamic correction is made, eq. (13) must be used to compute sizes and elevations of the intermediate baffles in the system.

6. Monte-Carlo Simulations

The various collimator systems were run through Monte-Carlo simulations to estimate the resolution. Details are given in ref. [7]. Two forms of perfect scatterers were considered: either every neutron was scattered with exactly the same magnitude of the momentum transfer (δ-function Q), or else the scattering law was that of non-interacting hard spheres of uniform radius. Neutrons reaching the detector were binned vs. radius and time, with the radial bins 3.0 mm wide and logarithmic time bins of width

$\Delta t = t/600$. Normalized contour plots of three constant-Q runs are given in fig. 7. The radial variable has been converted to

$$\Psi = \frac{4\pi\, m\, L}{h} \sin(\theta/2), \tag{16}$$

so that

$$Q = \Psi/t \tag{17}$$

and a line of constant Q is a straight line with slope +1 on the log-log plot.

The histogram bins are wide in the Ψ direction (especially at small Ψ) and very short in t, as shown in fig. 8. A Q bin is a diagonal band, which includes contributions from many Ψ-t bins. Our binning procedure is to take t equal to the mid-value of the bin, and to compute the fraction of each log(Ψ) bin which falls within the Q bin. We then take the average of the normalized count rate from each contributing old bin weighted inversely as its variance. All position and/or time dependent corrections must be performed before rebinning. The weighted average may then be multiplied by the area of the new bin to produce an "intensity."

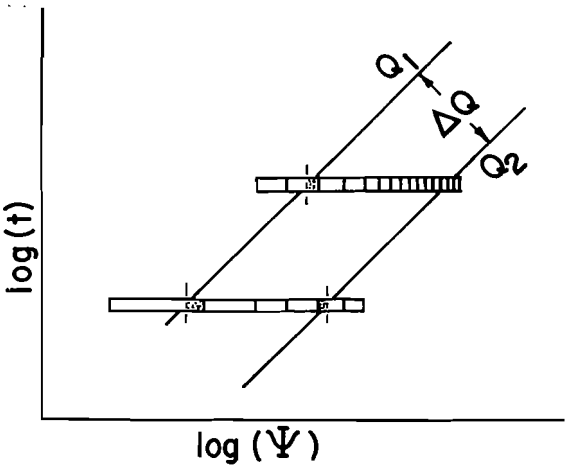

Fig. 8. Relationship of Q bins to Ψ and t bins.

Fig. 9 shows the resulting intensity vs. Q when all data are summed. (Note that a square-root scale is used to emphasize the tails of the distributions.) Comparing to fig. 7, it is clear that the long tails in fig. 9 result from including short wavelength data from the innermost annuli of the detector, where the resolution is poor. If we omit data in the lower-left corner of fig. 7, the result is fig. 10. On this figure, I is the fraction of all detected neutrons which is retained. Note the greatly improved standard deviations, σ.

The same data-reduction procedure was applied to the hard-sphere simulations. We have also used a fitting program for spheres and a Guinier analysis program, both including propagation of errors, to investigate the statistical precision which may be obtained. The resulting intensity distributions and fitted parameters are shown for the case of R = 30 Å in fig. 11. With the source operating at 100 μA, and a 1% scattering sample, the data-collection time for this number of neutrons would be less than 1 s.

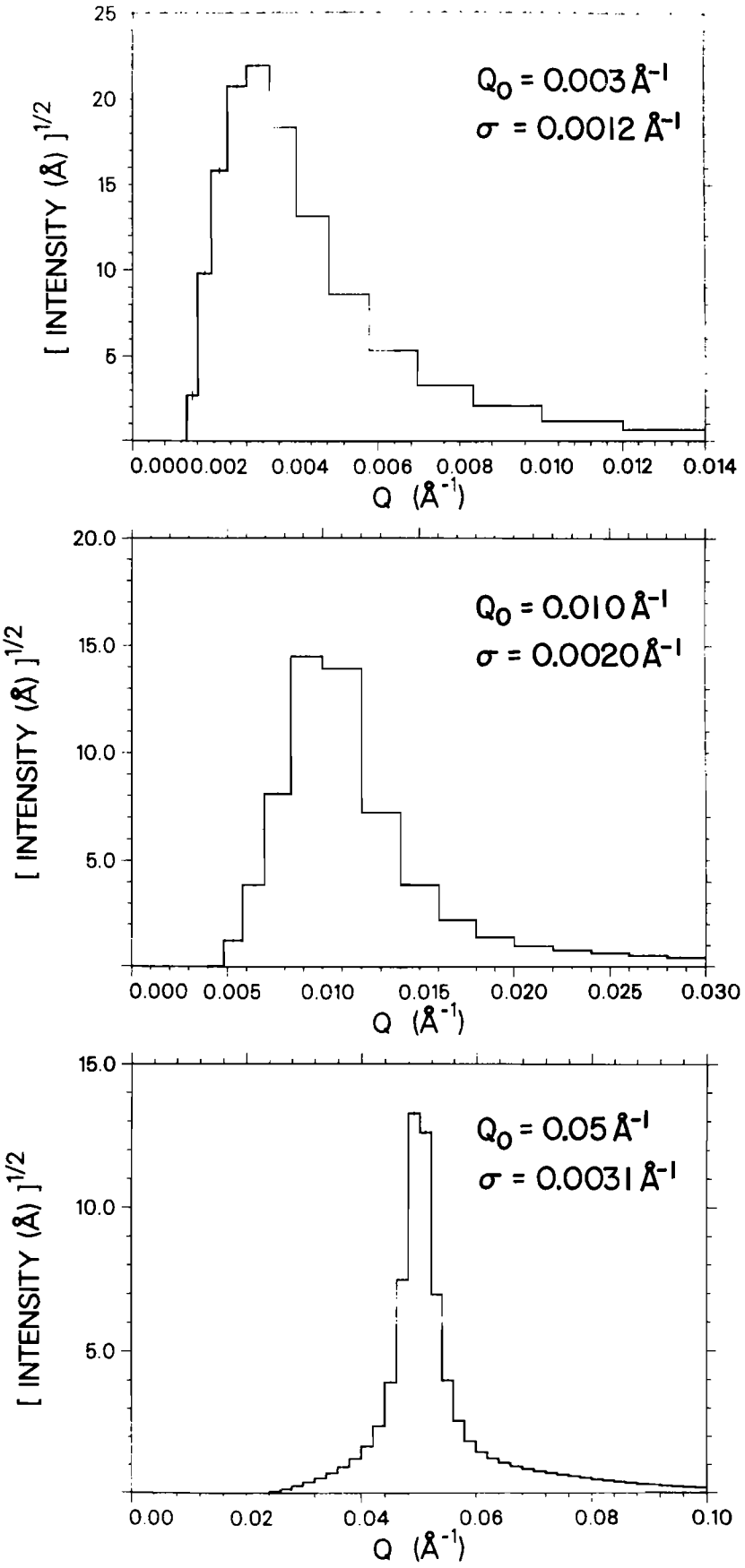

Fig. 9. Sum of data of all wavelengths, for three constant Q simulations.

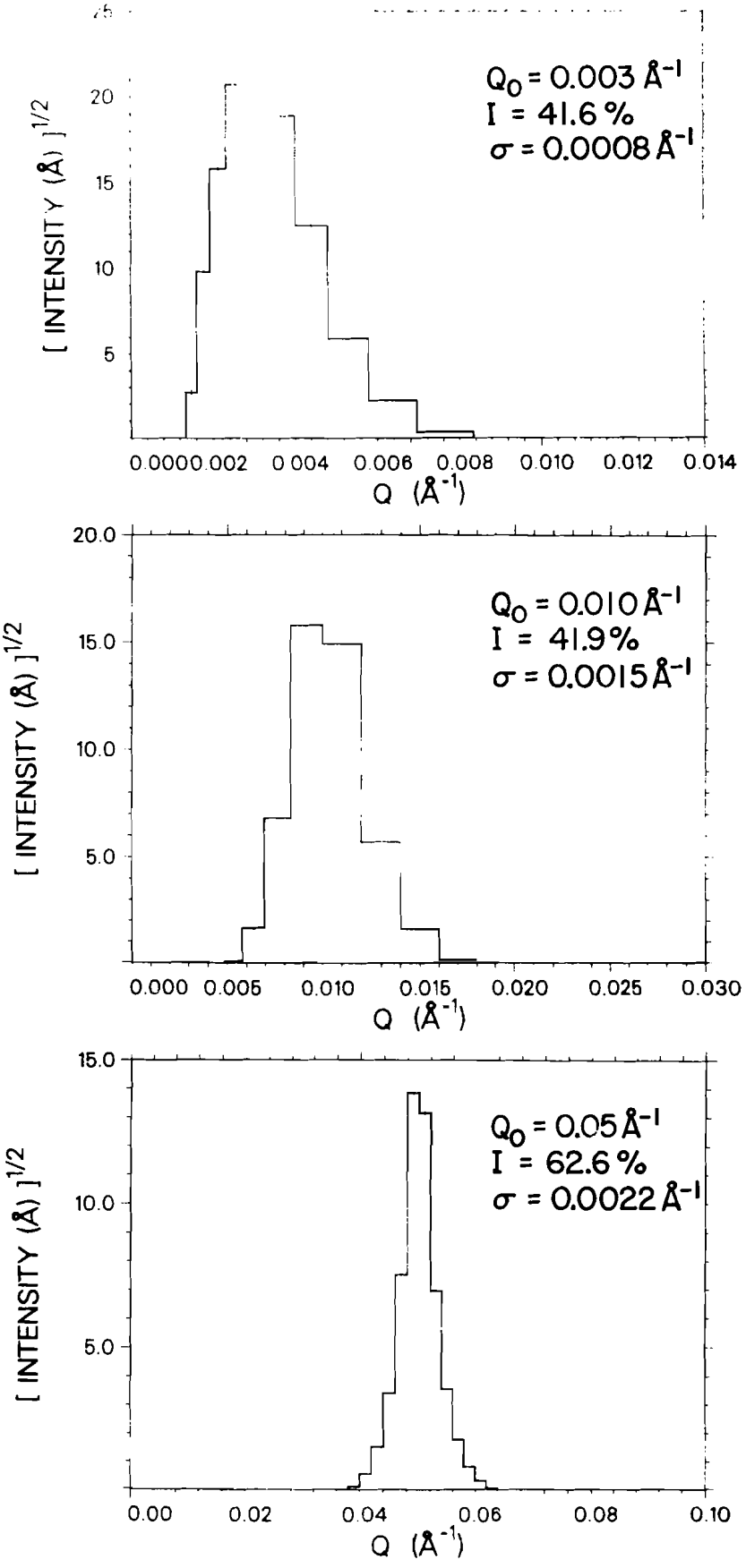

Fig. 10. Sum of data, excluding lower-left corner from fig. 7.

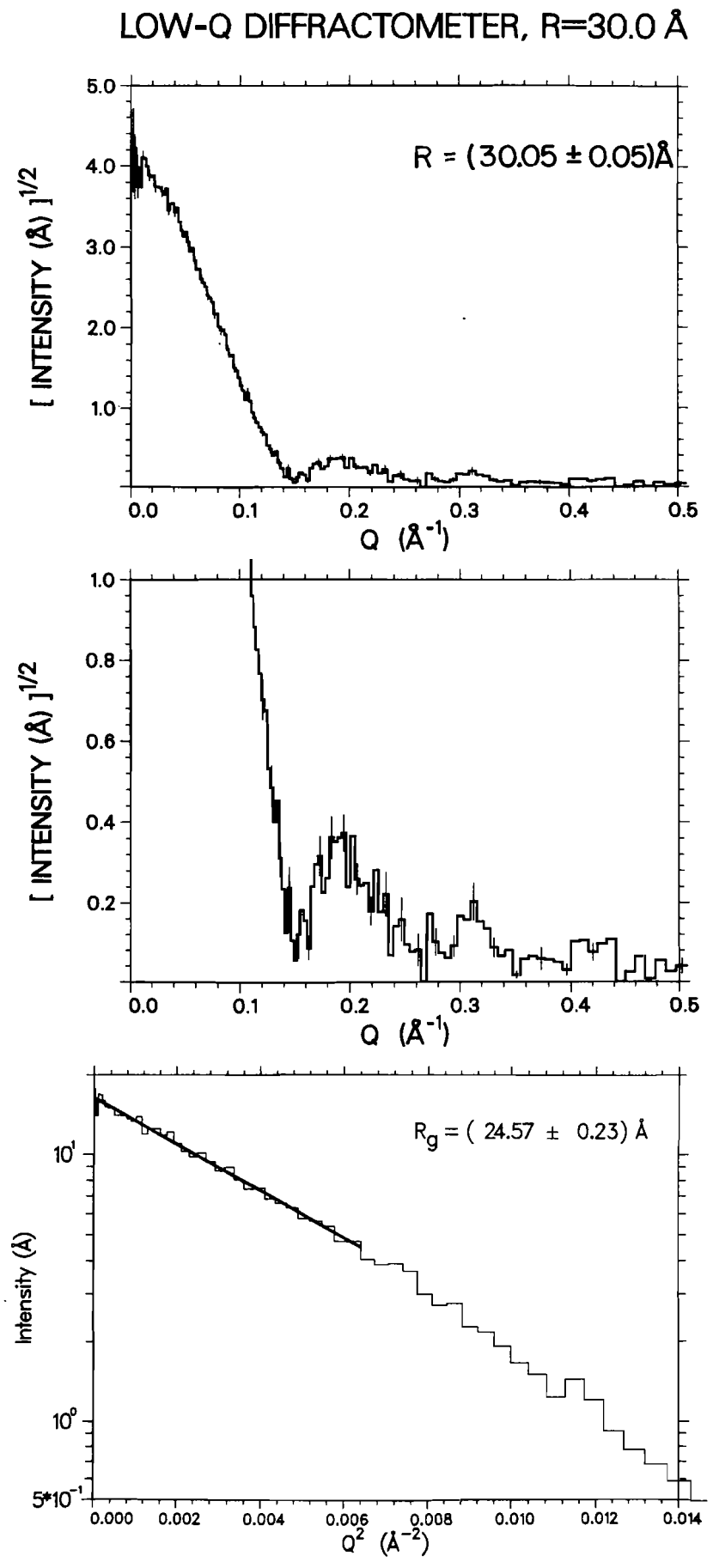

Fig. 11. Simulated data for hard sphere scattering with R = 30 Å.

A significant feature of the LQD is that a broad range of Q is measured in a single experiment without any collimation or detector changes. This will allow high prescision model fits in the range of sizes from 10 to 300 Å to be obtained in slightly less time than at D-11. On the other hand, to obtain the same precision as D-11 for a Guinear fit will require about four time as long.

Acknowledgments

This work was permformed under the auspices of the U.S. Department of Energy, Office of Basic Energy Sciences.

References

[1] T.D. Perring, A.D. Taylor, and D.R. Perry, Rutherford Appleton Laboratory report RAL-85-029 (1985).

[2] P.A. Seeger, I.E.E.E. Trans. Nucl. Sci. **NS31** (1984) 274.

[3] P.A. Seeger and M.J. Nutter, this conference (1985).

[4] P.A. Seeger, Proceedings of the International Neutron Scattering Conference, Santa Fe, August (1985).

[5] P.A. Seeger, Nucl. Instr. and Meth. **178** (1980) 157.

[6] D.F.R. Mildner and J.M. Carpenter, J. Appl. Cryst. **17** (1984) 24.

[7] P.A. Seeger and R. Pynn, submitted to Nucl. Instr. and Meth. (1985).

[8] Committee members were J.M. Carpenter, J.E. Epperson, J.B. Hayter, R.Pynn, K. Rhyne, J.M. Rowe (chair), D. Schaefer, and J.W. White.

[9] I.I. Gurevich and L.V. Tarasov, "Low-Energy Neutron Physics" (North-Holland, Amsterdam, 1968) p. 58.

Proceedings of the Eighth Meeting of the International Collaboration on Advanced Neutron Sources (ICANS-VIII)
8-12 July 1985, Rutherford Appleton Laboratory Report RAL-85-110

TOF TYPE SMALL ANGLE SCATTERING SPECTROMETER SAN AT KENS PULSED COLD NEUTRON SOURCE

By Y. Ishikawa and M. Furusaka

Physics Department Tohoku University, Sendai 980 Japan

N. Niimura

Laboratory of Nuclear Science Tohoku University, Sendai 980 Japan

M. Arai

National Laboratory for High Energy Physics, Tsukuba, Ibaraki, 305 Japan

and K. Hasegawa

Department of Engineering, University of Tokyo, Tokyo 106 Japan

Abstract

The paper describes the configuration and performance of a new TOF type small angle neutron scattering spectrometer SAN installed at the pulsed cold neutron source in the National Laboratory for High Energy Physics(KEK). The spectrometer has a special advantage over the conventional small angle scattering machine in following two points. One is its ability for simultaneous measurements of wide Q range (3×10^{-3} $A^{-1} < Q < 4$ A^{-1}) and another is new information which it provides by employing the wavelength dependence of scattering. For example, the inelastic scattering can be separated from the elastic one without making energy analysis. The discussions have also been made on the design principle of this type of spectrometer.

§ 1. Introduction

The small angle neutron scattering spectrometer (SANS) is a special machine for investigating macro-structures and it becomes now one of the most important instruments for neutron scattering because of its application to wide scientific fields as solid state physics, chemistry, material sciences, polymer and biology.(Kosterez 1979) The demand for this machine is still increasing and therefore this machine is installed or at least planned to be installed in most of the research reactors in the world. The situation would be the same for the pulsed spallation neutron sources which are just coming out in the world as the next generation neutron sources, but because of its new feature; pulsed character, there was no agreement on the design principle of the TOF type SANS when we planned to install our small angle neutron scattering spectrometer "SAN" at the cold moderator of our spallation neutron source KENS in National Laboratory for High Energy Physics (KEK) (Ishikawa and Watanabe 1978). Only few papers had been published to report the results of preliminary tests of this type of spectrometers (Cser, 1975, Borso, 1981). Some people even suspected the installation of this machine to the spallation neutron source, partly because of small advantages of spallation neutron source (pulsed short wavelength neutrons) to this machine and the complexity of handling the 3 dimensional (3D) data (2D-position sensitive detector + TOF channels).

We have shown, however, by our four year's successful utilization, that the small angle neutron scattering spectrometer is also quite an appropriate spectrometer for the spallation neutron source, giving new information which is difficult to obtain with the conventional small angle scattering machine

installed at the reactor. The paper describes in the next section the overall layout and configuration of the spectrometer. Some instrumental devices newly developed for this spectrometer such as the two dimensional (2D)-converging Soller slit, which would also be useful for the conventional SANS, are also discussed in this section. Then the characteristics of the TOF-SANS are summarized in Section 3 with experimental results obtained with our spectrometer SAN. In the final section the design principle of the TOF-SANS is discussed in comparison with that of the conventional SANS in the steady reactor. The design principle of this spectrometer(SAN) as well as its scientific yields are reported in many short papers published in KENS Report I(1980)-V(1985) and in a review article (Ishikawa, 1983). The problems for data analysis of this spectrometer are discussed separately in a succeeding paper (Furusaka et al, 1985).

§2. Structure of SAN at KENS

2.1 Overall Layout

The layout of the SAN is displayed in Fig.1(a) and (b). The spectrometer is installed at the exit of a bent neutron guide from the KENS cold moderator with effective dimensions of h =10 cm, w = 8 cm, d = 5 cm made by solid methane at 20K (Ikeda et al., 1983). The distance between the source and sample is fixed to be ℓ_S = 19 m, where are located a 3.5 m long straight guide, a tail cutter C_1, a 11m long bent guide tube and a 2m long 2D-converging Soller slit. A 2D-position sensitive detector (PSD) (60 x 60 cm^2) is accommodated inside a large vacuum scattering chamber, 10^{-2} mmHg in pressure and the distance between

the sample to the detector ℓ_2 can be changed between 1 and 5 m without breaking vacuum. The SAN is also equipped with several normal ^{3}He counters noted as A, B, ..., F in the figure in order to expand the dynamical range of the Q measurements. The 2D-PSD consists of an array of 43 1D-PSD as described later in detail. The photograph of the SAN spectrometer as well as the 2D-PSD inside the vacuum chamber are shown in Fig.2. The tail cutter C_1 is designed to avoid the frame overlap of pulsed white neutrons operating with 20 Hz at the position of the detector, 25 m apart from the source. A range of wavelength [λ], which can be employed in the experiment is [λ] = 8 A and we usually use the neutrons with 3 A $\leq \lambda \leq$ 11 A. The range of momentum transfer Q covered with this wavelength band is displayed in Fig. 3 for four different 2D - PSD positions noted as G_1 - G_{10}(ℓ_2 = 1, 3, 5 and 10 m). The last position G_{10} is still in a stage of planning. The solid straight lines (A - F) are the ranges of Q covered with six single ^{3}He counters. From this figure, it is seen that the SAN with 2D - PSD at the position of 5 m can measure simultaneously a wide Q range between 3 x 10^{-3} A^{-1} and 4 A^{-1}.

2.2 Vacuum scattering chamber

In order to meet the requirement that the vacuum pressure of the large scattering chamber, 1.2 m in diameter, 6 m long, should be always 1 x 10^{-2} mm Hg, while that of the sample chamber can be varied between 10^{-6} mmHg and 1 atmospheric pressure depending on the experimental conditions, we put a specially designed vacuum shutter in between both chambers as shown in Fig. 4. The shutter valve in the open state is equipped with an immovable thin Al foil window, 0.3 mm thick and 200mm in diameter

which serves to keep two chambers in different vacuum states of 10^{-2} mmHg and 10^{-6} mmHg respectively. When we need to make the sample chamber to the atmospheric pressure for sample exchange or installation of other equipment as an electromagnet, a thick Al plate shutter with a 2mm thick Al window was closed behind the thin Al foil to support it against the atmospheric pressure. This device reduces significantly the time for changing the experimental conditions and saves the machine time.

Another convenient device we designed is a movable beam stopper in front of the 2D-PSD. It is preferable that the direct beam stopper can be removed for the transmission measurement or can be moved for centering. Therefore we put first a movable beam stopper which was hanged vertically by a rod of 10 mm wide and was driven electronically from outside in both horizontal and vertical directions. This system was, however, found not ideal because it reduces the detecting efficiency behind the hanging rod as shown in Fig. 5(a) where we demonstrate the scattering intensity from water detected by 2D-PSD. The time channels are integrated for simple demonstration. The beam stopper we finally adopted consists of a thin Al plate 0.4 mm thick covering the whole 2D - PSD with a small beam stopper(42 x 42 mm^2) made of Cd at the center of the plate which is shown in Fig. 6. The Al plate can be moved in the horizontal direction from outside. This system insured the homogeneity of the detecting efficiency as shown in Fig. 5(b).

2.3 2D-Converging Soller slit and background level of SAN

Although the principle of the 2D-converging Soller slit had been reported earlier(Nunes, 1978), no small angle neutron

scattering machines had hitherto adopted this slit, partly because of the difficulty of fabricating it and partly because of the anxiety for increasing the background level due to this slit. We designed a simple two dimensional converging Soller slit and found that the adoption of the slit is particularly important for the TOF type small angle neutron scattering machine.

The principle of the converging Soller slit is displayed in Fig. 7. This is the Soller slit system which collimates the incident neutrons so as to converge them into the center of the 2D-PSD. Therefore the scattering angle ϕ of the neutrons scattered from any sample position is conserved even if we use the large sample ($\phi = \phi_o$ in Fig. 7(a)). The layout of the 2D converging Soller slit finally we designed is shown in Fig. 8. The slit consists of two sets of one dimensional converging Soller slits, each making the neutrons converge in horizontal and vertical directions respectively. The slit is made of Gd_2O_3 coated thin iron plates, 0.2 mm thick. The results of using the 2D converging Soller slit is displayed in Fig. 9, where the incident neutron beam divergences at the position of 5 m from the sample are displayed as the contour maps of equal intensity for three different wavelengths. The lower curves correspond to the case without the slit, while the upper one is the result of insertion of the slit. We can see in the lower figure that without collimation (i) the divergence of the beams is larger for longer wavelength corresponding to the larger critical angle $\theta_c(\lambda)$ of the neutron guide and (ii) the beam intensity is shifted to the left hand side for 4 A because of existence of garland type reflections inside the guide for this wavelength. Note that the concavity of the intensity map at the left hand side is due to

the presence of the beam stopper. Such a difference in the divergence as well as the inhomogenous intensity distribution for different wavelengths are completely disappeared, when we use the Soller slit as shown in the upper figures. Since the spacial homogeneity of the intensity is usually achieved by connecting a long straight guide to the bent guide, we found that the converging Soller slit is particularly useful for the TOF machine which requires a shorter flight path than the conventional SANS.

The effect of the background by this collimator was examined as shown in Fig.10, where the background under four different conditions are compared with the scattering from a standard sample, SiC powder. The background marked as Al window is the case where the sample case has two Al windows, 0.5 mm thick, while in case of Si(Single), the windows are replaced by single crystal Si plates, 3 mm thick.(See also Fig. 4). In the latter case, the background level was found to be reduced almost to the real background (BG) which corresponds to the case of no window. The background is of course three order of magnitude smaller than the signal intensity for small Q values. The background at high Q values was also compared with the scattering from pure water, 2 mm thick in Fig. 11, which indicates that the S/N ratio is about 100 for $Q > 0.02\ A^{-1}$, sufficiently high for the study of solution, but the background starts to increase below this Q value. The increase of background is partly due to a small leakage of the direct beam and presumably partly to the small angle scattering from the Soller collimator. Although the S/N ratio in this Q range reduces less than 1/5 for water, the situation is much improved for the actual small angle scattering because of the increase of signal intensity at small Q side.

Total neutron intensity is about 10^6 of the background at Q = 0.01 A^{-1}. Note that the 2D-PSD has no shield and the scattering chamber is shielded only by a Cd sheet, 0.5 mm thick.

The incident beam collimation realized by the converging Soller slit is quite important, because it determines the final resolution of the spectrometer as will be discussed in Section 4.3, all other resolutions can be matched to this resolution. Referring to Fig. 7(a), the angular resolution of the converging Soller slit is given by

$$\Delta\phi^2 = \frac{1}{2}\left[\left(\frac{2d_o}{\ell_1}\right)^2 + \left(2d_1 \cdot \left(\frac{1}{\ell_1} + \frac{1}{\ell_2}\right)\right)^2 + \left(\frac{2d_2}{\ell_2}\right)^2\right]^2 , \qquad (1)$$

where $2d_o$, $2d_1$, and $2d_2$ are respectively the slit widths at the positions of entrance of the collimator, and that in front of sample and detector. The characteristic feature of the converging Soller slit is that $\Delta\phi$ does not depend on R_o or R_s, the positions of the incident beam on the collimator or sample. If the beam convergence is ideally realized (Fig. 7(a)),

$$2d_o/\ell_1 = 2d_1 \quad (1/\ell_1 + 1/\ell_2) \qquad (2)$$

This relation also corresponds to the resolution matching. Therefore

$$\Delta\phi^2 = \frac{1}{2}\cdot\left[2\left(\frac{2d_o}{\ell_1}\right)^2 + \left(\frac{2d_2}{\ell_2}\right)^2\right] = \Delta\theta^2_{col} + \Delta\theta^2_{det} . \qquad (3)$$

The momentum resolution $\Delta Q/Q$ is then given by

$$\left(\frac{\Delta Q}{Q}\right)^2 = \left(\frac{\Delta\lambda}{\lambda}\right)^2 + \left(\frac{\Delta\phi}{\phi}\right)^2 . \qquad (4)$$

Since $\Delta\lambda$ = 0.25A for SAN, $(\Delta\lambda/\lambda)^2$ ($<<$ 0.01) can be practically neglected in (4). The minimum 2D - PSD resolution being about $\pm$5 mm and $\Delta\theta_{det}^2 \simeq 1/2(1/500)^2 = 2 \times 10^{-6}$ for ℓ_2 = 5m. Therefore

$$\frac{\Delta Q}{Q} \cong \frac{\Delta\theta_{col}}{\phi} \quad \text{or} \quad \Delta Q \cong \Delta\theta_{col} \frac{2\pi}{\lambda} \quad . \tag{5}$$

Our convergning Soller slit having an angular divergene $\Delta\theta_{col}$ = 2.9×10^{-3}, ΔQ_{min} = 1.65×10^{-3} A^{-1} for λ = 11A, which is about 1/2 of Q_{min} (= 3×10^{-3} A^{-1}) of our spectrometer.

In case of 3 m scattering; ℓ_2 = 3 m, we use a half set of our converging Soller slit, one pair of vertical and horizontal collimators, each being 50 cm long. $\Delta\theta_{col}$ then becomes 5.8×10^{-3}. This configuration, however, breaks the condition of beam convergence (Fig. 7(b)), resulting in adding another term $\Delta\theta^2_{nc}$ in Eq(3). A simple geometrical calculation shows that $\Delta\theta^2_{nc}$ is given by (Ishikawa et al 1980)

$$\Delta\theta^2_{nc} = \frac{1}{2} \left(\frac{R_s}{\ell_2^0} \cdot \frac{\Delta\ell}{\ell_2}\right)^2 , \tag{6}$$

with notations defined in Fig. 7(b). By putting R_s = 18 mm, ℓ^o_2 = 5 m, ℓ_2 = 3 m, $\Delta\ell$ = 2 m, to Eq(6), $\Delta\theta nc^2$ = 2.9×10^{-6} is obtained, which is much smaller than $\Delta\theta^2_{col}$ = 3.4×10^{-5}. Therefore the converging Soller slit given in Fig. 8 can be used for both 5 m and 3 m scattering measurements. The latter configuration increases the intensity of incident neutrons by a factor four compared with the 5 m scattering and can cover the momentum transfer higher than 0.01 A^{-1}. For the 1 m scattering, we use only a vertical convergning Soller slit with appropriate dimension.

2.4 Detector system

The 2D-PSD we adopted consists of an array of 43 x 1 D - PSDs, 1/2" in diameter and 24" in active length with 6 atom ^3He originally developed at Missouri University (Berlinger et al. 1981) (Reuter - Stokes). This is the charge sensitive PSD with low resistive anode wire (3.6kΩ), particularly suitable for the TOF measurement because of rapid time response. Since the 2D - PSD with a bank of 90 preamplifiers is accommodated inside a vacuum scattering chamber with a typical operating pressure of < 1.5 x 10^{-2} mmHg, a voltage as high as 1900 V can be safely applied to each 1D - PSD, enabling a position resolution of 7 mm to be achieved. We could not apply more than 1 kV in atmospheric pressure because of high humidity in Japan.

A block diagram of the data processing system for the 2D - PSD is shown in Fig. 12. The neutron event position is calculated by charge division method. The position is determined by the following expression

$$X = \frac{Q_A}{Q_A + Q_B} \quad , \tag{7}$$

where Q_A and Q_B are the charges detected at each end of a 1D - PSD. Charge sensitive preamplifiers convert Q_A and Q_B to voltage signal, directed to the main amplifiers and its outputs are summed and fed to a single channel pulse height analyzer (Discriminator). When the sum of Q_A and Q_B is within a preset limit, a standard set signal is generated, which is used as a gate signal for the sample & holder circuit, analogue to digital converter (ADC) and time analyzer. Since the conversion speed of the ADC is prompt (5μ sec), a single ADC

can handle the signals from 4 different detectors. The digitized values of Q_A and $Q_A + Q_B$ are transferred to the address register of the P-ROM, where the positions calculated according to the expression (7) are tabulated. The operation time for calculation of the position is reduced to be 1 μ sec - access time of P-ROM by this table. The discriminator output is used to determine the neutron time of flight. Finally the data corresponding to the position, detector number and time of flight creates one address and add-one process is performed to this address of a bulk memory.

The advantages of adopting the array of 1D - PSDs for the TOF-2D-PSD are summarized below.

(i) The interference between X and Y directions can be avoided absolutely.

(ii) Some troubles of a single detector never result in a fatal wound. This is particularly true for the TOF measurement because the same information can be obtained from different detectors by employing different wavelengths.

(iii) The total dead time of the detector can be reduced (50 μ sec in our system).

We encountered little troubles of 2D-PSD during four years operation.

§ 3. Characteristics of TOF type SANS
- experimental results obtained with SAN -

3.1 Simultaneous measurements of wide Q range

The most important characteristic of SAN is its potential for measuring simultaneously a wide range of momentum transfers as shown in Fig. 3. Such a wide dynamical range of measurements

is indispensable when we study nonequilibrium phenomena as phase separation process (Furusaka et al 1983). One typical example of the results obtained with SAN is displayed in Fig.13, where we plot the temporal variation of the scattering function $I(q,t,T_a)$ of an $Fe_{60}Cr_{40}$ alloy in a process of phase separation when the sample is annealed at T_a = 550 C for annealing time t. Note that simultaneous measurements of nearly two order of magnitudes of momentum transfers ($0.02 \leq Q \leq 0.6$ A^{-1}) are required to get the complete profiles of the scattering functions of I(Q,t,Ta) in the whole decomposition process, which is impossible to practice with the conventional SANS employing a monochromatized beam as indicated by a line in a lower part of the figure. We have shown in a previous paper (Furusaka et al, 1985) that the measurements of the tail part of the scattering function are quite important to distinguish the early stage of decomposition from the late stage. In the latter stage the scattering function obeys the Q^{-4} law for large Q and the scaling law holds, while in the early stage the tail part obeys the Q^{-2} law and the scattering function cannot be scaled in a similar way.

Another typical example of the simultaneous measurement of wide Q range is provided by the study of the magnetization process in a single crystal of $90FeTiO_3$-$10Fe_2O_3$, a typical cluster type spin glass (Arai et al 1985 a, b). In this study, in addition to the small angle scattering detected by 2D - PSD, the magnetic scattering around the (1,0,1) and (1,0,-0.5) reciprocal lattice points was measured simultaneously with two ^3He counters placed at high angles as shown in Fig. 14. The (1,0,1) scattering is equivalent to the (0,0,0) scattering and they give an information on the ferromagnetic short range correlations,

while the (1,0,-0.5) scattering suggests the presence of amplitude modulation of the ferromagnetic correlations inside the short range order. The scattering patterns around three different Bragg points are displayed in Figs.14(a), (b) and (c). We have studied the effect of the magnetic field on the scattering around these three reciprocal lattice points (Arai et al, 1985 b) and found that no change occurs in the magnetic structure inside the short range order if the magnetic field is less than 5 kOe. Such simultaneous measurements of small angle scattering and Bragg reflections are quite important for the study of the irreversible process, but cannot be realized with the conventional SANS.

3.3 Studies of small angle Bragg scattering with single crystals

The TOF type small angle scattering machine is particularly suitable for the study on the single crystal, as described in the previous section. In case of small angle Bragg scattering with SAN, the same Bragg reflections around (0,0,0) are detected by different wavelengths at many different positions on the 2D - PSD. A typical example of measurements is provided by the scattering from a single crystal of MnSi which is known to have a helical spin structure with a long period of 180 A along <111> below T_N = 29.5 K.(Ishikawa et al, 1976) Therefore four satellites appear at $\langle q_s, q_s, q_s \rangle$ with q_s = 0.035 A^{-1} as shown in Fig. 15, but in many different positions on the 2D - PSD for different wavelengths. The value of q_s determined with different λ is plotted against λ in Fig. 16(a), which indicates that q_s does not vary with λ. This is the best way to check the accuracy of the position determination of 2D - PSD and the result

indicates it satisfactory. Thus $q_s = 0.035 \pm 0.005$ A^{-1} is determined at 13 K (Ishikawa et al, 1984), in good agreement with a previous measurement with D 11 spectrometer at ILL (Ishikawa et al, 1976). Fig. 16(b) is plotted the intensity of the satellite reflections as a function of λ. The λ dependence of the satellite intensity can be understood, if we consider that the simultaneous detection of four satellites in the (1,1,0) reciprocal plane with the 2D - PSD placed perpendicular to the incident beam is a result of the finite size of the satellites as shown in Fig. 17(a); the Ewald sphere can cross with the satellites even if it does not cross the (1,1,0) plane. Thus the gradual decrease of intensity of the satellites with increasing λ is due to the decrease of overlapping area because of the decrease of the radius of the Ewald sphere. The size of the satellites can be determined directly from the rocking curve which is obtained by rotating the sample around the vertical axis. The rocking curve thus obtained has a FWHM of 2.57 degs as shown in Fig. 17(b), which corresponds to the momentum spread Δq_B of 1.57×10^{-3} A^{-1}. The helical spin structure of MnSi has therefore a coherent length $\xi = 2\pi / \Delta q_B = 4000$ A. The λ dependence of the intensity of satellites can be calculated by using this satellite size and the result of calculation is plotted by a broken line in Fig. 16(b). The agreement between observation and calculation is quite satisfactory, indicating that the satellite size can be determined automatically from the λ dependence of the intensity without rotating the crystal. In Fig.16(c) are plotted the width of satellite $(\Delta q/q)^2$ plotted against $1/\lambda^2$. The solid line is calculated by (22) which takes into account the instrumental resolution as will be discussed later. The agreement

between the observation and calculation is again satisfactory, indicating that the instrumental resolution can accurately be taken into account for SAN. The extrapolation of $\Delta q/q$ to $1/\lambda^2 = 0$ gives in principle the resolution free momentum spread Δq_B, but the previous method (Fig. 16(b)) can make a better determination. Thus a single measurement of Bragg reflections with our SAN provides much more information than that obtained with the conventional SANS.

3.4 Separation of inelastic scattering with a chopper

One of the important problems for small angle scattering is to distinguish the scattering due to the heterogeneity (static origin) from inelastic scattering as magnon scattering. This can in principle be performed by chopping the incident neutrons in front of the sample and by measuring the TOF spectra of the scattered neutrons. Since, however, it looses significantly the neutrons to be used in the experiment and increases the size of data memory bank by one order of magnitude, only few experiments have ever practiced the separation of the inelastic scattering.

Our spectrometer is quite suitable for this purpose. It is enough for us to put a chopper(C_2 in Fig.1(a)) in front of the sample. Our SAN is equipped with two different types of choppers for different purposes. One is a chopper with many windows (Fig. 18(a)) to modulate in time (wavelength) the incident neutrons and another has only one windows (Fig. 18(c)) to monochromatize incident neutrons, both are operated with a frequency of 80 Hz synchronizing with the neutron pulse(20 Hz). The former is used to reject the inelastic part, while the latter for measuring the inelastic scattering as schematically shown in Fig. 18(b) and

(d). One example of the test experiments with the first type chopper is shown in Fig. 19, where the time spectra measured with three different detectors are demonstrated. The upper two figure are the spectra obtained with a fixed counter at the position of 150 degs scattering while the lower two are those with different 1D - PSD by disregarding the positional information to increase the counting rate. The lowest pattern obtained with 22th 1D-PSD shows the time modulation of incident neutrons, thus it corresponds to the pattern of elastic scattering. Except this case, the modulated spectra do not go to zero because of presence of the inelastic part, suggesting that the inelasticity is involved in the scattering. The elastic part can be separated by deconvoluting the modulated part. The energy resolution of the spectrometer with 2D - PSD at 3 m from the sample is about o.6 meV for 4 A. Although the measurement is still in a stage of preliminary test, the method will be applied successfully in some practical problems.

3.5 Separation of magnon scattering without chopper

We have also found that the inelastic scattering as magnon scattering can be separated from the small angle scattering of static origin simply by analyzing the dependence of the scattering functions. The principle is that, in case of elastic scattering, the scattering function is independent of the wavelength of incident neutrons, which is not the case if the inelasticity is involved in the scattering. In case of magnon scattering with a momentum and an energy transfers of q and h_m respectively, the scattered neutron wave vector k_f varies from the incident neutron wave vector k_i as

$$\frac{h^2 k_i^2}{2m} - \frac{h^2 k_f^2}{2m} = \pm\hbar\omega_m \,, \tag{8}$$

$$k_i - k_f = \pm q.$$

Since $\hbar\omega_m = Dq^2$, a simple calculation shows that the scattering occurs within the critical angle ϕ_c given by (Hatherly et al, 1964)

$$\phi_c \cong \frac{\hbar^2}{2m}\frac{1}{D} \,, \tag{9}$$

which is independent of the incident neutron wavelengths. In Fig. 20(a), we plot the small angle scattering from Fe_3Pt for different wavelengths separately against Q, which shows clearly that the scattering at high Q side has a dispersion for different wavelengths, but if we plot the scattering intensity multiplied by k_i^2 against scattering angle θ (Fig.20(b)), all the scattering for different wavelengths fall on a single line suggesting that the small angle scattering at high Q side is due to the magnon scattering. Thus the measurement of the wavelength dependence of the scattering function gives an information on the existence of inelastic scattering and in case of magnon scattering we can separate its contribution from the small angle scattering of other origins, which is difficult to practice with the conventional small angle scattering machine. In this way, we successfully measured the small angle scattering of static origin in Fe_3Pt and the results as well as the detailed method for analysis will be published separately.

3.6 Real Time Spectroscopy

By real time spectroscopy, we mean the measurement of the slow relaxation phenomena with a relaxation time of order of 10^{-3} 1 sec, where the external condition as magnetic field or temperature is varied abruptly and the change of positional correlations which follows is measured in real time. Though this technique can also be applied to the conventional small angle scattering machine at the continuous reactor, the TOF type SANS is more effective than this because of the simultaneous measurement of wide Q range. In order to make the real time spectroscopy possible, the KENS-SAN is equipped with a large external memory bank of 2 M bites so as to make possible the collection of data in eight different conditions sequentially as shown in Fig. 21 which show a preliminary result of measurements of variation of the spin glass state under a pulsed magnetic field. The squared pulsed field of 5 kOe was applied in a certain time interval with a rise time of 10 m sec and the variation of the spin correlations in a typical cluster type spin glass of 0.9Fe-TiO_3-0.1Fe_2O_3 was observed in a time interval of 50 m sec.

This experiment was realized by employing a micro-processor LSI 11/23 and a bulk memory bank of 2M bites. The schematic diagram of the SAN's data acquisition system for this purpose is shown in Fig. 22. The pulsed magnetic field is applied synchronizing with the neutron source and the 2D -PSD data giving the temporal variation of the spacial correlations were sent successively to eight different memory area in the external bulk memory by the control of the μ processor. The system is particularly suitable for studying the nonequilibrium phenomena with relaxation time more than 50 msec. The detailed result of

the relaxation phenomena in the spin glass system will be published in a separate paper.

§4 Design Principle

The design principle of the TOF type small angle neutron scattering spectrometer installed at the pulsed neutron source should be somewhat different from the conventional one because of employing a band of wavelengths. In this section we will discuss this problem based on our experience.

4.1 Neutron Source

The intensity of scattered neutrons with wavelength between λ and $\lambda + \Delta\lambda$, from a sample with cross section , $I(\lambda)\Delta\lambda$ is given in general by

$$I(\lambda)\Delta\lambda = i(\lambda)\Delta\Omega_i \frac{d\sigma}{d\Omega}(\phi) S \Delta\Omega_d \eta_s \eta_d \Delta\lambda \ , \tag{10}$$

where $i(\lambda)\Delta\lambda$ is the intensity of incident neutrons with λ between λ and $\lambda + \Delta\lambda$ and is given by

$$i(\lambda) = \frac{\lambda_T^4}{\lambda^5} \exp(-\lambda_T^2/\lambda^2) \ . \tag{11}$$

λ_T is the characteristic wavelength of the moderator at temperature T defined by

$$\lambda_T = h/\sqrt{2mkT} \ . \tag{12}$$

$\Delta\Omega_i$, and $\Delta\Omega_d$ are the solid angles of initial and final beams respectively. $\Delta\Omega_i$ is given by squares of $\Delta\theta$: angular resolution of the incident beam. If we define the momentum resolution ΔQ, by the request of the measurement, $\Delta\theta$ depends on λ and is given

by

$$\Delta\theta = \frac{\lambda}{2\pi}\Delta Q \ , \tag{13}$$

while in the 2D-PSD, $\Delta\Omega_d$ can be determined so as to satisfy the relation

$$\frac{d\sigma}{d\Omega}(\phi)\ \Delta\Omega_d = \frac{d\sigma}{d\Omega_Q}(Q)\Delta Q^2 \ , \tag{14}$$

independent of λ. $d\Omega_Q$ being the solid angle in the Q space, η_s is the scattering efficiency at the sample and may be proportional to $1/\lambda$, if the neutron absorption by the sample obeying the 1/v law. The detecting efficiency η_d can be assumed as 1 for cold neutrons. $\Delta\lambda$ is determined by the TOF time channel width Δt_c and can be selected to satisfy.

$$\frac{\Delta\lambda}{\lambda} = \frac{\Delta t_c}{t} \cong \frac{\Delta Q}{Q} \ . \tag{15}$$

If $\Delta Q/Q$ is selected to be 0.1, Δt_c can be much longer than the neutron pulsed with Δt_m which is about 150 μ sec for λ = 6 A, t, total flight time being an order of 30 msec.

Finally by assuming that $d\sigma/d\Omega_Q$ is independent of λ, the λ dependence of the scattered neutrons $I(\lambda)$ in Eq(10) is reduced to be

$$I(\lambda) = \frac{\lambda_T^4}{\lambda^4} e^{-\lambda_T^2/\lambda^2} C(\Delta Q)^4 \ . \tag{16}$$

The optimal wavelength λ_{opt} giving the maximum intensity is therefore given from $dI/d\lambda = 0$ to be

$$\lambda_{opt} = \frac{1}{2^{1/4}} \lambda_T \cong 0.84 \lambda_T \cdot \quad (17)$$

The incident neutron collimation $\Delta\theta_{col}$ is determined as

$$\Delta\theta_{col} = 2 \cdot \frac{\lambda_{opt}}{2\pi} (\Delta Q)_{min} , \quad (18)$$

since ΔQ_{min} is usually determined referring to the smallest Q value. The total scattered neutron intensity $I_T(\lambda_T)$ in case of employing the incident neutrons with λ between λ_{min} and λ_{max} is given by

$$I_T(\lambda_T) = C \int_{\lambda_{min}}^{\lambda_{max}} I(\lambda) d\lambda \cong C \lambda_T^4 \int_0^{\infty} \frac{1}{\lambda^4} \exp(-\lambda_T^2/\lambda^2) d\lambda = C\sqrt{\pi} \lambda_T . \quad (19)$$

The result indicates that even in case of the TOF type small angle scattering machine which utilizes all wavelengths, it is preferable to use the cold neutron source. Note that the peak intensity is higher for the normal moderator than the cold moderator as shown in Fig. 23 where the neutron spectra from the KENS normal moderator (polyethylene plate at 295 K) and cold moderator (solid CH_4 at 20 K) are compared in a normalized scale.

Note also that, in case of small angle scattering machine at the steady state reactor, the employment of the cold neutrons is indispensable to avoid the multiple Bragg scattering, but the TOF small angle scattering machine inevitably uses the shorter wavelength than the Bragg cut off in order to expand the dynamical range of measurements. The effect of multiple Bragg scattering can be estimated because of making the same measurement with longer wavelengh. Therefore the neutron source spectra should

have good intensities for both of shorter (λ < 4 A) and longer wavelengths. The cold moderator is better than thermal one to satisfy this condition.

4.2 Neutron Guide

In case of the continuous reactor, it is preferable that the SANS is installed at the exit of the bent neutron guide, because it significantly reduces the background. This principle is not necessarily applicable to the TOF-SANS with the pulsed neutron source because the background due to the high energy neutrons can automatically be separated from the signal by time channels. The first merit of using the guide tube is to conserve the beam divergence in long distance. The situation is demonstrated in Fig.24. If we don't use the neutron guide, the beam divergence $(\Delta\theta)^2$ is determined by the solid angle $(\Delta\theta_m)^2$ which the cold moderator spans to the sample;

$$(\Delta\theta_m)^2 = \frac{h \cdot w}{\ell_s^2} \quad . \tag{20}$$

In case of KENS cold moderator with h_{eff} = 10 cm and w_{eff} = 8 cm, the solid angles for ℓ_s = 9 m is given by 98.8 $(mrad)^2$ and for ℓ_s = 19 m, 4.8 $(mrad)^2$ assuming the cross section of flight path to be 3 cm^w x 5 cm^h, independent of λ. If the neutron guide with Ni coated mirror is employed, the critical angle $\theta_c(\lambda)$ being given by

$$\theta_c(\lambda) = 1.73 \times 10^{-3}\lambda \ (A) \quad . \tag{21}$$

The beam divergence is then determined by the collimator $\Delta\theta_{col}$ for longer wavelength and for λ for which $\theta_c(\lambda) < \Delta\theta_{col}$, the

divergence follows a $\theta_c(\lambda)$ line in Fig. 24 and for $\theta_c(\lambda) < \Delta\theta_m$, the divergence becomes equal to the direct glancing angle $\Delta\theta_m$, independent of λ. In case of the bent guide tube with cut off wave length λ_c (4 A in case of KENS), there is a steep decrease of intensity of neutrons with λ less than λ_c as shown by solid lines in Fig. 24. The difference in total intensity on the sample in three cases of without guide (NG), with straight guide (SG) and bent guide at the positions of 9 m and 19 m are more clearly seen in Fig. 25, where the energy spectra of these three cases are plotted against λ. We can see clearly that the neutron guide significantly increases the neutron total intensity and the gain in the intensity for the straight guide against the bent guide in the short wavelength region becomes also more significant for shorter ℓ_s. Therefore if the fast neutrons contribution to the background is not important, it is better to install the SANS spectrometer as close as possible to the source by using the straight guide. In KENS we finally adopted the bent guide because of the unknown factor for the background coming from fast neutrons. This choice was found successful and we have encountered no troubles for the background even if the 2D - PSD has no shield as described in the previous section. If the emphasis is put on the lower Q measurements, our choice would be still correct, because no difference in the intensity appears for longer λ which is important for low Q measurements.

4.3 Resolution

In the TOF-SANS, it is better to define the resolution not by $\Delta Q/Q$, but by ΔQ, because the incident neutron collimation $\Delta\theta_{col}$ being fixed, the incident neutron resolution $\Delta Q/Q$ varies

with λ. The total momentum transfer resolution ΔQ is given by

$$\Delta Q^2 = \left(\frac{\Delta\lambda}{\lambda}\right)^2 Q^2 + \left(\frac{\Delta\phi}{\phi}\right)^2 Q^2 + \Delta Q_{anal}{}^2$$
$$= \left(\frac{2\pi}{\lambda^2}\phi\right)^2 \Delta\lambda^2 + \left(\frac{2\pi}{\lambda}\right)\cdot(\Delta\theta^2{}_{col} + \Delta\theta^2{}_{det}) + \Delta Q_{anal}{}^2 , \quad (22)$$

where the last term $\Delta Q^2{}_{anal}$ is the momentum resolution introduced in a process of data analysis. Since $\Delta\lambda$ (time resolution) and $\Delta\theta_{det}$ (positional resolution on 2D-PSD) as well as ΔQ_{anal} should be chosen so as to match to $\Delta\theta_{col}$ in data analysis, it is better to select the original time and PSD channel widths as small as possible. Eq(22) shows that for a given ΔQ^2, $(\Delta Q/Q)^2$ varies with as $1/\lambda^2$ as actually found in the measurement of Bragg reflections (Fig. 16c). Note that the slope of the solid line in this figure is determined not by $\Delta\theta_{det}$ by ΔQ_{anal}.

§5. Conclusion

The TOF type small angle scattering machine SAN we have installed at KENS cold neutron source has been proved to be a unique and useful machine, having provided many interesting results in many fields of sciences in this four years. Note that the cold neutron source of KENS is very small; it is cooled by a small refrigerator of 40 W (15 K). The machine is particularly powerful for the study of nonequilibrium phenomena because of its unique ability for the wide Q measurements. The separation of inelastiac scattering will be another promising aspect of this spectrometer. We should also remark that the machine was also found to give good results for the studies of polymer (Okano et al, 1983) and biological materials (Hirai, 1985) in solution. One reason is that the contrast matching of solvent can

accurately be realized by measuring the λ dependent transmission (Hirai et al, 1985). We believe that the utility of this type of SANS will be increased more by further studies.

Although we have thus found that our SAN is quite satisfactory, we suggest that the installation of SAN directly to the straight guide from the cold neutron source would give a better performance, which we would like to test one day. Finally we should also remark that the TOF-SANS should be installed as close as possible to the source to avoid the frame overlapping problem and the improvement of the positional resolution of 2D-PSD is indispensable for it.

Acknowledgement

The authors would thank H. Sasaki, N. Watanabe and Y. Endoh for their interests and encouragements. Their thanks are also due to S. Ikeda for his assistance in construction in the early stage and to all members of the SAN's machine group, particularly to K. Kurita, S. Yamaguchi, Y. Fujino and M. Hirai for their collaborations in the measurements.

References

Arai, M., Ishikawa, Y., Saito, N. & Takei, H. (1985 a)
J. Phys. Soc. Jpn 54 781 - 794.

Arai, M. & Ishikawa, Y. (1985 b)
J. Phys. Soc. Jpn 54 795 -802.

Berlinger, R., Mildier, D.F.R., Pringle, O.A. & King, J.S. (1985)
Nucl Instru. Meth. 185 481 - 495.

Borso, C.S., Carpenter, J., Williamson, F.S., Holmblad, G.L.
Muller, H., Faber, J.Jr., Epperson, J.E. & Danyluk, S.S.(1982)
J. Appl. Cryst. 15, 443 - 448.

Cer L. (1975), Neutron Scattering for the Analysis of Biological Structures pp. V113 - V1129. BNL Report - 50453, BNL, New York, USA.

Furusaka, M., Ishikawa, Y., Yamaguchi, S & Fujino, Y. (1983)
Physica 120B 383 - 386.

Furusaka, M., Ishikawa, Y. & Mera, M. (1985 a)
Phys. Rev. Letts 17 2611.

Furusaka, M., Arai M. & Ishikawa, Y. (1985 b)
J. Appl. Cryst. succeeding paper.

Hatherly, M., Hirakawa, K., Lowde, R.D., Malett, J.F.,
Stringfellow, M.W. & Torrie B.H. (1964)
Proc. Phys. Soc. 84 55 - 62.

Hirai M. (1985), Neutron Small Angle Scattering Study of Nucleosome Core, ph. D. Thesis Tohoku Univ.

Ikeda, S., Ishikawa, Y. and Inoue, K. (1981)
Proc ICANS- IV, KENS Report II, 200 - 209, KEK, Tsukuba, Japan.

Ishikawa, Y., Tajima, K., Bloch, D. & Roth, M. (1976)

Solid State Commu. 19 525 - 528.

Ishikawa, Y., Furusaka, M., Arai, M., Niimura, N., Ikeda, S. & Hasegawa, K. (1980), KENS Report 1, 101 - 126, KEK, Tsukuba, Japan.

Ishikawa, Y. (1983), Physica 120 B 3 - 14.

Ishikawa, Y. & Arai, M. (1984) J. Phys. Soc. Jpn 53 2726 - 2733.

Kosterez, G. (1979) Treatise on Materials Science and Technology Vol 15, Neutron Scattering, ed. by Kostorz, G. pp 227 - 289, Acad. Press. London, UK.

Okano, K., Kurita, K. Nakajima, S. Wada, E., Furusaka, M. & Ishikawa, Y. (1983) Physica 120 B 413 - 417.

Figure Captions

Fig. 1 Layout of KENS SAN (a) overall arrangement and (b) around sample and detector chambers.

Fig. 2 (a) Photograph of SAN's vacuum scattering chamber and (b) 2D position sensitive detector installed inside the vacuum chamber.

Fig. 3 Ranges of wave vector Q measured with SAN. Solid lines are ranges covered by single counters, while broken lines are those by 2D-PSD installed at four different positions.

Fig. 4 SAN's vacuum scattering chamber with a special vacuum shutter to separate the sample chamber from the detector chamber.

Fig. 5 Scattering intensities from water detected by 2D-PSD in cases of (a) employing a movable beam stopper hung from the top and (b) adopting a new beam stopper described in the text.

Fig. 6 (a) A new movable beam stopper system composed of a large thin Al plate of 0.4 mm with a Cd beam stopper at the center. The Al plate can be moved horizontally by an electric device. (b)its photograph.

Fig. 7 Principle of converging Soller collimator system (a) in converging condition and (b) in non converging condition.

Fig. 8 SAN's converging Soller slits designed for 5 m 2D-PSD.

Fig. 9 Direct beam profiles without Soller(lower figures) and with (upper figures) converging Soller collimators.

Fig. 10 Comparison of backgrounds with signals from SiC sample

detected by 5 m 2D-PSD in case of with only thin Al windows, Si single crystal windows and without any window materials (BG).

Fig. 11 Comparison of background with signal from water detected by 5 m 2D-PSD.

Fig. 12 Block diagram of data processing system for TOF-2D-PSD.

Fig. 13 Temporal variation of scattering functions measured with SAN for $Fe_{60}Cr_{40}$ at room temperature in a process of phase separation ,when the sample was annealed at T_a = 550 C. (Furusaka et al. 1983).

Fig. 14 Simultaneous measurements of (a)small angle scattering and (b) and (c) Bragg reflections from a single crystal of $90FeTiO_3$-$10Fe_2O_3$ which exhibits a typical characteristics of cluster type spin glass. (Arai et al 1985 a) Detector configuration is shown on the reciprocal lattice plane in a upper left part of the figure.

Fig. 15 Four satellite reflections from MnSi at 15 K around (0,0,0) in the (0,1,1) reciprocal plane. The satellites along [1 0 0] and [0 1 1] would be multiple reflections.

Fig. 16 (a) Wavelength dependence of satellites position q_s, (b)integrated intensity of satellites I, and (c)linewidth of satellites $\Delta q/q$. A broken line in (b) and solid line in (c) are calculated (see text).

Fig. 17 Observation of satellites in the (0,1,1) plane by neutrons with different wavelengths impinging perpendicular to the plane. (a) Ewald spheres and satellites with finite sizes. (b) Rocking curve (open circles) of a satellite obtained with a single wavelength by rota-

ting the crystal around a vertical axis.

Fig. 18 Second chopper C_2(Fig. 1) for inelastic scattering. (1) chopper for rejecting inelastic scattering and (2) chopper for measuring inelastic scattering.

Fig. 19 Time modulation of small angle scattering from Fe_3Pt at room temperature when a chopper of the first type in Fig. 18 was operated. (a) time spectra at 150° counter, (b) a part of (a) indicated by a horizontal line is plotted in an enlarged scale. (c) time spectra of 24th 1D-PSD, where positional information was disregarded. (d)time spectra of direct beam obtained with 22th 1D-PSD which corresponds to the case of elastic scattering.

Fig. 20 (a) Small angle scattering from Fe_3Pt, plotted against Q for different wavelengths, (b) that plotted against scattering angle .

Fig. 21 Time variation of small angle scattering from $90FeTiO_3$-$10Fe_2O_3$, when a squared pulsed magnetic field of 5 kOe was applied to the sample.

Fig. 22 Block diagram of data acquisition system for real time spectroscopy.

Fig. 23 Energy spectrum of solid methane cold moderator at 20K, compared with that of polyethylene plate at 295 K.

Fig. 24 Beam divergence of neutrons with and without guide and with an appropriate collimator.

Fig. 25 Wavelength dependence of neutron intensity at different positions. SG(9m) (SG(19 m)): at the exit of straight neutron guide 9m (19 m), far from cold neutron source, BG: at the exist of bent guide with a cut off wavelength λ_c = 4 A. NG: at the position of 19 m far from cold moderator, but without guide.

KENS-SAN Arrangement

(a)

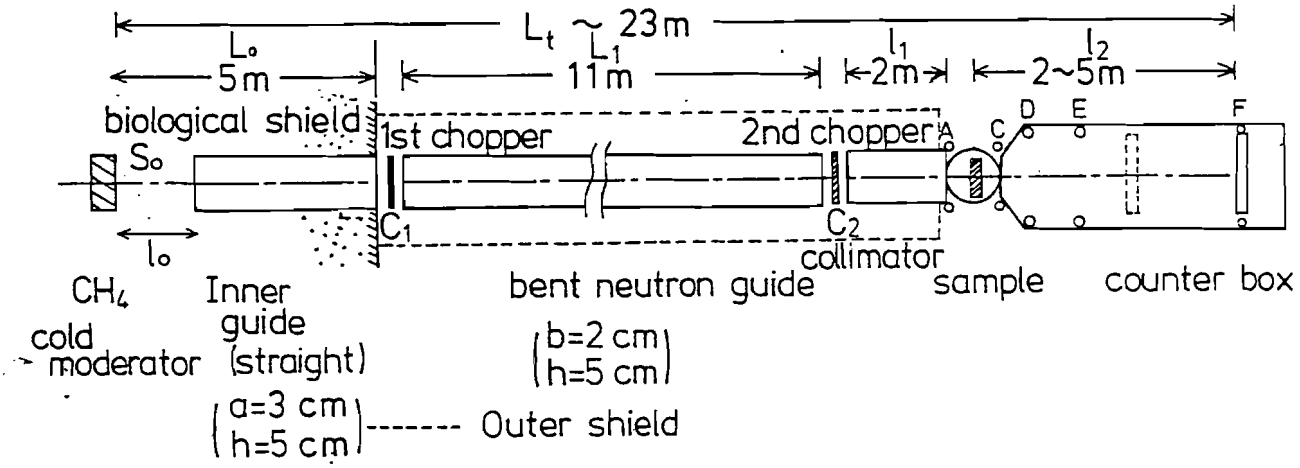

(b)

A-E ; fixed ^{3}He counter

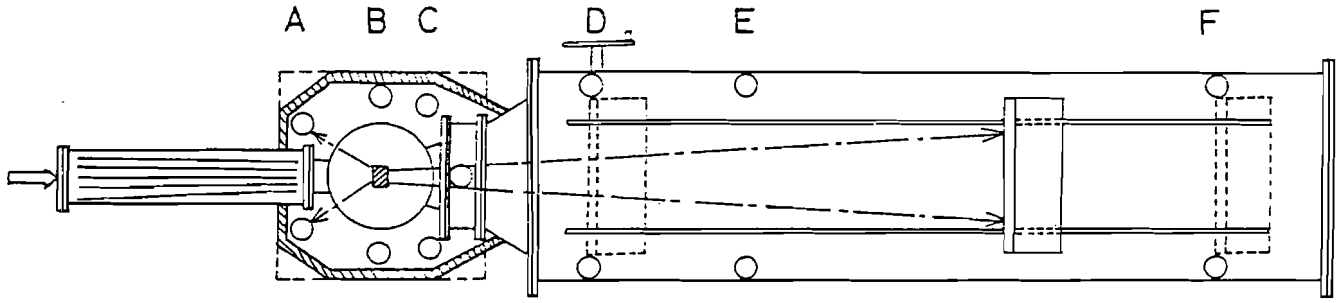

Sample case

Converging Soller collimator

Vacuum shutter

Vacuum chamber

2D-PSD

Fig. 1

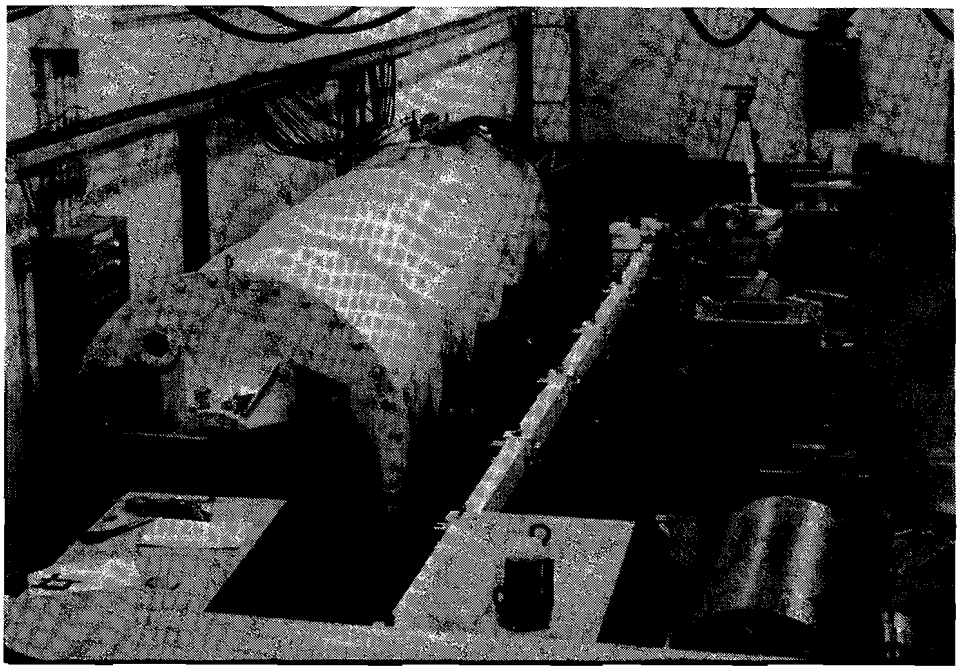

(a)

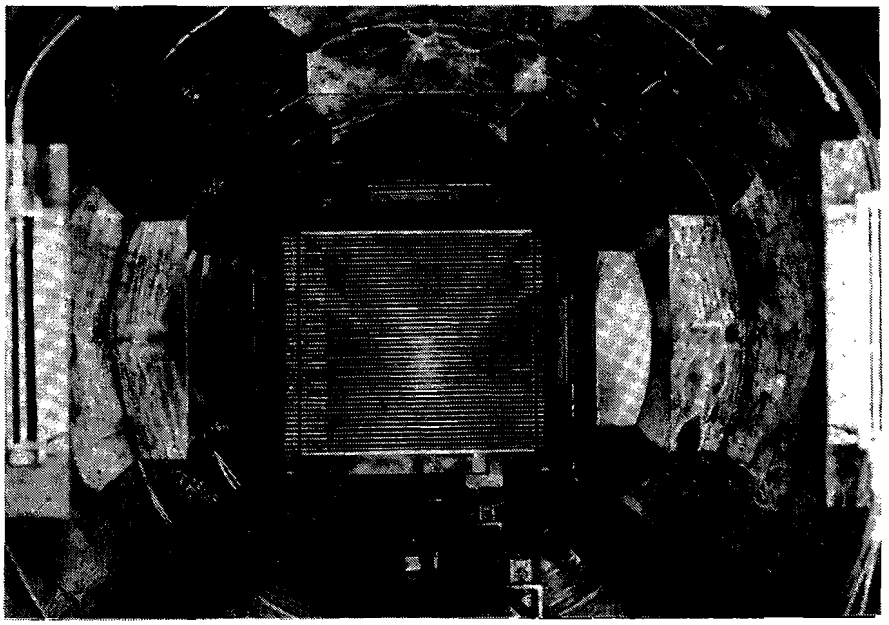

(b)

Fig. 2

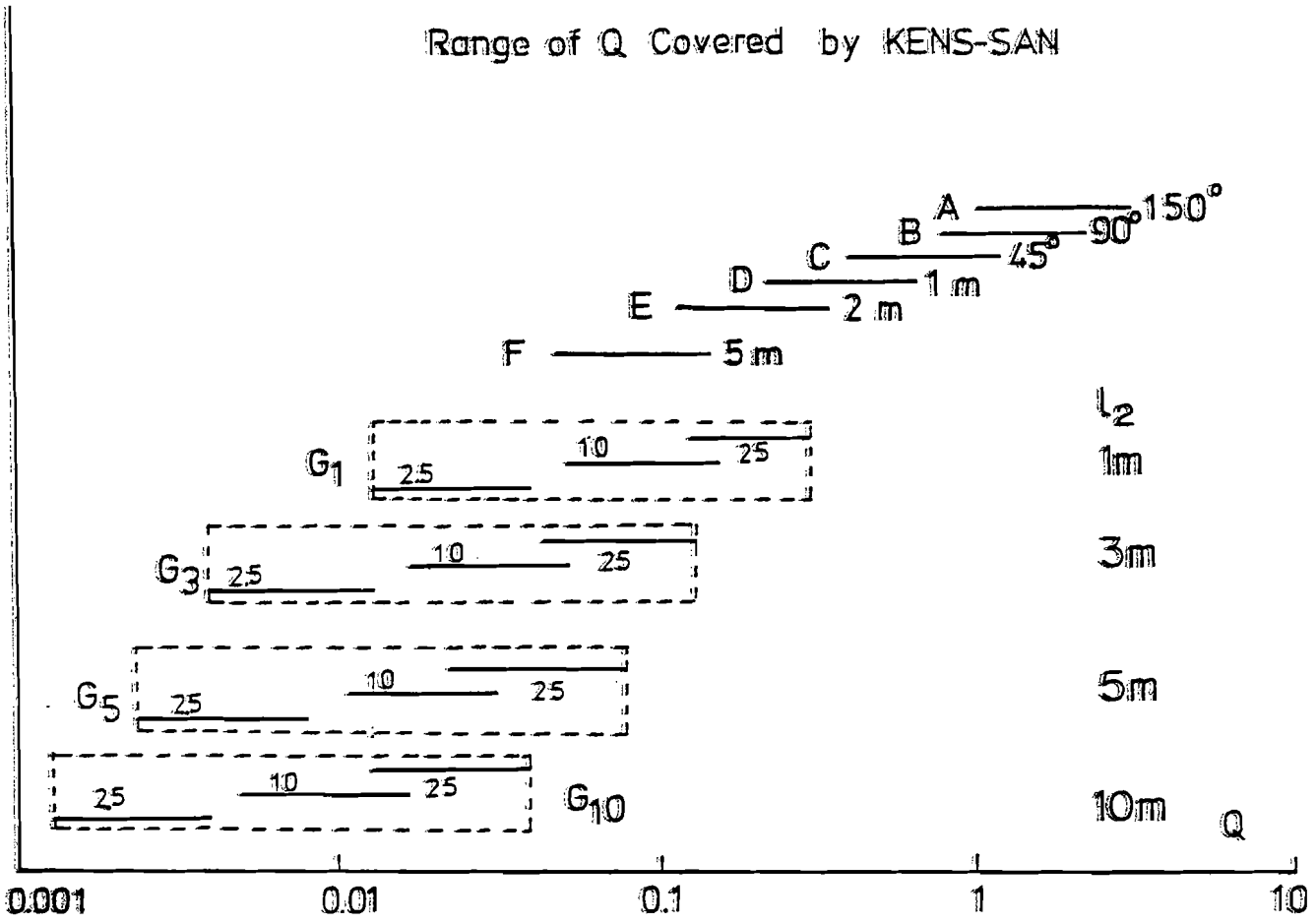
Range of Q Covered by KENS-SAN
A
150°
B
90°
C
45°
D
1 m
E
2 m
F
5 m
L_2
G_1
1m
G_3
3m
G_5
5m
G_{10}
10m
25
10
25
Q
0.001
0.01
0.1
1
10

Fig. 3

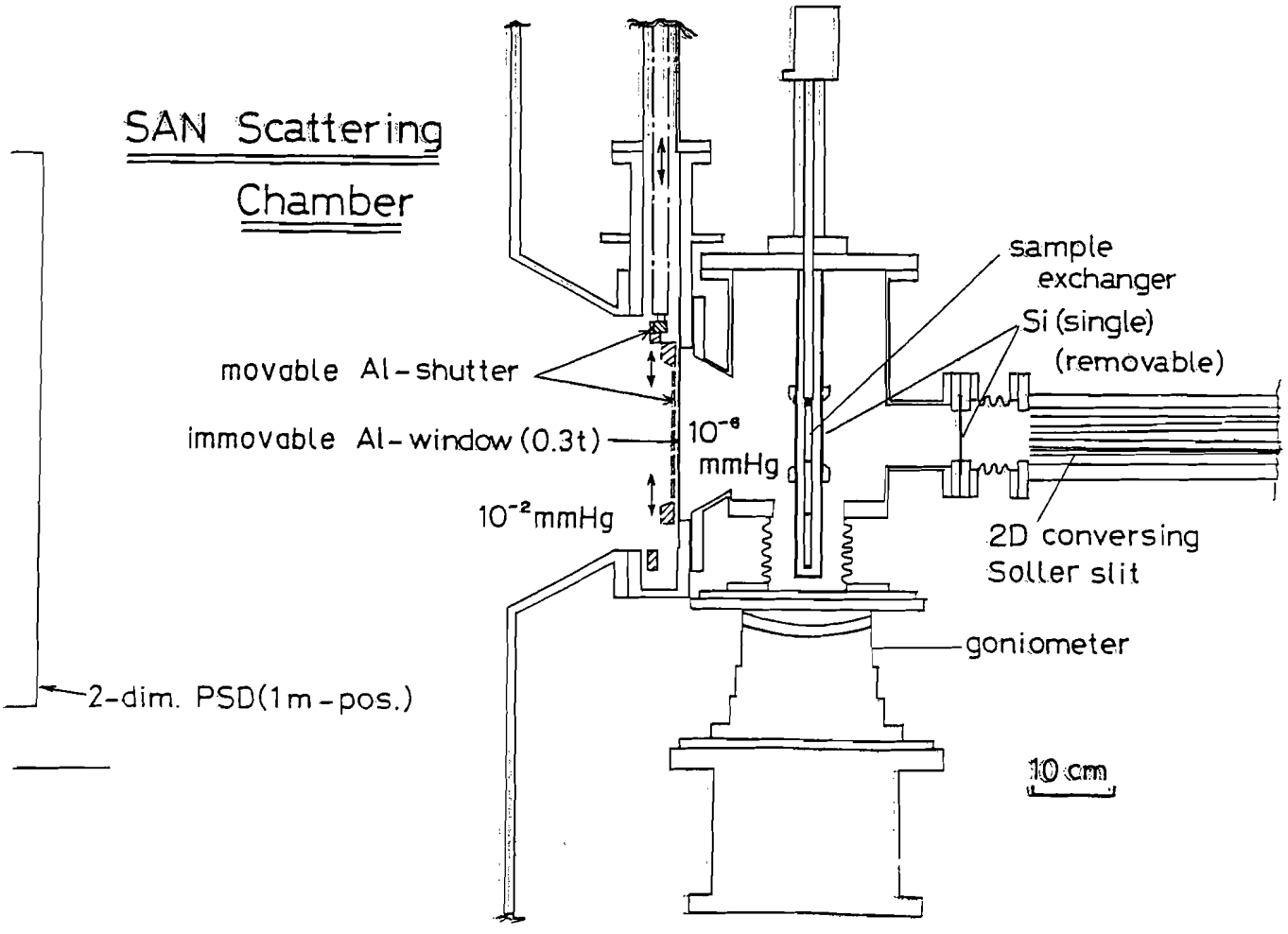
SAN Scattering
Chamber
sample
exchanger
Si (single)
(removable)
movable Al-shutter
immovable Al-window (0.3t)
10^{-6}
mmHg
10^{-2}mmHg
2D conversing
Soller slit
goniometer
2-dim. PSD(1m-pos.)
10 cm

Fig. 4

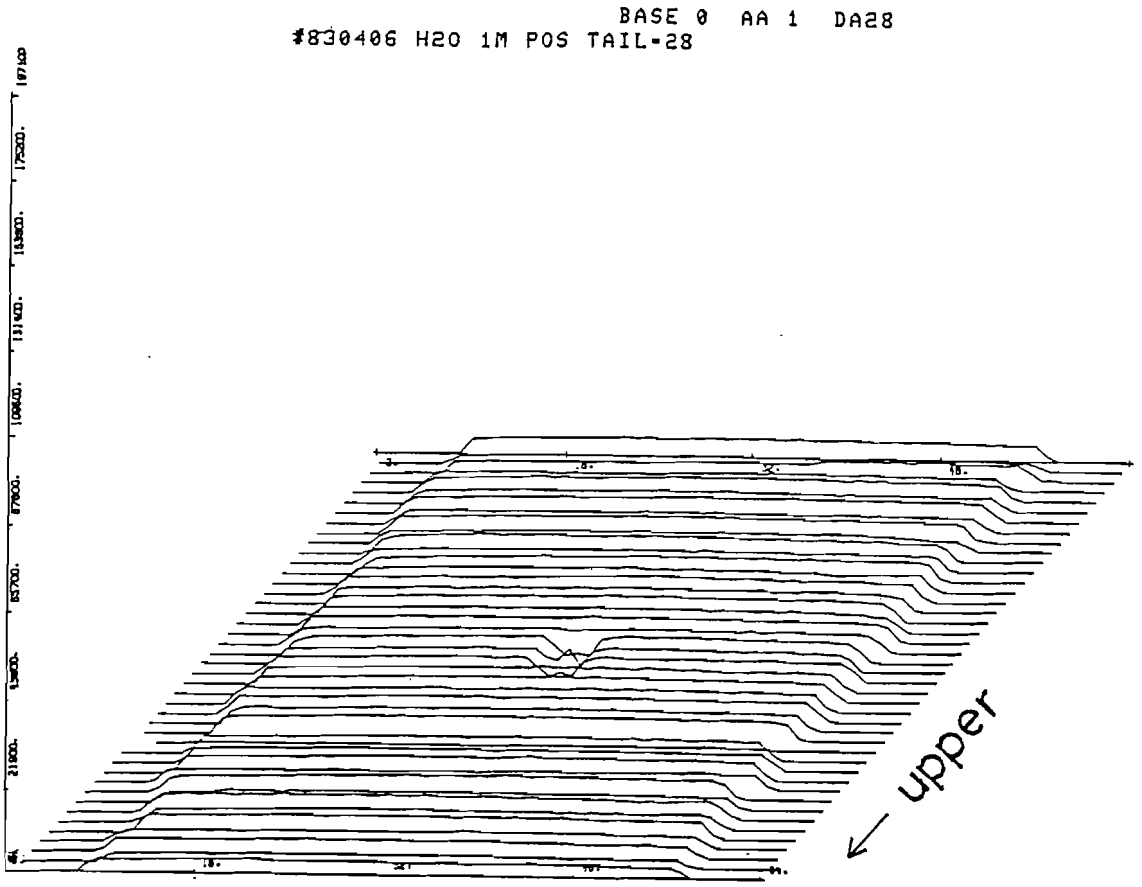

(b)

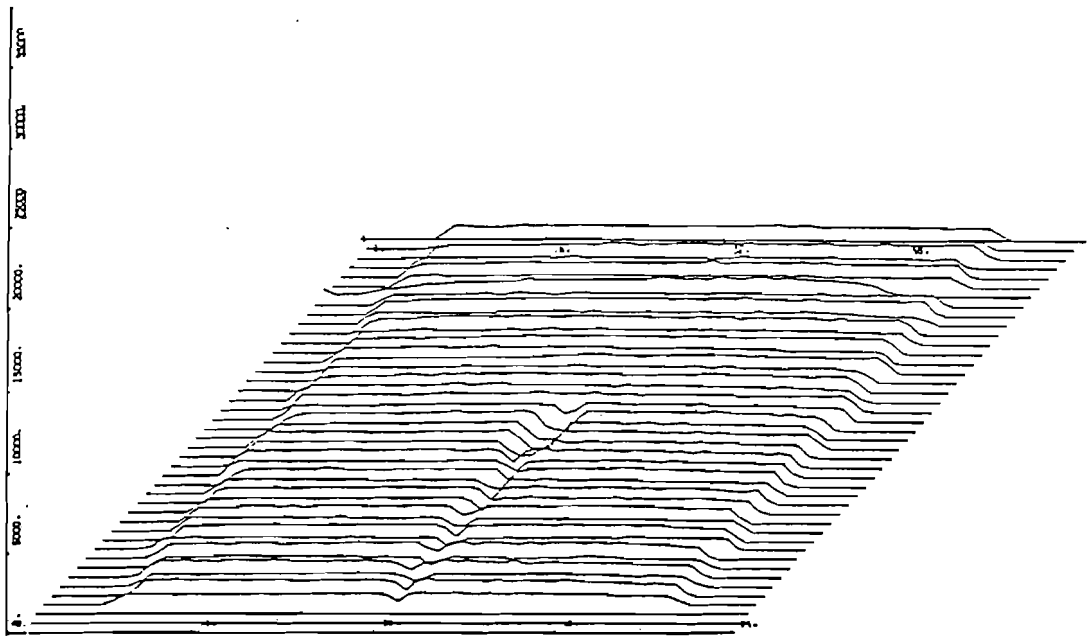

(a)

Fig. 5

(a) SAN 2-dim. PSD & Beam Stopper

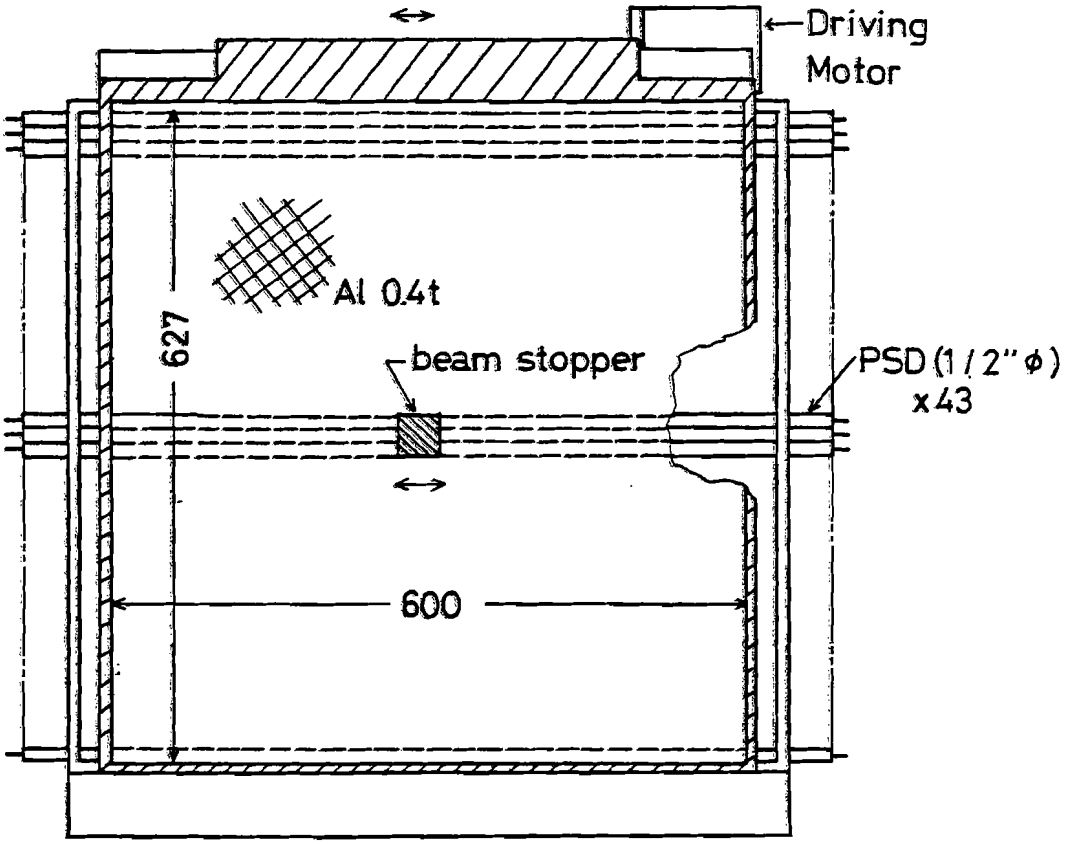

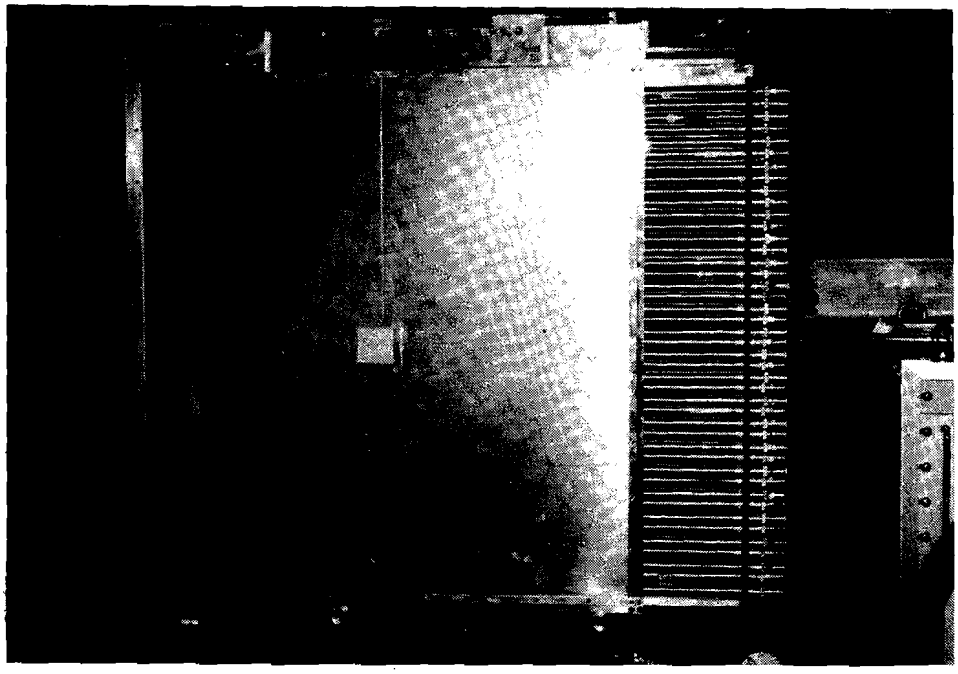

Fig. 6

(a) Converging Slit Collimator System.

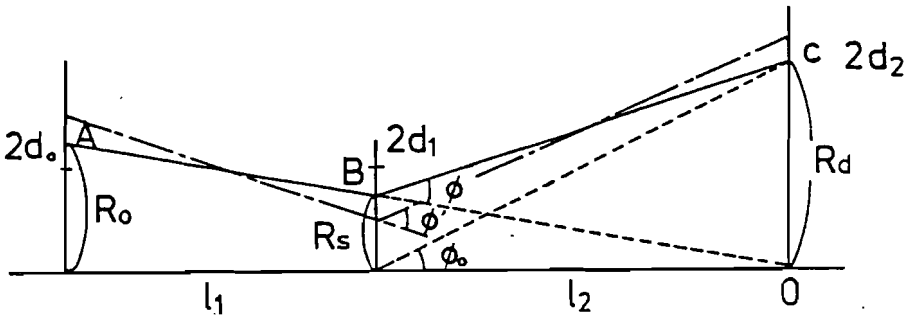

(b) Non Converging Condition

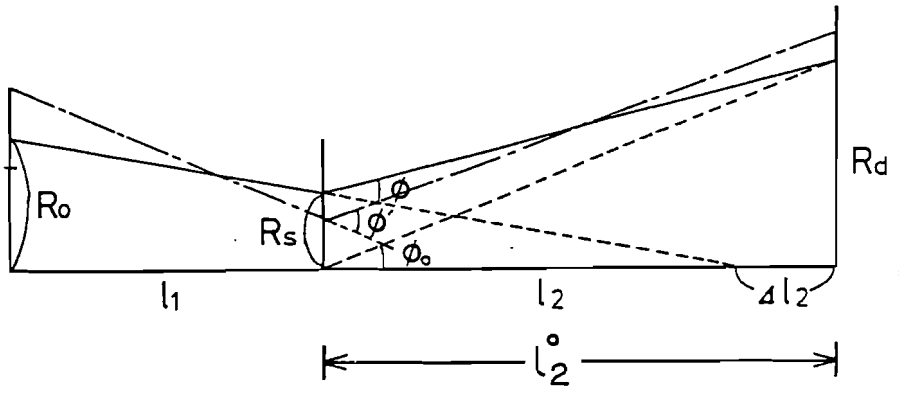

Fig. 7

KENS-SAN CONVERGING SOLLER SLIT

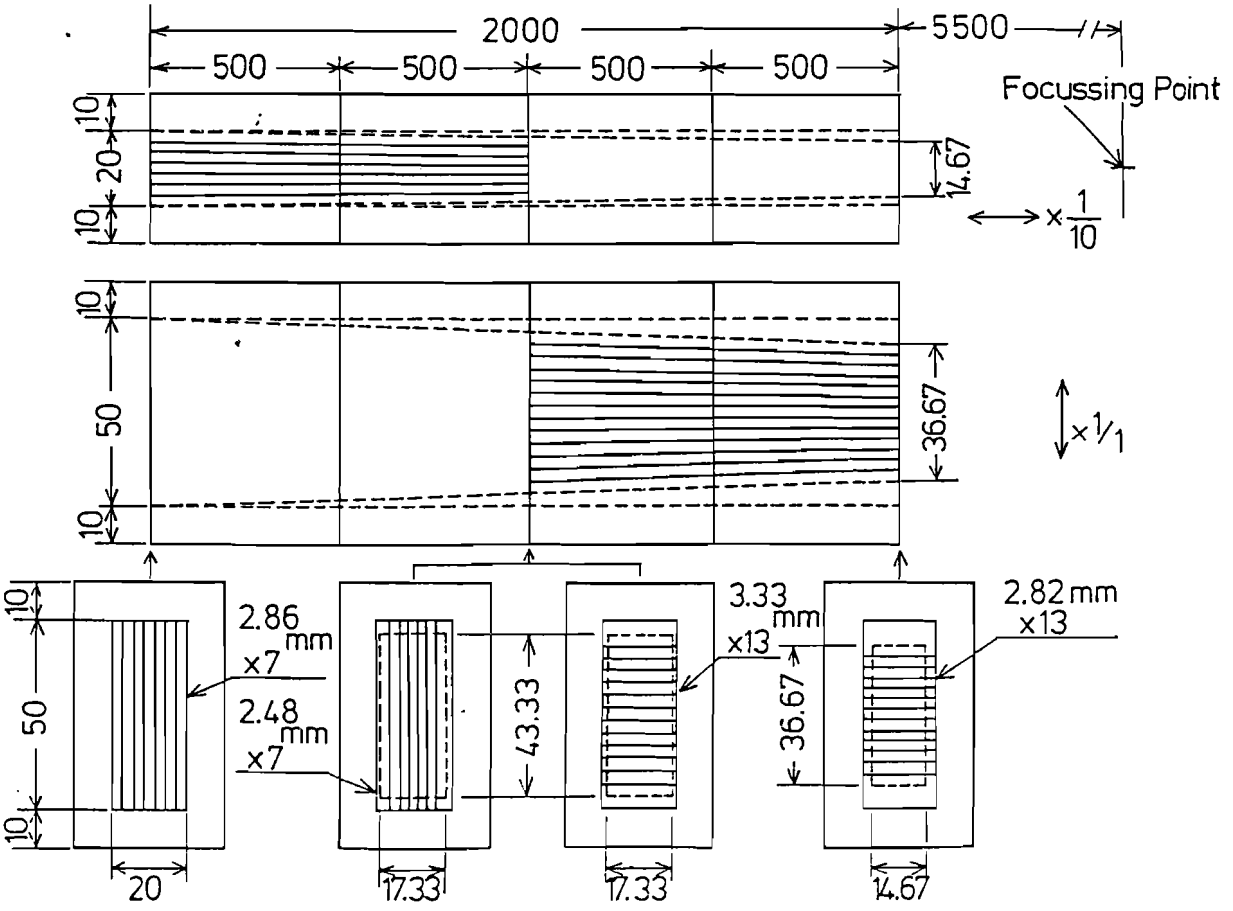

Fig. 8

Direct Beam Profiles

(5 m position)

with collimator

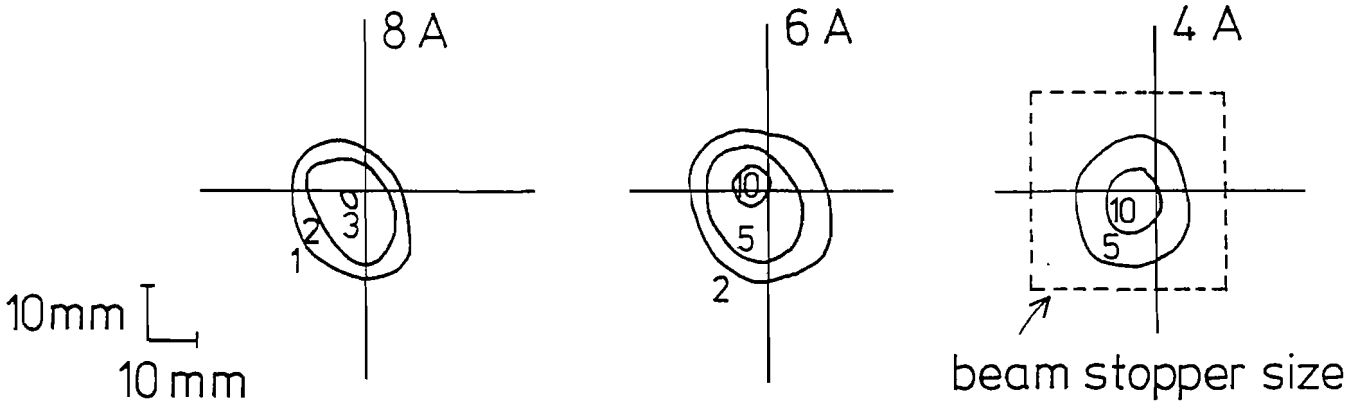

without collimator.

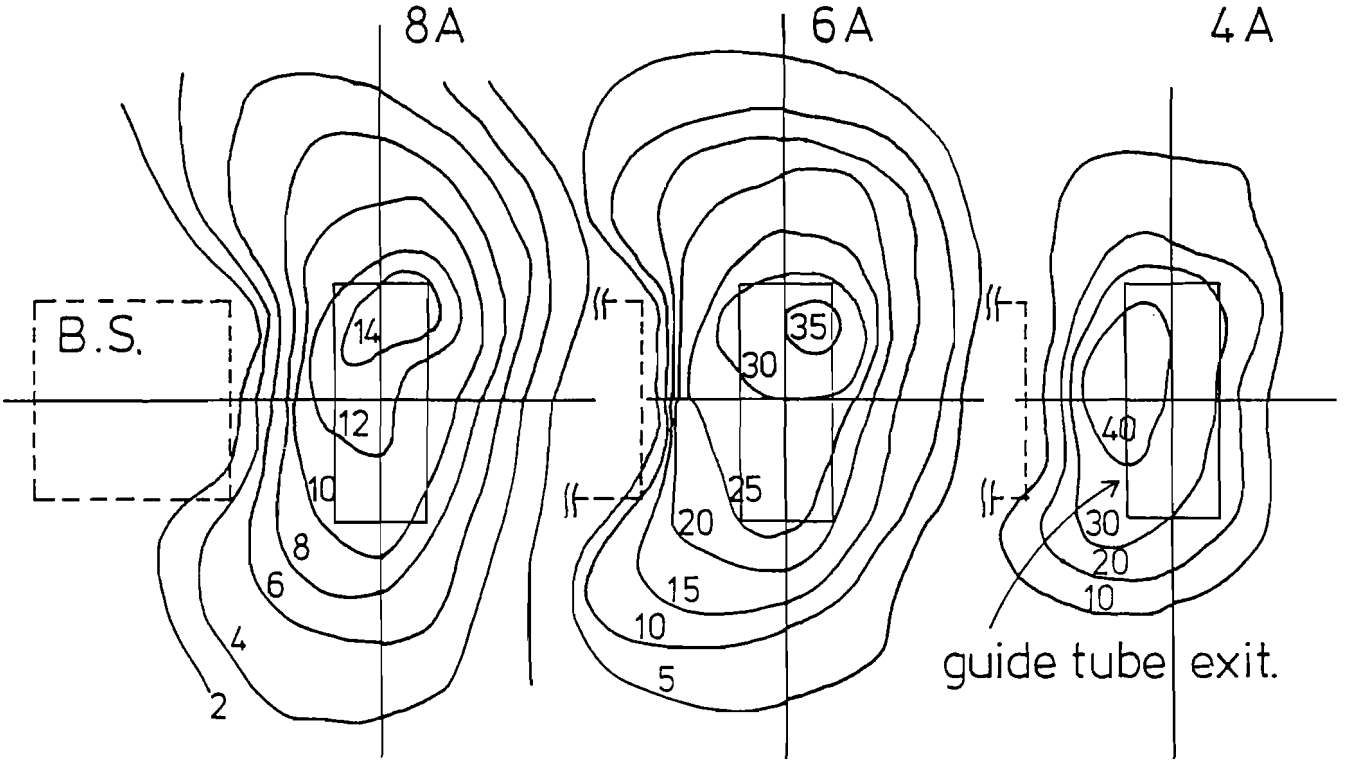

Fig. 9

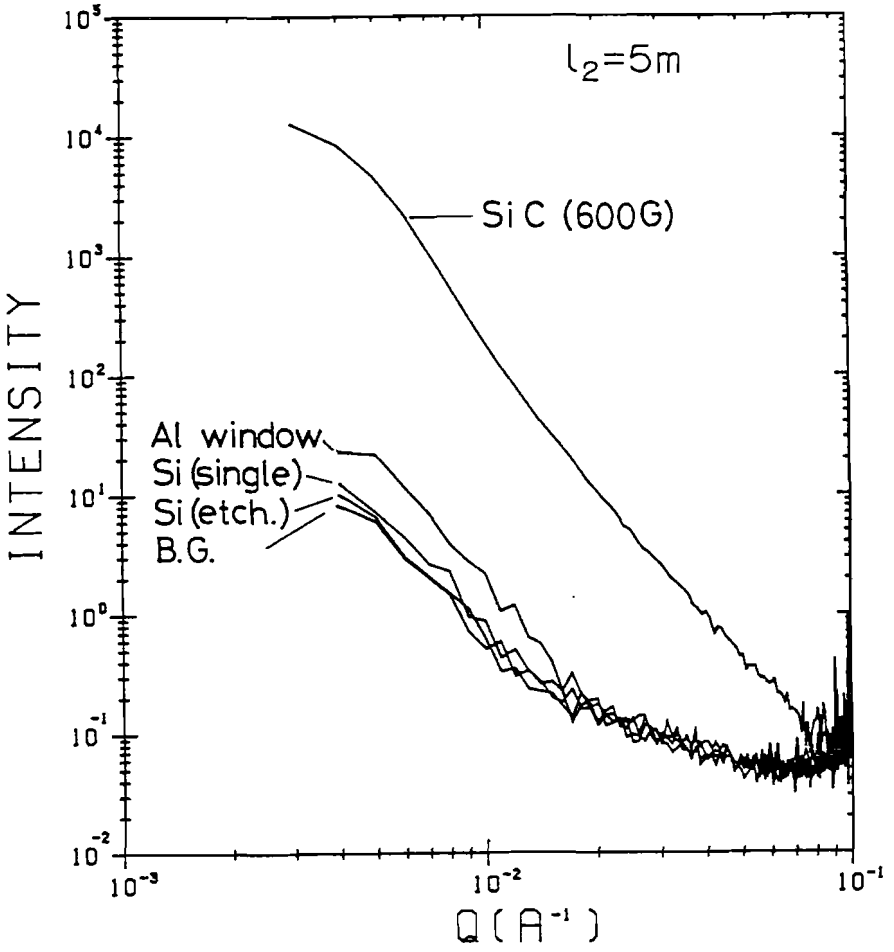
l_2=5m
Si C (600G)
Al window
Si (single)
Si (etch.)
B.G.
INTENSITY
Q(Å^{-1})

Fig. 10

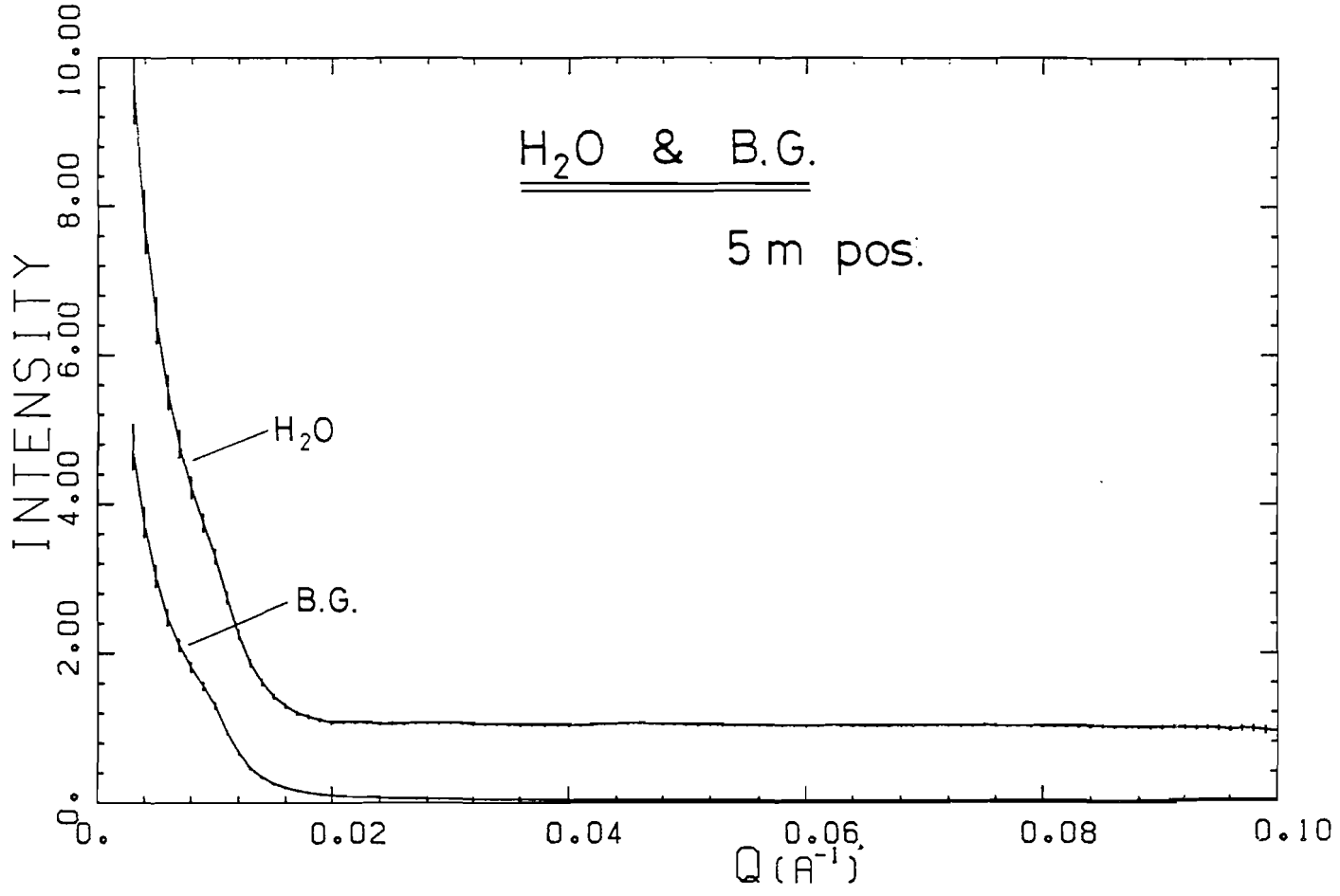
H_2O & B.G.
5 m pos.
H_2O
B.G.
INTENSITY
Q(Å^{-1})

Fig. 11

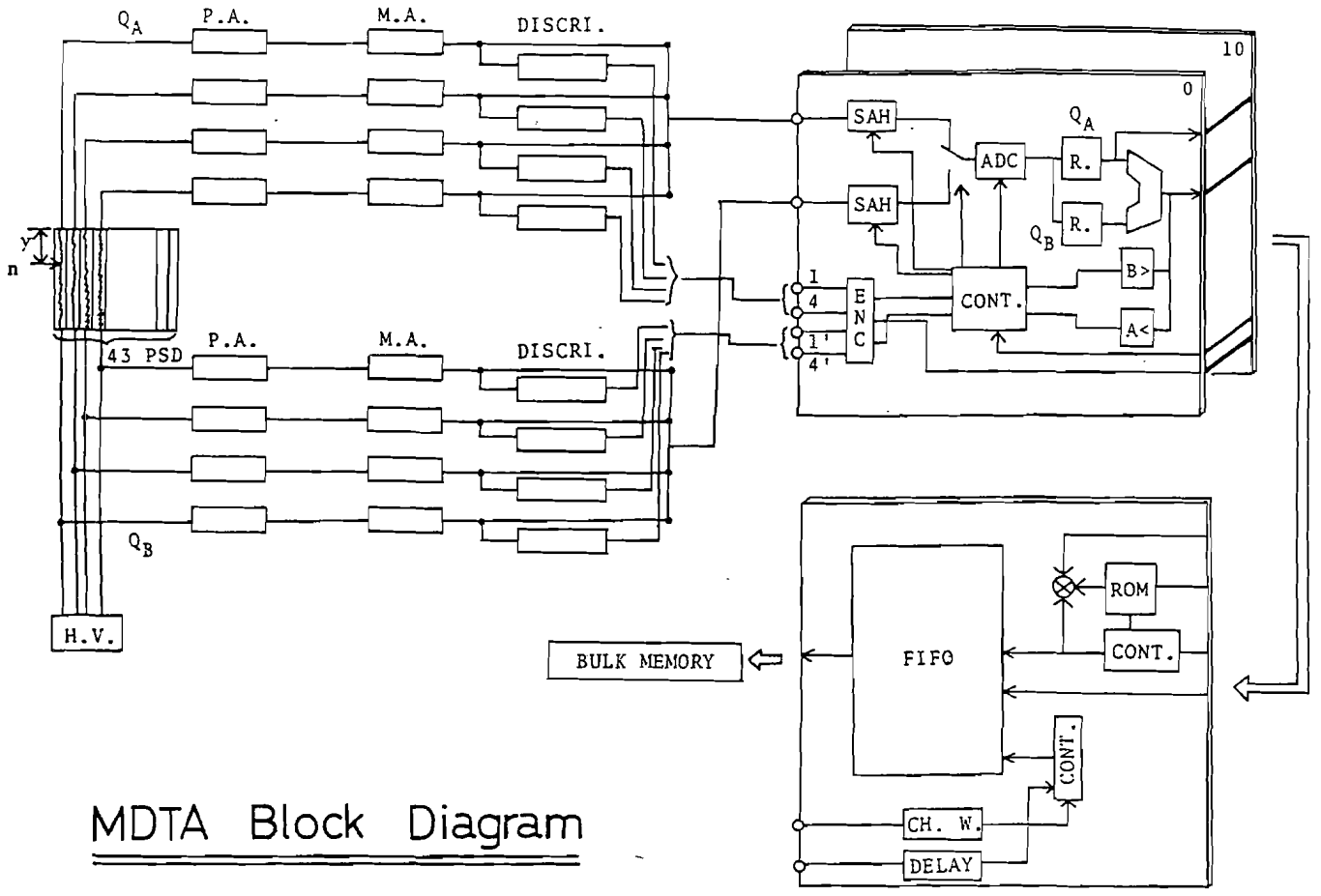
Q_A
P.A.
M.A.
DISCRI.
10
0
SAH
SAH
ADC
Q_A
R.
R.
Q_B
B>
A<
CONT.
1
4
E
N
C
1'
4'
y
n
43 PSD
P.A.
M.A.
DISCRI.
Q_B
H.V.
BULK MEMORY
FIFO
ROM
CONT.
CONT.
CH. W.
DELAY
MDTA Block Diagram

Fig. 12

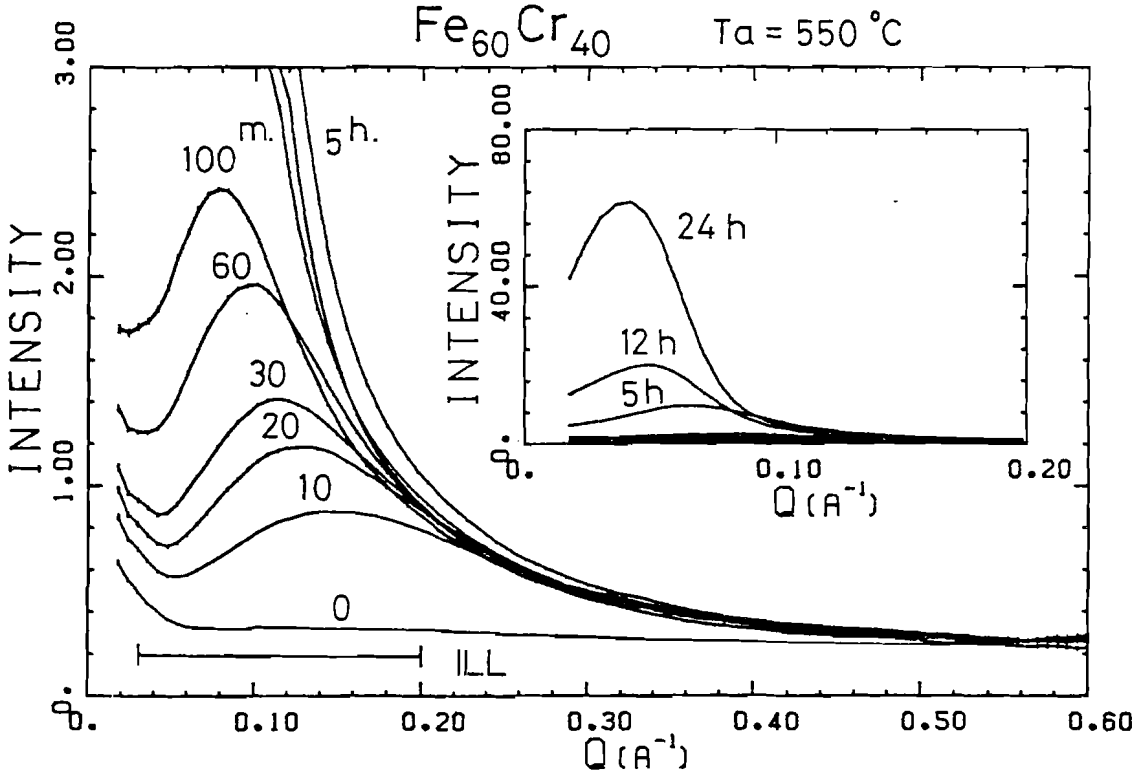
Fe60Cr40
Ta = 550 °C
INTENSITY
3.00
2.00
1.00
0.
100 m.
5 h.
60
30
20
10
0
ILL
0.10
0.20
0.30
0.40
0.50
0.60
Q (A^-1)
80.00
40.00
24 h
12 h
5h
0.10
0.20

Fig. 13

$90FeTiO_3-10Fe_2O_3$

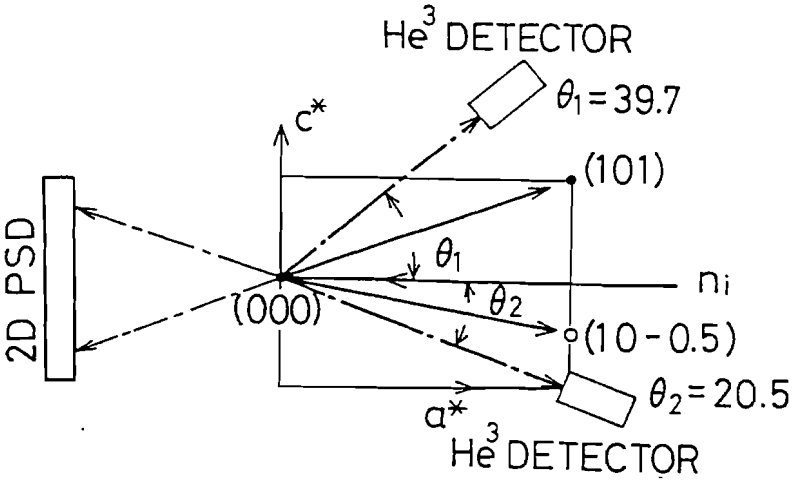

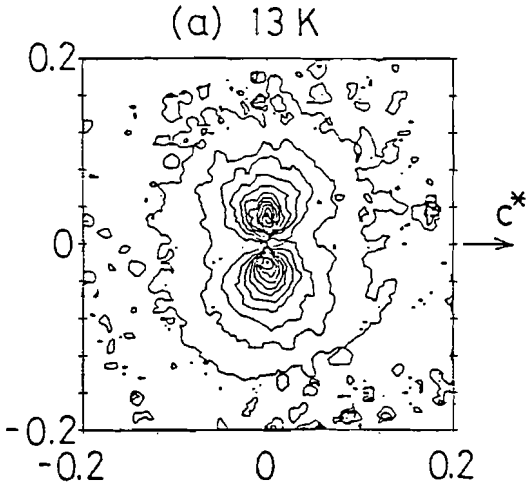

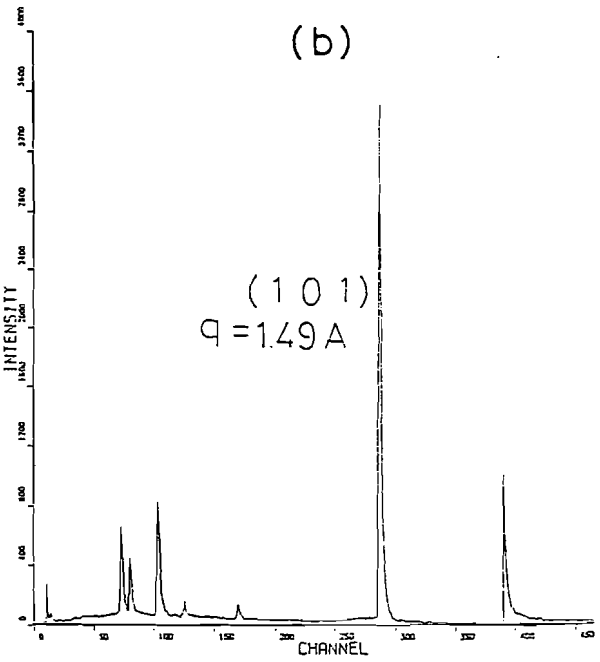

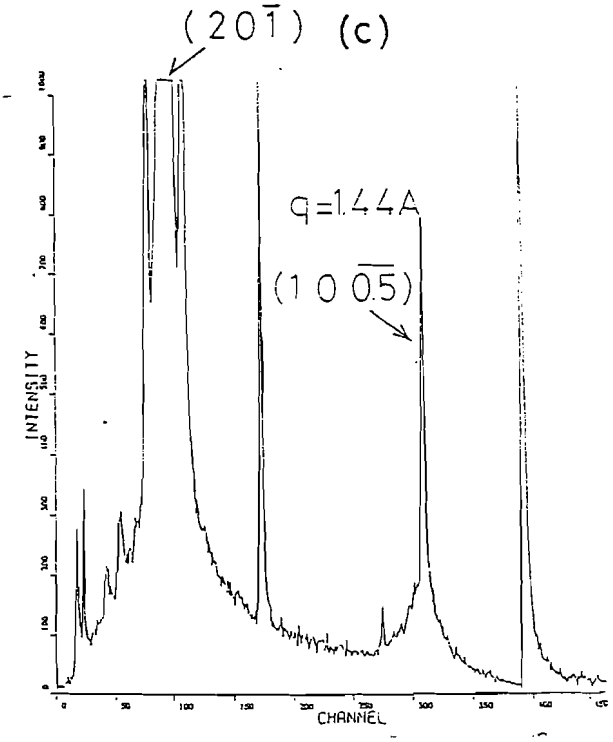

Fig. 14

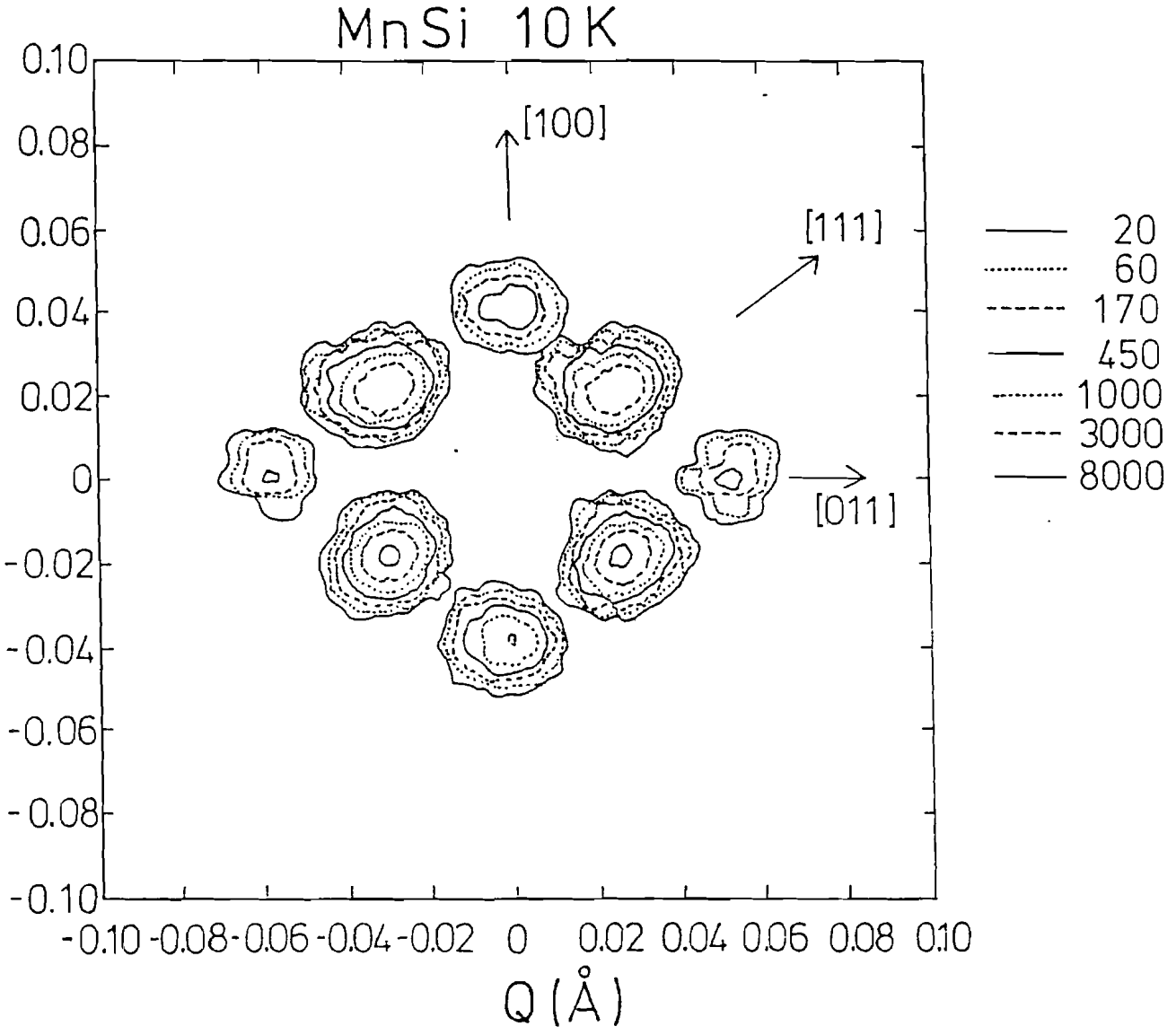
MnSi 10K
[100]
[111]
[011]
20
60
170
450
1000
3000
8000
0.10
0.08
0.06
0.04
0.02
0
-0.02
-0.04
-0.06
-0.08
-0.10
-0.10 -0.08 -0.06 -0.04 -0.02 0 0.02 0.04 0.06 0.08 0.10
Q (Å)

Fig. 15

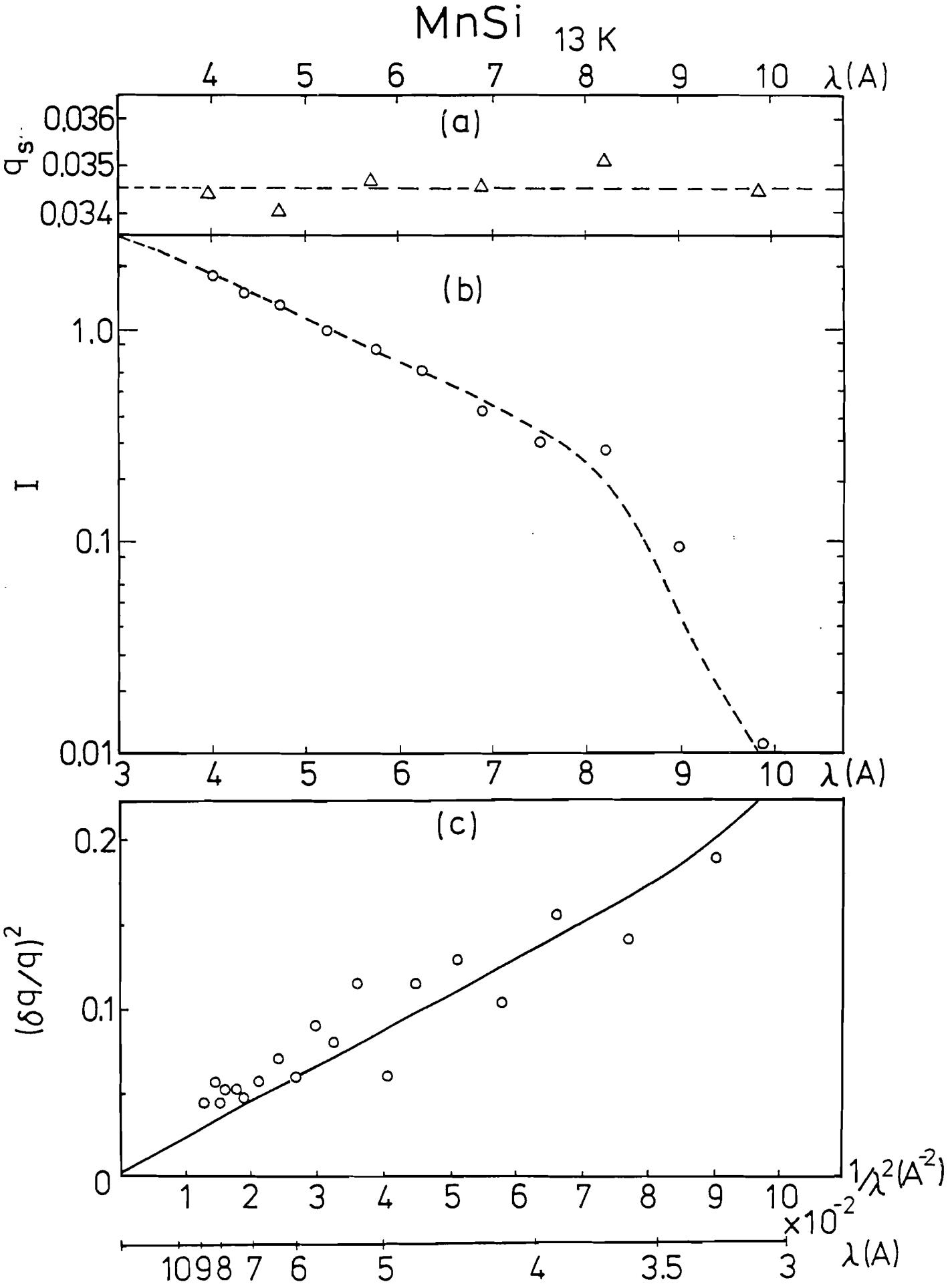
MnSi 13 K
4 5 6 7 8 9 10 λ(A)
(a)
q_s
0.036
0.035
0.034
(b)
I
1.0
0.1
0.01
3 4 5 6 7 8 9 10 λ(A)
(c)
$(\delta q/q)^2$
0.2
0.1
0
1 2 3 4 5 6 7 8 9 10
$1/\lambda^2(A^{-2})$
$\times 10^{-2}$
10 9 8 7 6 5 4 3.5 3
λ(A)

Fig. 16

(a)

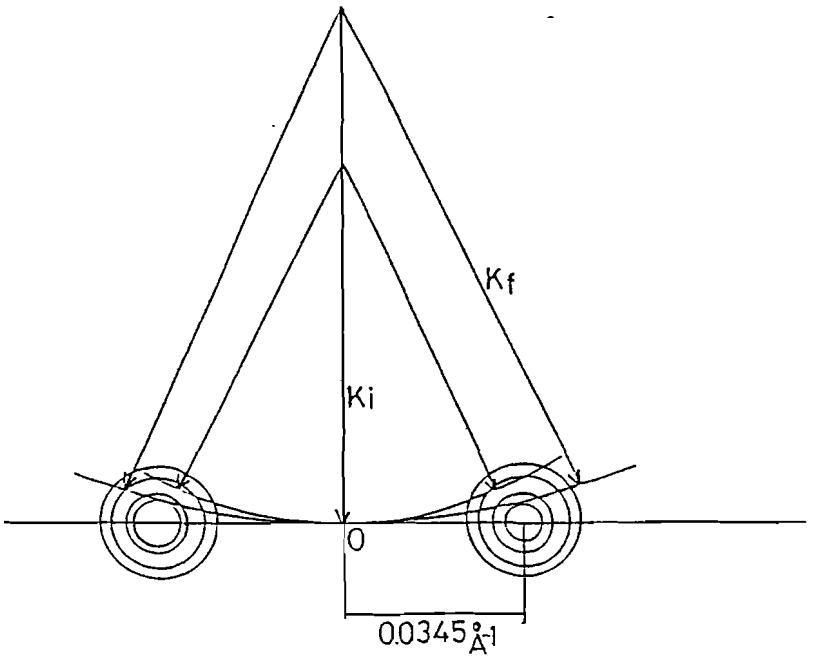
Kf
Ki
0
0.0345Å-1

(b)

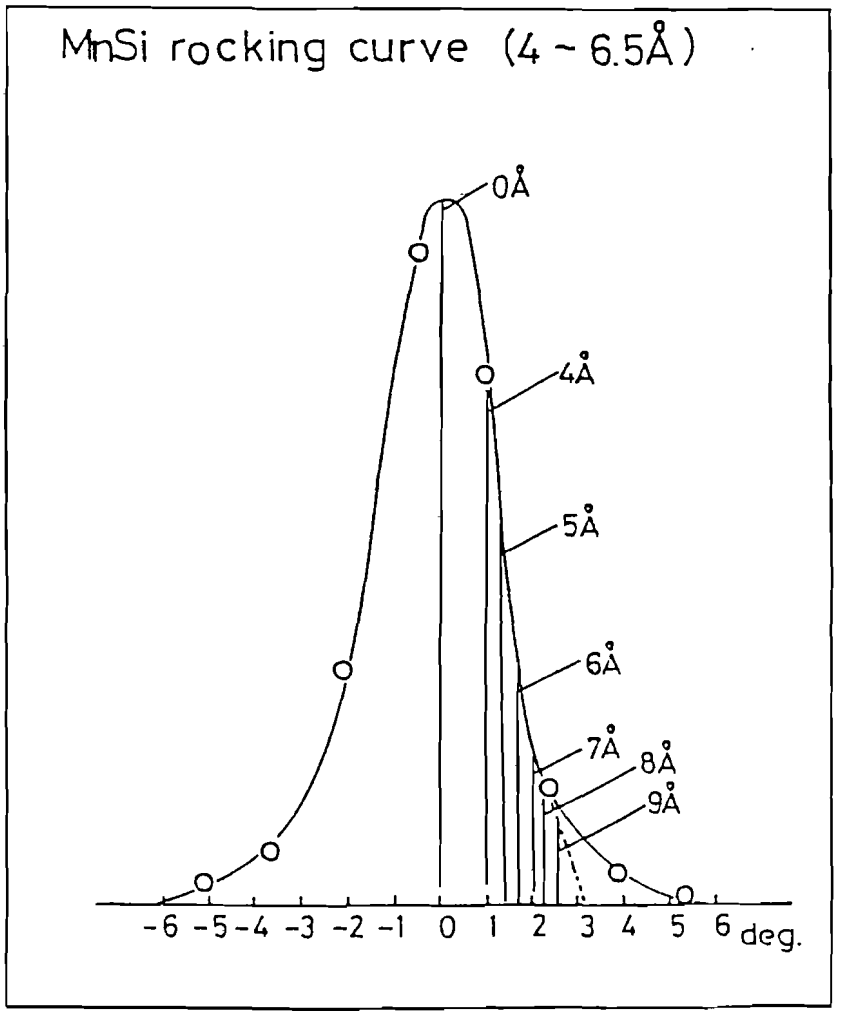
MnSi rocking curve (4 ~ 6.5Å)
0Å
4Å
5Å
6Å
7Å
8Å
9Å
-6 -5 -4 -3 -2 -1 0 1 2 3 4 5 6 deg.

Fig. 17

(1) Chopper for Rejecting Inelastic Part

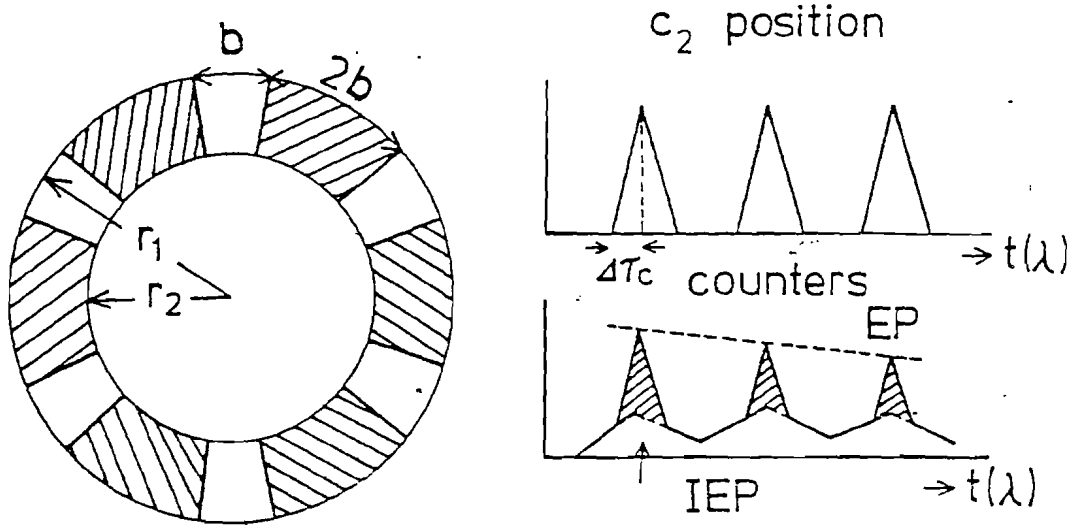

(2) Chopper for Inelastic Scattering

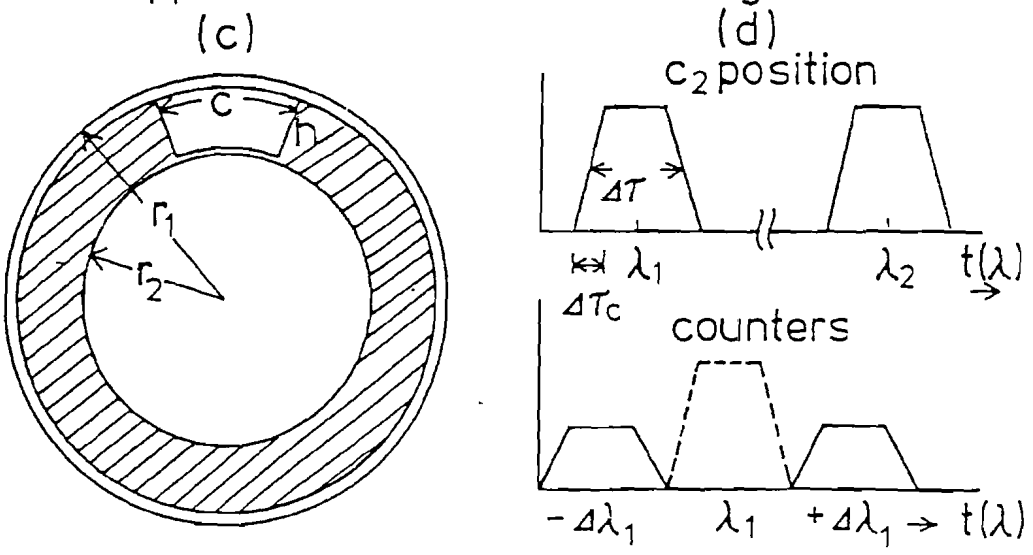

Fig. 18

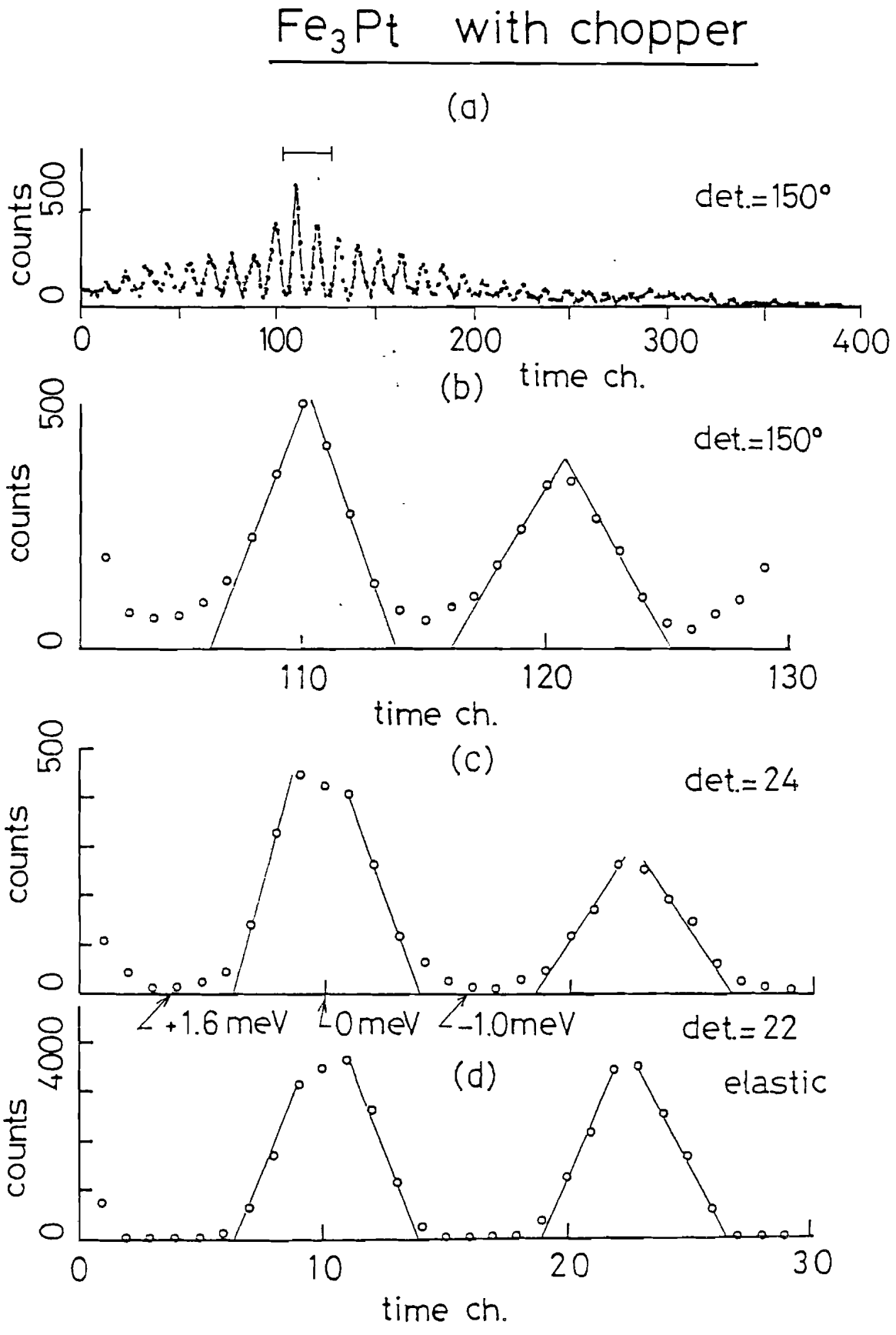
Fe3Pt with chopper
(a)
counts
500
0
det.=150°
0
100
200
300
400
time ch.
(b)
counts
500
0
det.=150°
110
120
130
time ch.
(c)
counts
500
0
det.= 24
+1.6 meV
0 meV
-1.0meV
det.= 22
(d)
elastic
counts
4000
0
0
10
20
30
time ch.

Fig. 19

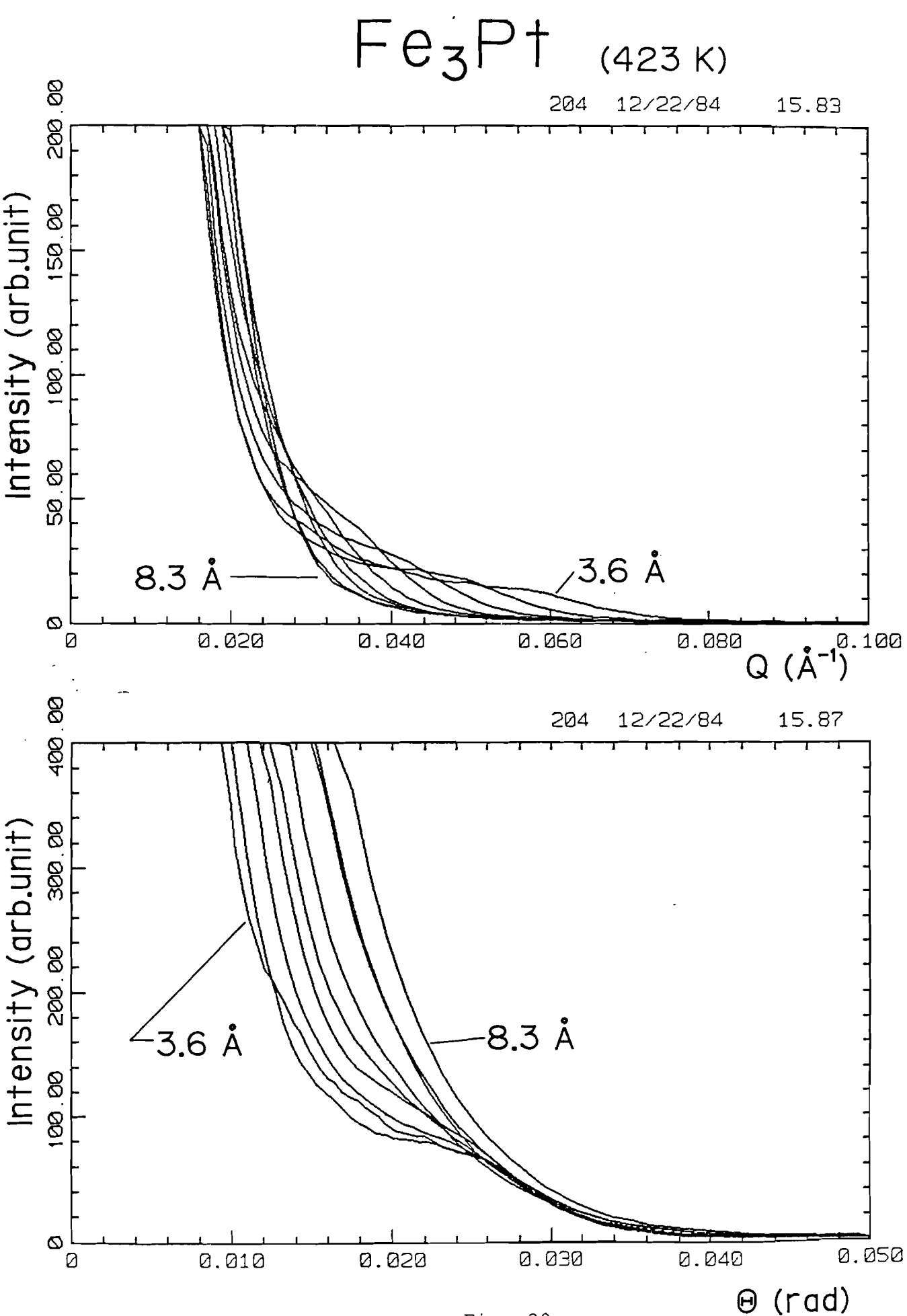
Fe3Pt (423 K)
204 12/22/84 15.83
Intensity (arb.unit)
200.00
150.00
100.00
50.00
0
8.3 Å
3.6 Å
0
0.020
0.040
0.060
0.080
0.100
Q (Å-1)
204 12/22/84 15.87
Intensity (arb.unit)
400.00
300.00
200.00
100.00
0
3.6 Å
8.3 Å
0
0.010
0.020
0.030
0.040
0.050
Θ (rad)

Fig. 20

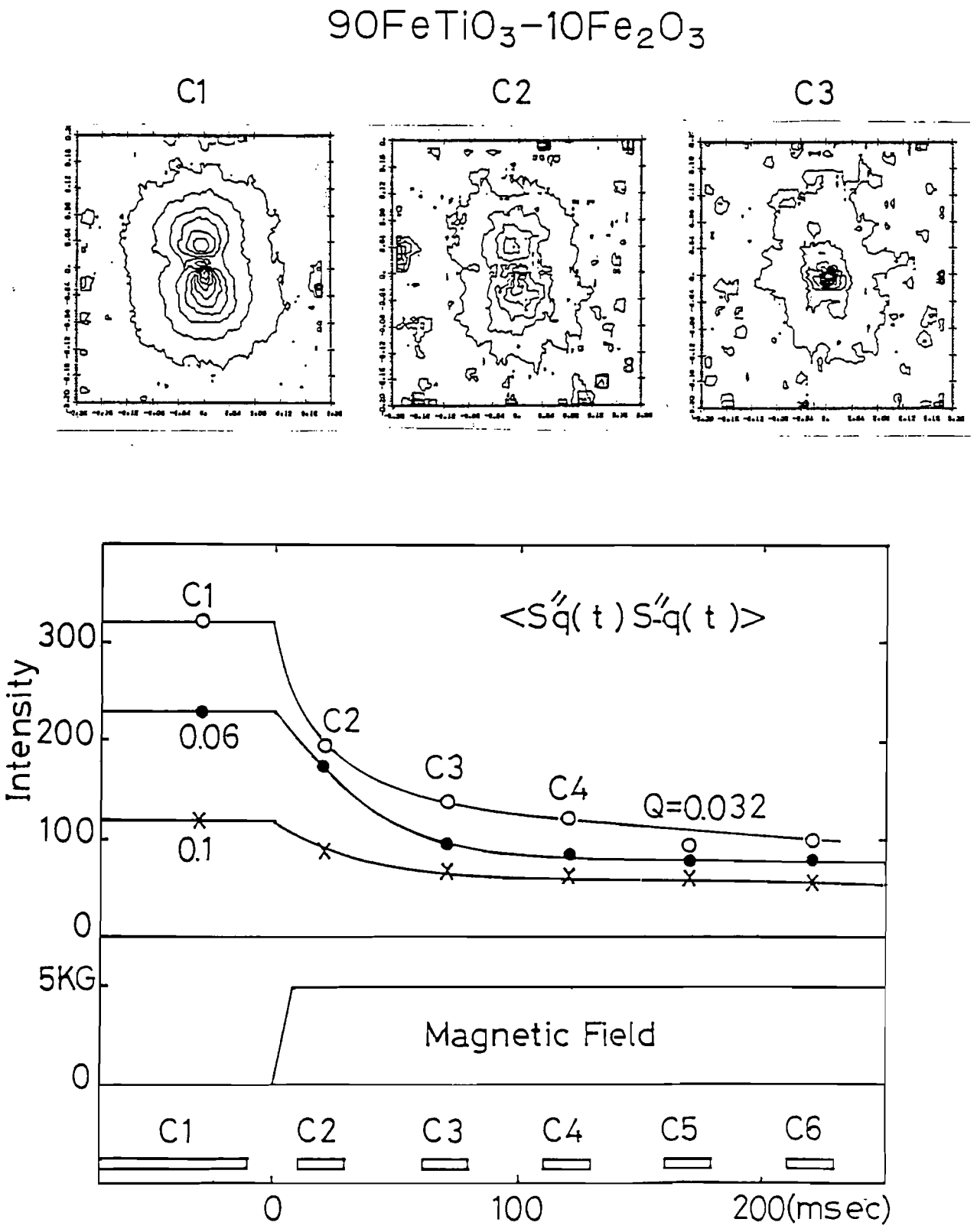
90FeTiO3−10Fe2O3
C1
C2
C3
<S''q(t) S-''q(t)>
Intensity
300
200
100
0
0.06
0.1
C1
C2
C3
C4
Q=0.032
5KG
0
Magnetic Field
C1
C2
C3
C4
C5
C6
0
100
200(msec)

Fig. 21

BLOCK DIAGRAM OF THE BULK MEMORY

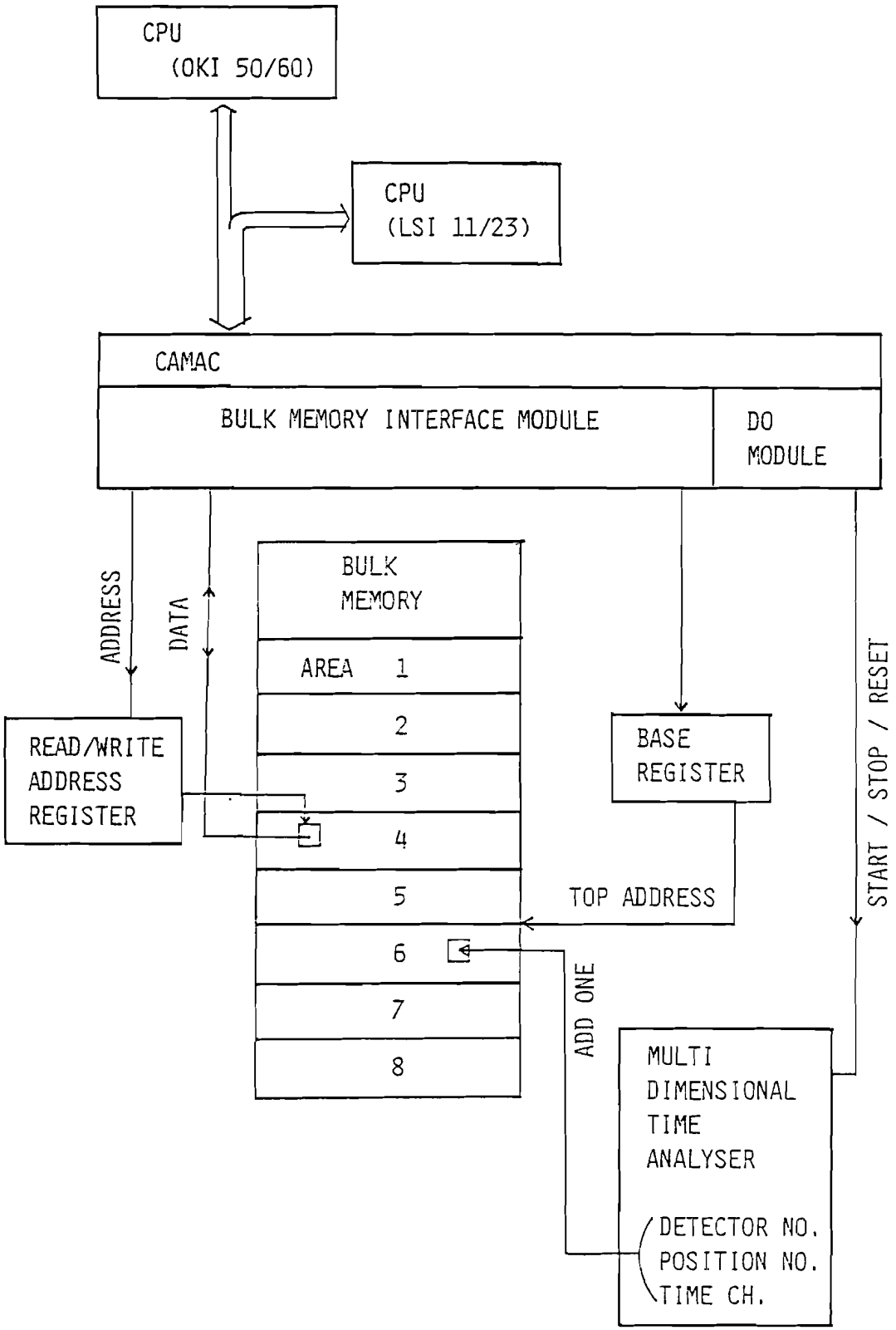

Fig. 22

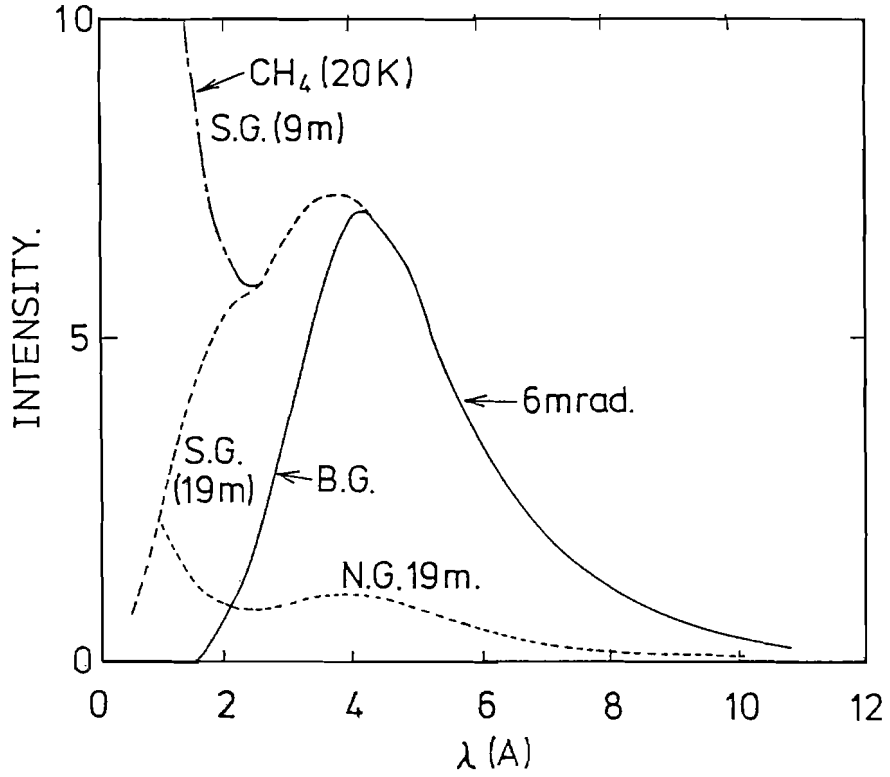
10
5
0
INTENSITY.
CH4 (20K)
S.G. (9m)
6mrad.
S.G.
(19m)
B.G.
N.G. 19m.
0
2
4
6
8
10
12
λ (A)

Fig. 25

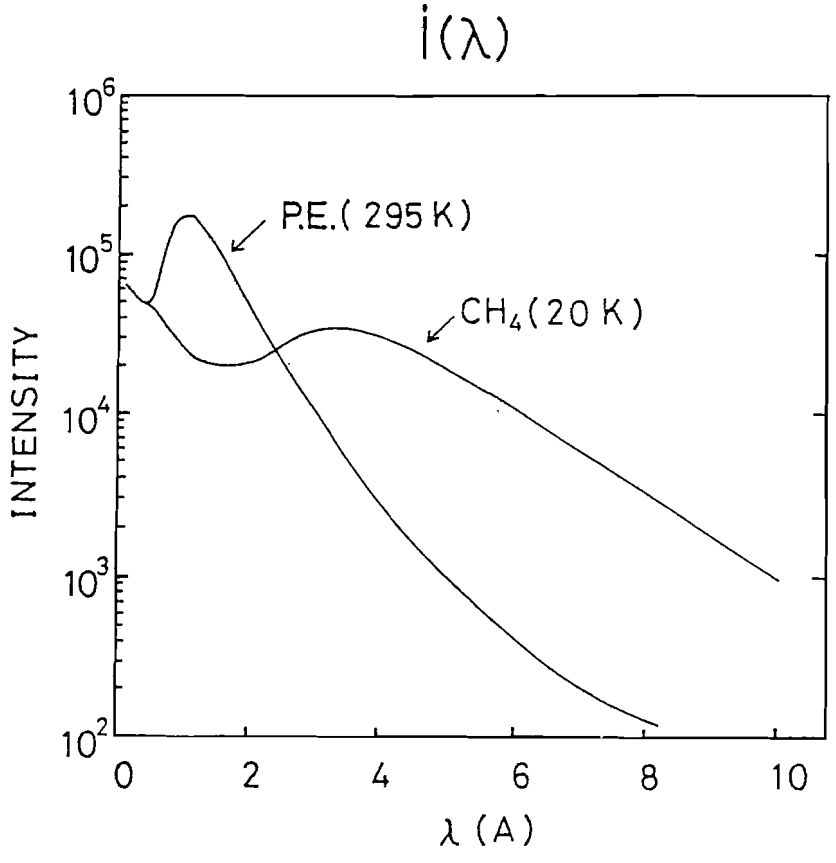
I(λ)
10^6
10^5
10^4
10^3
10^2
INTENSITY
P.E. (295 K)
CH4 (20 K)
0
2
4
6
8
10
λ (A)

Fig. 23

GUIDE TUBE EFFICIENCY

(SAN)

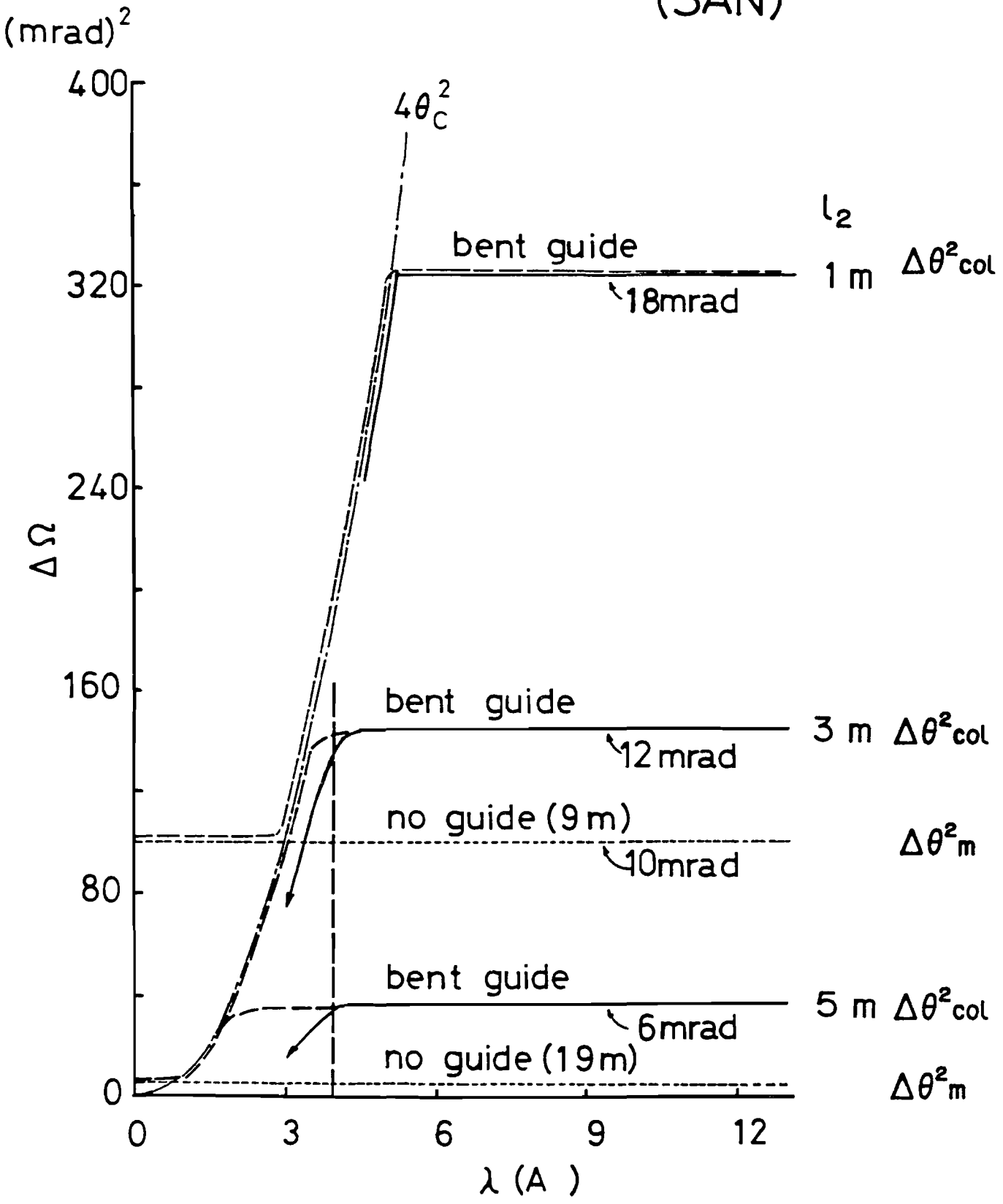

Fig. 24

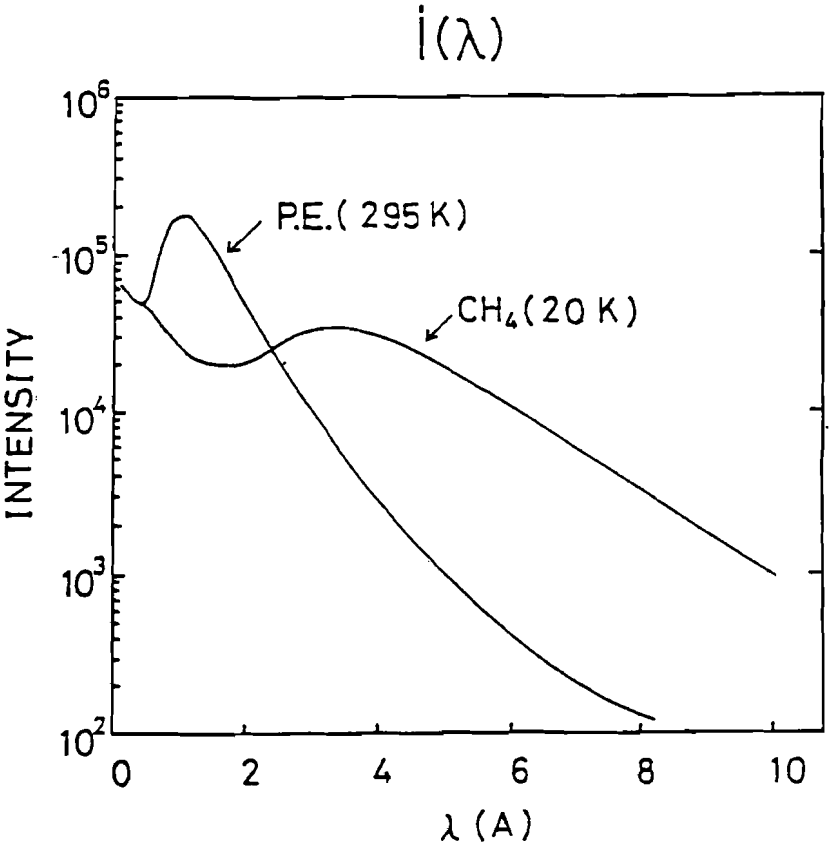
I(λ)
INTENSITY
P.E.(295 K)
CH4(20 K)
λ (A)

Fig. 23

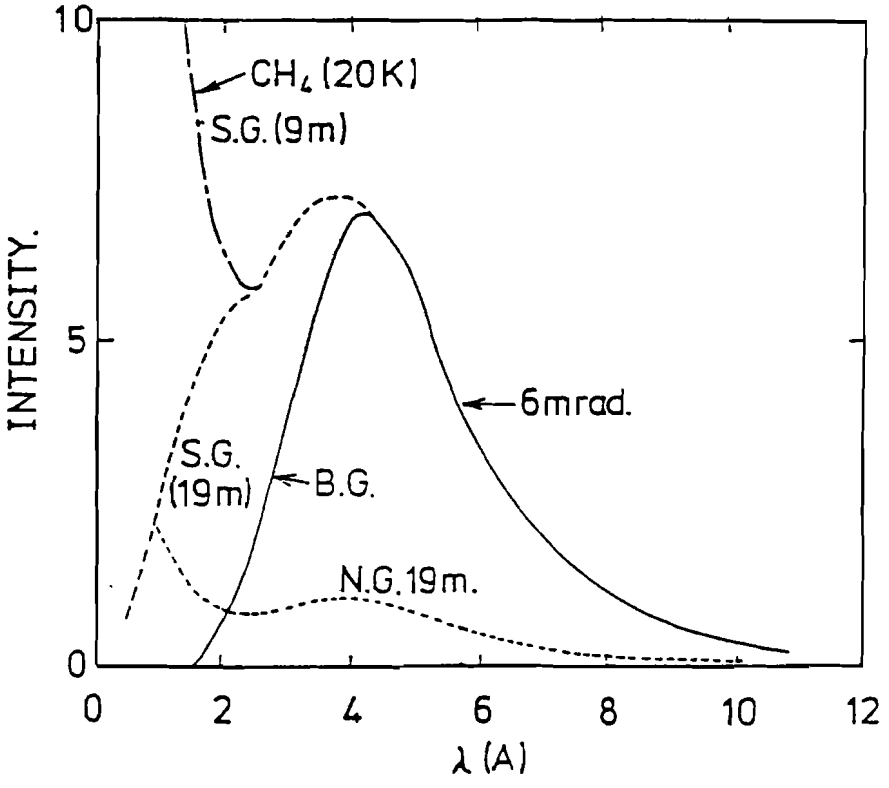
INTENSITY.
CH4 (20K)
S.G. (9m)
6mrad.
S.G.
(19m)
B.G.
N.G.19m.
λ (A)

Fig. 25

Proceedings of the Eighth Meeting of the International Collaboration on Advanced Neutron Sources (ICANS-VIII)
8-12 July 1985, Rutherford Appleton Laboratory Report RAL-85-110

A Proposal for a Multi-Function Materials Facility for the Spallation Neutron Source

Colin G Windsor and Roger N Sinclair

Materials Physics and Metallurgy Division, AERE, Harwell , OX11 0RA.

Summary. A neutron beam instrument is proposed which will allow the simultaneous study of the microstructural, crystalline phase, internal stress, defect, local order, texture, diffusional and vibrational properties of materials. The penetration of neutrons permits all these properties to be studied in a bulk specimen *in situ* during a heat treatment or chemical reaction as a function of time. The possibility of using narrow incident and scattered neutron beams allows the simultaneous monitoring of these properties as a function of position across the sample. Only by using the polychromatic neutron beam from a pulsed source, can all these properties be studied at the same time and at the same point on the specimen. The proposed instrument is designed for installation on the Spallation Neutron Source recently commissioned at the Rutherford Appleton Laboratory. Its performance is evaluated for a series of key experiments in applied science and shown to permit a complete neutron examination of the sample within minutes.

1. Introduction

Conventional neutron instruments are restricted to just one of the many neutron techniques which can be applied to a sample. Their counters record only a tiny fraction of the precious neutrons scattered by the sample. This proposal demonstrates that the restriction can be overcome by using a variety of detector banks together with the wide incident wavelength band given by a pulsed source. A series of techniques can be matched together in a single *multi-facility* with little compromise on the performance of any one mode. The present design considers an instrument optimised for the resolution and intensities required when applying neutron techniques to materials science.

The ability of neutron beams to penetrate several centimetres of most materials makes them uniquely useful in materials science(1). Whole components may be studied with little surface preparation or sensitivity to surface effects. The same penetrating ability allows easy containment of the component in a furnace, stress cell or reaction vessel. This makes possible the *in situ* study of irreversible processes such as the ageing of steels, the creep to fracture of a tensile specimen, or the setting of a cement. The several techniques of neutron beam science are often performed consecutively on different specimens and on different instruments. The proposed instrument allows the principal neutron beam techniques to be applied to the same specimen at the same time. A second feature of this instrument is its use of a thin *pencil* incident neutron beam to scan the properties of the sample as a function of position across its surface. For example the microvoids, defect structure, minority phases and stress could be measured across a fracture specimen with resolution of a few millimetres. Its 90^0 angle counters allow properties, such as residual stress and texture within a weld, to be measured as a function of three-dimensional position within the volume of the sample.

The thinking behind this instrument is illustrated by recent developments in electron microscopy. When a feature of interest is found by transmission microscopy, a battery of techniques— electron diffraction, X–ray analysis, Auger analysis and electron energy loss spectroscopy can all be applied to the same area of the specimen. Neutron scattering offers an even wider range of complementary techniques.

The wide range of usable neutron scattering angles and incident wavelengths enables a series of diffractometers to be tailored to different scientific objectives. These are characterised by different, if overlapping, ranges in the scattering vector $Q=4\pi\sin(\phi/2)/\lambda$ depending on the scattering angle ϕ and wavelength λ . The size range monitored is given roughly by $L\approx 2\pi/Q$ so that the different Q ranges are analogous to the different magnifications of a microscope. The accessible Q values span a range of 10^4 from 0.004 to 40 Å^{-1} implying a size range from many hundreds to a fraction of an Angstrom. The range of resolution ΔQ feasible in neutron diffraction is equally wide. It needs to be matched to the required precision in the size of the object under study. Even at the same value of Q there is a need for both high resolution and low resolution measurements. For example around Q = 2 Å^{-1} , corresponding to typical interatomic spacings, high resolution diffraction defines the sharp d-spacings of crystallites. At the same time local order in a defect structure or multi-component liquid reveals short range structure which requires only low resolution. The need is for the widest possible range of Q vectors to be covered at a range of resolutions ΔQ . Such is the objective of this instrument.

A unique feature of neutron scattering is that it embraces both structural studies through diffraction, and dynamic studies through the Doppler shifts caused by atomic motions. Diffusion in the sample gives quasi-elastic broadening with a width proportional to the rate of diffusion, while vibrations give inelastic modes at the energy transfer $\hbar\omega$ corresponding to the vibrational frequency ω. Most inelastic experiments have lower counting rates than is usual in diffraction. This instrument uses only configurations of relaxed resolution that can be operated together with diffraction in time and spatially resolved experiments.

2. The principal fields in materials science covered by neutron scattering.

A recent review considered the contributions of neutron beam techniques to applied materials science (2). The principal areas are given in table 1 together with complementary techniques.

(i) Microstructure.
The use of Small Angle Neutron Scattering (SANS) to probe microstructure in the size range 30 to 1000 $Å^{-1}$ has proved one of the most powerful fields of materials science (3) . Although its upper size range is covered by electron microscopy, SANS offers an easy and quantitative route to a defect diameter distribution function and volume fraction measurement. As conventionally practised, with a Q value range from of order 0.006 to 0.3 $Å^{-1}$, SANS has the important limitation that the nature of the defects being observed is not known except when evident from other information. However many defects studied by SANS will also give an observable diffraction pattern. For example, a 200 Å diameter particle gives a diffraction peak at a 2Å d-spacing with acceptable 10^{-2} line broadening. Thus a combination of medium resolution diffraction and SANS is an important aid to the interpretation of small angle scattering data.

(ii) Phase identification.(4)
Larger diameter phases, including those too large to be resolved by small angle scattering, can be resolved at very low volume fractions by high resolution powder diffraction. In practice neutron diffraction allows volume fractions below 1% to be estimated quantitatively. This is appreciably better than is possible with X–rays, where Compton scattering and fluorescence spoil the signal to noise ratio from the minority phase. The techniques of multi-phase Rietveld refinement allow the structure of minority phases to be refined in their normal environment rather than after extraction. Their growth as a function of heat treatment time would be an important application of this instrument. Some phases, such as those from age-hardening alloys, would first appear in SANS, but as their size increased the SANS pattern would become too narrow and the diffraction pattern would become visible by high resolution powder diffraction.

(iii) Internal stress determination.(5)
Neutrons are unique in being able to measure non-destructively the internal stress within a specified volume of a bulk component. The method is the three-dimensional analogue of X–ray surface-stress measurement. High resolution diffraction measures the lattice strain from the small shifts in d-spacing of order 10^{-4} in $\Delta d/d$. In order to observe the largest strains the neutron scattering vector Q should be directed along the direction of maximum strain. For many samples this is only possible if the scattering takes place at angles close to 90^0. In particular the back-scattering geometry so often used on pulsed sources can often measure the strain only through the Poisson's ratio effect, and so give observed shifts only around a third of the maximum shift. An essential feature of this instrument is therefore the provision of high resolution powder diffraction at 90^0 scattering angle. The required resolution is of order 3×10^{-3} in $\Delta d/d$. A second feature possible with 90^0 diffraction is the definition of both in-going and out-going neutron beams by apertures to define a scattering volume within a component. Both minority phase analysis and stress analysis can then be mapped out as a function of position within the sample. By rotating the specimen about this position, the full stress tensor can be determined.

(iv) Defect scattering.(6)
For defect sizes below 50 Å electron microscopy becomes increasingly difficult, and often impossible to perform quantitatively. However the Q values between 0.25 to 1 $Å^{-1}$ needed to observe these sizes are often not accessible using SANS except by changing the counter position or the wavelength. This instrument proposes a special *diffuse scattering* bank with the same relatively relaxed resolution of order $\Delta Q/Q=0.1$ conventional in SANS extending the range of Q values that can be measured simultaneously by SANS. This permits the extension of power-law models revealing the shape of the scattering centres, and giving a good surface area measurement from the Porod law. Perhaps equally important, the extension of the Q range into the region between the first Bragg peak and the origin allows a precise determination of the background. A wide Q range and a precisely subtracted background are the two essentials for successful transformation of SANS results to give the real-space diameter distribution function.

(v) Local ordering.(7)
Disordered systems, such as alloys, glasses, polymers, liquids, gels and ionic solutions, show a diffraction pattern at Q values in the range 0.6 to 3 $Å^{-1}$ characteristic of local order over distances of a few atomic spacings. Although measurable by X–rays, neutrons enjoy the opportunity of isotopic substitution to give the partial structure factors essential to the understanding of local order. However these are often expensive and available only in small quantities, so that an essential feature of this instrument is its high count-rate and ability to pick out the most appropriate resolution for a particular Q value. This is done by employing a wide range of counter angles. An advantage that neutrons have over X–rays in the area of local atomic ordering is that neutron scattering lengths are constant over the Q range of interest, making possible a cleaner separation of scattering components caused by size effects and by atomic ordering.

(vi) Texture measurement. (8)
Neutron diffraction reveals the preferential alignment of crystallites over an appreciable volume of the sample, and so can give a statistically smooth orientation distribution function (ODF). In contrast X–rays see only a surface layer of crystallites and so give an imprecise ODF depending on the chance number of crystallites within the much smaller beam area. Texture measurements can be made by rotating the sample or, as proposed here, by using many counters spread over a wide azimuthal angle, but with the same scattering angle. Texture variations are then immediately apparent from the azimuthal variation. By using a pulsed beam, several partial pole figures are obtained simultaneously giving inverse pole figures from which the ODF can be obtained from only one, or at most two, sample orientations. The ODF could then be followed as a function of time together with the related microstructural and stress properties. For the interpretation of many mechanical properties in terms of texture, the inverse pole figure along the incident beam direction given by this instrument provides exactly the necessary information.

(vii) Diffusion measurements.(9)
Appreciable diffusion of the molecules in a material leads to a quasi-elastic broadening of the normal elastic scattering. For example the motion of free or bound water molecules can be used to determine the fraction of chemically bound water molecules in a material. The method is complementary to those using nuclear magnetic resonance but can be used in high water content situations where the NMR signal is damped out. The bound molecules will usually give a diffraction spectrum so that simultaneous diffraction would be an important aid in determining the nature of the diffusing species. Quasi-elastic measurements could also give an important guide to the interpretation of SANS from semi-aqueous materials such as setting cement, where the nature of the contrast is not clear. The applications of quasi-elastic scattering extend as the energy resolution is made more stringent. However in practice comparable count-rates between the quasi-elastic scattering and SANS and diffraction are only achieved if a modest energy resolution is specified. The resolution needed to resolve free and bound water is of order 0.1 meV.

(viii)Vibrational spectroscopy.(10)
The vibrational spectrum of materials characterises the strength of the bonds between its molecules. The motions of hydrogen atoms are particularly well seen because of their large cross-section. The vibrational spectra of hydrocarbons reveal their local environment, for example their orientation on a catalytic site. Measurements generally need to be taken over a wide energy range up to a few hundred meV, with a resolution of a few meV. Beryllium filters, including Be/BeO difference techniques , and Be edge differential techniques cover the range adequately with high intensity. The neutron method has two important advantages over infra-red and Raman scattering which cover the same energy range. The neutron scattering intensities are readily calculated on an absolute scale leading to precise interpretation of the results. Secondly the large hydrogen cross-section aids the assignment of modes, which can be identified by deuterium substitution.

The ranges of the scattering vector Q and energy transfer $\hbar\omega$ specified for the multi-facility are summarised in table 2.

3. The design principles of a multi-instrument for the SNS.

It is a unique feature of pulsed neutron scattering that it permits all the neutron techniques described in the previous section to be performed at the same time. This can occur only because the pulsed source is polychromatic and can extend from the cold 4 to 8 Å wavelength neutrons needed for small angle, diffuse and quasi-elastic scattering to the thermal and epithermal 0.1 to 4 Å neutrons needed for diffraction and vibrational scattering. The time-of-flight scans used by all modes of the instrument mean that all the results appear at the same time. A reactor-based instrument with the same objectives would need to scan the incident neutron wavelength over a wide range and so give the results only sequentially.

The Spallation Neutron Source (SNS) at the Rutherford Appleton Laboratory in the UK(11), as the world's highest mean flux fast pulsed source, is the natural site for this instrument. It does impose some important constraints.

(i) The pulse repetition frequency of the SNS is fixed at 50 Hz. Although this can be reduced by pulse-removal choppers this would not be desirable for many of the modes of this instrument and will not be considered here.

(i) Its moderators are at ambient,100K and 20K temperatures. For this instrument with its requirement for good time resolution at thermal energies yet with good cold neutron intensities for small angle scattering the 100K moderator is the best choice.

The key parameter of the multi-facility is its total flight path length L. The period between source pulses τ = 20000 μs limits the wavelength band $\Delta\lambda$ observable to (12)

$$\Delta\lambda = \frac{hL}{m\tau} = 0.3956\, x\, \frac{20000}{L(cm)} \quad \text{Å}. \qquad 1.$$

The required 0 to 8 Å wavelength can be achieved within a single *frame* of the time scan only for a total flight path less than 10 metres. The original design for this instrument had a total flight path of order 20 metres utilising the 0 to 4 Å frame for diffraction and the 4 to 8 Å frame for small angle scattering chosen by a velocity selector *after* the specimen. This had to be rejected because of down scattering through the velocity selector from the intense epithermal flux near the start of the next frame.

Within the key constraint of a total flight path of order 10 metres the remaining parameters must be chosen to satisfy the specifications of table 2, and yet at the same time give appropriate count-rates for key experiments on the various facilities. The arrangement of the counter banks for each facility is shown schematically in figure 1. They were considered with following order of priority:

(i) The small angle facility.
The resolution requirement $\Delta Q = 0.006$ Å^{-1} at 8 Å wavelength implies a matched incident and scattered collimation

$$\alpha_0 = \alpha_1 = \frac{\sqrt{2}\,\lambda\,\Delta Q}{4\pi} \qquad 2.$$

equal to 0.2^0 . This collimation is sufficiently fine that an incident guide tube is not a sensible option. A nickel guide only achieves 0.2^0 for wavelengths below 1.2 Å. The natural collimation arising from the moderator width W_m and the incident flight path L_0 is given by

$$\alpha_0^{natural} = \frac{W_m}{L_0}. \qquad 3.$$

With the full SNS moderator width of 10 cm an incident flight path of 27.6 metres is required to give a natural collimation equal to the required value of 0.2^0. Thus if the facility is to operate within the required 10 metre total flight path it is essential to employ a converging collimator. These have been successfully used on many SANS facilities (13). The design would employ *pepper pot* irises containing several apertures aligned so that they converge on the detector. The small iris surface means that their

low-angle scattering is reduced. The key parameter is the diameter d_1 of a single aperture at the sample position. This should be matched to the resolution of the counter elements d_2. We shall assume 0.5 cm for both d_1 and d_2, as used in many conventional SANS cameras. The scattered flight path L_1 giving the required scattered beam resolution α_1 of 0.2^0 is given by

$$\frac{\sqrt{d_1^2 + d_2^2}}{L_1} = \alpha_1 \qquad 4.$$

or $L_1 = 2$ metres. The constraint that $L_0 + L_1 = 10$ metres then defines the incident flight path $L_0 = 8$ metres. It is assumed that 6 metres of this which passes throught the beam shutter and bulk shield of the SNS is available for the converging collimator. The 0.2^0 constraint then implies an aperture size varying from 0.5 cm diameter at the specimen to 2 cm at the start of the converging collimator and viewing a 2.5 cm diameter area of the moderator. Assuming 8 such apertures distributed over a 10 cm diameter of the moderator surface ensures that half the total moderator area is used. The whole cluster of apertures subtends an angle $\alpha_{cluster} = W_m/L_0 = 0.72^0$ and has a diameter of 2 cm at the sample. For experiments performed as a function of position over the sample area using a pencil thin beam, only the central aperture would be used. Very cold neutrons with wavelengths above 8 Å would be excluded from the beam by reflecting nickel-coated plates.

If the detector active diameter were 32 cm, its maximum angle would be 9.1^0, and its Q range for wavelengths above the iron Bragg cut-off of 4.06 Å would be from 0.004 to 0.24 $Å^{-1}$. By using neutrons with thermal energies from 0.5 to 4 Å the Q range would be extended to cover from 0.01 to 2 $Å^{-1}$.

(ii) The back-scattering diffraction facility.
The resolution requirement $\Delta Q/Q = 0.004$ of this facility is chosen to give a high count rate from minority phases. The refinement of new structures is not expected to be a common mode for the facility. With an incident flight path $L_0 = 8$ m and a scattered flight path $L_1 = 2$m, the overall resolution at a scattering angle ϕ is

$$R = \frac{\delta_m}{L_0 + L_1} + \cot\left(\frac{\phi}{2}\right)\frac{\Delta\phi}{2}. \qquad 5.$$

Putting $\delta_m = 2.8$ cm, the back-scattering resolution $R_{180} = 0.003$. For a 2 cm sample and counter element the scattering angle spread $\Delta\phi$ has components of 1.1^0 from the sample size and 0.72^0 from the angular spread of the converging collimator giving the specified resolution R=0.004 for scattering angles ϕ above 150^0. With a maximum scattering angle of 175^0, the counter bank extends from a minimum diameter of 8.7 cm to a maximum diameter of 45 cm, to give a total area of order 6000 cm^2, and subtending a solid angle of 0.6 sterad. The wide d-spacing range extending up to 4 Å would be particularly valuable for identifying structures in multi-phase problems.

(iii) The 90^0 stress facility.
The achievement of the specified resolution $\Delta d/d = 0.003$ at scattering angles of 90^0 is quite demanding. If the timing and angular terms in equation 5 are matched, then the total flight path needs to be of order 13 metres, while the matched angular collimations $\alpha_0 = \alpha_1$ need to be of order 0.2^0. Thus high angular collimations are essential and even long guide tube instruments would require additional incident collimation at many wavelengths.

The centre aperture of the converging collimator has the required 0.2^0 collimation, so that for samples using the 0.5 cm diameter central aperture, the required $\alpha_1 = 0.2^0$ collimation could readily be obtained from a single 1.5 cm diameter detector placed 5 metres from the sample. The relatively long scattered flight path increases the total flight path to the required 13 metres, and also gives angular collimation without the use of Soller slits. With the 90^0 scattering angle a 50 cm long counter subtending 10^0 in

the vertical plane would not degrade the resolution or the precision of the stress direction to any significant extent. No scattered beam intensity is sacrificed by the long scattered beam flight path. In practice it would need to be inclined at say 30^0 to the horizontal in order to avoid interaction with neighbouring beam paths.

For larger samples the most important requirement is for sample angles at 45^0 to the incident beam direction so that the scattering vector Q lies along the length of the specimen. This is particularly true for rod-like test specimens where an external stress needs to be applied parallel to the scattering vector. For this case a focussing technique has been devised to offset the changes in scattering angle across the converging collimator by corresponding changes in the total flight path. The method is detailed in appendix 1. For a counter at a scattering angle ϕ, at a distance L_2 from a thin specimen angled to lie along the scattering vector,focussing occurs when, with the notation of figure 3,

$$(L_0 + L_2)\left(\frac{1}{L_1} - \frac{1}{L_2}\right) = 4\left(\tan\frac{\phi}{2}\right)^2. \qquad 6.$$

For example with $\phi = 90^0$, $L_0 = 8$ m and $L_1 = 2$ m the focussing distance when all apertures of the converging collimator arrive with the same flight time is given when $L_2 = 5.12$ m. L_2 decreases as the scattering angle ϕ is reduced, or as the SANS flight path L_1 is reduced. This arrangement allows the full 2cm wide multi-aperture to be used with the resolution appropriate to a single aperture. For most applications a set of 20 counters spaced 0.5^0 apart and covering scattering angles from 85 to 95^0 would be acceptable. These counters could be *computer focussed* to give a total scattered beam solid angle of 0.006 sterad with a corresponding increase in effective count rate. The maximum observable d-spacing extends to 4.3 Å, giving a wide range of simultaneously measurable crystal orders.

(iv) The diffuse scattering facility.
The diffuse counter bank is proposed to cover scattering angles from 10^0 to 30^0 and so extend continuously the range of Q values covered by the SANS detector. Resolution in $\Delta Q/Q$ can be relaxed back to the 5% level by shortening the flight path to 1 metre. The focussing effect of the converging collimator will be reduced, so we propose a 1cm wide sample and detector element to give an angular spread of 0.8^0 matching the incident collimation of the whole converging cluster giving around 4% resolution at 30^0 scattering angle. The Q range for cold neutrons of from 4 to 8 Å will be from 0.15 $Å^{-1}$ to 0.8 $Å^{-1}$. Using thermal neutrons from 1 to 4 Å extends the Q range to 3.2 $Å^{-1}$. Although the counter might be used with still shorter wavelength neutrons, its resolution would be insufficient for general amorphous structure determination. It is considered much more important to maintain intensities for the generally weak diffuse scattering by providing full azimuthal detector coverage. This would extend from a radius of 17 cm at 10^0 scattering to 30 cm at 30^0, giving a total area of 6900 cm^2 and subtending a solid angle of 0.69 sterad.

(v) The local order facility.
The objective of this detector bank is to cover the important Q range from 0.4 $Å^{-1}$ to 3 $Å^{-1}$ using a wide variety of wavelengths and resolutions. Both cold and thermal neutron wavelengths are needed. It is proposed to cover the 4 to 8 Å wavelength band using a set of counters from 30^0 to 150^0 scattering angles. By employing wavelengths from 1 to 4 Å, the important Q range from 3.2 $Å^{-1}$ to 12 $Å^{-1}$ of conventional reactor diffractometers is covered. High resolution diffraction will be performed on other counter banks so that this bank will have a range of more modest Q resolutions of a few percent. With a scattered flight path L_1 of 50 cm, counters 2 cm wide and 20 cm high give 2.3^0 angular resolution which is sufficient to give $\Delta Q/Q$ of 7.5% at 30^0 scattering angle, improving to 0.7% at 150^0. Spaced every 2.5^0 in scattering angle, the whole 48 counters would occupy 1900 cm^2 and subtend 0.77 sterad.

(vi) The texture facility.
For texture measurement to be possible with one or at any rate few sample

orientations, it is necessary to cover as wide a range of scattering angles as possible, both horizontally and vertically. The local order bank provides scattering plane information, but the wide range of wavelengths at which any one reflection is seen makes the immediate interpretation of the texture difficult. It is therefore proposed to build a texture bank on both sides of the sample covering the wide range of azimuthal angles from + 60^0 to − 60^0 at a fixed scattering angle of 100^0. The angular spacing between counters need be only 5^0 to give adequate spatial resolution in the pole figures. 48 counter elements of size 2 x 4 cm^2 at a 50 cm flight path are proposed. These have a total area of 384 cm^2 and a solid angle of 0.15 sterad. The angular resolution with a 2 cm sample would be 3.2^0 giving the required resolution $\Delta d/d$ = 0.03.

(vii) The quasi-elastic facility.
The LAM spectrometer built by Inoue *et al* in Japan has proved of great utility in materials science (14). The LAM40 instrument uses an incident flight path of 5.7 m and achieves quasi-elastic resolution of 0.1 meV as specified as most useful for the multi-facility. The counter arms are 60 cm to the analyser and 60 cm from analyser to counter. The analyser is a time-focussed array of 100 cm^2 area of pyrolytic graphite of 1.2^0 mosaic spread. Sample scattering angles of 45^0, 60^0 and 75^0 are proposed as most suitable for the separation of free and bound water problems.

(viii) The beryllium filter facility.
The required high count rates necessary for including vibrational scattering on a multi-facility are only feasible by using the wide scattered energy window of a beryllium filter. By using a short scattered flight path and large scattered neutron solid angle, energy resolutions of order 10 meV are possible up to around 100 meV energy transfer. The spread in scattered flight times is also minimised by using the shortest possible scattered flight path. A value of 22 cm is proposed. The spread of scattered neutron flight times can also be essentially removed by observing the *beryllium edges* caused by vibrational peaks rather than the peaks themselves.(15)

4. The performance of the multi-facility for key experiments

The essence of a successful multi-facility is that its various components have count rates that enable the required information to be obtained in comparable counting times. It is therefore necessary to consider at this stage a set of key experiments and the information required from them so that the various counter-banks can be appropriately matched. It is by no means a question of equating counter bank solid angles, or even counting rates, since the cross-sections to be measured differ, as does the method of interpreting the data. For example the diameter distribution of an alloy hardening phase needs to be measured in a time comparable to that needed for the volume fraction of an embrittling inter-metallic minority phase, and for measurements of the internal stress and texture in the alloy matrix. The evolution of the glassy structure of cement gel during setting needs to be measured in comparable times to its microporosity distribution, its free to bound water content and its vibrational spectrum. Table 4 lists a set of simple key experiments with well-defined cross-sections for each component of the multi-facility. The counting time for each experiment is calculated using the program SIP (16) for the configuration detailed in table 3 installed on the SNS. The statistical requirements are different for different experiments. For the broad distributions of SANS, defect, local order and vibrational scattering, a requirement of 1% statistical accuracy per resolution element is made. For the stress, texture and quasi-elastic broadening, a requirement of 1% statistical accuracy integrated over the peak is assumed to be sufficient. The SANS, defect, back diffraction, stress and texture experiments are based on an iron or steel sample 2 mm thick. The local order, quasi-elastic, vibrational and SANS calibration are based on a light water sample 1 mm thick. All samples see the same incident flux. For the SNS source with a 1 ev flux of $8x10^{12}$ s^{-1} $ster^{-1}$ eV^{-1} and a Maxwellian total flux of 3.5 x 10^{12} s^{-1} cm^{-2} the cold neutron flux incident on a full sample is some $4x10^5$ s^{-1} integrated over the wavelength range from 4 to 8Å. The thermal flux from 0.4 to 4 Å is of order $9x10^7$ s^{-1}.

(i) SANS from 0.1% of voids in 2 mm thick steel.

The thermal annealing of irradiated steels suffering from void swelling is a classic example of the need for a multi-facility. The void size distribution broadens, other minority phases are induced – for example ferrite in stainless steel, and distortion stresses are relieved. The SANS contrast from voids is of course unusually large, but it is seen that at $0.05Å^{-1}$, within the Guinier range $QR_g \approx 2$, the scattering is strong enough to give a 2.3 minute counting time per radial element for 1% statistics.

SANS calibration from 1 mm thick water.
The absolute calibration of SANS intensities is one of its most valuable features. Good 1% statistics per radial element are obtained in a 1.3 hour calibration run.

(ii) Back diffraction from 1% ferrite in 2 mm thick stainless steel.
The body centred ferrite phase is one of several phases induced by irradiation in stainless steel. At a 1% volume fraction it is typical of the crystalline phases needed to be identified by the back diffraction facility. The 220 peak is considered. At 150^0 scattering angle it corresponds to $Q = 6.2\ Å^{-1}$ at $\lambda = 1.96$ Å. The count rate integrated over the peak is $251\ s^{-1}$ giving 1% statistics in 0.6 mins.

(iii) 90^0 stress diffraction from a 3x3x3 mm^3 volume of steel.
For this important application, the integrated intensity of the 220 steel peak is calculated for a pencil beam 3x3 mm^2 in area using just the central aperture of the collimator. The 220 peak is appropriate since its modulus corresponds closely to the isotropic modulus. The counting rate for all 10 counters is $30\ s^{-1}$ giving 1% statistical error in 5.5 mins.

90^0 stress diffraction from a 2 mm thick steel plate.
Using the full collimator area in a focussing orientation gives a count rate of $176s^{-1}$ integrated over the 220 peak corresponding to 1% statistical error in 0.9 mins.

(iv) Diffuse scattering from 1% of 25Å voids in 2 mm thick steel.
The large range of the pore size distribution potentially measurable using neutrons, if a wide enough Q range can be covered, is most important. The scattering from the smaller end of the void distribution is considered at $Q = 0.5\ Å^{-1}$ in the Porod law region ($QR_g \approx 5$). Scattering of 4.4 Å neutrons then occurs at 20 degrees scattering angle in the diffuse bank. The count rate over a 1 cm annulus is $29\ s^{-1}$ giving 1% statistics in 34 minutes.

(vi) Texture in 2 mm thick steel.
The integrated intensity of the iron 220 peak is considered measured on a single 2 x 4 cm^2 element of the azimuthal texture bank at 110^0. The count rate is $55\ s^{-1}$ giving 1% statistics in 3 mins. Some 10 pole figures should be measurable simultaneously to give the full orientational distribution function in around 10 mins.

(vii) Quasi-elastic scattering from a 1mm thick water sample.
Turning again to the 1 mm light water sample, the requirement is to measure the quasi-elastic profile with sufficient statistical precision to enable the area under the broad free water distribution to be separated from the narrow bound water peak. A 1% precision in the integrated area under the whole peak is assumed sufficient for this. The count-rate of a single focussed analyser operating at 4.3 Å with 0.1 meV resolution is $4.7\ s^{-1}$ giving a 35 minute count time for 1% statistics.

(viii) Vibrational scattering from 1 mm water at 60 meV energy transfer.
The objective of most neutron vibrational spectroscopy experiments is to identify hydrogenous vibrational modes and so help assign modes and enable inter and intra-molecular force constants to be determined. The vibrations of water molecules are typical and show a broad peak at around 80 meV energy transfer caused by torsional motions. The molecular cross-section at 80 meV is some 35 barns $sterad^{-1}eV^{-1}$. This gives rise to a $20\ s^{-1}$ count rate within a 1 meV scattered energy window. This might be given by a Be/BeO window spectrometer or by a Be edge differential analysis with a 1 meV stepsize. It corresponds to a 8.5 minute run time for 1% statistics.

5. Information presentation: following the *neutron profile* .

A new way of performing neutron experiments is opened up by the multi-facility. The choice of which Q range and resolution is of most importance can be postponed until after the experiment has been completed since the experiment follows the heat treatment or chemical reaction under study, over several ranges and resolutions simultaneously. The battery of facilities would give a *neutron profile* of the sample over any one time period or volume within it. Its display would need great ingenuity to enable the experimenter to follow changes in the profile, rather than be swamped by a deluge of data! It might feature a simultaneous display of processed data. The user would have specified previously the *windows* of interest in which embrittling phase diffraction peaks occur, the unstressed matrix peak positions measured on the 90^0 counters, and the untextured matrix peak intensities measured on the texture counters. He could then view the changes in the defect size distribution, the embrittling phase volume fraction, the internal stress changes and the texture changes as they occur during the experiment.

6. Conclusions.

The count rate predictions for key experiments given by table 4 show the practicality of this instrument, and its ability to employ all the main techniques of applied neutron scattering simultaneously. Its main advantage is its use in kinetic experiments to relate together the many different processes which may take place at the same time. A second advantage is the neutron economy achieved by the wide range of information gathered in a single experiment. The relatively low cost of a complete process study using this instrument will open the door to project managers at present not able to afford the unique information neutrons can give in materials science.

Appendix 1. Wide angle diffraction focussing using a converging collimator.

The achievement of high resolution in diffraction at wide scattering angles requires a high degree of angular collimation. The following method enables the collimation from a single aperture of a converging collimator to be applied to all its beams. The change in flight time caused by the slightly different scattering angles across the collimator is cancelled by the change in flight path. Figure 3 represents a collimator from the moderator M incident on a sample at distance L_0 and converging on a small angle counter at a further distance L_1. The sample is placed so as to lie along the bisector to the counter, which is placed at a distance L_2 from the sample at a scattering angle ϕ. The flight time at a displacement x across the sample is given by

$$t = \frac{m(L_0+L_2)}{h}\, 2d \sin\frac{\phi}{2}$$

$$= \frac{2dm}{h}\left(L_0 + L_2 - 2x\cos\frac{180-\phi}{2}\right)\sin\left(\frac{\phi}{2} + \frac{x\sin\frac{180-\phi}{2}}{2L_1} - \frac{x\sin\frac{180-\phi}{2}}{2L_2}\right)$$

$$= \frac{2dm}{h}\left((L_0 + L_2)\sin\frac{\phi}{2} + x\left((L_0+L_2)\left(\frac{1}{2L_1} - \frac{1}{2L_2}\right)(\cos\tfrac{\phi}{2})^2 - 2(\sin\tfrac{\phi}{2})^2\right)\right). \quad \text{A1.}$$

Focussing then occurs for any value of x when

$$(L_0 + L_2)\left(\frac{1}{L_1} - \frac{1}{L_2}\right) = 4\left(\tan\frac{\phi}{2}\right)^2. \quad \text{A2.}$$

For the special case of 90^0 scattering this reduces to

$$(L_0 + L_2)\left(\frac{1}{L_1} - \frac{1}{L_2}\right) = 4. \quad \text{A3.}$$

References

(1) *Neutron Scattering* Methods of Experimental Physics, K Skold and D L Price (Eds) Academic Press,(1985).

(2) C G Windsor, A J Allen, M T Hutchings, C M Sayers, R N Sinclair, P Schofield and C J Wright, *Neutron Scattering in the 90's* IAEA, Vienna (1985) 575.

(3) G Kostorz, in *Treatise in Materials Science and Technology,* Vol 15, *Neutron Scattering* ,Ed G Kostorz, Academic Press (1979)

(4) G F Slattery and C G Windsor, J Nucl Materials 118 (1983) 165.

(5) A J Allen, M T Hutchings, C G Windsor and C Andreani, Adv Phys (1985) (In Press).

(6) W Schmatz, in *Treatise in Materials Science and Technology* , Vol 15 in *Neutron Scattering* Ed Kostorz, Academic Press,(1979)

(7) C N J Wagner, J of Non Crystalline Solids 42 (1980) 1.

(8) H J Bunge, *Technological applications of texture analysis* Texture of Materials (Proc 7th Int Con Noordwijkerhowt, (1984) Zwijndrecht 447.

(9) T Springer, *Quasi-elastic Neutron Scattering for the Investigation of Diffusive Motions in Solids and Liquids.* Springer Tracts in Modern Physics, Vol 64, Berlin,(1978).

(10) C G Wright and C M Sayers, Rep Prog Phys 46 (1983) 773.

(11) D A Gray in *Neutron Scattering in the 90's* IAEA, Vienna (1985) 261.

(12) C G Windsor, *Pulsed neutron scattering* Taylor and Francis, London, (1981).

(13) A C Nunes Nucl Inst Meth., 119 (1974) 291.

(14) K Inoue, Y Kiyanagi, H Imasa, Y Sakamoto, Nucl Inst Meth, 178 (1978) 447.

(15) J M Carpenter, G H Lander and C G Windsor Rev Sci Inst 55 (1984) 1019.

TABLE 1 Neutron scattering compared to other techniques.

	Neutrons	Electrons	X rays	NMR	Light
Microstructure	SANS	TEM	SAXS		
Phases	Diffraction	Diffracti-on	Diffraction		
Internal strain	90^0 diffraction		Surface diffraction		
Defects	Diffuse	TEM	Diffuse		
Local order	Diffraction		Diffraction		
Texture	Azimuthal diffraction		Diffraction		
Diffusion	Quasi-elastic			Resonance lifetime	
Vibrational	Be filter				Raman Infrared

TABLE 2 Design specification for the multi-facility.

	λ_{max}	λ_{min}	Q_{min}	Q_{max}	ΔQ_{min}	$(\frac{\Delta Q}{Q})_{min}$	$\hbar\omega_{max}$	$\Delta\hbar\omega$
	Å	Å	$Å^{-1}$	$Å^{-1}$	$Å^{-1}$	percent	meV	meV
SANS	8	4	0.008	0.24	0.004	6		
	4	0.1	0.24	5	0.3	6		
Back diffraction	8	0.1	1.6	125	0.006	0.4		
90^0 diffraction	8	0.1	1.5	88	0.004	0.3		
Diffuse	8	4	0.15	0.8	0.03	4		
	4	1	0.8	3.2	0.1	4		
Local order	8	4	0.8	3	0.06	0.7		
	4	1	3	12	0.2	0.7		
Texture	4	0.4	2.2	22	0.03	1.5		
Quasi-elastic	4.3	4.3	1	2	0.1	10	5	0.1
Be filter	4	0.1	7.5	21	1	10	200	10

TABLE 3 Proposed parameters of the SNS multi-facility.

Moderator: Liquid methane 100K: 10x10 cm^2 area: 20000μs period

Incident path: Converging collimator: 8 m flight path: 10 apertures.
Collimation $\alpha_0=\beta_0=0.2^0$

Sample 2 x 2 cm^2 area Standard SNS 40 cm diameter enclosure.

	Scattered path L_1	Angular range ϕ_{min} $\Delta\phi$ ϕ_{max}	Counter elements (widthxheight) xnumber	Total area	Solid angle
	(m)	(deg)	(cm^2)	(cm^2)	(sterad)
SANS	2	0(0.14)9	0.5x0.5x12000	3217	0.08
Back diffraction	1	153(1)175	2x2x1526	6107	0.6
90^0 diffraction	5	85(0.5)95	1.5x50x20	1500	0.006
Diffuse	1	10(0.5)30	1x1x6907	6907	0.7
Local order	0.5	30(2.5)150	2x20x48	1920	0.7
Texture	0.5	110	2x4x48	380	0.15

Quasi-elastic: 60 cm sample-analyser: 60 cm analyser-detector: Wavelength 4.3 Å.
Graphite analyser: 002 planes: $2\theta_A=80^0$: 10x10 cm^2 area: 1^0 mosaic.

Be filter: 22 cm scattered path: 15 cm thickness:
$120–159^0$ scattering angle: 10x10 cm^2 area:
Scattered energy window $\Delta\hbar\omega$ = 1 meV.

TABLE 4 Performance of key experiments on the multi-facility.

	Facility	Experiment	ϕ	Q,ω	Counting Time
			deg.	$Å^{-1}$ meV	min
(i)	SANS	0.1 % of 100Å voids 2mm thick iron.	2	0.05	2.3
		1 mm water calibration.			78
(ii)	Back diffraction	1 % volume fraction 220 bcc peak 2 mm stainless steel.	150	6.2	0.6
(iii)	90^0 stress diffraction	220 bcc peak steel $3x3x3mm^3$ volume.	90	6.2	5.5
		2 mm thick plate.			1.0
(iv)	Diffuse	1% of 25Å voids 2 mm thick iron.	20	.05	34
(v)	Local order	1% amorphous iron 10Å hard spheres 2 mm thick iron.	45	2	16
(vi)	Texture	220 integrated peak 2 mm thick iron.	110	6.2	3
(vii)	Quasi-elastic	1mm thick water Integrated intensity.	45	1.1	35
(viii)	Vibrational	1mm thick water 1 meV window.	140	ω=80	8.5

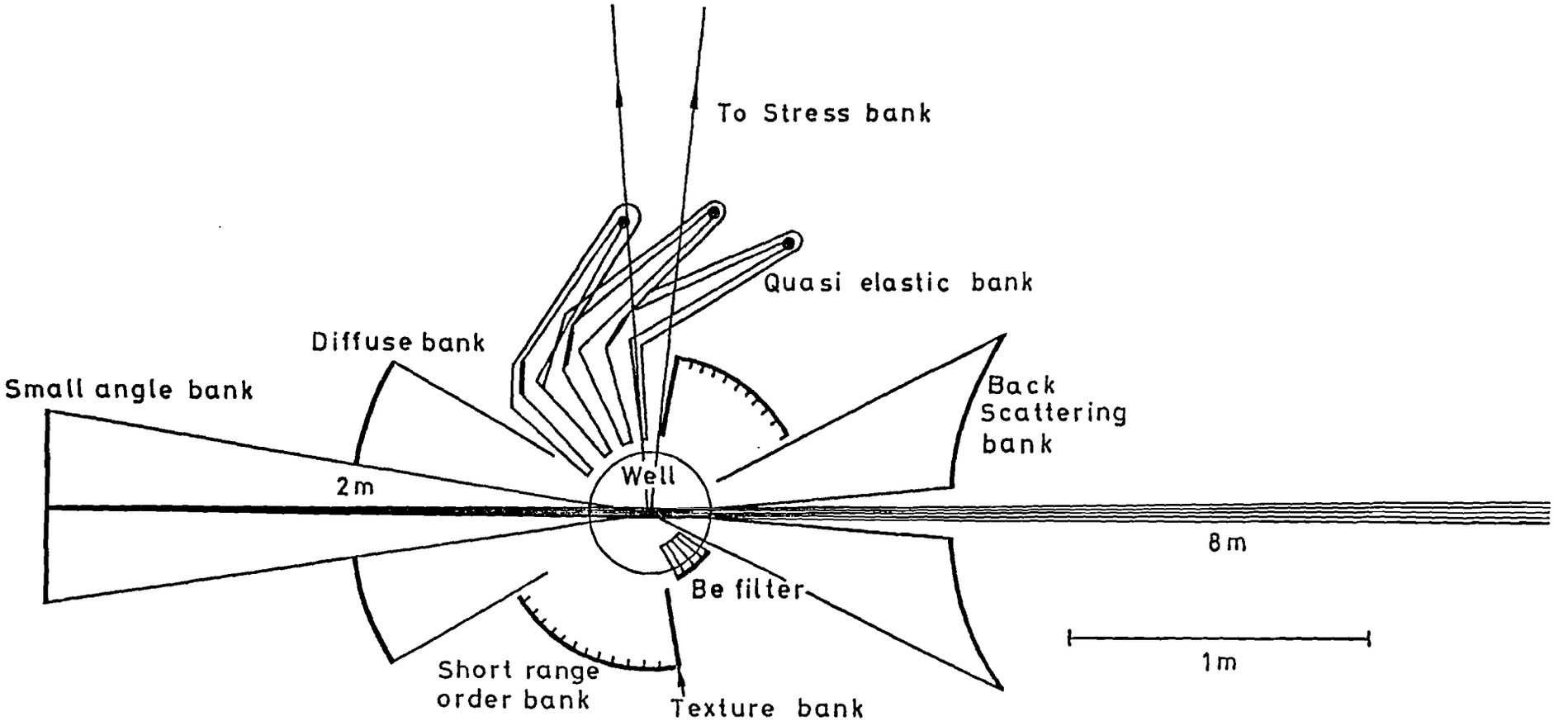

Figure 1. A schematic layout of the proposed materials multi-facility for installation on the SNS. Its various counter banks are able to obtain information simultaneously using the principal techniques of applied neutron scattering.

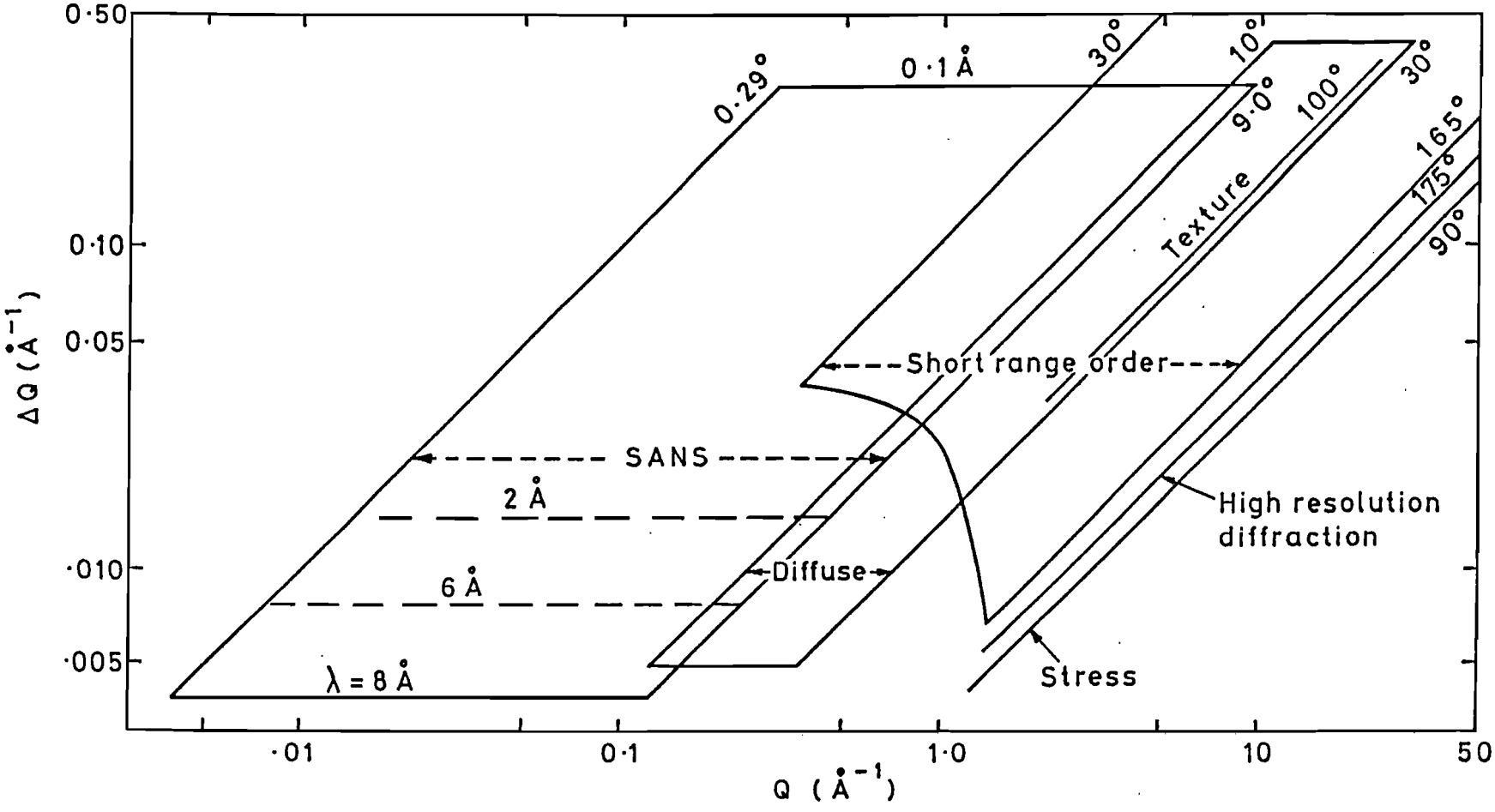

Figure 2. The ranges of scattering vector Q and its resolution ΔQ which can be covered simultaneously using the various counter banks of the multi-facility.

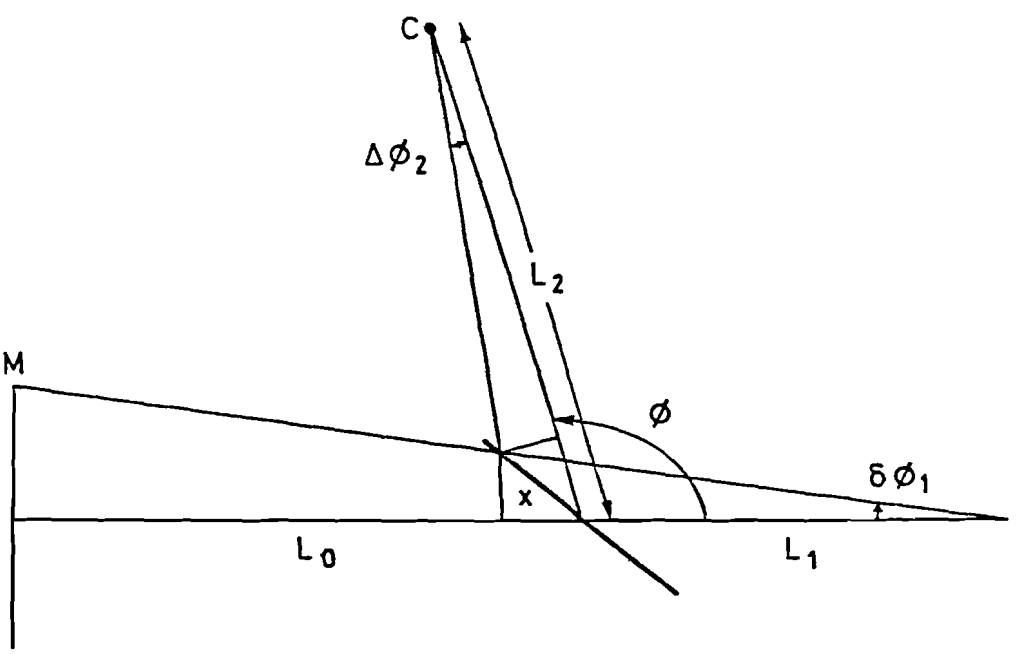

Figure 3. The time focussing for wide angle diffraction possible using a converging collimator.

Proceedings of the Eighth Meeting of the International Collaboration on Advanced Neutron Sources (ICANS-VIII)
8-12 July 1985, Rutherford Appleton Laboratory Report RAL-85-110

LOQ - The Small Angle Diffractometer at the SNS

R K Heenan
Rutherford Appleton Laboratory
Chilton, Didcot
Oxon OX11 0QX

A pulsed spallation source such as the SNS is not generally considered ideal for small angle scattering since it is not optimised to produce long wavelength neutrons. In fact the LOQ machine at the SNS (Figure 1) will be very competitive with reactor based instruments such as D11 at the ILL. The wide range of scattering vector Q accessible in a single measurement (Figure 2) on the SNS means that many experiments could be performed more quickly than on D11.

LOQ looks at a liquid hydrogen moderator, the sample is situated at 16m and there will eventually be 5 "telescopic" detector banks moving independently inside an evacuated tank (20m long, 1.8m internal diameter). Longer wavelength neutrons are selected by a super mirror bender thereby reducing neutron backgrounds at the detector and allowing thinner chopper blades and collimating apertures. A set of three mechanical disc choppers attempt to eliminate frame overlap and define the range of wavelengths used. The pulse rejection chopper could not in practise be placed close enough to the moderator so in some cases a small overlap of long wavelength neutrons occurs at certain detector positions. It is planned to eliminate these with nickel coated silicon crystal mirrors.

Beam diameters at the sample range from 2mm to 25mm. Some guesses have been made for time averaged intensity at the sample assuming full SNS output, allowing for all window transmissions and detector efficiency etc (Figure 3). Taking 1 in 4 pulses (12.5Hz) and selecting 4-10Å neutrons gives a wide Q range and about 3×10^5 neutrons/cm^2/sec. Using 1 in 2 pulses and 2-6Å neutrons reduces Q range and worsens resolution but increases intensity to over 10^6 neutrons/cm^2/sec. These figures compare well to D11 if it is set up with similar collimation. (In the long term a dedicated SNS cold source could do much better as longer moderation times could be tolerated without worsening resolution. Other instruments needing the hydrogen moderator prevent this at present.)

1) LOQ General Arrangement

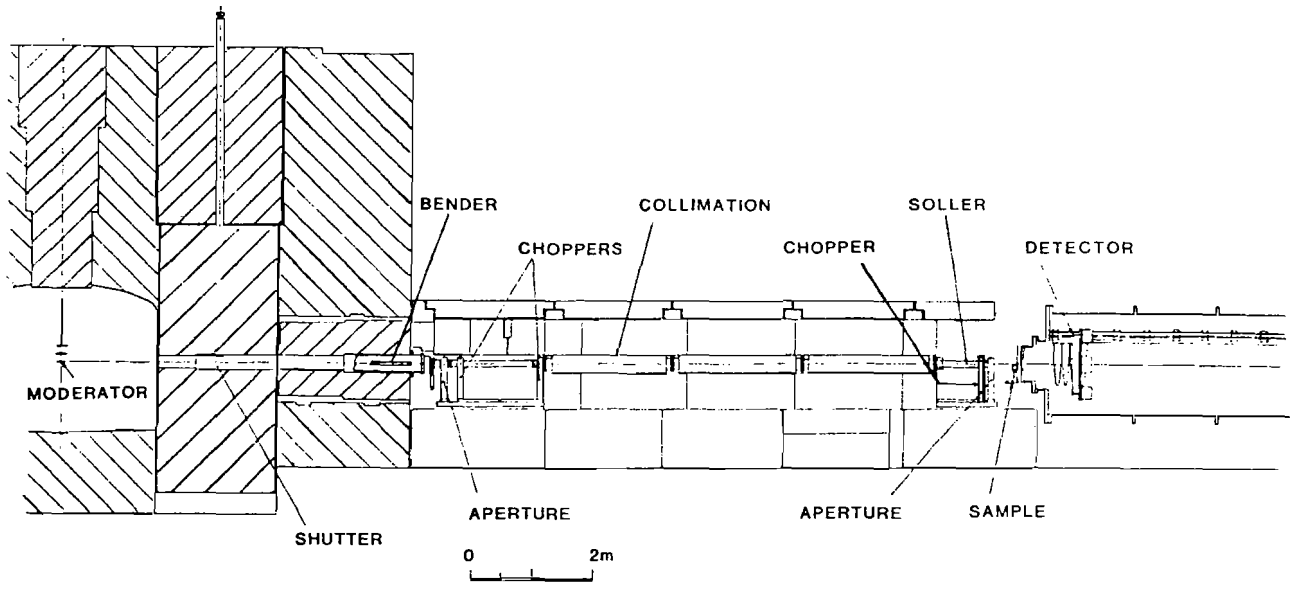

2) LOQ Ranges of Q as a function of detector positions and wavelengths used.

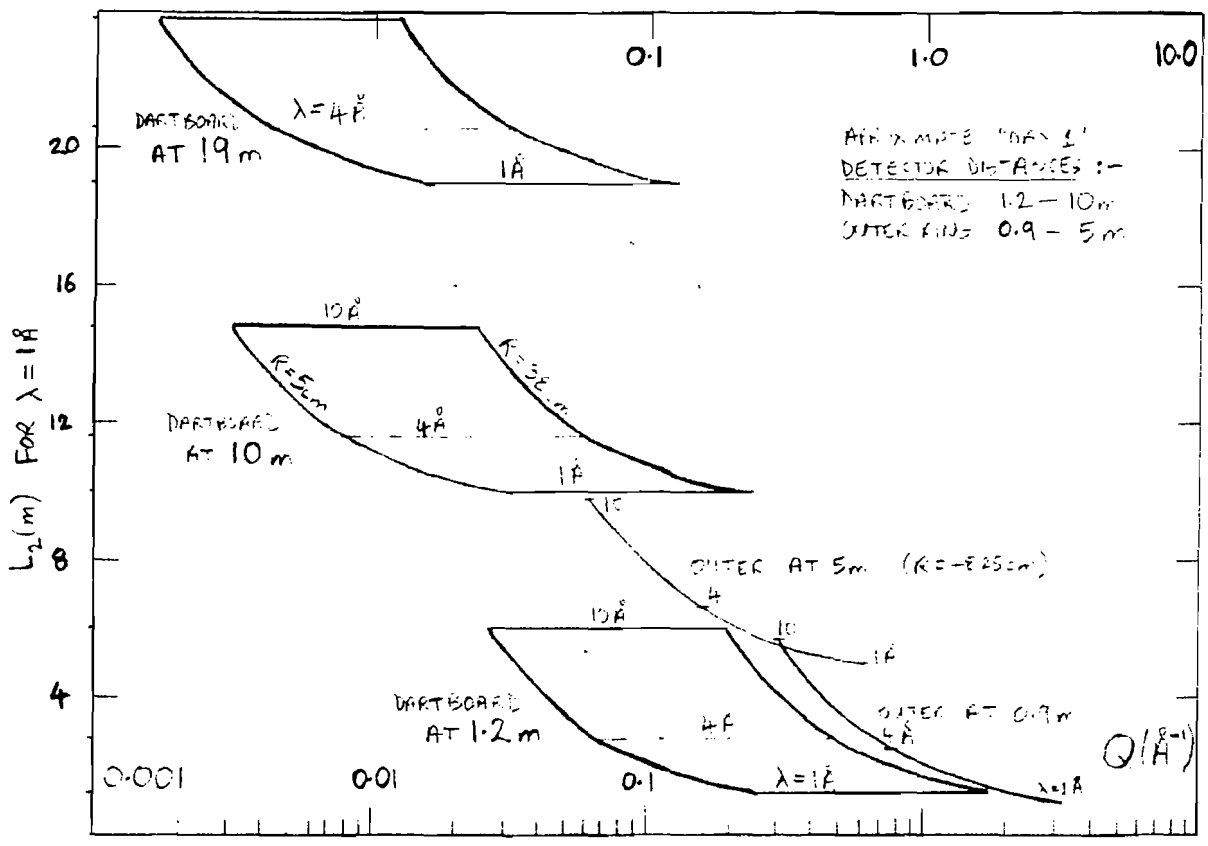

Circularly symmetric detector banks, diameter 1m, are of glass scintillator elements with fibre optic encoding to many fewer photomultiplier tubes. Constructional details are presented in a separate paper. A central scintillator detector array should allow measurement of transmission coefficients as a function of wavelength simultaneously with the diffraction measurements.

Data reduction is quite complex, with various routes possible dependent on the nature of the experiment and quality of data. The discussion given in the paper by P A Seeger et al is relevant here. A modified version of their Monte-Carlo program has also been used to simulate LOQ data. A VAX 11-730 computer is attached to the experimental apparatus for initial display and analysis of data, it runs independently of data collection.

The LOQ apparatus can be tailored to give the best compromise of intensity and resolution for a particular experiment by careful choice of beam size, detector positions, and wavelength range selected. At the time of writing the beam line is still under construction and preparations are being made for a test of the first 1/9 detector segment (560 elements connected to 16 photo-tubes) in the recently delivered 10m section of the vacuum tank.

3) LOQ Estimated intensities at sample.

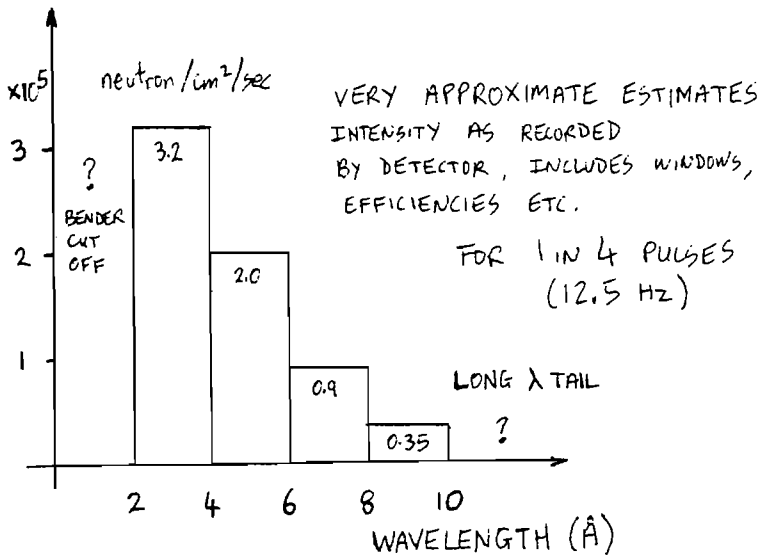

Proceedings of the Eighth Meeting of the International Collaboration on Advanced Neutron Sources (ICANS-VIII)
8-12 July 1985, Rutherford Appleton Laboratory Report RAL-85-110

IRIS - A pulsed source quasielastic and inelastic spectrometer

R C Ward, C J Carlile, P S Goyal* and J L Altrip
Rutherford Appleton Laboratory, Chilton
* Bhabha Atomic Research Centre, Bombay

Abstract

The backscattering technique for high resolution quasielastic and inelastic spectroscopy, used in the investigation of the dynamics of condensed matter, has been extended by its application to pulsed neutron sources. Whilst the wavelength band for reactor based spectrometers is obtained by using complicated instrumental techniques (e.g. Doppler shifting or temperature scanning), the pulsed source variant of such a spectrometer is provided with the wavelength band relatively simply by utilising the pulsed nature of the source and the time of flight dispersion of the neutrons over an incident flight path. Not only is the wavelength band selected by this technique wider than that from other methods but, by simply rephasing the waveband selection chopper to different energies, truly high resolution inelastic spectroscopy can be performed.

The above method has been used in the design of the IRIS spectrometer which is being commissioned on the Spallation Neutron Source at RAL. The incident beam resolution is defined by the dispersion of the narrowly pulsed beam over a ~ 30 metre incident flight path and the scattered beam is analysed by backscattering techniques. The spectrometer will use three different analyser systems which are being installed in phases. The first phase, which is now operational, uses a double polycrystalline beryllium filter and provides elastic resolutions of ~ 50 μeV over an energy transfer range of ~ 20 meV and at Q's up to 3 $Å^{-1}$. The second phase, to be installed in 1986, uses pyrolytic graphite analysers in backscattering and provides an elastic resolution of ~ 12 μeV over the same energy transfer range and at Q's up to 2 $Å^{-1}$. The third phase will use silicon analysers and will provide elastic resolutions of ~ 1 μeV over the same ranges of $\hbar\omega$ and Q.

IRIS will be fully operational by the end of 1986 and will provide an extension of the facilities available for the study of diffusive molecular motions. It will also greatly increase the energy transfer range available for microvolt inelastic scattering spectroscopy.

References

C J Carlile, 'High Resolution Inelastic Spectrometer', Proceedings of the 4th Meeting of International Collaboration on Advanced Neutron Sources (KENS Report II) p588, 1980.

B A Dasannacharya, P S Goyal, P K Iyengar, N S Satya Murthy, J N Soni and C L Thaper, 'ΔT-Window Spectrometer', Proceedings of the International Conference on Neutron Scattering in the '90s IAEA Vienna 1985 p443

Proceedings of the Eighth Meeting of the International Collaboration on Advanced Neutron Sources (ICANS-VIII)
8-12 July 1985, Rutherford Appleton Laboratory Report RAL-85-110

FIRST RESULTS ON THE CRYSTAL ANALYSER SPECTROMETER, TFXA, AT THE SNS

J Penfold
J Tomkinson
M Lobo
I Davidson

Presented are the first preliminary commissioning results obtained on the crystal analyser spectrometer TFXA at the SNS.

The Time Focussed Crystal Analyser TFXA is an indirect geometry inelastic scattering spectrometer using a time-focussed pyrolytic graphite analyser to give good count rates and energy transfer resolution over a wide range of energy transfers.

TFXA is located on the N8 beam at 12m from the ambient poisoned moderator at the SNS.

The spectrometer is based on the time focussing geometry described by Ikeda et al[1], and is shown in figure 1. In addition to the time focussing, the Marx principle is used to provide energy focussing[2]. This reduces the positional uncertainty in the analysing energy E_2, and is a feature not previously exploited on crystal analyser spectrometers. It enables good energy transfer resolution to be maintained down to energy transfers of a few meV.

Figure 2 shows the calculated energy transfer resolution for TFXA. The improvement in resolution from the energy focussing at energies of less than 100 meV is clearly shown. Further improvements in resolution are expected by removing the uncertainty in scattered flight path due to the thickness of the BF_3 gas detectors.

The spectrometer has been installed with half the final detector solid angle, comprised of eight 1" BF_3 gas detectors. The full detector solid angle and scintillator detectors will be installed later in 1985.

The initial commissioning results have been obtained using a 30% scatterer of zirconium hydride at mean currents on the SNS of between 0.05 and 0.5 μA. Figure 3a shows the raw time of flight data summed over the eight detectors. The suppression of the higher order reflections from the graphite analyser by the cold beryllium filter is excellent. Low levels of background are seen at both short and long times of arrival. Figure 3b shows the raw time of flight data of the individual detectors, where the importance of the variation in final energy for the different detectors at low values of energy transfer is clearly demonstrated by the variation of the position of the elastic line. An initial calibration of the important distances L_1 and L_2 and the final energies E_2 for each detector have been performed. Figures 4a and b show the raw data of figure 3 transferred to an energy transfer scale and corrected for incident spectral shape. The elastic line shown in figure 4a has a fwhm ~ 0.27 meV compared with a calculated width ~ 0.3 meV. Figure 4b shows the fundamental vibrational mode and three overtones of zirconium hydride. The absence of any significant background bodes well for the future. Intensity calculations are in reasonable agreement with the data. The inherent width of the zirconium hydride features does not place any demands on the instrumental resolution. It is intended to demonstrate the resolution with more suitable samples in the near future.

Acknowledgements

We wish to acknowledge the advice of D K Ross and R N Sinclair, and the advice and help of colleagues at RAL.

References

(1) S Ikeda, N Watanabe and K Kai, Physics 120B (1983) 131

(2) D K Ross - private communication

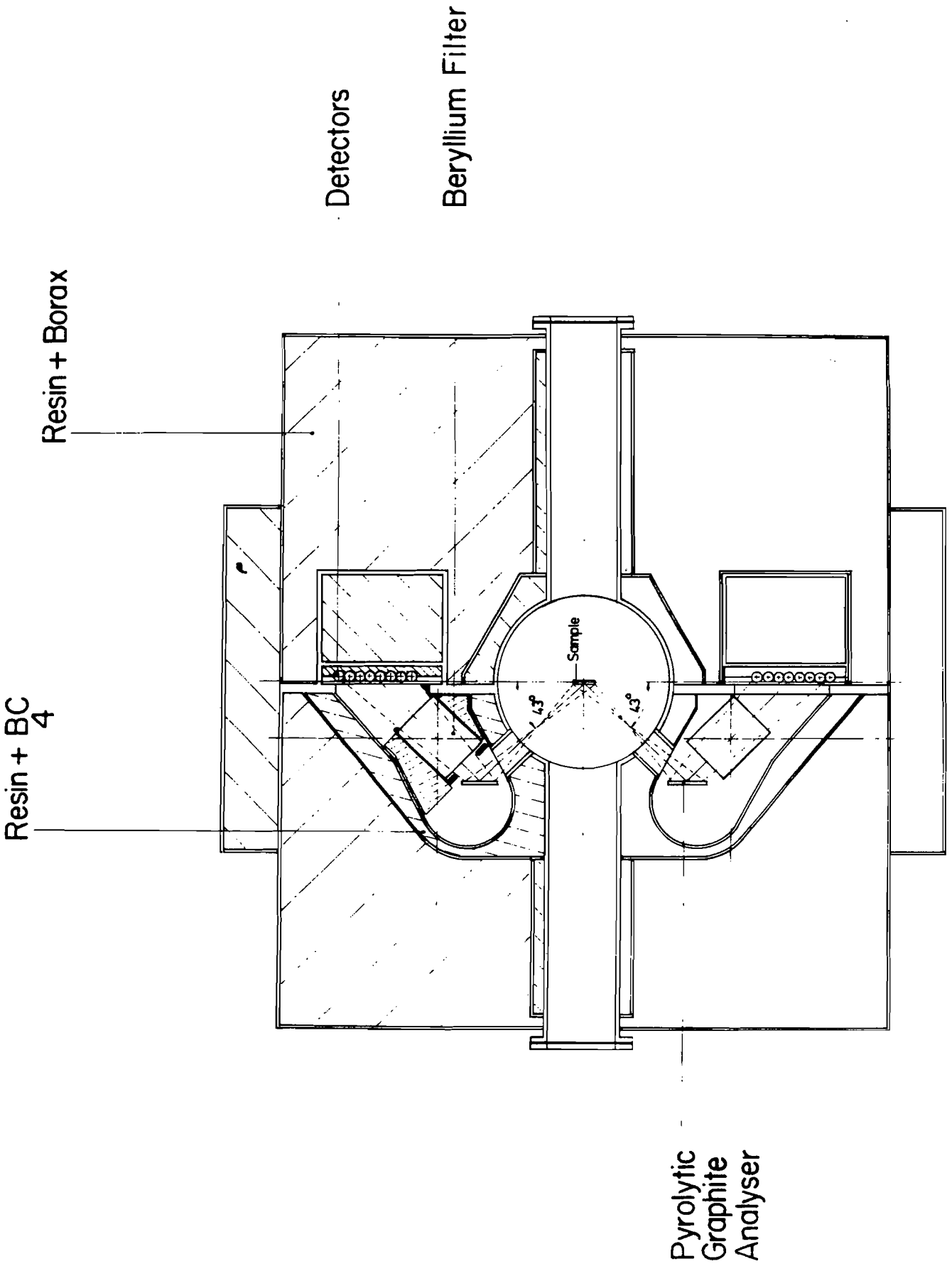

(1) Layout of the time focussed crystal analyser spectrometer.

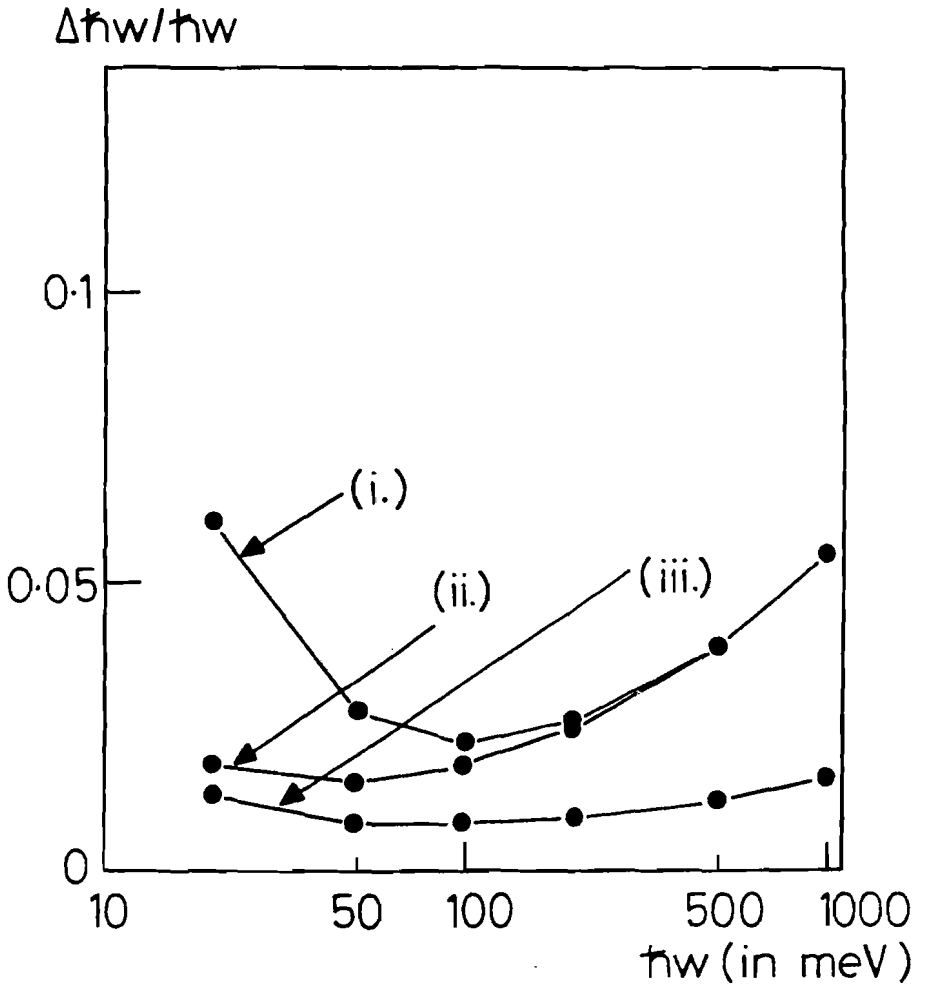

(2) Time focussed crystal analyser spectrometer energy transfer resolution $\Delta h\omega/h\omega$ for (i) 1" BF_3 detectors, (ii) as (i) but with energy focussing and (iii) as (ii) but with an improved detector system.

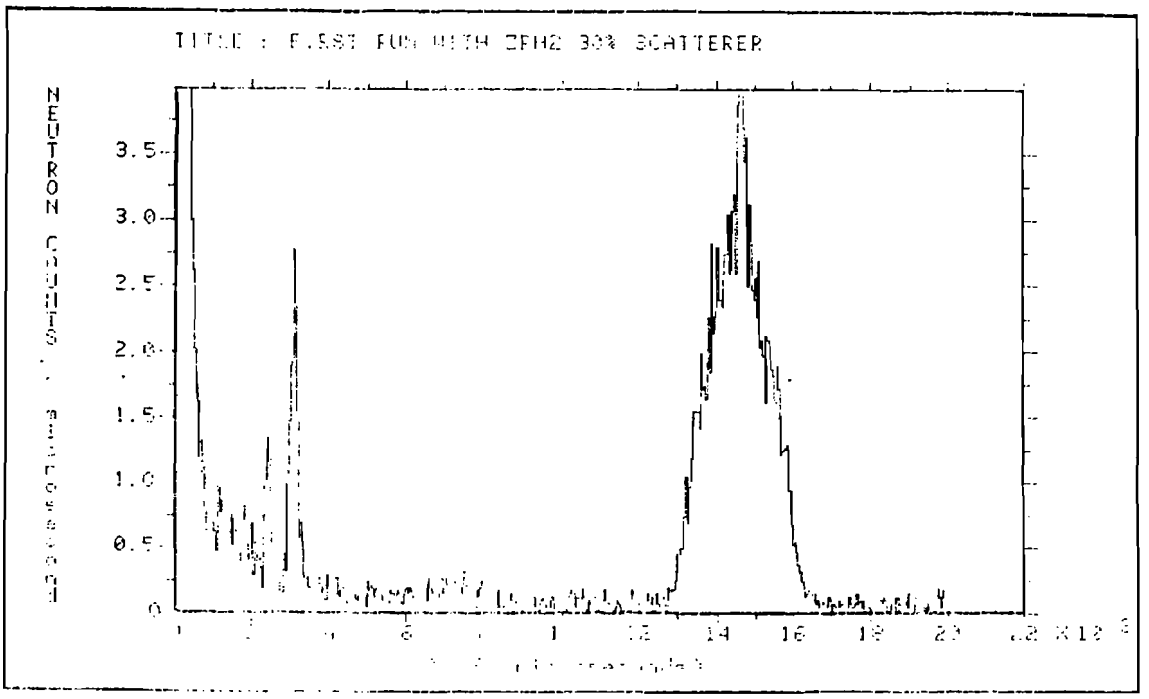

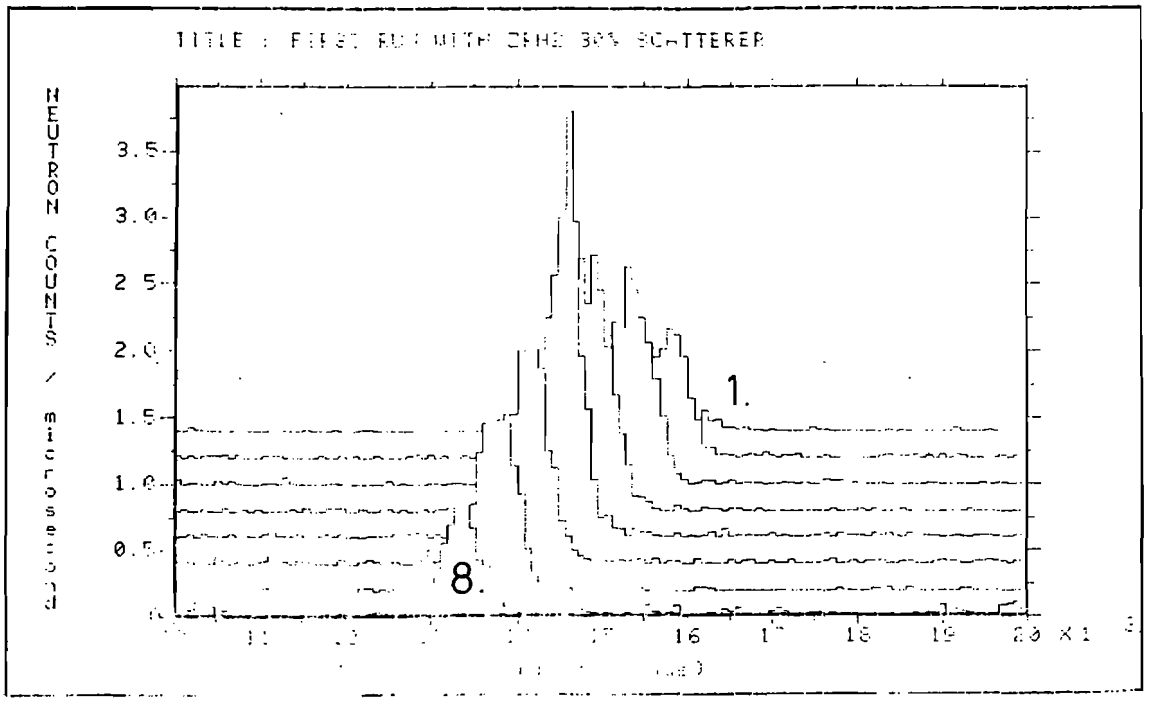

(3) (a) Raw tof data of ZrH_2 for the sum of the eight detectors.

(b) Raw tof data of ZrH_2 from the individual detectors.

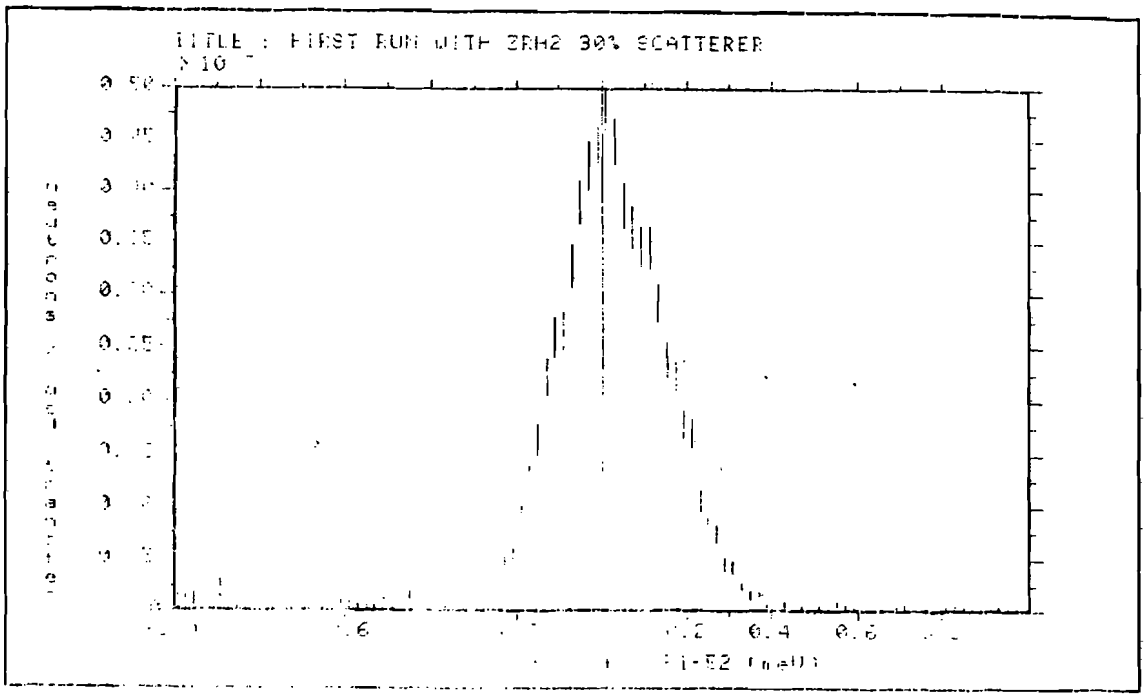

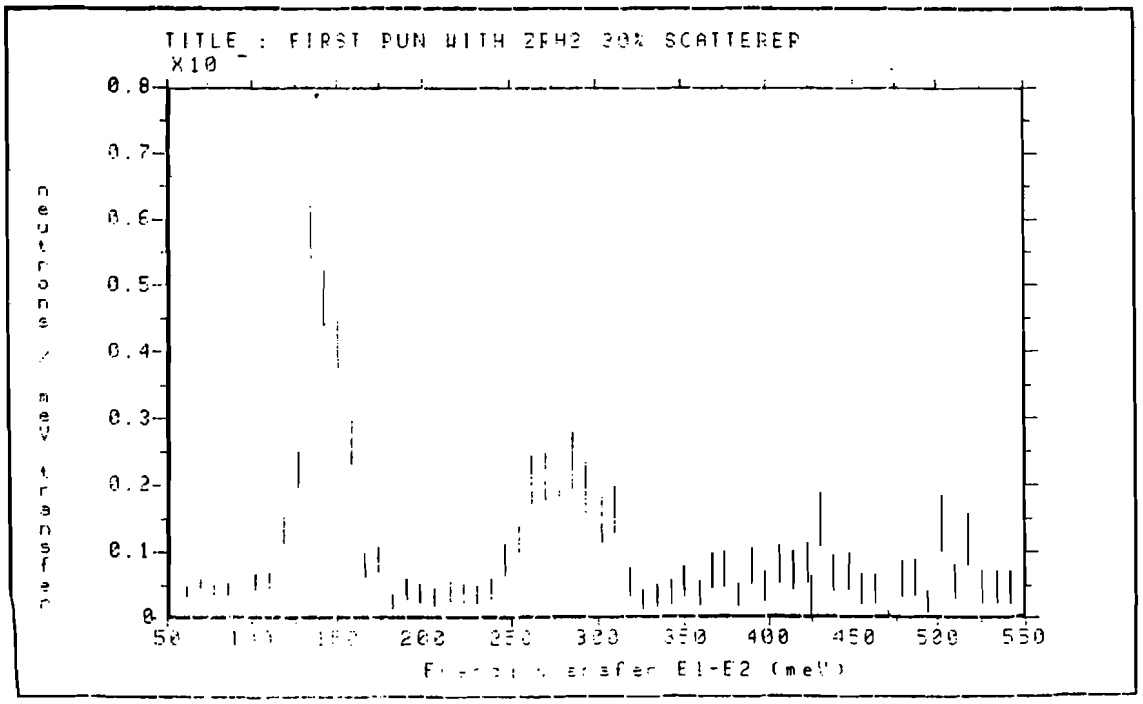

(4) ZrH_2 data corrected for incident spectral shape and transferred to a energy transfer scale

(a) Elastic line

(b) Fundamental vibrational mode and overtones

Proceedings of the Eighth Meeting of the International Collaboration on Advanced Neutron Sources (ICANS-VIII)
8-12 July 1985, Rutherford Appleton Laboratory Report RAL-85-110

MARS - A MULTI-ANGLE ROTOR SPECTROMETER FOR THE SNS

C J Carlile, A D Taylor and W G Williams
Neutron Division, Rutherford Appleton Laboratory

Abstract

The design concept for an optimised direct geometry inelastic spectrometer on the SNS is discussed with the emphasis on the choice of the monochromating method. The resolutions, dynamic ranges and fluxes achievable with crystals and phased choppers are calculated for the incident energy range $20 \leqslant E_1$ (meV) $\leqslant 500$. We also consider the practicalities of realising a spectrometer to provide 1% energy transfer resolutions over a large (Q, ε) range. It is shown that the chopper spectrometer is the better choice for the major part of this incident energy range, but that the crystal method, particularly in a double monochromator arrangement, may offer advantages at the lowest energies. While anticipating that most applications will require the rotor option we consider that the most versatile spectrometer is a hybrid one, and make recommendations on a suitable spectrometer design. Full details of this work have been reported in Rutherford Appleton Laboratory report RAL-85-052.

Proceedings of the Eighth Meeting of the International Collaboration on Advanced Neutron Sources (ICANS-VIII)
8-12 July 1985, Rutherford Appleton Laboratory Report RAL-85-110

FIRST RESULTS FROM THE HIGH ENERGY TRANSFER SPECTROMETER HET AT THE SNS

B C Boland, Z A Bowden, T G Perring*
and A D Taylor

Neutron Division
Rutherford Appleton Laboratory
Chilton, Didcot, Oxon, OX11 0QX
UK

THE HET SPECTROMETER

The HET spectrometer [1] at the SNS is a direct geometry chopper spectrometer designed to study systems at high energy transfer ε with low associated momentum transfer Q and good resolution $\Delta\varepsilon$. The chopper [2], which spins at 600 Hz, has been successfully phased to the accelerator via a master clock. The burst time of the chopper is matched to the moderator pulse width and the spectrometer views the moderator at an angle of 27° to the normal to minimise the scan time contribution. Three chopper slit packages, optimised for 250 meV, 500 meV and 1000 meV are envisaged, but all commissioning to date has been done with the intermediate energy package.

The layout of the spectrometer is illustrated in Figure 1. The monochromating chopper is located at 10m and the primary flight path is

---

* Permanent address: Cavendish Laboratory, Cambridge, CB3 0HE

11.8m. The low angle detector bank, covering 3° to 7°, has a secondary flight path of 4m. The detectors are 10 atmosphere ^3He tubes arranged in 5 banks with azimuthal symmetry. One bank is in the horizontal scattering plane for single crystal excitations and has an angular resolution of 0.25°. A bank of direct coupled scintillator detectors, again with azimuthal symmetry, covers scattering angles of 9° to 29° with 2° resolution. Currently 32 of the eventual 256 elements are available. A high resolution scintillator bank covering these angles with 0.5° resolution is located in the horizontal plane. The kinematic space covered by these banks is illustrated in Figure 2 for three values of incident energy. The difficulty of achieving high values of energy transfer subject to the constraint that $Q \leq 4 \text{Å}^{-1}$ is illustrated in Figure 3. The chopper performance has been estimated using a Monte Carlo calculation and the resulting energy resolution, using the approach of reference [3], is given in Figure 4.

In addition the spectrometer has the capability of making measurements at high momentum transfer, an important region for the study of quantum fluids. For this purpose, a high angle bank, consisting of six scintillator elements at a secondary flight path of 4m, has been constructed, see Figure 1. Its scattering angle may be varied between 80° and 140°.

FIRST RESULTS

Excellent progress has been made with low intensity commissioning of the spectrometer. Beam profiles have been measured and show that B_4C collimation is extremely effective, see Figure 5. The bulk shield shutter position has been optimised for signal to noise. 126 detectors are being used and show good signal to noise, even at low scattering angles. With the chopper removed, timing and length calibrations have been carried out using resonance foils and Bragg diffraction.

Figure 6 shows the raw time-of-flight spectrum of ZrH_2 ($6\ 10^{21}$ H atoms/cm^2 with a beam area of 4 x 4 cm^2) taken with an incident energy of 526 meV. Data have been summed over all detectors between 3° and 7°. The total time to measure this spectrum was 6.9 μA-hr, which corresponds to 2 minutes at full SNS intensity. The measured elastic line at 1.6ms has a resolution of $\Delta E_o/E_o = 0.82\%$ which compares well with the predicted value

of 0.79%. The inelastic features at 1.67ms, 1.79ms and 2.05ms correspond to the 140 meV, 280 meV and 420 meV simple harmonic oscillator transitions in ZrH_2. The momentum transfer associated with these features is 2.6$Å^{-1}$, 5.2$Å^{-1}$ and 8.8$Å^{-1}$ respectively. These data, transformed to an energy scale, but not corrected in any other way, are shown in Figure 7.

The user programme planned for HET includes experiments on the vibrational spectroscopy of metal hydrides, and hydrogen bonded systems, crystal field levels in actinide and rare earth metal systems, itinerant magnetism and momentum distributions in quantum systems. Data from a 26 μA-hr preliminary study of the ferroelastic KH_2PO_4 are shown in Figure 8.

REFERENCES

[1] B C Boland, 'High Energy Inelastic Spectrometer' in 'Proceedings of ICANS-IV, October 1980', published as KENS Report II (1981).

[2] T J L Jones, J H Parker, J K Fremerey, K Bowden and I Davidson, 'Experience with the KFA-Julich Magnetic Bearing System on an SNS Neutron Chopper', these proceedings.

[3] C J Carlile, A D Taylor and W G Williams, 'MARS - A Multi-Angle Rotor Spectrometer for the SNS', Rutherford Appleton Laboratory Report RAL-85-052 (1985).

Figure 1

HET Spectrometer

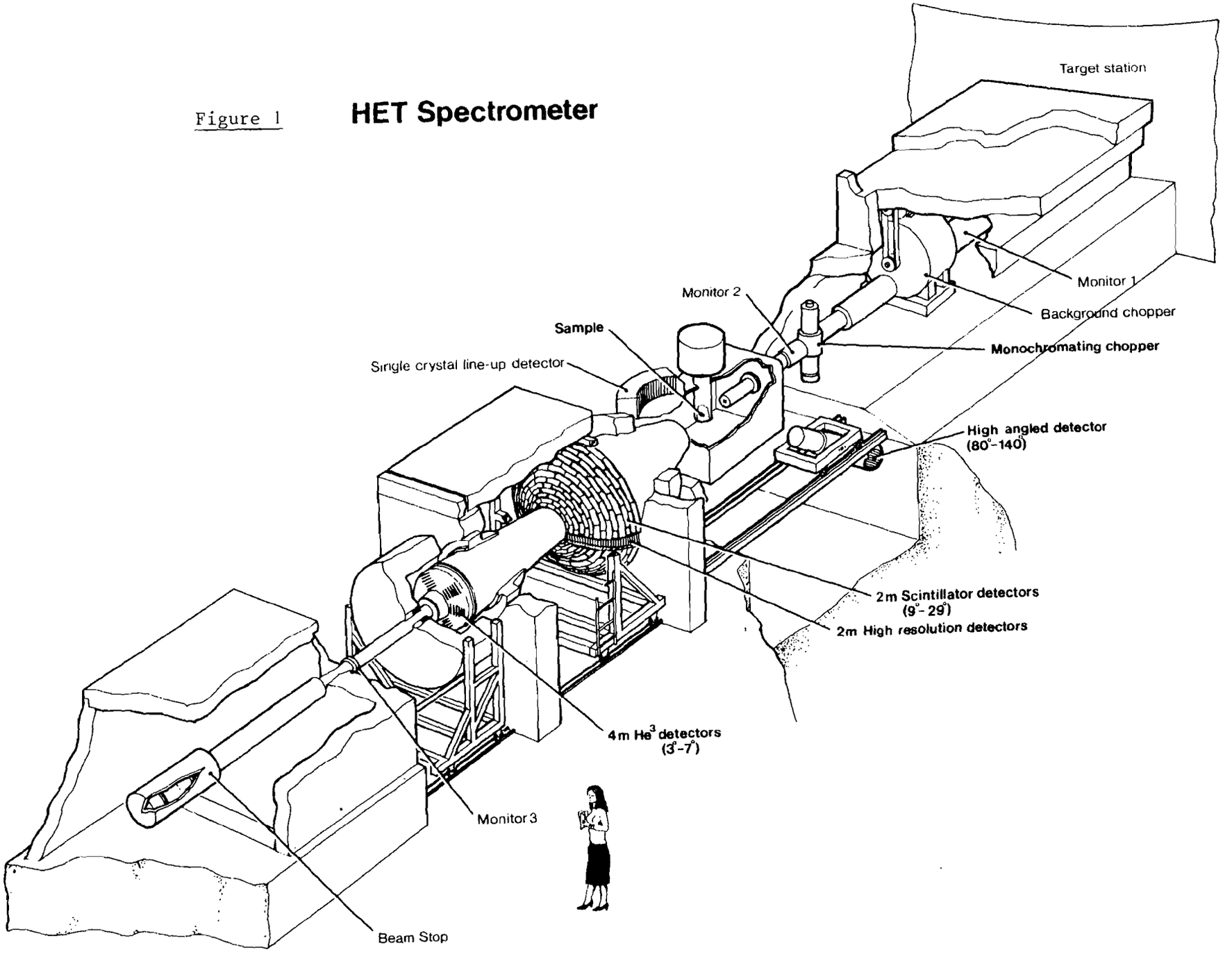

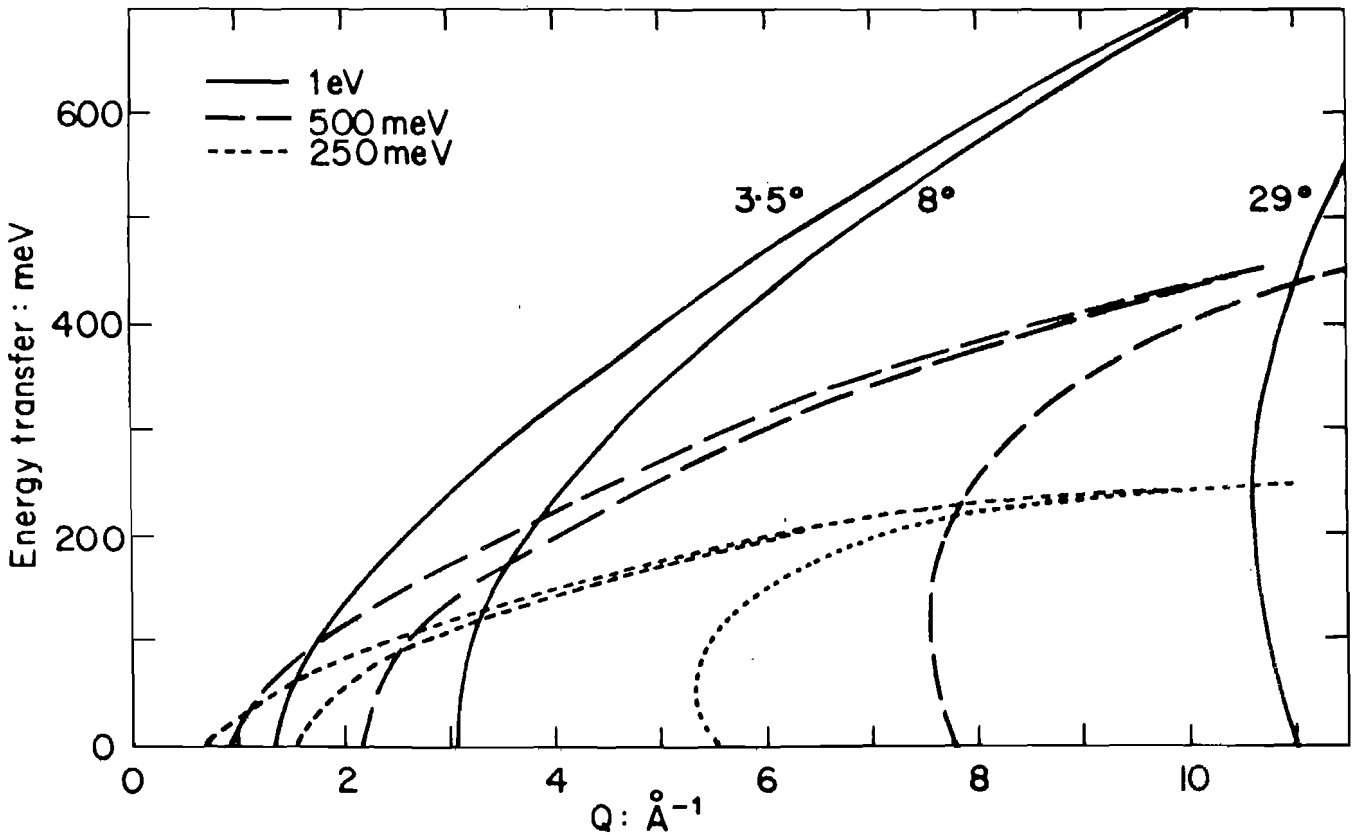

Figure 2 Kinematic space accessible by the 4m bank (3.5°-8°) and the 2m bank (8°-29°) for three values of incident energy

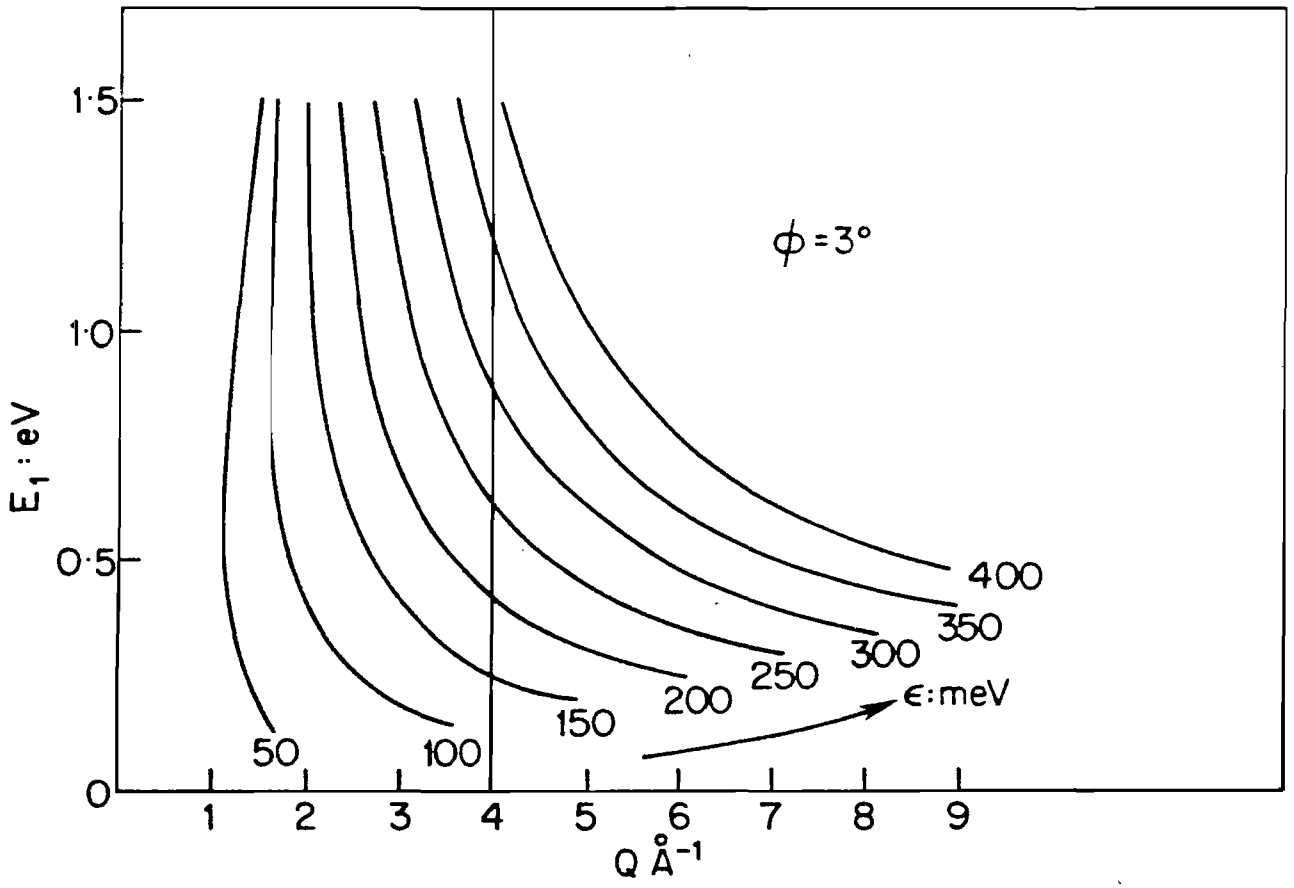

Figure 3 Plot of incident energy against momentum transfer for the lowest scattering angle illustrating the incident energies required to achieve a given energy transfer subject to the condition $Q \leq 4Å^{-1}$

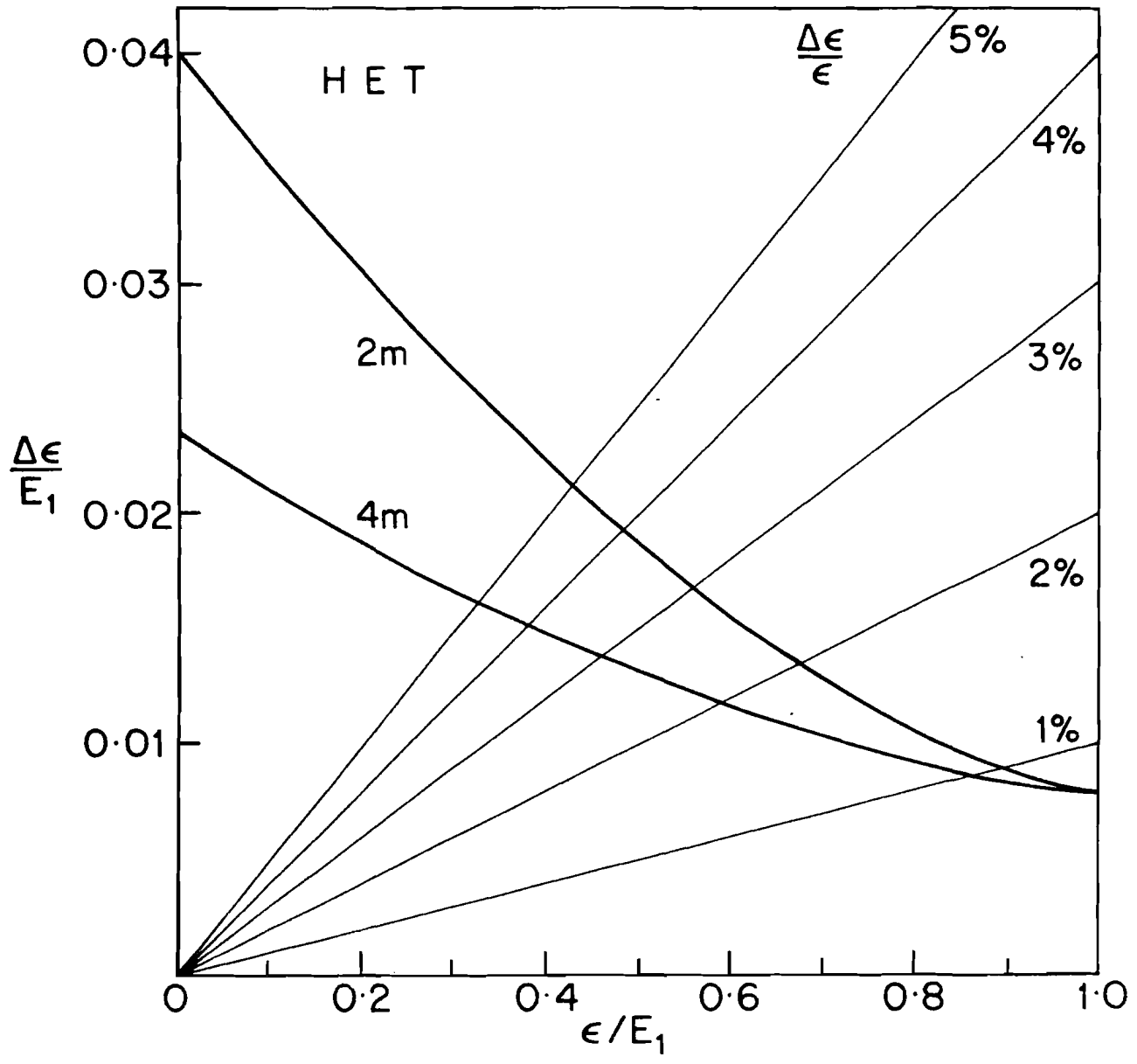

Figure 4 The energy transfer resolution of the HET 2m and 4m banks in reduced units. Fractional energy transfer resolutions are also indicated

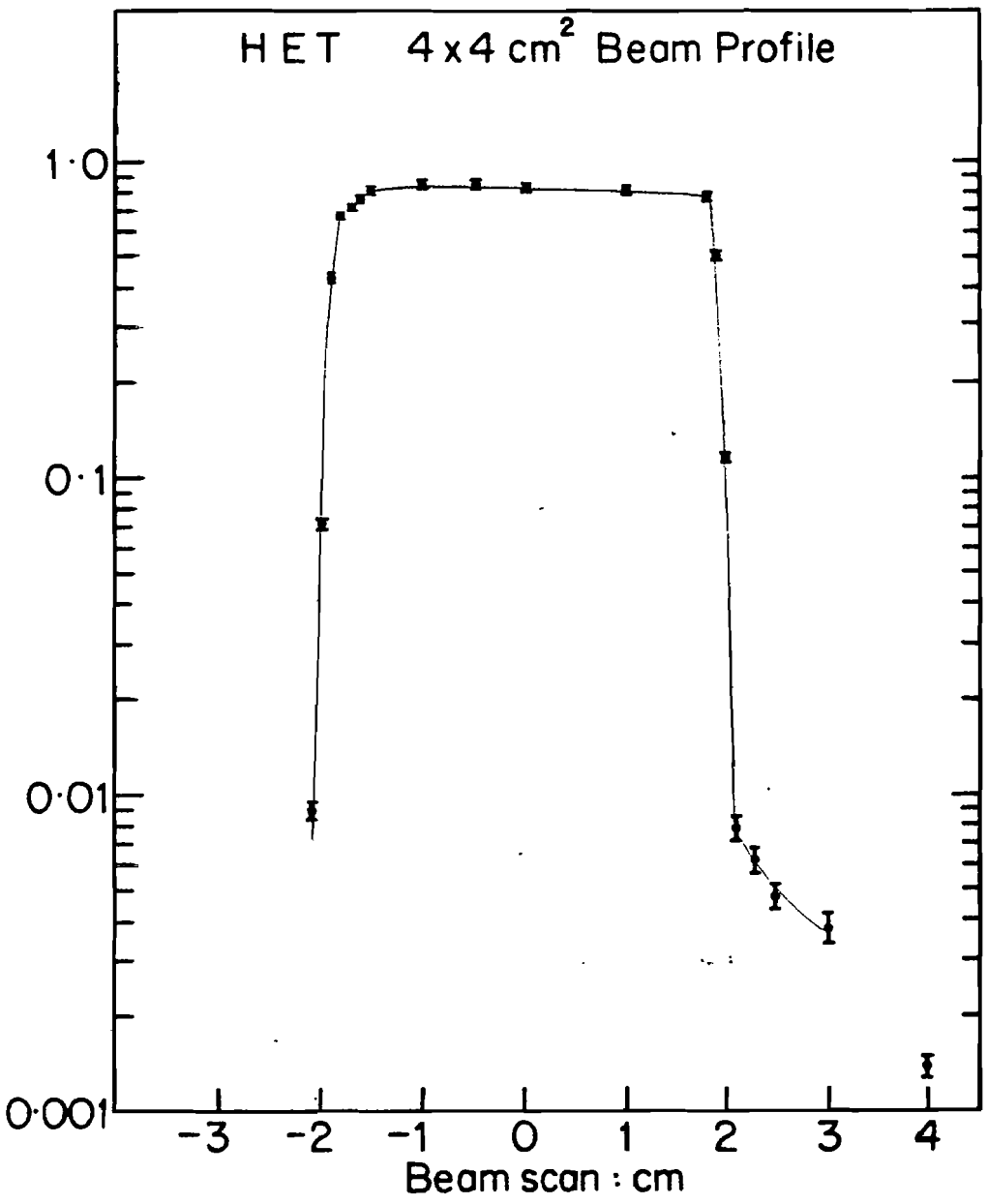

Figure 5 The measured HET beam profile at the sample position

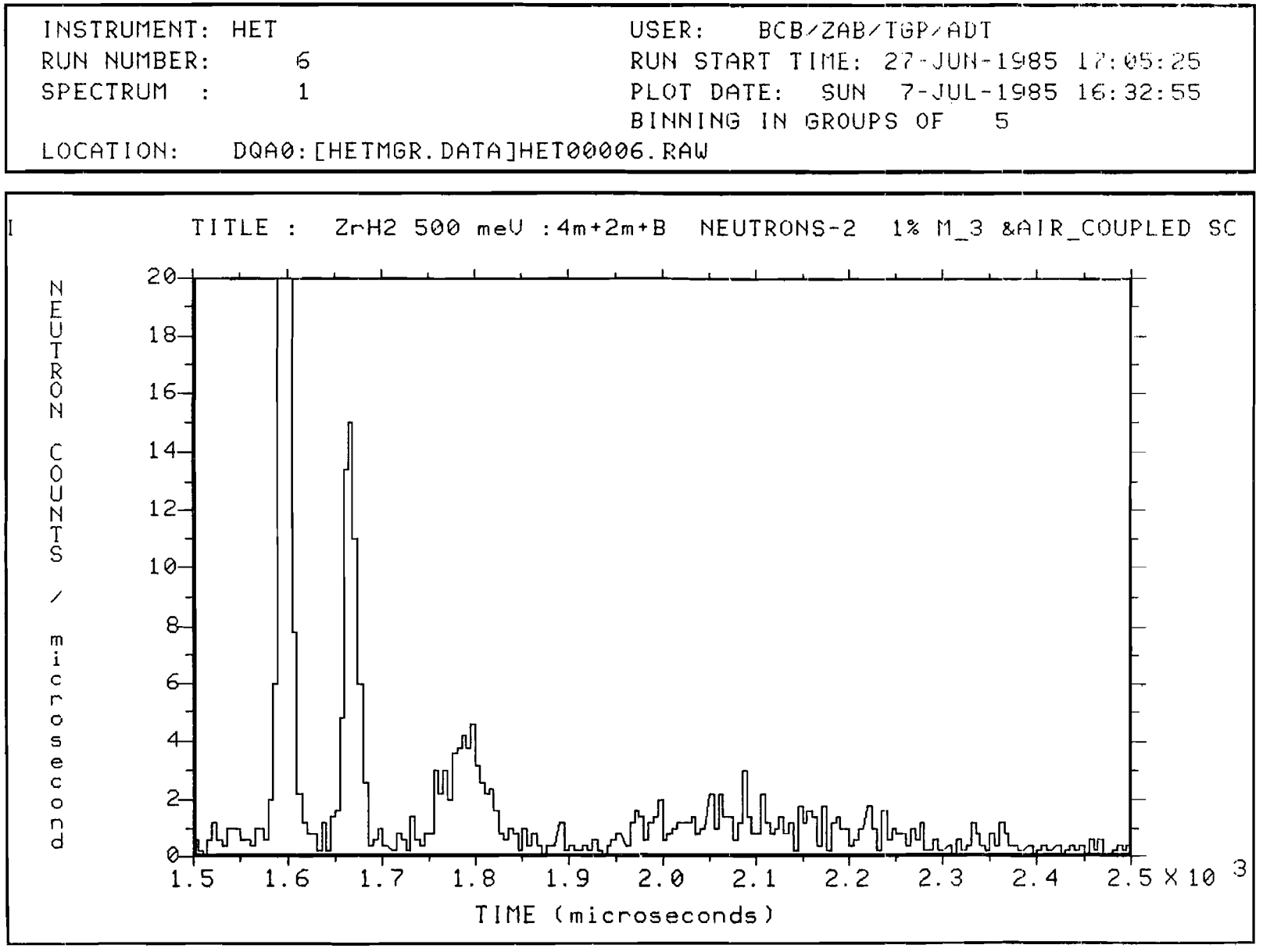

Figure 6 The raw time-of-flight spectrum of ZrH_2 taken in 6.9 μA-hr with an incident energy of 520 meV

INSTRUMENT: HET
RUN NUMBER: 6
SPECTRUM : 1

LOCATION:

USER: BCB/ZAB/TGP/ADT
RUN START TIME: 27-JUN-1985 17:05:25
PLOT DATE: WED 7-AUG-1985 18:16:32
BINNING IN GROUPS OF 4

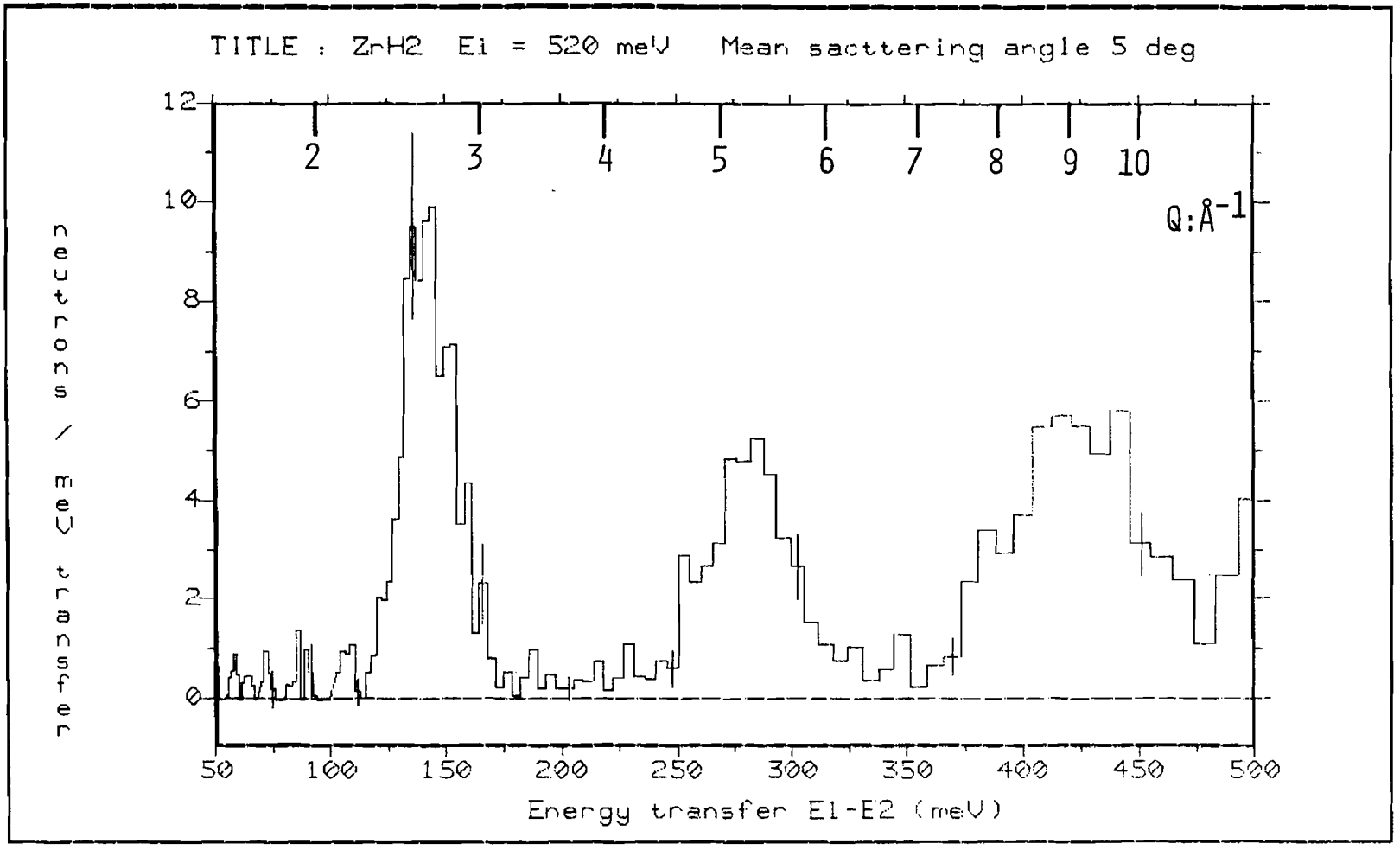

Figure 7 The data of Figure 6 converted to an energy transfer scale

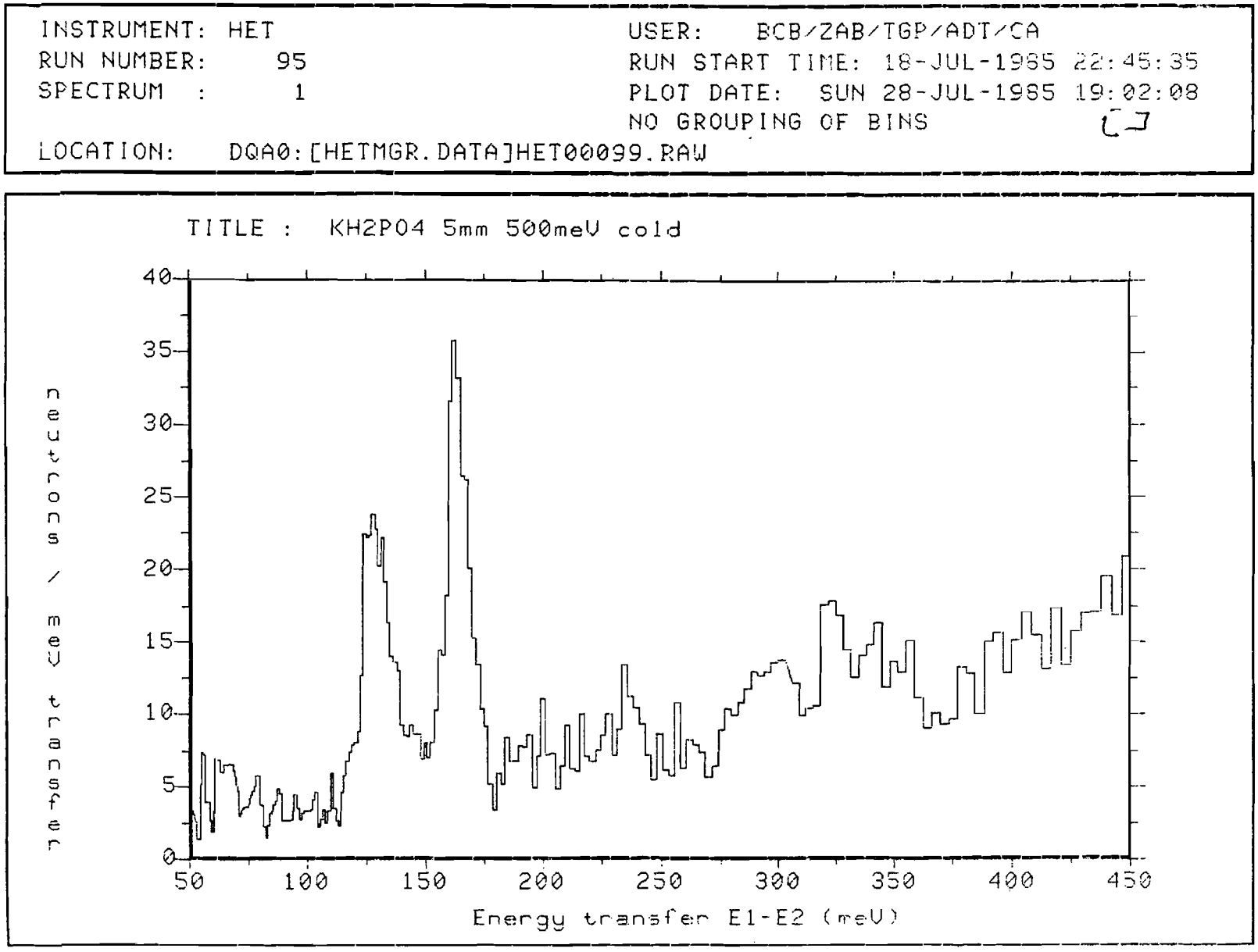

Figure 8 Data on KH_2PO_4 taken in 26 μA-hr with an incident energy of 495 meV

Proceedings of the Eighth Meeting of the International Collaboration on Advanced Neutron Sources (ICANS-VIII)
8-12 July 1985, Rutherford Appleton Laboratory Report RAL-85-110

SPECIALISED NEARELASTIC SPECTROMETER FOR RELAXATIONS IN ATOMIC LIQUIDS

by P.A. Egelstaff

Physics Department

University of Guelph, Guelph, Ontario

Abstract

For the study of gases, liquids and glasses it is useful to make inelastic scattering measurements at low q using neutrons of ~1Å. The case for this type of research is demonstrated through the recent analysis[1] of inelastic scattering data on dense gases taken at the 1N4 spectrometer. Until the development of the new pulsed neutron sources, the combination of reasonable resolution with reasonable counting rates in this regime was difficult or impossible to achieve. However by exploiting the new sources it seems possible to open up this field with a new spectrometer for nearelastic scattering, and a prototype instrument is described.

Introduction

The study of collective excitations in dense gases, liquids and glasses has a long history during which the importance of the transition regime between hydrodynamic behaviour and a collision dominated regime has been stressed. There is an extensive theoretical and experimental literature and several controversies are unresolved.

In terms of the dynamic structure factor, $S(q,\omega)$ the transition regime occurs for $0.1 < q < 0.6$ A^{-1} and $\omega \sim vq$, where v is the velocity of sound. These boundaries are not clearly defined and vary from sample to sample, but for many materials lie beyond the capabilities of commonly used neutron spectrometers (e.g. the 1N4 at the I.L.L. and the conventional 3-axis instruments). Only a few demonstration experiments have been attempted so far. One reason for this is the coupling between q and ω in neutron experiments, which is shown in figure 1. In this figure the ratio $y = \omega/v_n q$ (ω/q is the velocity of sound when a mode is observed and v_n is the neutron velocity) is plotted against the ratio (x) of the momentum transfer ($\hbar q$) to the neutrons momentum (mv_n). For this plot a mode having an approximately linear ω-q relationship will correspond to y=constant. Since the range of q is pre-determined, x cannot be large unless the incident neutrons velocity (v_n) is small: but in this case y will be large and outside the experimentally accessible range shown in the figure. Thus, as is well known, a relatively large neutron velocity is needed for these experiments: for practical purposes it should be greater than v. Because v varies between ~ 700 m/s for gases and ~ 3000 m/s for low temperature glasses, a reasonable choice is $v_n \sim 5000$ m/s ($\lambda \sim 1$Å). To reduce the experimental difficulties a lower velocity could be used for gaseous samples, and so an instrument offering a few fixed wavelengths in the 1 to 2 Å range would be suitable. The hatched area in figure 1 shows the area bounded by these requirements on q, v and v_n. The main point is that angles less than 5^o are needed.

The resolution requirements are also rather stringent, because the mode frequency is ~ 10^{12} $rads^{-1}$ for gases and a resolution width of ~ 1/10 of this frequency is needed. For example, a conventional time-of-flight experiment using 1 Å neutrons would involve ~ 15 m paths with time channels ~ 2.5 μsec. However if we ask that the 5 degree angular range is divided into ~ 0.1^o intervals, the sample dimensions would be ~ 2 cms at 15 m. Fortunately the samples in this field may be fabricated conveniently in this

size. Moreover a position sensitive detector of dimensions ~ 1 m diameter and ~ 2 cm resolution is a reasonable possibility. Thus although these characteristics are unusual, they are not inconceivable for an intense pulsed neutron source and modern instrument techniques.

Other details of a proposed instrument will be given later, but meanwhile a brief theoretical background will be given.

2. Brief Theory of R.A.L. via S(Q,ω)

The hydrodynamic theory of relaxations in atomic liquids may be used to derive an expression for $S(q,\omega)$. This expression, valid for $q \to o$, is the sum of three Lorentzians; one centered on $\omega = o$ related to non-propagating modes and one each centered at $\omega = \pm vq$ related to propagating sound modes. For larger values of q a generalised version of this expression has been derived in many papers, and may be written:

$$S(q,\omega) = \frac{1}{\pi} \frac{\frac{kT}{M} q^2 \, \mathrm{Re}[M(q,\omega)]}{\left| \omega_o^2 - i\omega \, M(q,\omega) - \omega^2 \right|^2} \qquad (1)$$

where $\omega_o^2 = kT\, q^2/MS(q)$, and $S(q)$ is the static structure factor. $M(q,\omega)$ is the Laplace transform of the memory function for the current-current correlation function in one form of the theory, and is the generalised viscous damping function for propagating modes in another form. Egelstaff and Gläser[1,2] rewrite equation (1) in terms of a normalised frequency $x = \omega/\omega_o$ and a normalised daming function, σ, i.e.:-

$$S(q,x) = \frac{S(q)}{\pi} \cdot \frac{\sigma_1/c}{\left| \frac{\sigma}{c}(1-x^2) + ix \right|^2} \qquad (2)$$

where $S(q,\omega) = \omega_o S(Q,\omega)$, $\sigma = \omega_o c/M^*(q,\omega)$ and $c = \pi\, S(q,x=o)/S(q)$. This form makes it clear that $S(q,x)$ depends on only two functions σ_1/c and σ_2/c (where $\sigma = \sigma_1 + i\sigma_2$). In a simple model where equation (1) is the sum of three Lorentzians having ω-independent parameters which satisfy the zero, second and fourth frequency moments of $S(q,\omega)$ we find $\sigma = 1 + i\omega\tau$ where τ is

an unknown constant. If we make no corrections to this model for the very high frequency behaviour of $S(q,\omega)$ then τ may be related to the fourth moment, and the memory function is an exponential function of time. Lovesey[3] employed this model and called it "a simple visco-elastic model." An advantage of the function $S(q,x)$ - equation 2 - is that σ_1 and σ_2 are weakly dependent on ω, in contrast to the stronger ω-dependence of $M(q,\omega)$ for example. Thus the approximation $\sigma = 1 + i\omega\tau$ is a good first approximation, and it would be useful to make measurements and perform analyses of sufficient precision that departures from this approximation are readily seen.

The inversion of $S(q,x)$ to find σ is, in principle, straightforward[1]. However in practice serious errors arise in the necessary Fourier-Laplace transform procedure for three reasons:-

(i) the experimental data extend over a finite ω-range

(ii) the errors tend to be large on a relative scale, at high ω,

(iii) equation (1) is a classical equation, and can be used only for

$$\hbar\omega \lesssim kT/3.$$

It has been shown[1] that the range of ω over which $M(q,\omega)$ exhibits significant intensity is considerably wider than that for $S(q,\omega)$, and therefore these three restrictions limit ω in real data to a "near-elastic" range as far as $M(q,\omega)$ is concerned. Thus we need to invert $S(q,x)$ to σ in frequency space using a relatively narrow or nearelastic range of ω. This problem was solved in reference 1, and details will not be given here.

The principal feature considered in many of the papers written during the long history of this subject, is the damping of the propagating modes (particulary the magnitude of the damping) and often this is related to subjective criteria. By using the quantities σ_1/c and σ_2/c derived from $S(Q,\omega)$ a simple solution for the damping problem is obtained. In reference 1 (equation 33b) it is shown that the ratio ω_s/Z_s (where ω_s is the real and Z_s the imaginary part of acomplex frequency for the mode) is determined by the point $[\sigma_1/c;\ \sigma_2^o/c]$ in figure 2. Thus without discussing subjective features, such as the shape of $S(Q,\omega)$, a quantitative measurement of a

meaningful ratio is possible. The experimentally observed behaviour of ω_s/Z_s v.s. q, and the behaviour of σ_1 or σ_2^o v.s. q can, in some cases, be complicated, and examples will be given in the next section. While present experiments show structure as a function of q, it is evident that not all the structure has been observed and further data at lower q are required. This is particularly interesting since some of the structural features are not correlated with those in S(q).

3. Illustrative examples of the relaxation parameters

The scale factor appearing in equation (2) is $c = \pi\ S(q,o)/S(q)$ and may be evaluated easily from experimental data. Gläser and Egelstaff[2] present a summary of five sets of experimental data, and compare them with the predictions of a simple 'collision model.' The argon and krypton data are shown in figure 3 (see table 1 also). It can be seen that these data show structure as a function of q, which is not included in the simple model, but that the general level for $q > 1$ Å^{-1} is accounted for approximately. When q is less than 1 Å^{-1}, the collison model fails because collective effects become important and there is a transition towards the hydrodynamic regime. The data displayed extend to $q \sim 0.4$ A^{-1}, but their quality is not satisfactory for $q < 0.6$ A^{-1}. Thus the transition is not covered by these data.

Figure 4 is a plot of σ_1 v.s. q for argon and krypton (see lines 2 and 4 of table 1). For $\omega \sim 0.4\ \omega_o$ it does not differ significantly from its value at $\omega = o$ (i.e. $\sigma_1 = 1$). However for $\omega \sim 2\ \omega_o$ and $q < 1$ A^{-1}, σ_1 is greater than unity. In the hydrodynamic limit[1] it is $\sigma_1(\omega=\omega_o) = 1 + \nu C_v[D_T(C_p-C_v)]^{-1}$ where ν is the kinematic viscosity, D_T is the thermal diffusivity and C_v and C_p are the specific heats at constant volume and pressure respectively. This limit is much larger than the values given in figure 4, so that we expect a sharp increase at lower q. At figure 5, σ_2/ω is plotted as a function of q, and it can be seen that between $\sim 0.4\omega_o$ and $\sim 2\omega_o$, there is little change. In figure 6, the values of ω, corresponding to the data of figure 5 are shown. The magnitude corresponds

to times less than 0.1 ps., while the lowest values are comparable to h/kT. These small times indicate that M(Q,t) has some structure as a function of t, so that the area is small (σ_2 at low ω is proportional to this area). In the hydrodynamic regime σ_2/ω (for low ω) = $[D\ q^2]^{-1}$, and again we are clearly not yet at this limit. The structure in this function is fairly weak.

Thus measurements to lower q would cover some interesting changes in magnitude and possibly more structure in this function. It is interesting to calculate the value of σ_2 as $\omega \to \infty$, using formula (6) of reference 1. For this purpose the fourth frequency moment of $S(q,\omega)$ is required, and for the argon data this has been taken from reference 4. These data show less variation with q than the low ω data and some increase in σ_2 at high (beyond the range of measurement) is indicated. However the error on the determination of the fourth moment is large and thus the magnitude of the increase is not well determined.

It is well known that at high q and at low q we have satisfactory theories, and the diagrams in this section show that while present data merges onto the high q theory, it does not extend low enough to merge onto the low q theory.

4. A Specialised Nearelastic Spectrometer

In the previous two sections the case for studying the nearelastic region (i.e. $\hbar\omega < kT/3$) for krypton and argon when $0.1 < q < 1\ A^{-1}$ was developed. It may also be argued that this region of (q,ω) space is important for other materials and in general any "average energy resonance excitation" may fall into this category (including biological materials and composites). Thus a spectrometer designed to cover this region would be useful, and with the advent of powerful pulsed neutron sources it has become possible to build one. Figure 7 shows the layout for such a spectrometer. To achieve the high energy resolution it is necessary to employ a short pulse of 1 Å neutrons, and for this reason a 95 K methane moderator would be more useful than a room temperature one. Initially the moderator pulse could be employed but later an extra chopper near the source, to sharpen the

pulse, should be added to the design in figure 7. As indicated in the introduction flight paths of about 15 m are required.

It is proposed to use conventional 'reactor type' techniques to displace the detectors from the main beam and to remove the energetic component from the spectrum. Thus a stationary graphite crystal is used to deflect (00ℓ) reflections by 17^{o} for 002 or 35^{o} for 004, and a saphire filter is used to remove short wavelength components. Then a Fermi chopper having a 2.5 μsec pulse width is placed just before the sample to improve the energy resolution of the pulse falling on the sample and to remove other orders. A large position sensitive detector (100 cms square) - similar to those used in conventional SANS at reactors - is set up 15 m from the sample. However to allow for slightly larger angle deflections it may be moved on a track (roughly parallel to the incident beam) so that deflections to one side of the beam passing through the sample may be observed in addition to the conventional SANS arrangement. Finally since most of the incident beam passes through the graphite crystal, the same beam may be used for (at least) two other similar spectrometers employing slightly different wavelengths. It may be useful to design the system so that any wavelength may be chosen from the set, 2.0, 1.8, 1.6, 1.4, 1.2 or 1.0 Å. It does not seem necessary to scan the wavelength so that a choice from a fixed set would suffice to optimise the intensity for any given sample.

To estimate the counting rate it may be useful to compare the performance with that of 1N4 at the I.L.L. Grenoble (in its original form with 4 m paths). For the same size sample at both spectrometers the geometry is changed by a factor of ~ 1/50, while the energy resolution width is reduced by ~ 1/5 and the detector area per (low) angle is increased by ~ 5 times. Thus the net effect is a decrease in throughput by ~ 50, which may be offset by the more powerful source giving higher intensity at 1 Å.

5. Conclusions

The longstanding case for the study of excitations in the low q and nearelastic ω range has been restated, giving emphasis to the problem of

excitations in simple fluids. These particular problems have a long history stretching over 100 years and have often been a source of controversy. By exploiting the new generation of pulsed sources and building a new spectrometer to study this region, and also by using the newly developed techniques of interpretation it may be possible to resolve some of these long standing problems. Moreover such an instrument would be very productive, and its use could be extended to other materials and problems which have an interesting history as well.

Acknowledgement

I would like to thank Dr. W. Gläser for helpful discussions on the subject of this paper.

References

(1) Egelstaff P.A. and Gläser W. Phys. Rev. A 31, 3802, (1985).

(2) Gläser W. and Egelstaff P.A. "Properties of Collective Modes in Fluids - Experimental Results". To be published.

(3) Lovesey S.W. J. Phys. C. 6, 1856, (1973).

(4) van Well A.H., Verkerk P., de Graaf L.A., Suck J-B, and Copley J.R.D. Phys. Rev. A 31, 3391, (1985).

(5) Egelstaff P.A., Gläser W., Litchinsky D., Schneider E. and Suck J-B. Phys. Rev. A 27, 1106, (1983).

Table 1

Summary of Experiments

Case	Element	Temp. K	Density atoms/nm^3	Ref.	Mean Free Path ℓ(Å)	Wave-length(Å)	$\sqrt{\frac{kT}{M}}$ Å/ps.	H.S. dia d(Å)	ρd^3
1	Ar	120	20.1	4	0.25	0.60	1.666	3.4	.79
2	Ar	120	17.6	4	0.35	0.60	1.666	3.4	.69
3	Kr	297	13.8	5	0.48	0.24	1.717	3.53	.61
4	Kr	297	10.6	5	0.8	0.24	1.717	3.53	.47

Notes: H.S. dia is the effective hard sphere diameter deduced from a fit to the position and peak height of the principal peak in S(Q).

The wavelength is calculated for velocity $V_o = \sqrt{kT/M}$.

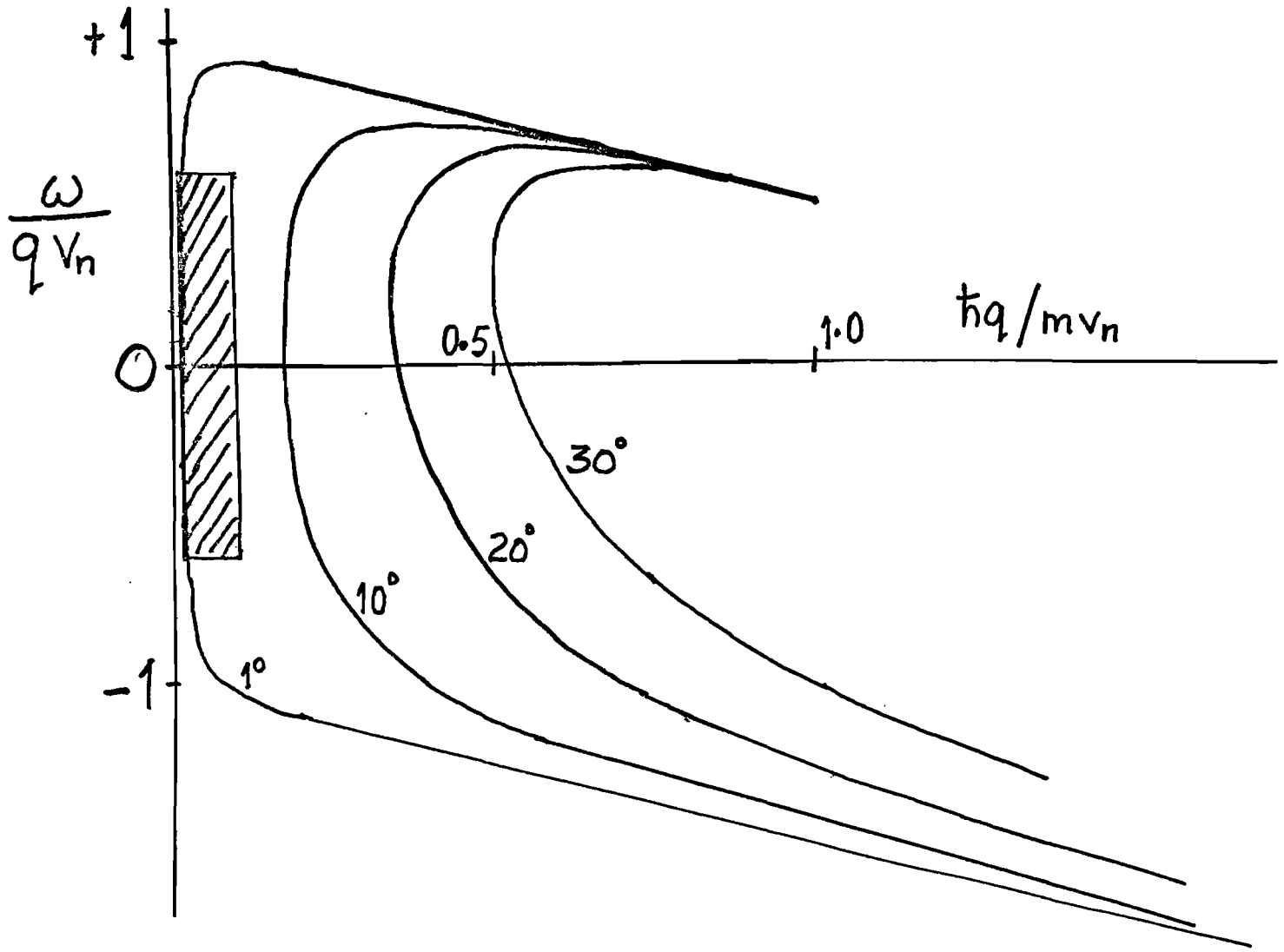

1. An ω-q diagram for nearelastic scattering. The ratio (ω/qv_n) where v_n is the neutron velocity is plotted against the momentum ratio $\hbar q/mv_n$ for several values of θ. The hatched region shows the part of the diagram discussed in this paper.

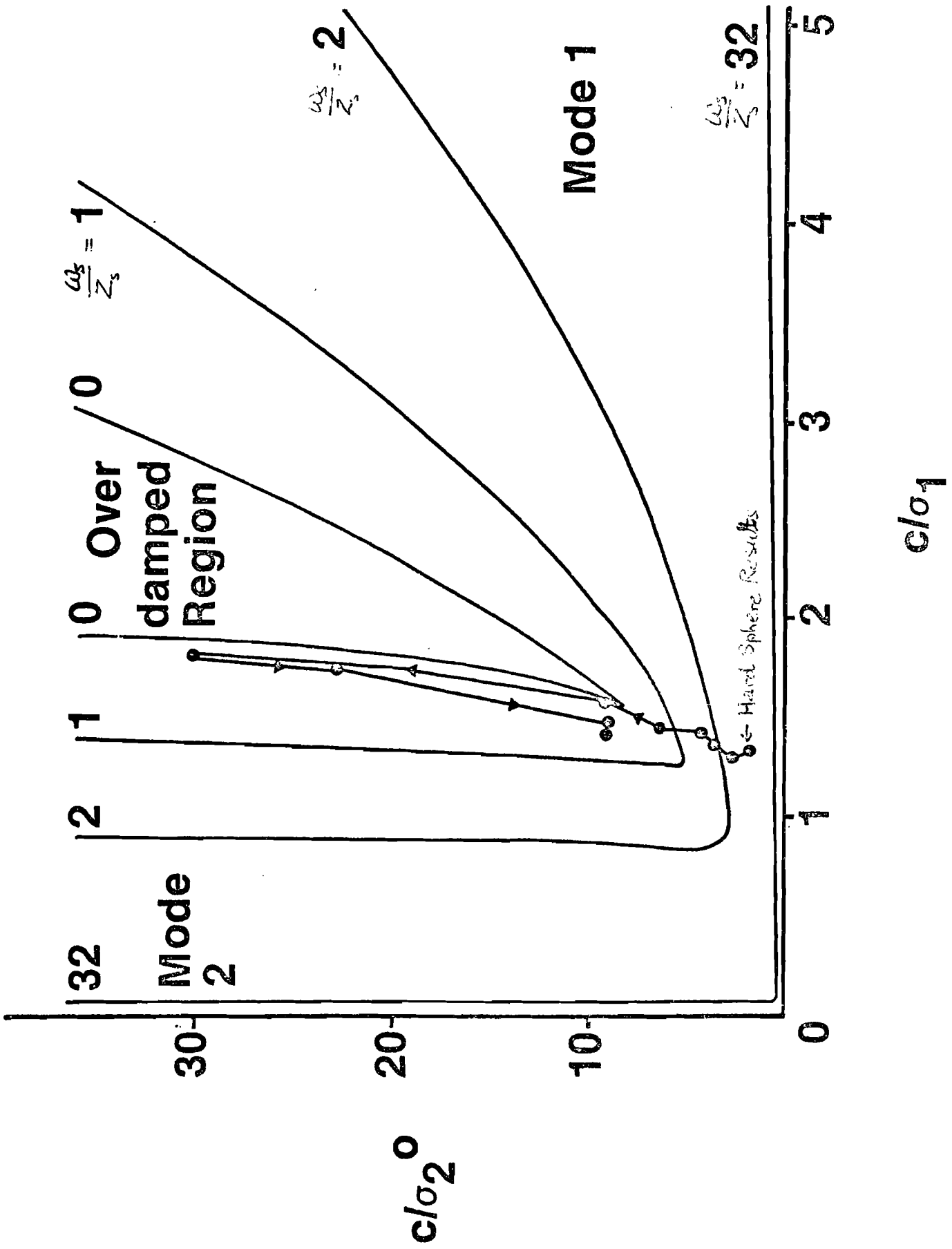

2. Propagating mode diagram[1]: the ratio c/σ_1 is plotted against c/σ_2 for different choices of ω_s/Z_s, where the mode frequency is $\omega_s + iZ_s$.

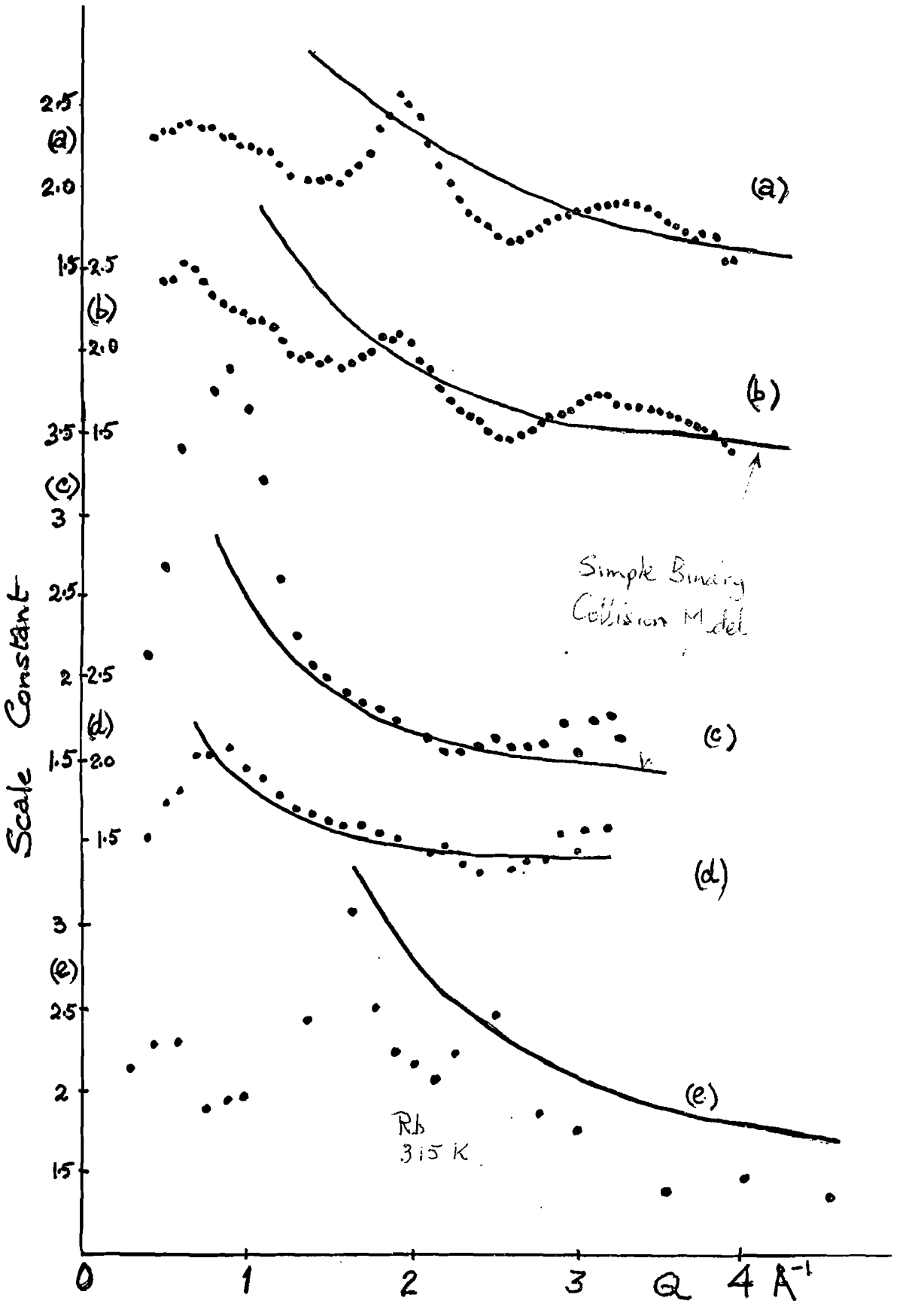

3. The scale constant c, appearing in equation 2, is plotted as a function of q for five sets of experimental data.[2] Details are given in table 1.

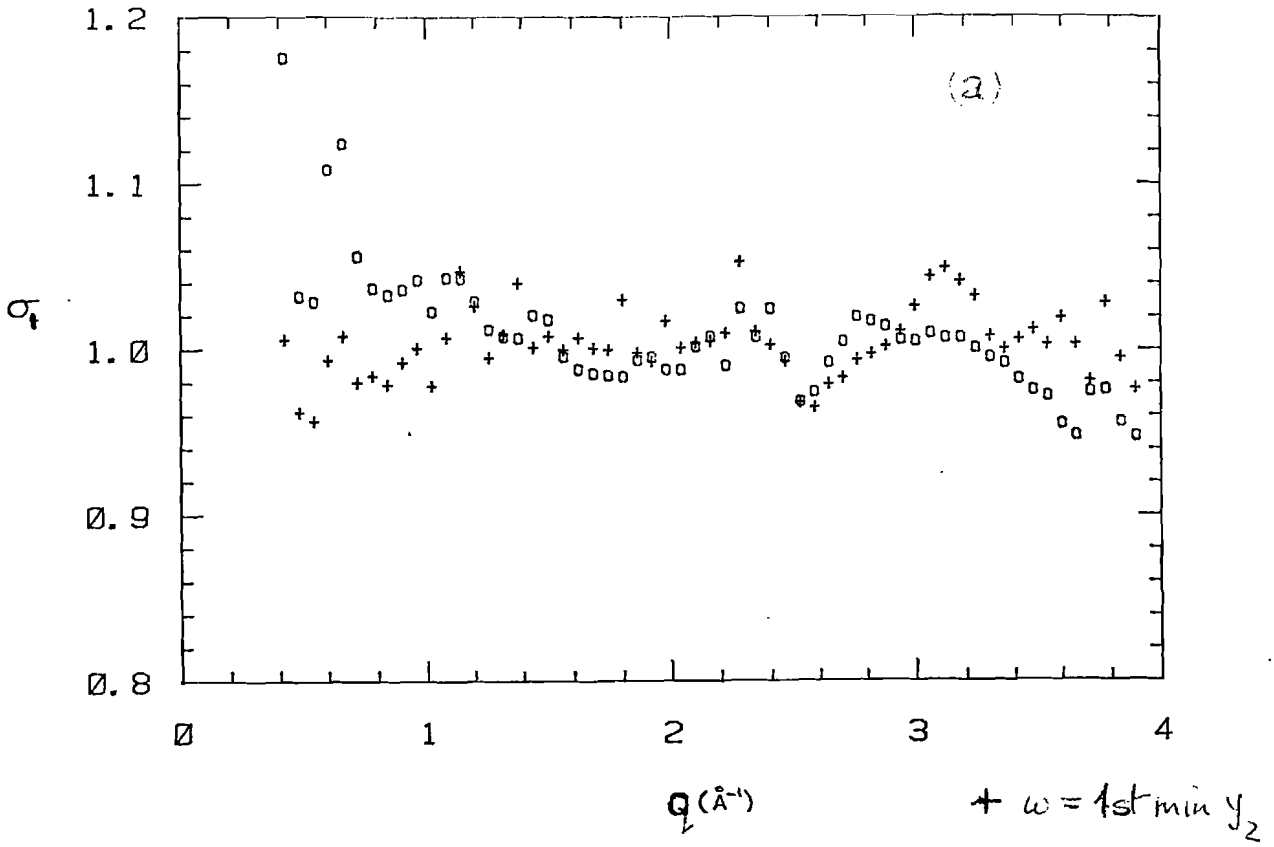

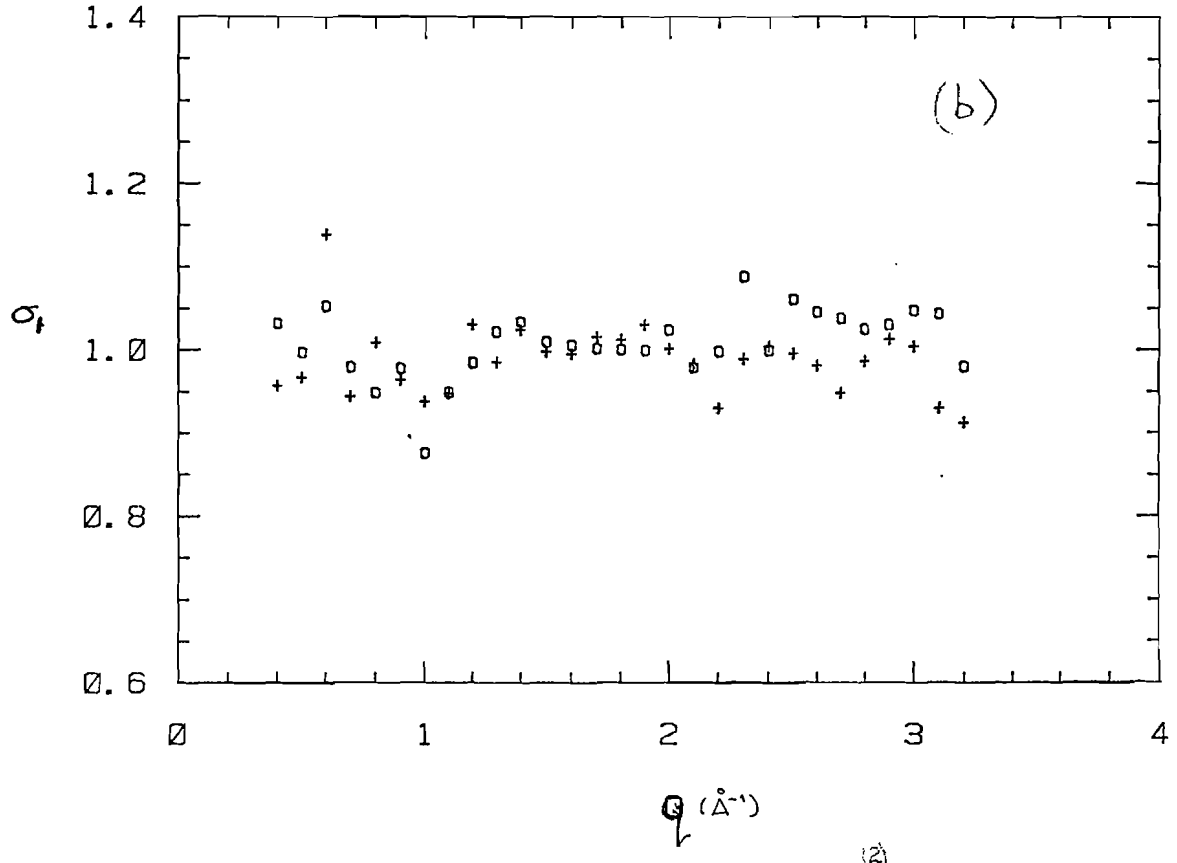

4. The real part of the damping function (σ_1) is plotted[2] as a function of q for the (a) Ar and (b) Kr experiments 2 and 4of table 1. The symbols indicate two different values of ω, the lowest ω shown in figure 6 and ω_0.

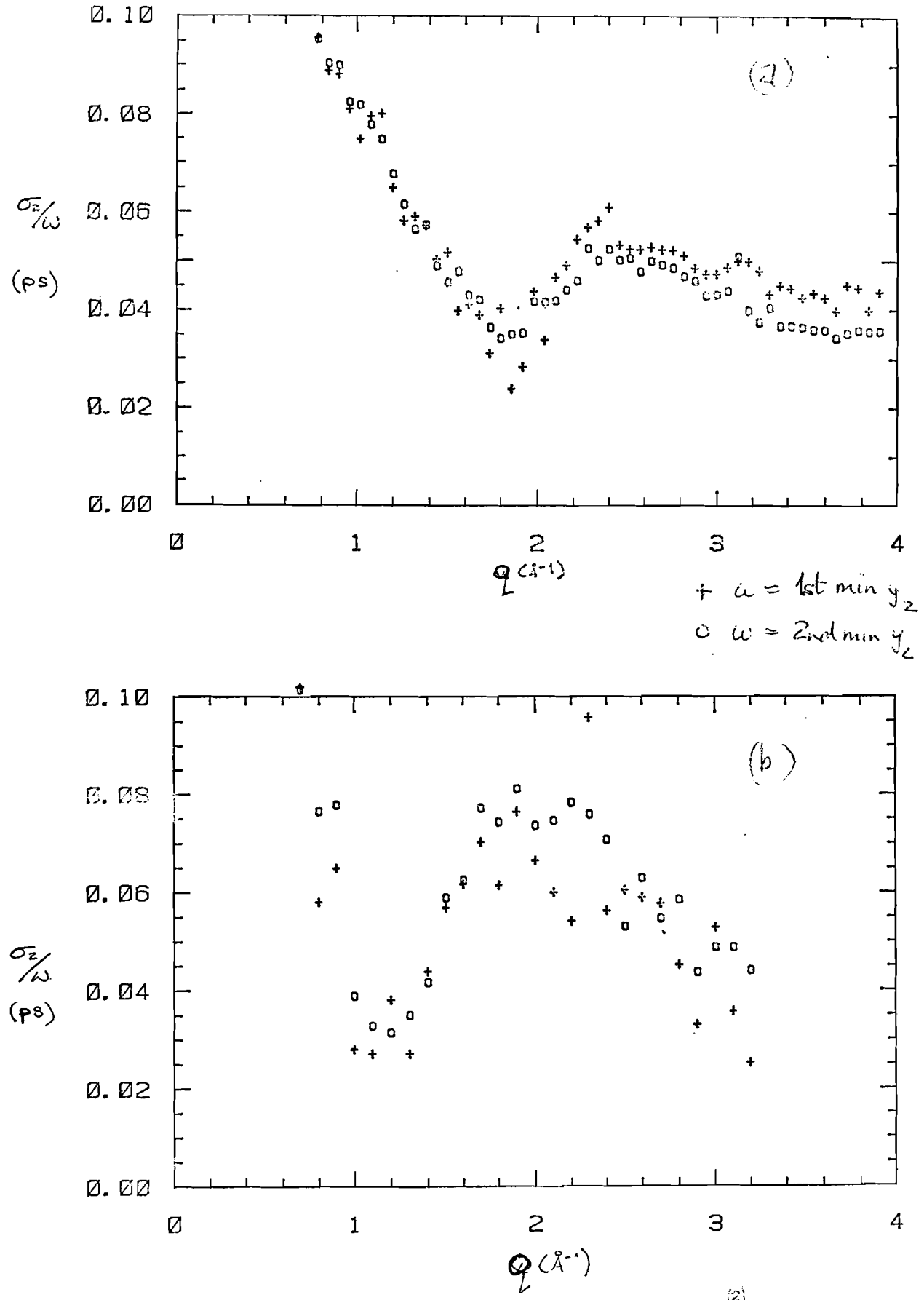

5. The imaginary part of the damping function (σ_2/ω) is plotted[2] as a function of q for the (a) Ar and (b) Kr experiments 2 and 4 of table 1. The symbols indicate two different values of ω shown in figure 6.

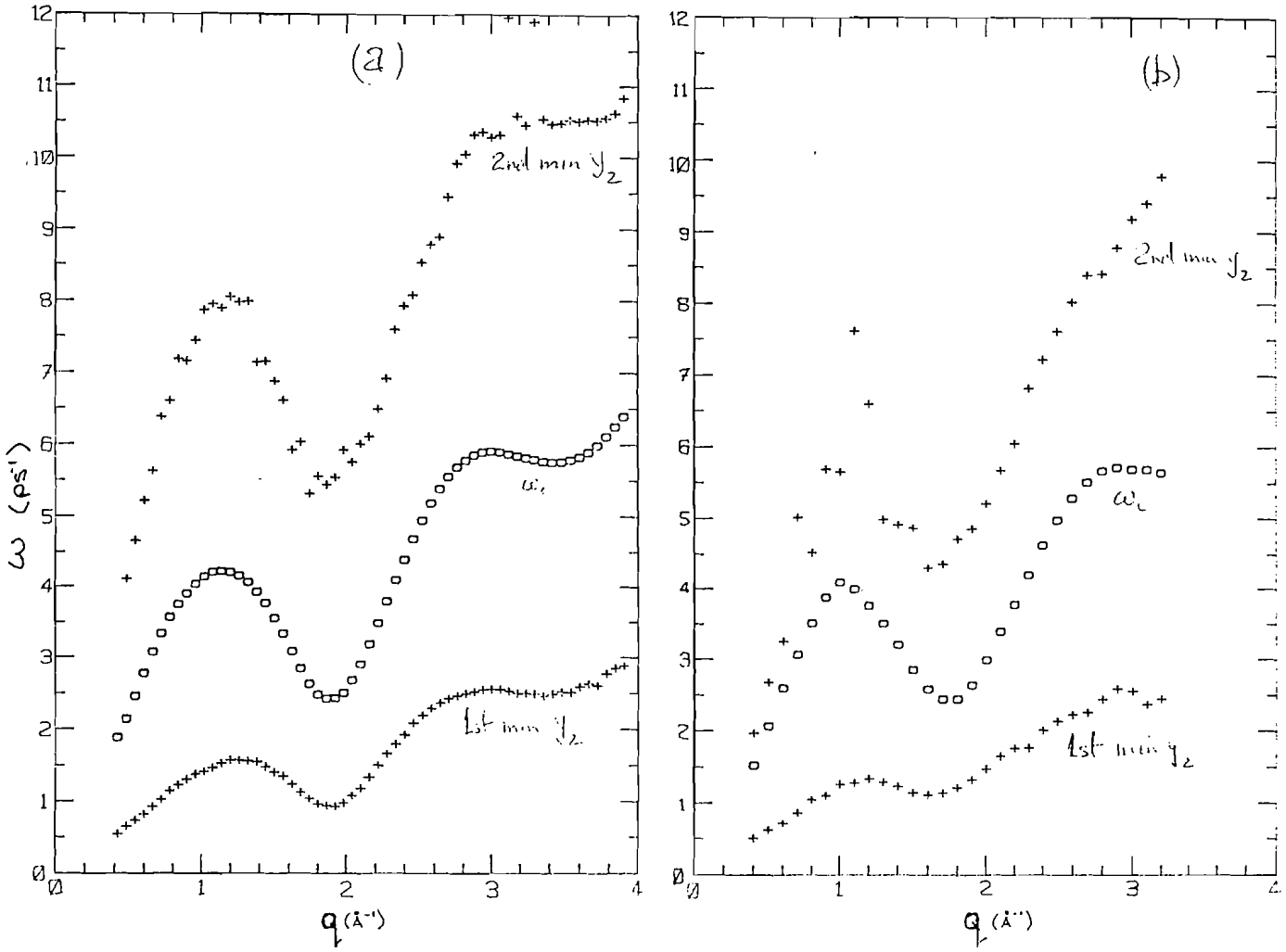

6. The values of ω for which minima are found[2] compared to $\omega_o = q\sqrt{\frac{kT}{MS(q)}}$. The data of figure 5 are for the upper and lower curves shown here.

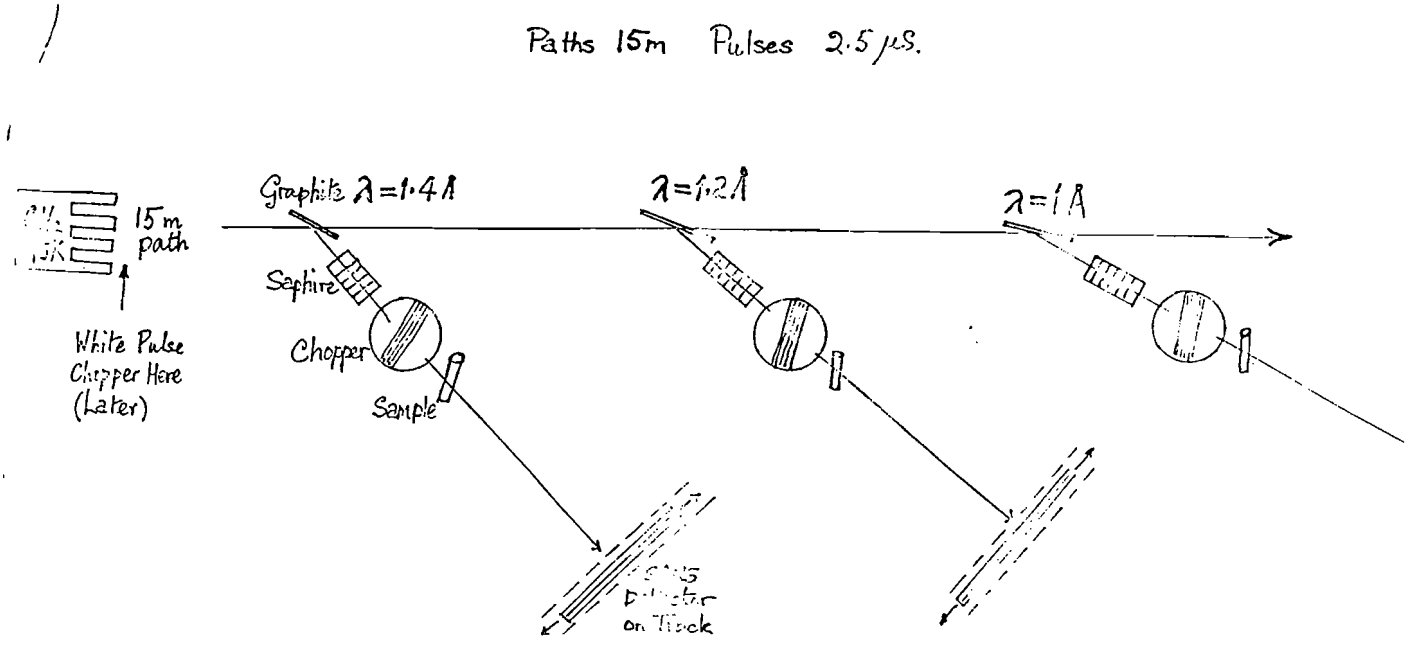

7. An SNS for RAL and AERE. A simple layout diagram for the specialised nearelastic spectrometer for relaxations in atomic liquids and for average energy resonance excitations as described in section 4.

Proceedings of the Eighth Meeting of the International Collaboration on Advanced Neutron Sources (ICANS-VIII)
8-12 July 1985, Rutherford Appleton Laboratory Report RAL-85-110

ELECTRON VOLT SPECTROSCOPY USING RESONANCE ANALYSIS AT THE SNS

R J Newport, M P Paoli*, V T Pugh,
R N Sinclair+, A D Taylor and W G Williams

Neutron Division, Rutherford Appleton Laboratory
Chilton, Didcot, Oxfordshire, OX11 0QX

+AERE Harwell,
Didcot, Oxfordshire OX11 ORA

*Clarendon Laboratory, Oxford University,
Parks Road, Oxford, OX1 3PU

ABSTRACT

A brief description is presented of the instrumentation which will be available in the early period of SNS operations for the development and scientific use of electron volt inelastic neutron spectroscopy.

I INTRODUCTION

The eVS project on the SNS has as its present aim the development and scientific use of a spectrometer in which the scattered neutron energy is determined using a nuclear resonance absorption filter. Two basic methods of using absorption resonances will be investigated in tandem on the one beam line. The resonance detector spectrometer (RDS) relies on the detection of promptly emitted γ-rays after resonant neutron capture. The resonance filter spectrometer (RFS), on the other hand, detects neutrons and utilises the difference in signal between the filter being out of and in the beam. This paper seeks to outline the present status of the eVS beam line instrumentation.

A principal feature of any eVS design must be the ability to measure high energy transfers with low associated momentum transfer $\hbar Q$ (see Figure 1). Of central interest here are magnetic and electronic excitations which

require $Q \leq 5\text{Å}^{-1}$. Because of the large electron-neutron mass difference, the "easiest" experiments will be those on tightly bound, high effective mass electrons. For high energy excitations, which we arbitrarily define as $\hbar\omega \geq 0.5$ eV, this can be realised only by using high energy incident neutrons ($E_o \geq 5$ eV) and detecting within a few degrees of the forward direction. Resolution requirements also place limitations on the science that can be done; the two "sharpest" nuclear resonance energies in this region are at 1.056 eV for ^{240}Pu and at 6.671 eV for ^{238}U and these can in principle provide $\hbar\omega$ and Q resolutions of ~ 10%. The intense epithermal spectrum of pulsed spallation sources also allows, for the first time neutron studies of condensed matter at high momentum transfer (see Figure 2). Values of $Q \sim 150\text{Å}^{-1}$ are attainable (e.g. using the 6.67 eV ^{238}U resonance and detecting at $\phi \sim 170°$); such Q values approach the impulse approximation.

A full review of the current status of eVS instrumentation development has been presented in a previous report [1], together with a discussion of some areas of scientific application. For more detailed descriptions of the techniques and experimental results see references [2] (RDS) and [3] (RFS) and the references therein.

The two detection methods will use a common collimation package, beam dump, data acquisition electronics (DAE), front end minicomputer (FEM), etc. and both view the same ambient (A) moderator. Incident and scattered beam neutron monitors will be common to the two instruments. The sample/detector tanks are sited within a blockhouse of wax/borax shielding tanks, thereby allowing relatively convenient close access. In this way a full assessment of the two methods can be made during early SNS operation, with the aim of determining the best eV spectrometer design.

II BEAMLINE LAYOUT

The eVS beamline has five major components beyond the moderator: the shutter, incident beam collimation, the Resonance Filter Spectrometer (RFS), the Resonance Detector Spectrometer (RDS) and the beam dump. The general layout of the beamline is shown in Figure 3. More detailed diagramatic information on the beamline components external to the biological shield can be found in Figure 4. Nominal RFS and RDS sample positions are at 10 m and 11.5 m respectively with secondary flight paths of ~ 1 m in both cases.

III COLLIMATION

The incident beam collimation package defines a circular beam of diameter ~ 30 mm at a sample position ~ 10 m from the moderator. The sample views a 100 mm diameter circle inscribed on the 100 x 100 mm ambient (A) H_2O moderator at 89.3° to the moderator surface.

To measure electron volt energy transfers in inverse geometry at low Q we are constrained to use relatively high energy neutrons and detect at scattering angles $\phi \sim 2°$. Implied in this statement is the importance of a design that limits both the sample and the detectors' view of collimation surfaces directly illuminated by the moderator, and a choice of materials that minimise problems associated with inelastic collimator transmission and γ-ray fluxes. The ability to collimate a relatively high energy neutron beam without introducing significant off-energy contamination is of paramount importance to the successful development of an eVS.

The eVS collimation may be divided into 3 sections: that within the shutter, the insert (i.e. within the biological shield) and that external to the biological shield. Figure 5 gives a schematic view of the assembly.

The shutter collimation consists of nine octagonal irises separated by iron spacing sections and held within an iron shot/borax/resin moulding which serves to decouple the collimation from the surrounding bulk shielding. The irises are formed from eight 6 mm thick sintered boron carbide tiles set at 45° to one another. The inner surfaces of the iron sections are set back from the B_4C - defined beam edge such that they cannot be viewed directly from the sample and should not, therefore, contribute to the instrument background as an extended secondary source.

Within both the insert and external collimator sections the beam is defined by a series of twenty 50 mm thick circular section B_4C/(10%) resin irises. This low hydrogen content mix should help to reduce the albedo of the inner, illuminated surface of the iris and moderation of the incident beam energies. The problem is ameliorated further by the intrinsic roughness (~ $\frac{1}{2}$ mm) of the iris inner surface. (Recent development work [4], motivated by the longer term requirements of the eVS project, has led

to B_4C/resin formulations with resin contents as low as 3%). Upstream of eight of the irises there is a 50 mm thick lead ring which serves to collimate the γ ray flux generated within both the target assembly and the collimation itself. γ collimation is particularly important when using a RDS-type system but will also be of benefit to a RFS-type system using Li-glass scintillator detectors. The lead rings are set back from the beam edge and cannot be viewed directly from either sample or detector positions, thereby avoiding the secondary neutron emission problem inherent in the use of lead. It is also worth noting that relatively pure lead (~ 99.8%) has been used in the fabrication to avoid possible background problems arising due to the large antimony content of most low grade lead stock: (antimony has a strong γ-emitting resonance at 6.24 eV). Downstream of each B_4C/resin iris there is a thin aluminium disc plasma spray coated with ~ 1 mm B_4C. These discs penetrate the epithermal beam sufficient to prevent a direct view of any iris from the sample or detector positions. These ensure that no hydrogenous collimator surface material may be seen directly by either the sample or by any detector.

The gaps between iris assemblies are filled with a lead + iron shot, borax and resin moulding with an inner suface lining of B_4C/resin. The inner surfaces of these are set well back from the beam edge.

The insert and most of the external collimation is evacuated to ~ 1 mbar, individual sections being separated by thin aluminium windows. The vacuum window immediately upstream of the spectrometers is sufficiently far from the RFS detector positions that it cannot be viewed at $\phi \geq 5°$, and lower angle detectors will have only a limited view. This arrangement also allows relatively easy access to the final three collimator irises for modification, if necessary. The final vacuum window is at the end of the beam dump drift tube. A gap in the collimation just outside the biological shield facilitates the insertion of resonance absorption blocking filters and will also allow direct geometry measurements.

The above collimation gives an umbra diameter of ~ 28 mm at the RFS sample position converging at 3.0 mrad, and, with a penumbra annulus of width ~ 4 mm which diverges at 6.8 mrad. At full SNS intensity the neutron flux through this sample position will be $\Phi \sim 3\ 10^7$ n eV^{-1} s^{-1} at E = 1 eV (note, $\Phi \propto E^{-0.95}$ for $E \geq 1$ eV). Within the umbra the flux is $\sim 5\ 10^6$ n eV^{-1} cm^{-2} s^{-1}. Provision has been made for the insertion of up to 250 mm

of beam trimming collimation just upstream of the RDS; assuming a nominal 30 mm diameter beam/sample within the RDS, this implies a flux of $4\ 10^6$ $eV^{-1}\ cm^{-2}\ s^{-1}$.

Two lithium glass scintillator monitors [5] may be installed using vacuum feedthroughs into the collimation (at either 6.5 m or 8.6 m from the target) and beam dump tube (at 13.5 m from the target). These low efficiency monitors have a fast response time, and their $E^{-\frac{1}{2}}$ efficiency (at $E \gg 1$ eV) makes them highly suitable for eV spectroscopy applications.

IV DETECTION SYSTEMS AND ELECTRONICS

As described above, there will be two detection systems under development within the eVS project, one downstream of the other. A prototype RFS sample/detector chamber has been installed on a beam line at the WNR facility, Los Alamos, for tests, but has now been returned to RAL to form the basis of a RFS on the SNS. The RDS equivalent will be based on the existing system installed on the Harwell Linac as part of a Harwell/Oxford University/RAL collaboration.

The two spectrometers will both use the same standard SNS instrument DAE package and VAX 11/730 FEM. The FEM will have access to the HUB computer via a Cambridge Ring and to all standard SNS instrument software packages.

Clearly, the two methods cannot be pursued simultaneously; during RFS runs the downstream RDS assembly will be left void (i.e. forming part of the beam dump drift tube), whilst for RDS runs it will be necessary to insert some collimation into the RFS sample/detector chamber. Having outlined the substantial areas of instrumentation overlap we now describe briefly the major features peculiar to each method.

(a) RFS. The prototype design has been discussed in some detail elsewhere [6] and the salient features only will be summarised here. The incident flight path is $L_1 \sim 10$ m, the scattered flight path will normally be $L_2 \sim 1$ m though there exists an option to reduce this to $L_2 \sim 0.75$ m. The 10 atm He-3 detector tubes are housed within a moulded B_4C/resin shielding block which allows the use of 1, 2 or 3 tubes (ganged or singly) at $\phi \sim \pm 10°$,

±15° and ± 20° and a four-detector square around the beam at $\phi \sim 5°$. It will be possible to extend the range to smaller scattering angles by installing an array of scintillator detector elements. Both the sample and the secondary beam fixed filters [3] are suspended from a sample tank flange. Rotary vacuum feedthroughs allow the user to perform a full double difference experiment without breaking vacuum. There is a liquid nitrogen feed through/cold finger assembly mounted on the sample flange which may be used to cool a filter or, exceptionally, the sample. The vacuum tank is lined internally with 6 - 8 mm of B_4C/resin (the resin concentration being limited to 3% in the sample tank and 5-10% elsewhere).

The inelastic scattering from ZrH_2 was studied during a series of test measurements at the WNR pulsed neutron source using both ^{149}Sm (E_R = 0.872 eV) and ^{181}Ta (E_R = 4.28 eV) analysers. Figure 6 shows the derived double difference spectra at ϕ = 5.5° as well as computer simulations based on an Einstein oscillator model.

(b) RDS. The RDS makes use of the detector and sample boxes previously used on the Harwell Linac. These are positioned to give an incident flight path of approximately 11.5 m and scattered flight path of 1 m, though variations are possible. An important component of the external shielding around the detector box will be a 100 mm layer of pure (antimony-free) lead to screen the detector from any γ-ray background. Initially the gamma ray detector will be a high resolution, high purity Ge detector (HPGe). The detector system has its own electronics, including an A.D.C., and can give output signals for events in pre-selected γ-ray energy bands as well as a digital signal which can be used to give 2-dimensional data analysis (i.e. T.O.F. and γ-ray energy) at some future date. Plans are well advanced to install a low resolution BGO detection system which will allow an investigation of coincidence techniques.

Initial development of the RDS on the Harwell Linac is described in [7]. This includes a comparison of HPGe and BGO detectors. A double difference spectrum obtained on the Harwell Linac for scattering from ZrH_2 at 15° using Sm analyser foils is shown in Figure 7.

V eVS DEVELOPMENT

It is impossible to define, a priori, the precise line of development that the eVS project will take but it is possible to indicate the general directions. Optimisation of the incident beam collimation together with both detector and general instrument shielding is important. The resonance filter technique must be pursued to lower scattering angles, which will necessitate the development of a low angle scintillator bank and a re-design of the scattered beam fixed filter assembly. The resonance detector must likewise be pushed to low angles using both high and low resolution γ detectors together with an investigation of coincidence or anti-coincidence techniques.

In parallel with the development of the instrumentation, and as a necessary part of it, the areas of science made accessible by the spectrometers will be investigated.

References

1. R J Newport, A D Taylor and W G Williams, RAL report RAL-84-047, 1984.

2. a) D R Allen, E W J Mitchell and R N Sinclair, J Phys E 13 639 (1980).
   b) J M Carpenter, N Watanabe, S Ikeda, Y Masuda and S Satoh, Physica 120 B + C, 126 (1983).
   c) H Rauh and N Watanabe, Nucl. Instr & Meth., 222, 507 (1984).

3. a) R J Newport, J Penfold and W G Williams, Nucl. Instr. Meth 224, 120, (1984).
   b) A D Taylor, R A Robinson and P A Seeger, Nucl. Instr. Meth 224, 133 (1984).
   c) P A Seeger, A D Taylor and R M Brugger, LANL report LAUR-84-1028 (1984).
   d) R J Newport, P A Seeger and W G Williams, RAL report RAL-84-113, 1984.

4. V T Pugh and B W Hendy, these proceedings, p670.

5. P L Davidson, RAL Report RAL-85-032 (1985)

6. R J Newport and W G Williams, RAL report RL-83-052 (1983).

7. M P Paoli, E W J Mitchell, R N Sinclair and A D Taylor, these proceedings

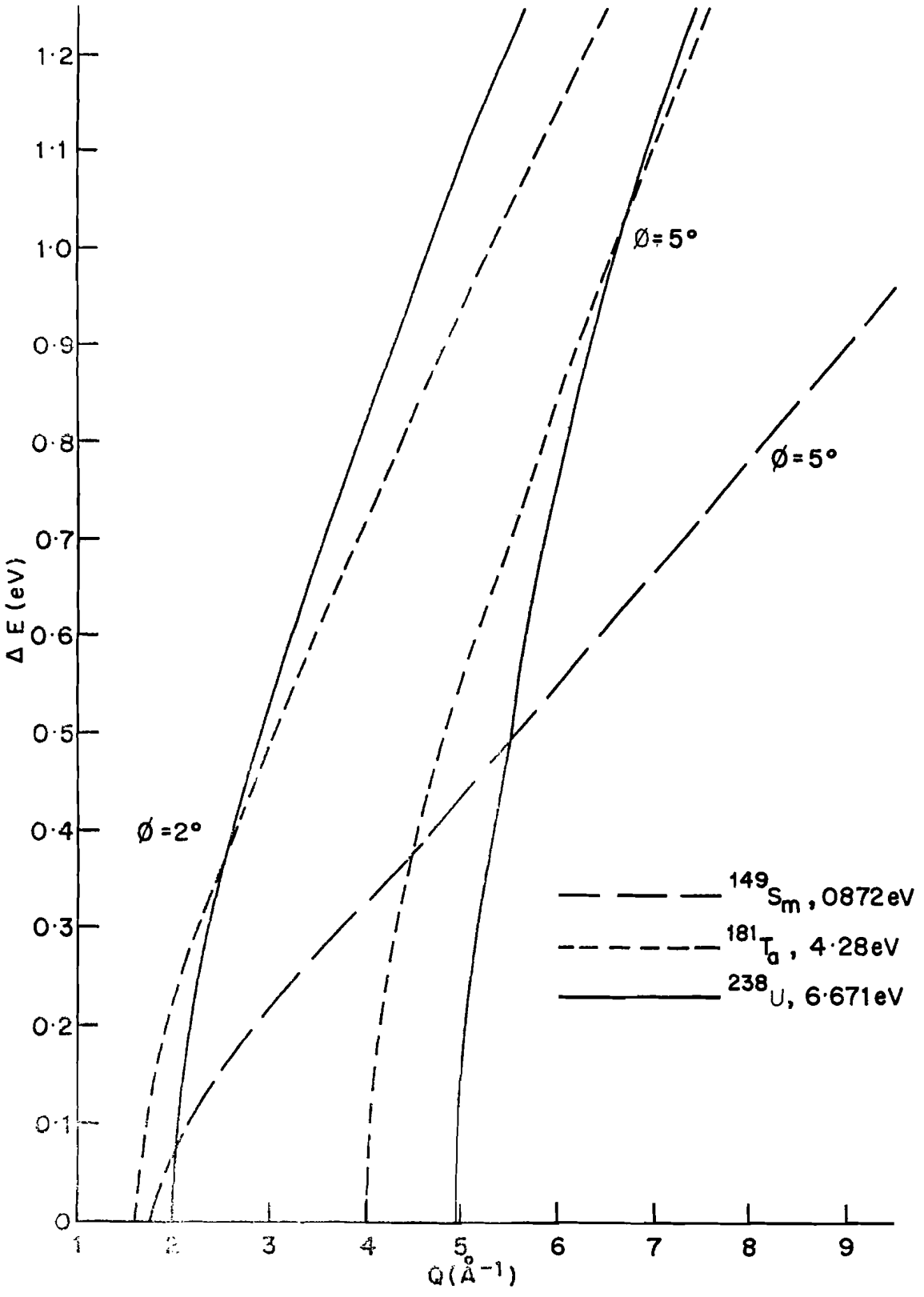

FIGURE 1 : DYNAMIC RANGE ACCESSIBLE WITH LOW ANGLE DETECTION

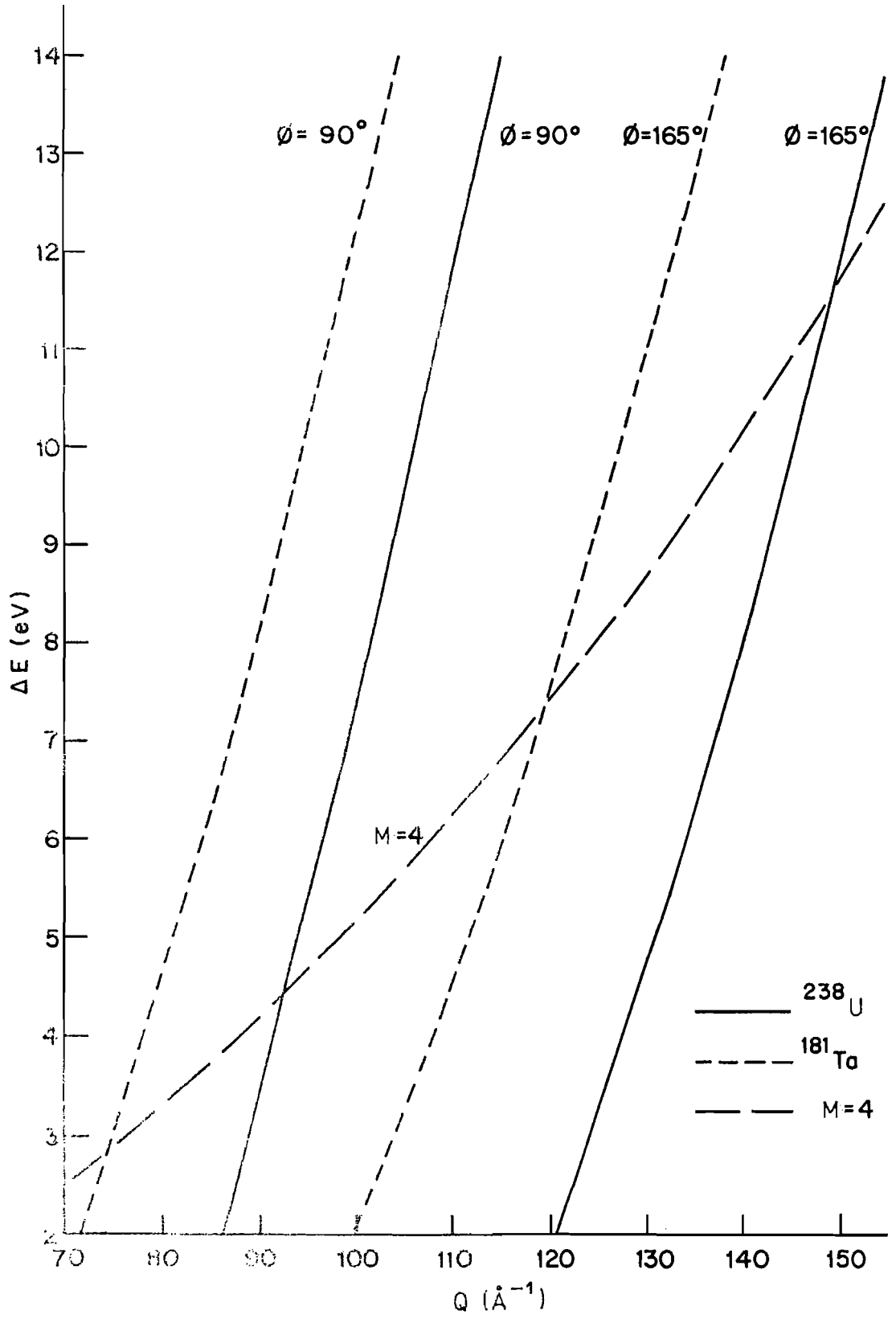

FIGURE 2 : DYNAMIC RANGE ACCESSIBLE WITH HIGH ANGLE DETECTION

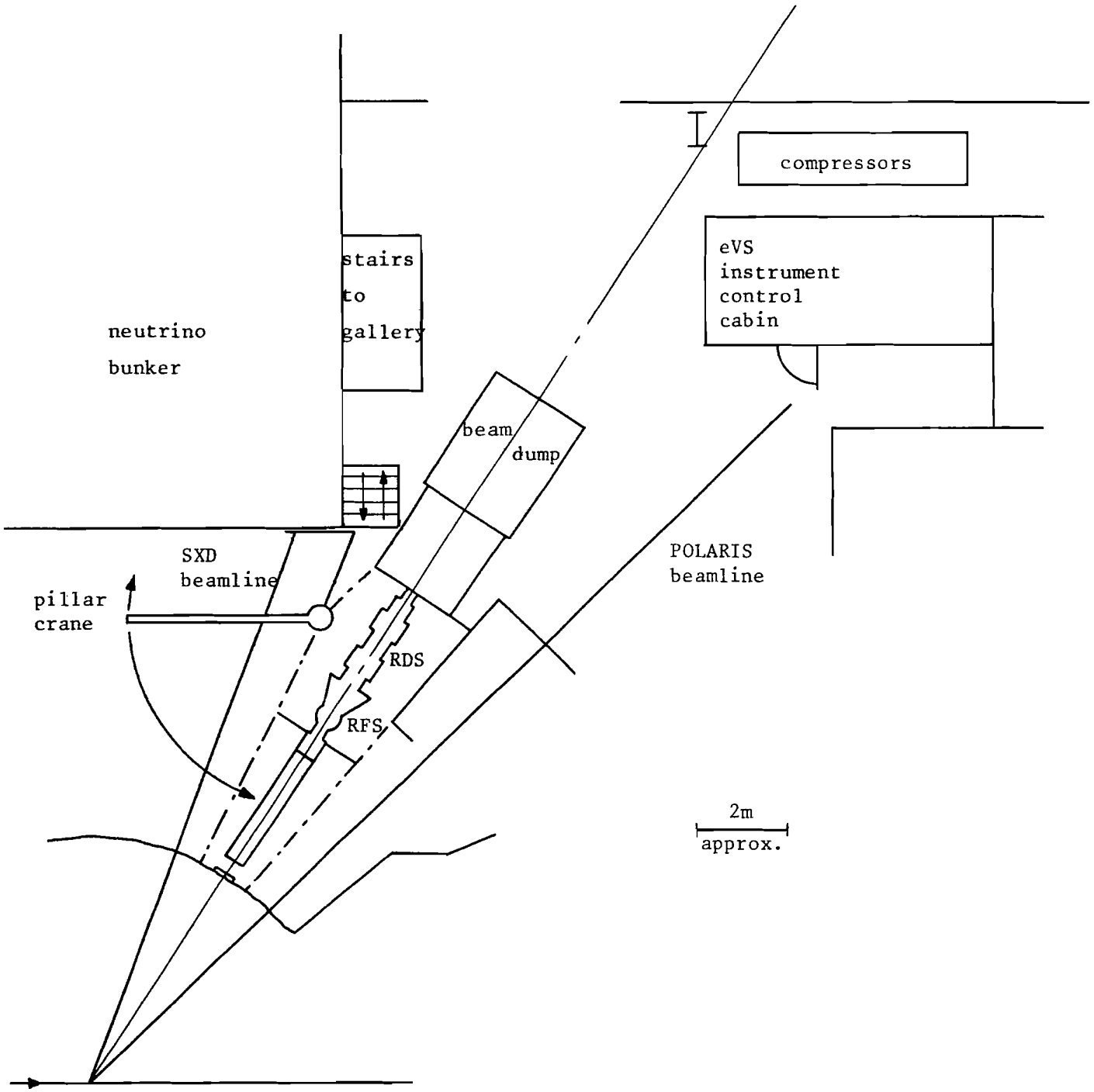

FIGURE 3 THE eVS BEAMLINE AND ITS ENVIRONS

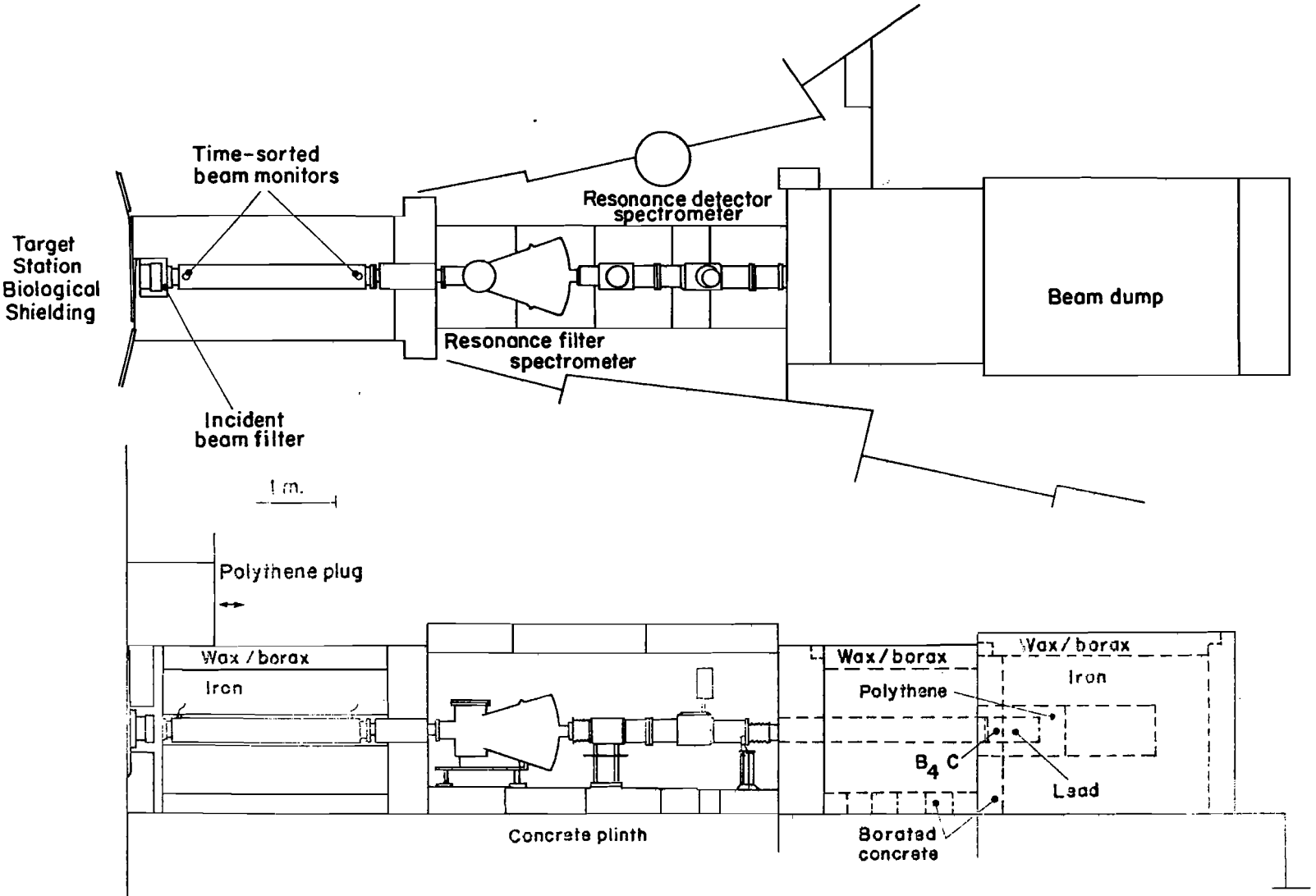

FIGURE 4 : Schematic Plan and Section of the eVS Beamline.

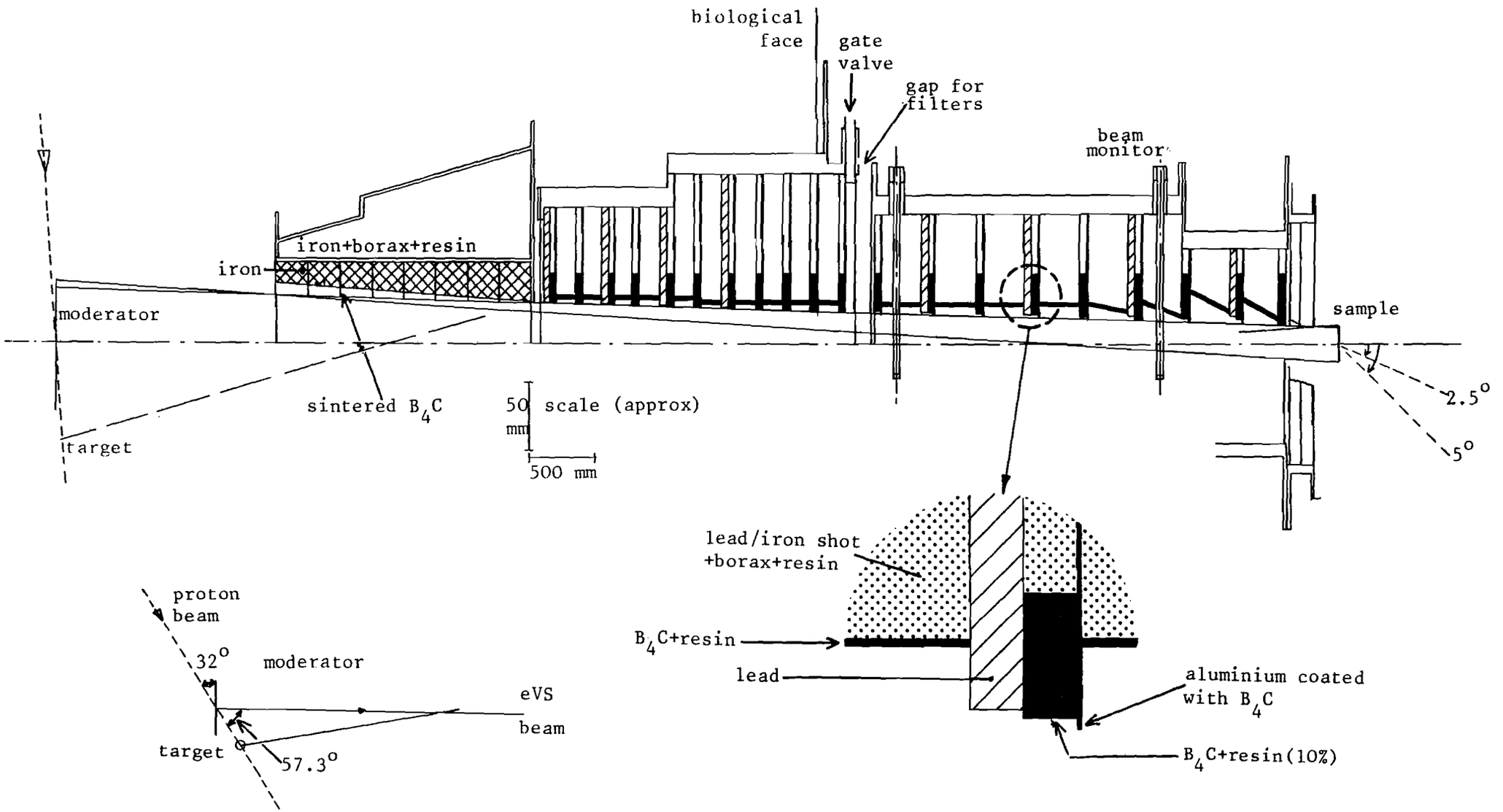

FIGURE 5 SCHEMATIC SECTION AND DETAILS OF THE eVS INCIDENT BEAM COLLIMATION ASSEMBLY

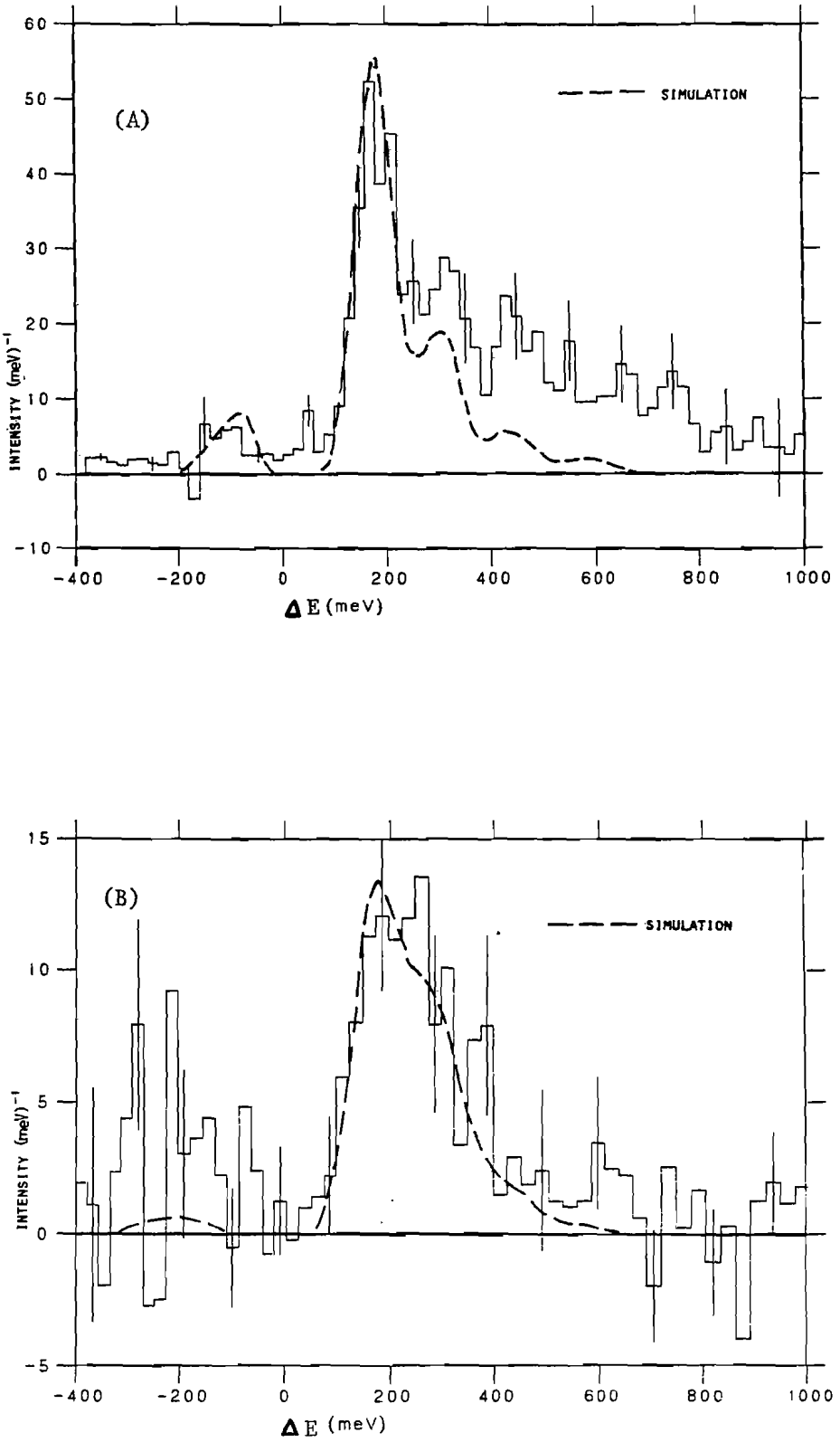

FIGURE 6 : INELASTIC SCATTERING FROM ZrH_2 USING THE RFS:

(A) SAMARIUM ANALYSERS

(B) TANTALUM ANALYSERS

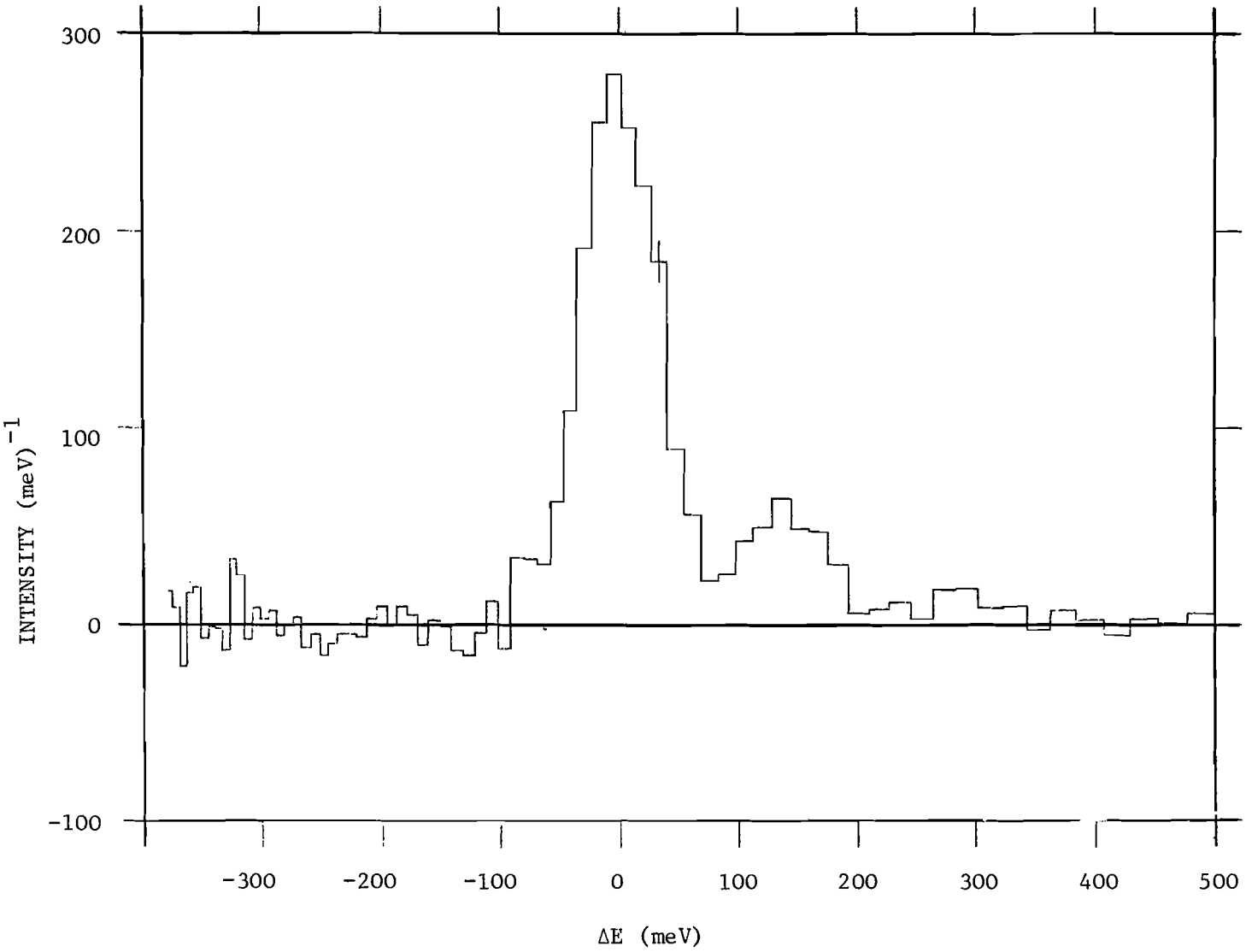

FIGURE 7 : INELASTIC SCATTERING FROM ZrH_2 USING THE RDS:

SAMARIUM ANALYSERS

Proceedings of the Eighth Meeting of the International Collaboration on Advanced Neutron Sources (ICANS-VIII)
8-12 July 1985, Rutherford Appleton Laboratory Report RAL-85-110

DEVELOPMENT OF A RESONANCE DETECTOR SPECTROMETER ON THE HARWELL LINAC

M P Paoli,
E W J Mitchell
Clarendon Laboratory
Oxford University
Parks Road
OXFORD
OX1 3PU

R N Sinclair
AERE Harwell
DIDCOT
Oxon
OX11 0RA

and

A D Taylor
Neutron Division
Rutherford Appleton Laboratory
Chilton
DIDCOT
Oxon
OX11 0QX

Abstract

Intense beams of epithermal neutrons are now available from accelerator based neutron sources. The neutron beam can be made monochromatic by using materials which resonantly absorb neutrons in this epithermal region. A Resonance Detector Spectrometer (RDS) uses a γ-ray detector to observe the γ-rays emitted when a neutron is absorbed by such a material. Development of an RDS system has been made at Harwell. This work included a background investigation, a comparison between a high resolution and a low resolution γ-ray detector, experiments using the double difference technique and experiments at high Q.

1. INTRODUCTION

Accelerator-based neutron sources provide intense beams of epithermal neutrons. These may be used to perform two new types of measurement. The first involves studying the excitation of single particles at large Q values, $\geq 100 Å^{-1}$, where the impulse approximation may be valid and so the final state of the particle can be neglected. The second is where excitation energies are large, ~ 1 eV, and Q values are small allowing magnetic and electronic excitations by keeping the magnetic form factor large [1].

For neutrons with energies above 1 eV rotors and crystal analysers are inefficient at monochromating the neutron beam. To make an epithermal neutron beam monochromatic it has been proposed that materials in which resonance absorption of neutrons occur can be used. There are two possible ways of using these materials. The first involves using the material as a filter. Performing with and without filter experiments then taking the difference gives the TOF spectrum due to neutrons with energy equal to that of the resonance. Experimental work using such a Filter Difference Spectrometer (FDS) is given in [2]. The second method, the Resonance Detector Spectrometer (RDS), makes use of secondary particle emission, particularly γ rays, when a neutron is resonantly absorbed [3]. In this paper we summarise the development work performed on an RDS system at the Harwell Linac. Further development will take place on the eV spectrometer on the SNS at the Rutherford Appleton Laboratory where RDS and FDS techniques will be pursued in parallel [4].

2. EXPERIMENTAL LAYOUT

The Harwell Linac accelerates electrons which then hit a Ta target. The bremsstrahlung radiation produced as the electrons slow down in the target cause (γ,n) reactions with the Ta nuclei and so give a pulse of high energy neutrons. These neutrons are then slowed down by an ambient water moderator. For the RDS, moderator to sample distance is 7m and the sample box to detector box distance is 2.4m. This was originally to allow scattering down to $2\frac{1}{2}°$. Shielding outside the detector box consisted of 10 cm of Pb surrounded by 25 cm of borated resin. The shielding inside the detector box varied but typically consisted of Pb to shield the γ ray detector and B_4C plates to screen all Pb blocks from neutrons. This internal shielding is shown in Figures 1a and 1b for scattering at 60° and 15°.

3. BACKGROUND INVESTIGATION

The first experiments were performed using a high resolution high purity germanium γ ray detector (HPGe). As the Linac uses γ rays to produce neutrons and as the target, moderator and spectrometer beam line are all colinear there is an intense γ flash when the electrons hit the target. Fast electronics are needed otherwise the γ flash saturates the detector which may not recover for several milliseconds, covering the time region of interest. Using the fast electronics enabled the detector to recover in times $\sim$ 10 μs.

A typical γ ray spectrum from a resonance capture consists of a continuum up to around 7 MeV with additional sharp γ ray lines. Figure 2 shows the lower end of the γ ray spectrum for neutron capture by Ta. There are Ta (n,γ) lines at 173 keV, 271 keV and 403 keV with background lines from Boron neutron capture at 482 keV and the positron annihilation line at 511 keV. A high resolution detector is needed if we wish to use the signal from the narrow (n,γ) lines as well as monitoring wide bands in the continuum. The initial experiments used a Ta analyser foil. Ta has two strong (n,γ) lines at 271 keV and 403 keV and these were used along with several broad bands in the region 520-3000 keV. The background was investigated using a Ta foil sample, and pure Pb sample scattering at 70° and 10° and a ZrH_2 sample scattering at 10° and 3° (both were $\sim$ 10% scatterers). The main source of background was caused by sample scattered neutrons being captured in Pb shielding. The Pb shielding blocks contain an Sb impurity which has neutron capture resonances and gives off γ rays when neutrons are captured. These resonances gave rise to a time structured background. To reduce this background B_4C plates were used to capture neutrons before they could be captured in the Pb blocks. Although boron also has a (n,γ) reaction, all the γ rays have energies around or below 482 keV. The other important background line was the 511 keV position annihilation line, thus most of the background occurs below this energy. Using B_4C plates improved the signal to background ratio above 520 keV but made worse the signal to background ratio below it.

The signal to background was best for the 1000-3000 keV band but very poor for the (n,γ) lines which both occur below 511 keV. If the sample is moved further from the detector this background problem is reduced

as the scattered neutron capture also occurs further from the detector. When the ZrH_2 sample was placed 2.3m from the detector, scattering angle 3°, the background level was reduced by 5 to the level if no sample were in the beam. However, the signal countrate was very low, being approximately one count per 1 μs channel per hour. This showed that the intensity of the Linac was too low to allow investigations of small angle scattering and so all further experiments were done at higher angles, 10°-70°.

4. COMPARISON OF HPGe AND BGO DETECTORS

As we had previously found that the best signal to noise ratio with the HPGe detector occurred when using a broad γ ray energy band rather than a specific (n,γ) line, this suggested that there may be advantages in using a higher efficiency, low resolution detector. A comparison was made between a high resolution, high purity intrinsic Ge detector consisting of a cylindrical crystal of Ge 6 cm long and 6 cm diameter and a low resolution Bismuth Germinate scintillator detector (BGO) consisting of a cylindrical Bismuch Germinate crystal 7.5 cm long and 7.5 cm diameter. The resolution of the HPGe was better than ¼% and for the BGO was in the range 20-30%.

Three types of comparison were made :

(i) Using a Ta foil as a sample.

(ii) Using Pb as a sample and scattering at 60° onto a Ta analyser foil.

(iii) Using ZrH_2 as a sample and scattering at 10° using Sm and Ta analyser foils.

For each type of experiment the geometries for the HPGe and BGO detectors were kept identical as was the internal collimation and shielding in the detector box. The external shielding close to the detector was marginally better for the BGO, as it would indeed be when the detectors are used in other experimental situations. However, in most previous experiments the external shielding was found to have little effect on the total background. For the Pb experiment the

incident flight path is around 9.4m and the secondary flight path 21 cm. For the ZrH_2 experiment where the scattering angle was 10°, the incident flight path was 8.75m and secondary flight path 75 cm. The principle background γ-ray lines came from boron capture, 482 keV, and the positron annihilation line at 511 keV. To avoid these lines using the low resolution BGO detector, a lower limit of 900 keV was chosen. Since the best signal to background ratio found previously occurred below 3000 keV, the principal comparison between the detectors used the gamma ray energy band 900-3000 keV.

For each type of experiment, the signal to background ratio and signal countrates were calculated and the results are shown in Table 1. These values are accurate to 10%. As expected when using the 900-3000 keV band, the signal to background ratios for both detectors were similar but there was a higher signal countrate for the larger BGO detector.

We also observed (n,γ) lines using the HPGe detector, 403 keV for Ta and 333 keV for Sm. The signal countrates for these lines are much lower than for the wide energy band. Previously we found that sample scattered neutrons were an important contribution to the background. A large amount of boron has to be used to stop neutron capture by the Sb impurity in lead shielding blocks. This produces a large number of background γ-rays of energy 482 keV and below. This background is highest when the sample is close to the detector as the neutron capture then also occurs near the detector. Thus we expect the background to be highest for the Pb scattering experiment, smaller for ZrH_2 experiments and insignificant for the thin Ta foil experiment. This explains our observations for signal to background. No signal could be seen on the background for the Pb experiment where as for the Ta experiment the signal to background was actually better on the 403 keV line than on the 900-3000 keV band.

An overall comparison does favour BGO as it is possible to get as good a signal to background ratio with a higher signal countrate than the high resolution detector and it is less expensive and more convenient to use (e.g. doesn't need to be cooled). Also a coincidence detector system, made of several BGO detectors, can be used and may improve the signal to background. However, using boron to capture sample scattered neutrons put observation of (n,γ) lines at a disadvantage. The signal

to background may improve if it becomes possible to use large amounts of Li instead of boron or if the sample is far away from the detector.

5. DOUBLE DIFFERENCE EXPERIMENTS

Improvements to the resolution of a spectrometer using resonance absorption foils can be made using the double difference technique [2c]. This method involves making measurements with two thicknesses of analyser foil. At the edges of the resonance absorption peak, the cross section is small and so the absorption scales linearly with foil thickness. At the centre of the resonance peak the cross section is high and the absorption scaling is not linear, (the exponential nature of absorption as a function of thickness is now important). If the fraction thin foil thickness divided by thick foil thickness is β ($\beta \leq 1$), then scaling down the thick foil spectrum by β and subtracting it from the thin foil spectrum cancels out the absorption at the edges of the resonance peak and leaves a contribution at the centre of the resonance peak equivalent to a narrower resonance. Any background, no foil spectrum, will have to be removed from both thin and thick spectra. The double difference spectra is given by

$$D.D. = (\text{Thin}) - \beta(\text{Thick}) - (1-\beta)(\text{No foil})$$

The pulse width of the linac was 5 μs for the experiments. If a Ta analyser foil was used, E_{res} = 4.28 eV, the linac pulse width would give a 132 meV resolution contribution whereas for Sm, E_{res} = 0.872 eV, it would only give a 12 meV resolution contribution. Hence Sm was used. A ZrH_2 sample was used and the scattering angle was 15°. The BGO detector was used as it had a greater countrate and the γ ray energy band 900-3000 KeV was selected.

The experiments consisted of a background run (no foil), a thin foil run and a thick foil run. The thin Sm foil was 0.107 mm thick (51% absorption) and the thicker foil was 0.348 mm thick (90% absorption). Figures 3 and 4 show the raw TOF spectra for the thin foil and thick foil runs respectively. The first excitation in ZrH_2 can be seen in the thin foil spectrum before the main elastic peak whereas with the thicker foil the resolution is too poor to see it, as expected. Figure 5 shows the double difference spectrum converted onto an energy

transfer scale. This spectrum shows two excitations in ZrH_2, the first can be seen much clearer than in the case of the original thin foil spectrum. From the spectra we estimate that the single foil spectrum has a resolution of 100 meV which is improved to 75 meV for the double difference data.

6. HIGH Q EXPERIMENTS

Due to the low intensity of the Linac, most experiments were performed at high scattering angles (high Q) with the sample close to the detector. Experiments were performed investigating recoil scattering from liquid He and from hydrogen in ZrH_2 and V_2H. At large Q, the Impulse Approximation may be valid so that the scattering function depends only on the initial state of the atom, the final state and interference effects being negligible.

In metal hydrides we wish to study the momentum distribution of the hydrogen and so get information on the potential that it is in. For these experiments a Ta analyser foil was used, E_{res} = 4.28 eV and the scattering angle was around 45°. This gave a Q value ~ 50 $Å^{-1}$. The BGO detector was again used selecting the gamma ray energy band 900-3000 keV. At this Q value the resolution of the spectrometer is not a problem as the H recoil scattering distribution becomes much broader than the instrument resolution. The TOF spectra for scattering from ZrH_2 with the background (no foil) spectrum removed, is shown in figure 6. The spectrum shows an elastic line from the metal a 365 μs and the broad recoil scattering from the hydrogen between 220 μs and 340 μs.

There is much interest in measuring the Bose-Einstein condensate fraction (zero momentum fraction) of the superfluid liquid He-II, particularly at large Q where the Impulse Approximation is valid. There is, however, a resolution problem as the scattering distribution from both the condensate and normal fractions of He-II are very narrow and so the instrument resolution must be kept to a minimum. The geometric arrangements of the moderator, sample and absorption foil cause variations in flight path length, scattering angle and so recoil energy of the He atoms. These variations cause a change in time of arrival of neutrons and can broaden a signal. The effect is particularly important for light atoms. Details of the theory of this

effect are given in [5]. Minimising this effect leads to a reduction in signal as the solid angles of the sample and detector foil are reduced. In this experiment a U^{238} analyser foil was used, E_{res} = 6.67 eV, and the scattering angle was 165° giving a Q value of 150 $Å^{-1}$. An only 1 cm thick sample was used, ~ 2% scatter, as the time difference between scattering from the front and back of the sample also broadened the signal. Again the BGO detector was used with a gamma ray energy window of 1300-3000 keV. The effects of having a greatly reduced signal, a sample container that was a 4% scatterer and limited time available to investigate background, made obtaining a good signal to background ratio impossible. The statistics on the data made it difficult to determine if a He signal was present, however, some indications of how to improve the signal to background were made and it should be possible to improve the experiment on the SNS. Reference [6] gives more details of a similar high Q experiment performed on liquid He on the KENS neutron source.

7. SUMMARY

Initial development of the RDS at the Harwell Linac has proved helpful for the development of the eV Spectrometer on the SNS at RAL. Although the epithermal neutron intensity from the Linac is much lower than will be available from the SNS, useful information has been found.

Firstly the need for extensive screening of Pb shielding by B_4C plates in order to reduce the background caused by sample scattered neutrons. This put observation of specific (n,γ) lines from the absorption foil, most of which have an energy below the (n,γ) line for boron, at a disadvantage. This meant that wide high energy bands had to be selected and so a high resolution γ detector had no advantage over a low resolution detector. In fact low resolution detectors have an advantage as they are less expensive, can be more efficient and a multi detector coincidence system may improve signal to background even further. However, high resolution detectors must still be considered if the sample scattered neutron background is reduced by, for example, increasing the sample-detector distance or replacing boron with lithium which does not give off γ rays when it captures neutrons.

The double difference technique was shown to improve the resolution for the RDS system. Also several high Q experiments were performed on

metal hydrides and He. The lack of neutron intensity made it difficult to extract information from the experiments but the results indicate that we may be optimistic for similar experiments on the SNS.

References

1. D R Allen, E W J Mitchell and R N Sinclair, J Phys E 13 639 (1980).

2. a) R J Newport, J Penfold and W G Williams, Nucl Instr Meth 224 120 (1984).

   b) A D Taylor, R A Robinson and P A Seeger, Nucl Instr Meth 224 133 (1984).

   c) P A Seeger, A D Taylor and R M Brugger, LANL report LAUR-84-1028 (1984), accepted by Nucl Instr Meth.

   d) R J Newport, P A Seeger and W G Williams, RAL report RAL-84-113 (1984).

3. a) J M Carpenter, N Watanabe, S Ikeda, Y Masuda and S Satoh, Physica 120 B + C, 126 (1983).

   b) H Rauh and N Watanabe, Nucl Instr Meth, 222 507 (1984).

4. R J Newport, M P Paoli, V T Pugh, R N Sinclair, A D Taylor and W G Williams, these proceedings.

5. J M Carpenter and N Watanabe, Nucl Instr Meth 213 311 (1983).

6. S Ikeda and N Watanabe, KENS Report V, p176 and 180 (1984).

Experiment			Detector	Gamma ray Energy (KeV)	Signal to Background	Relative Signal Countrate
Sample	Scattering Angle (deg)	Analyser Foil				
Ta	—	—	BGO HPGe HPGe	900-3000 900-3000 400-405	54 69 82	1.0 0.47 0.02
Pb	60	Ta	BGO HPGe HPGe	900-3000 900-3000 400-405	3.95 3.73 —	1.0 0.25 $\leq$ 0.02 (1)
ZrH_2	10	Ta	BGO HPGe HPGe	900-3000 900-3000 400-405	1.73 1.87 —	1.0 0.41 — (2)
ZrH_2	10	Sm	BGO HPGe HPGe	900-3000 900-3000 330-335	1.36 1.67 1.8	1.0 0.59 0.14

(1) No signal could be seen above the background

(2) Countrate too low to make measurements.

TABLE 1 Comparison of BGO and HPGe Detectors

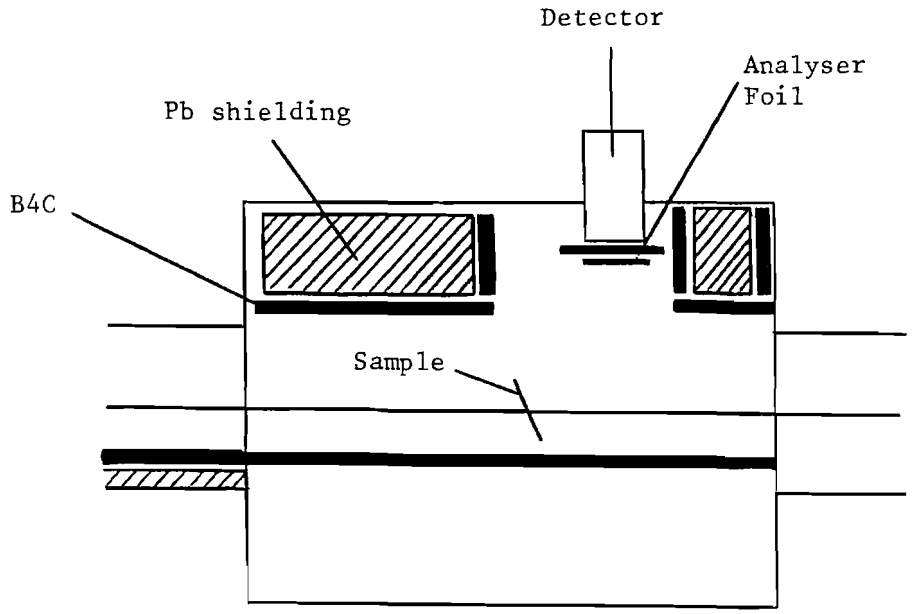

Figure 1a Internal shielding for scattering at 60°

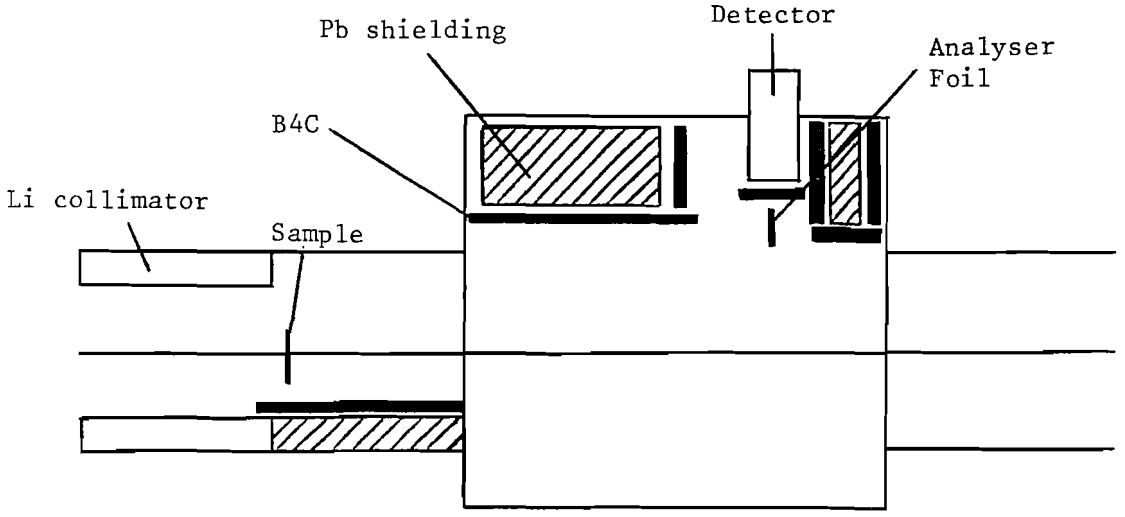

Figure 1b Internal shielding for scattering at 15°

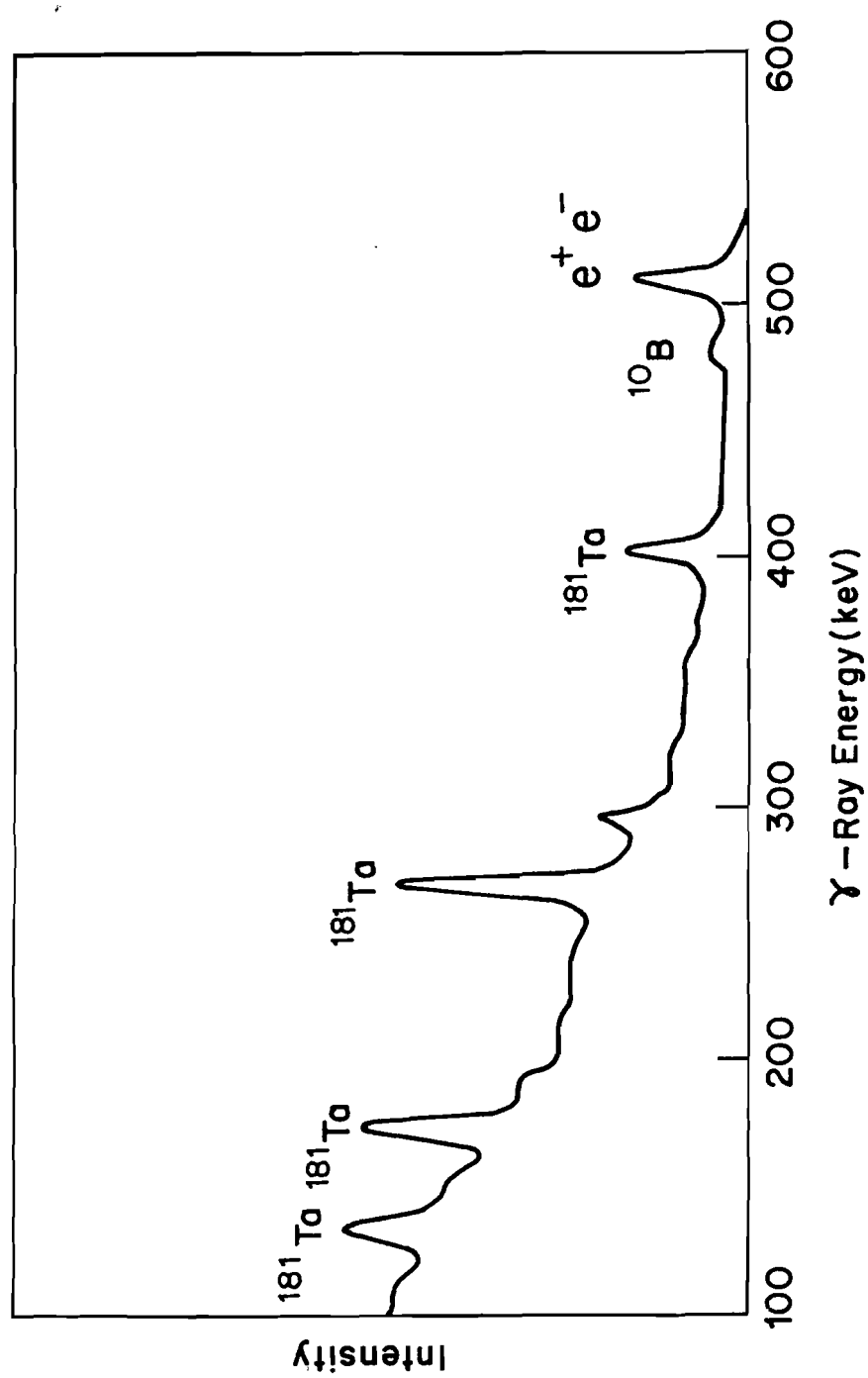

Figure 2 γ-ray Spectrum for neutron capture by Ta

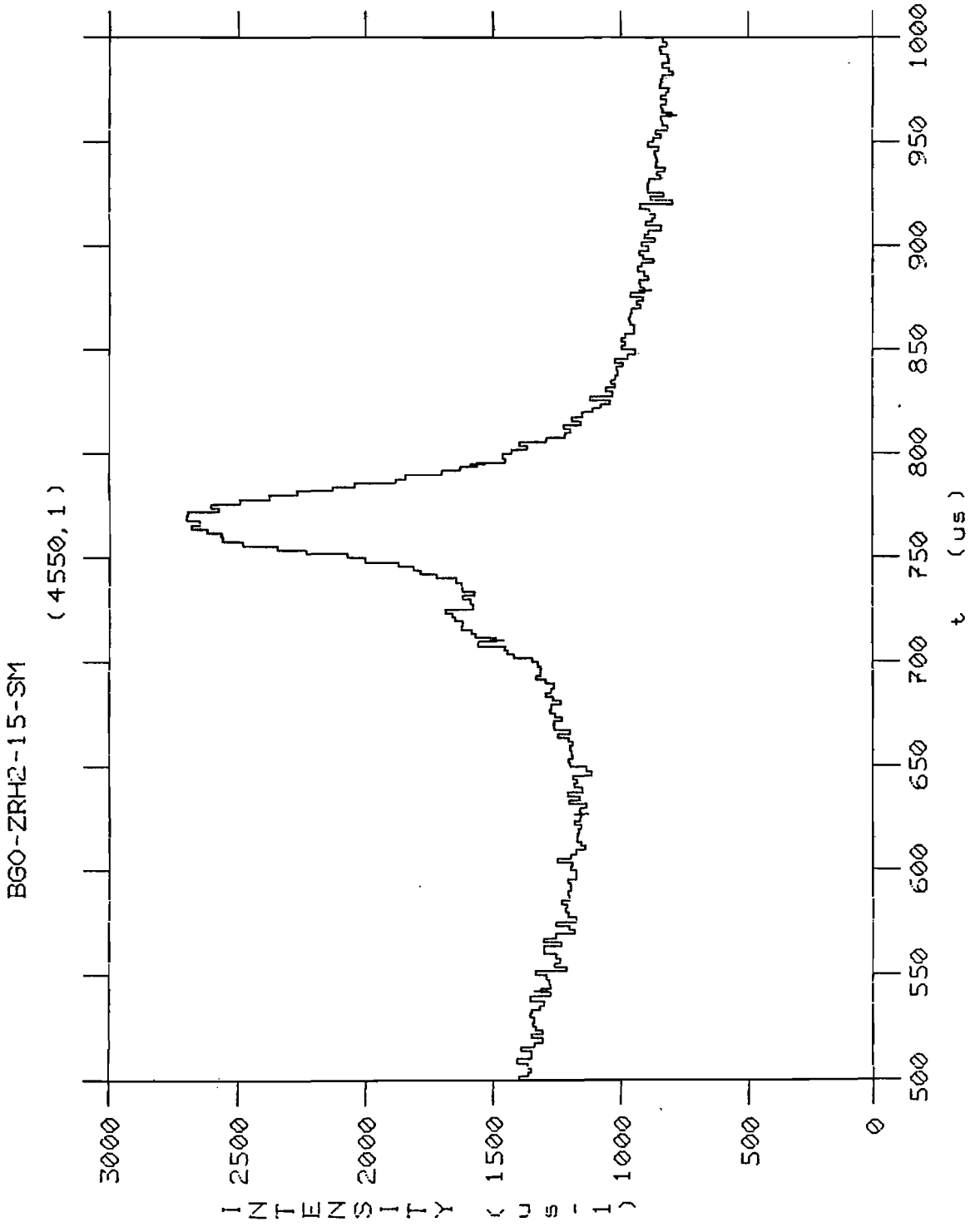

Figure 3 Scattering from ZrH2 at 15° using a thin Sm foil

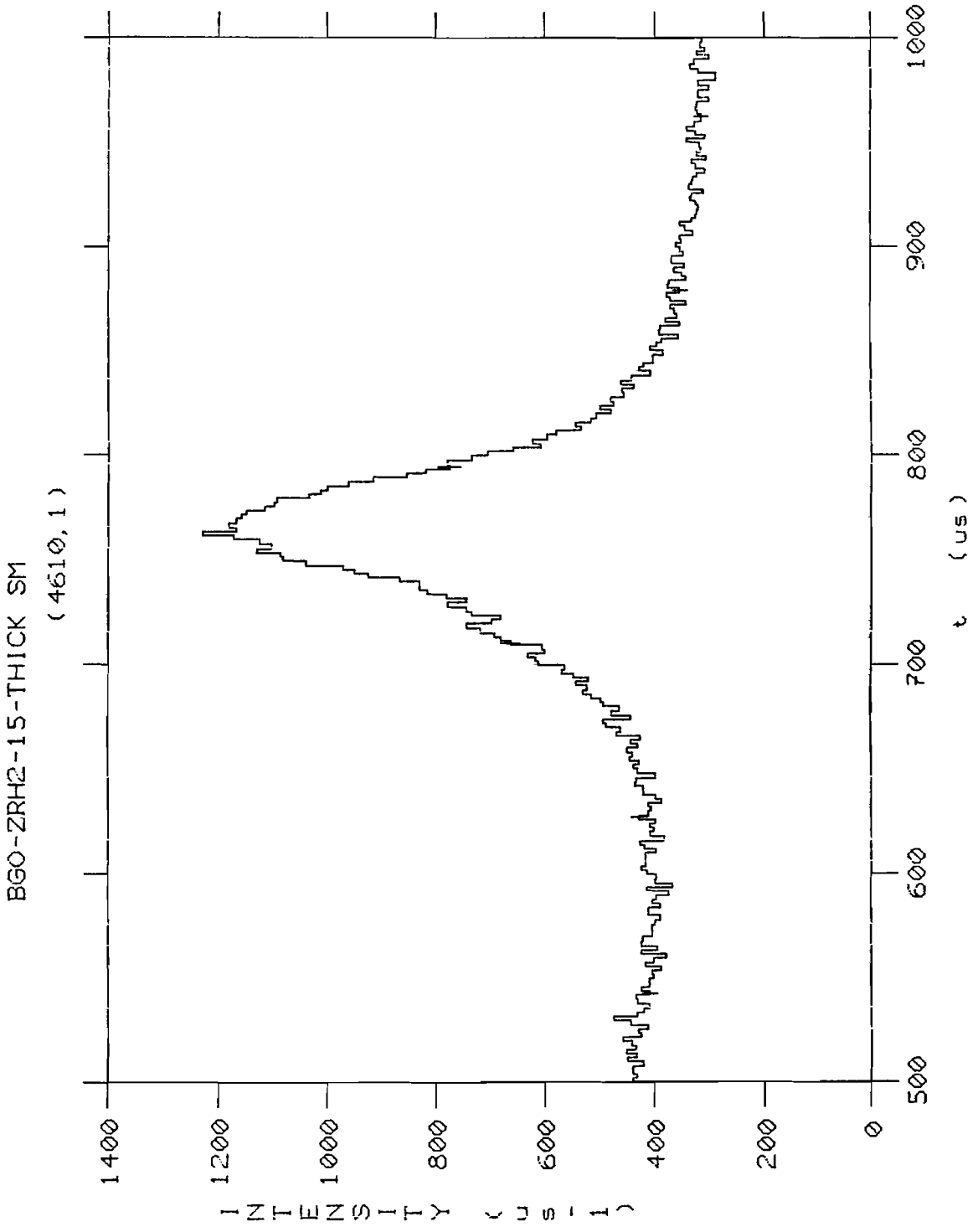

Figure 4 Scattering from ZrH2 at 15° using a thick Sm foil

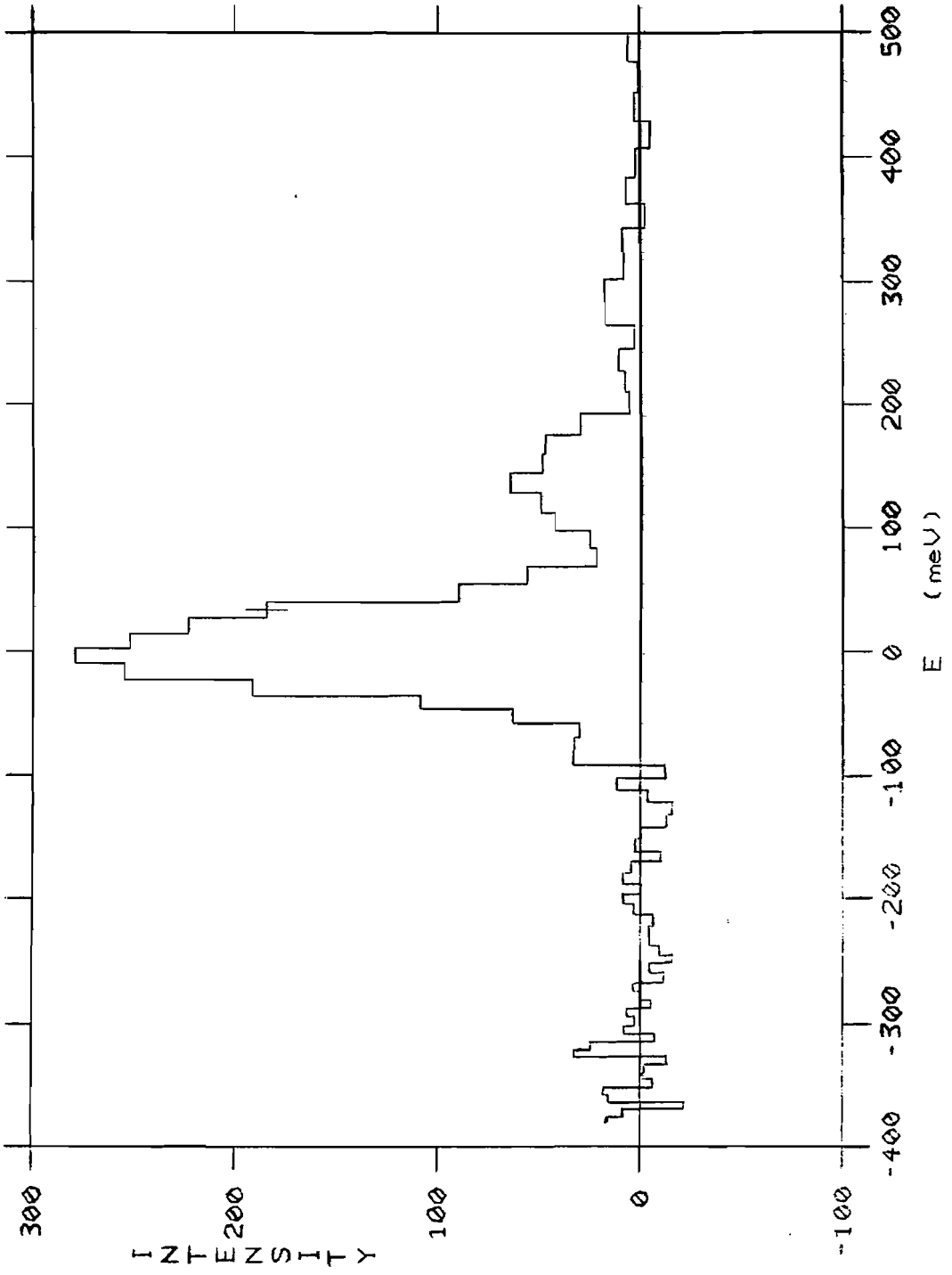

Figure 5 Double difference spectrum for ZrH_2 using Sm analyser foils.

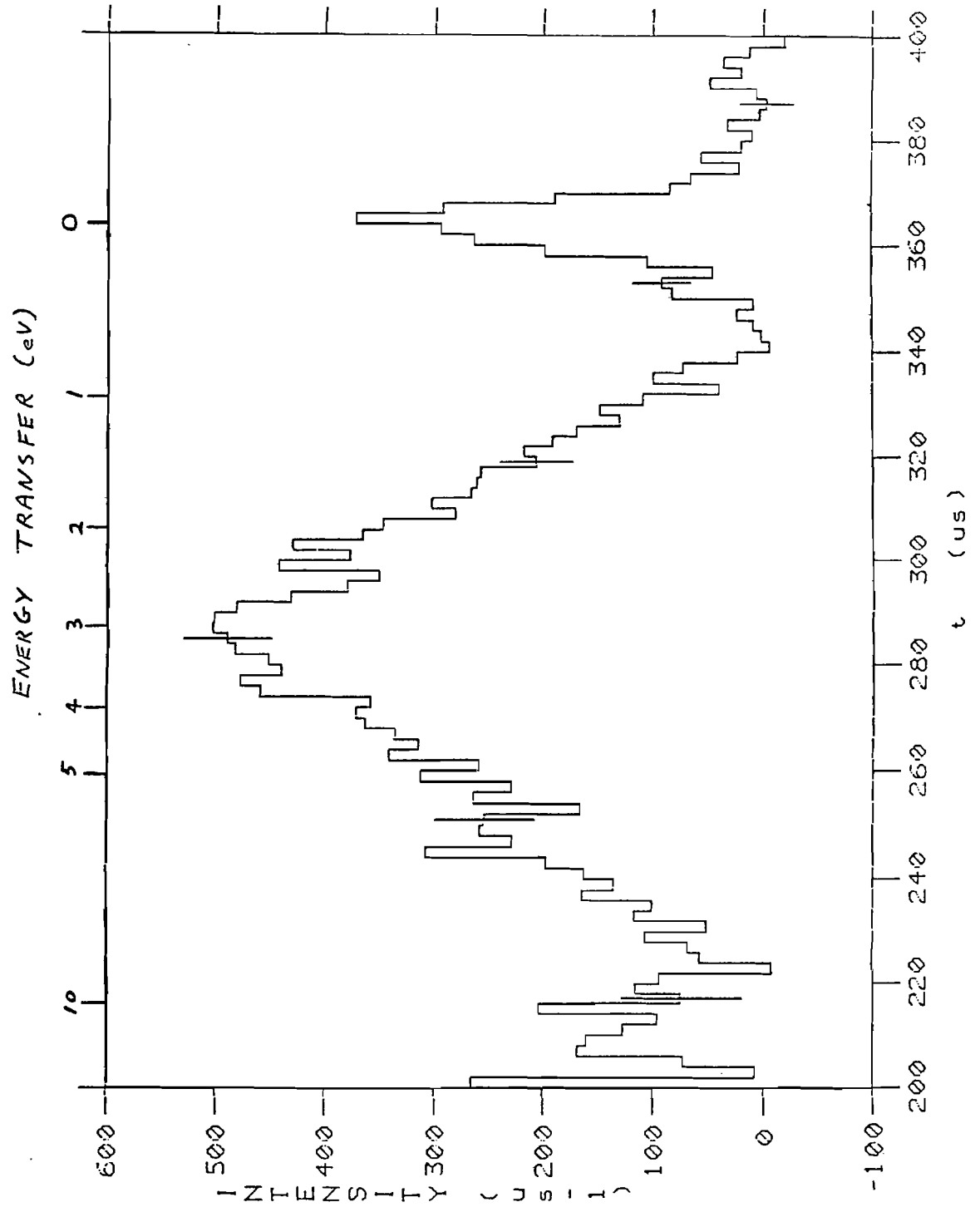

Figure 6 Scattering from ZrH2 at 45° (Background subtracted)

Proceedings of the Eighth Meeting of the International Collaboration on Advanced Neutron Sources (ICANS-VIII)
8-12 July 1985, Rutherford Appleton Laboratory Report RAL-85-110

Performance of the High Symmetry Spectrometer PRISMA to be installed at SNS

F. Sacchetti
Dipartimento di Fisica dell'Università di Perugia, Perugia, Italy
and
Istituto di Struttura della Materia del CNR, Frascati, Italy

The spectrometer PRISMA proposed in previous reports (Internal Reports ISM 1985/3 and 1985/4) is an High Symmetry Spectrometer designed to get high performance in measuring inelastic neutron scattering in single crystals. Therefore this instrument should be the analogue of the triple-axis spectrometers used in steady sources. A sketch of this spectrometer is shown in fig. 1, while in Table I the geometrical specification is given. The main point of present design is the relatively small angular distance between various analysers, still having a rather short sample to analyser distance. This last condition allows an almost free rotation of the analyser bank around the sample, thus leaving quite large degree of freedom in choosing the scattering triangles. Special care has been used in designing all moving parts to obtain the required performance as far as the angular reproducibility is concerned. In figs. 2a and 2b the sketch of the design of the main arm is given. Because of the small space available between analysers, special Soller collimators will be employed. In fact we have to use 0.2° collimators 25 cm long and the distance between two adjacent collimators is less than 2 cm. Moreover because of the necessity of having a large number of different

collimations to allow an easy change of resolution, relatively low cost collimators should be employed. In fact more than 100 collimators should be available. Therefore various collimators with different design are now being tested. Special care should be also devoted to the analyser crystals. These will be good quality squashed Ge cylinders with the (110) axis vertical. In this zone all the reflections up to (333) are available, thus giving very high flexibility in choosing the analyser d spacing. However these crystals must be as similar as possible to reduce calibration problems. The alignement of the sample will be obtained using five auxiliary counters in the range 100° to 120°, with different vertical collimations. All the counters will be ^{3}He detectors with filling pressure of 20 bars, thus providing a rather high efficiency also at relatively high energy. To have a rough estimate of the spectrometer performance in fig. 3 the expected intensity for an excitation having 20 meV energy is shown, choosing a spectrometer resolution of 3 meV FWHM and an average performance for the various components.

Geometrical characteristics of PRISMA

			Tolerance
L_o	Moderator to sample distance	9000 mm	1 mm
L_1	Sample to analyser distance	573 mm	0.2 mm
L_2	Analyser to counter distance	170 mm	0.1 mm
d	Diameter of sample, analyser and counter	12.5 mm	---
h	Height of sample, analyser and counter	60 mm	---
$\Delta\phi$	Range of sample scatt. angle	$\pm 135^\circ$	0.02°
$\Delta 2\theta$	Range of counter angles	$\pm 60^\circ$	0.005° x
$\delta\phi$	Separation of counters	2°	0.02°
η_c	Number of counters	16	---
α_1	Sample-analyser collimators	0.2° to 1.1°	
α_2	Analyser-counter collimators	0.4° to 3°	

x The counter arm is positioned by a stepping motor having a step of 0.036° and a reproducibility better than 0.005°.

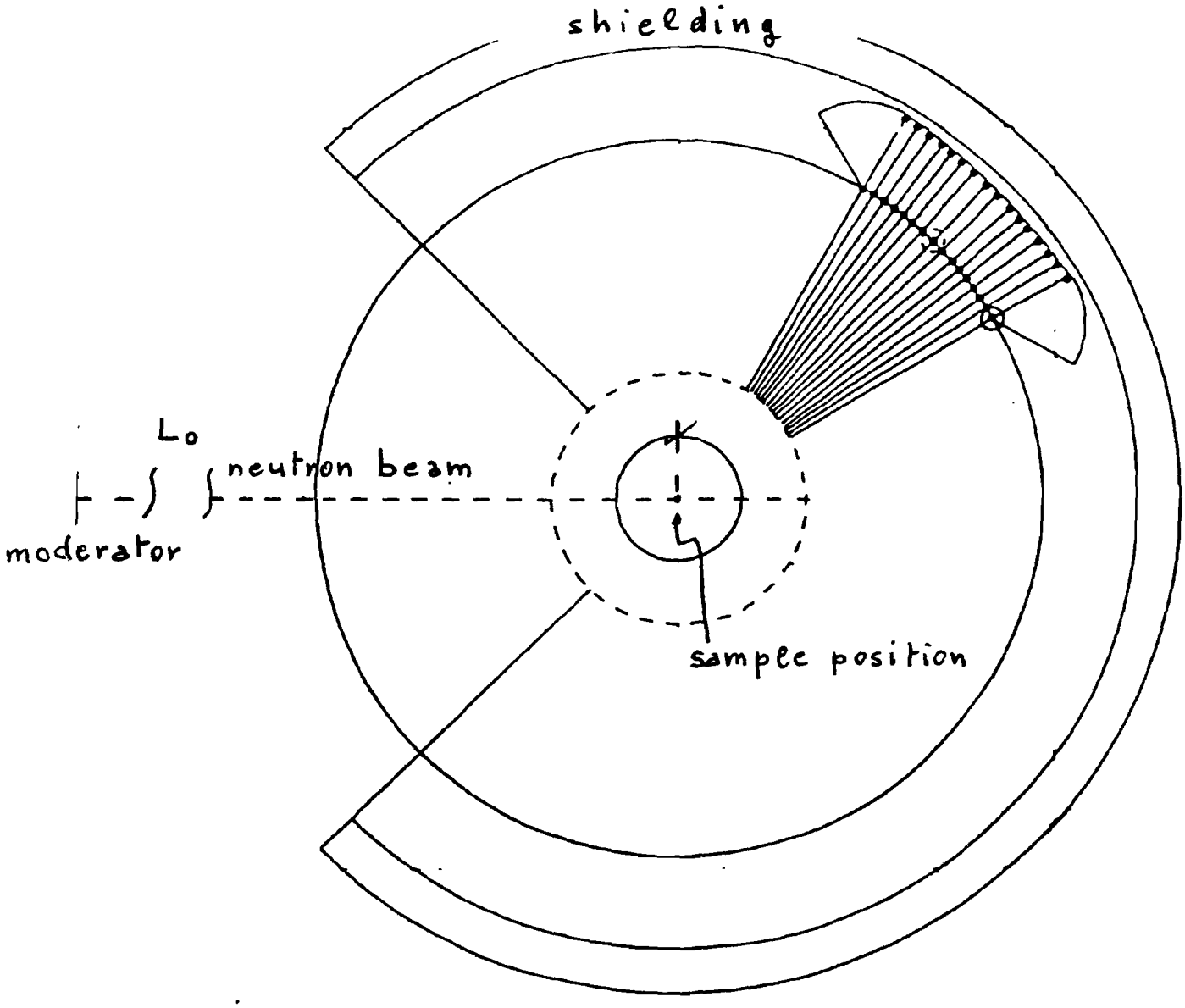

fig. 1

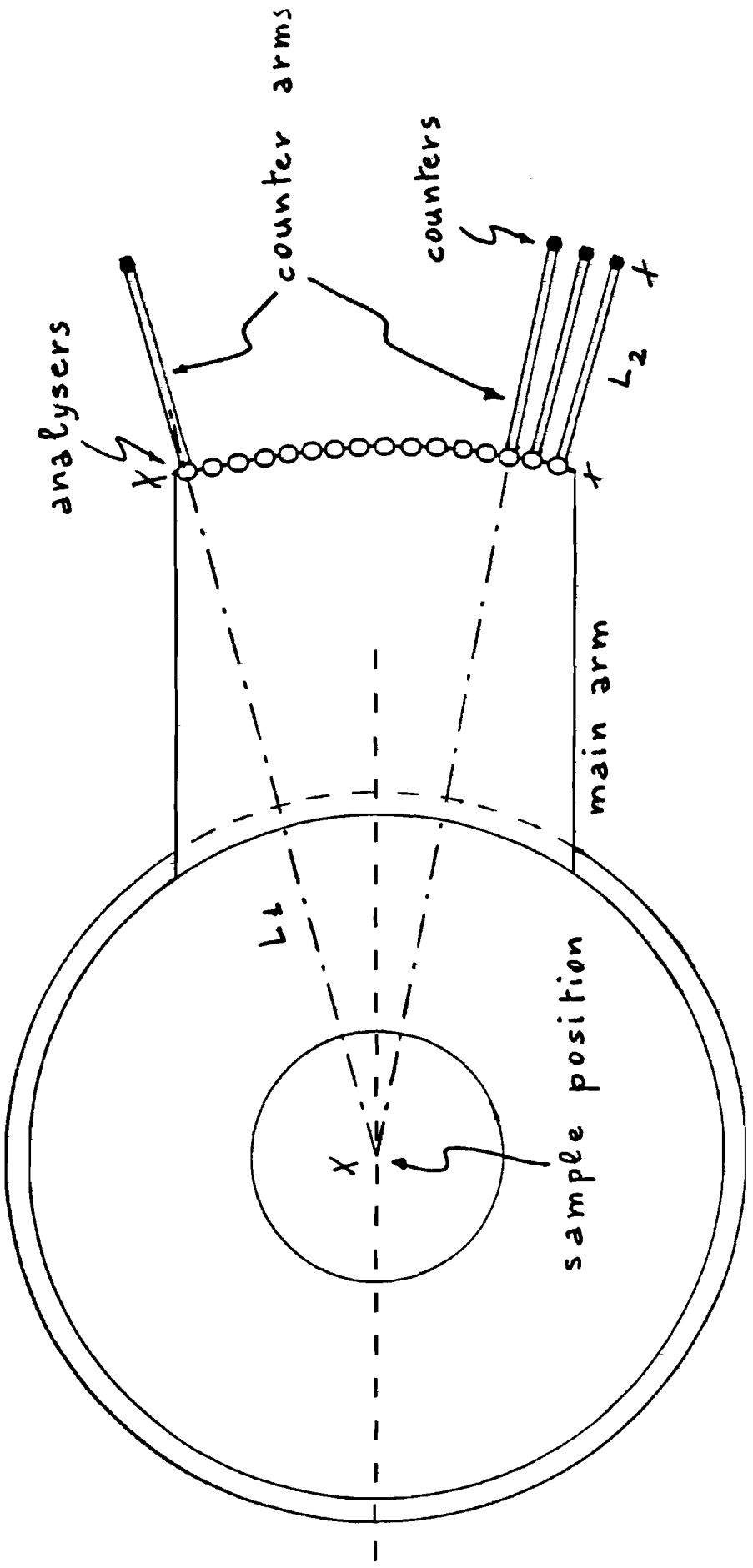
counter arms
counters
analysers
L_2
0
10 cm
main arm
L_1
sample position

fig. 2a

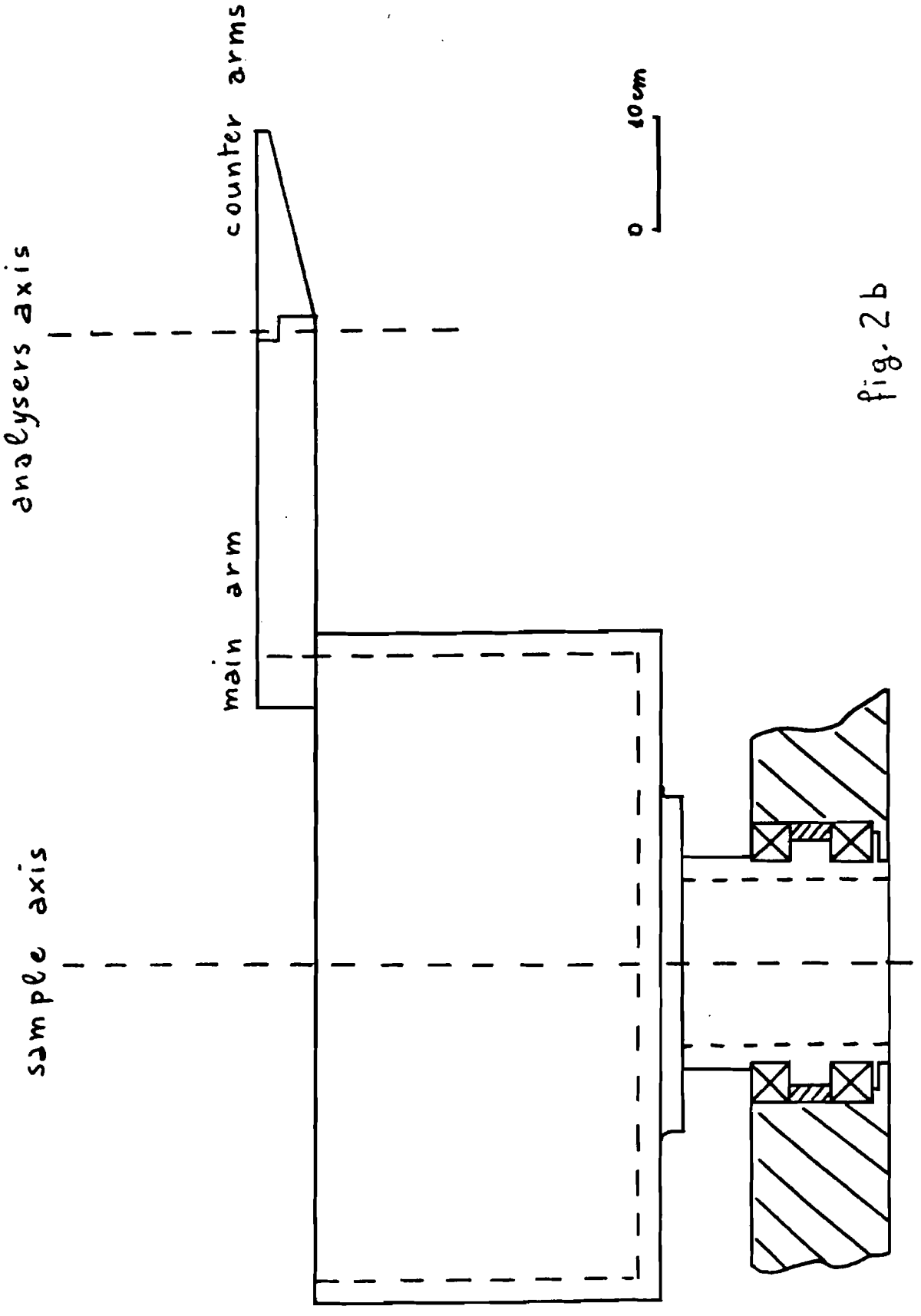

Fig. 2b

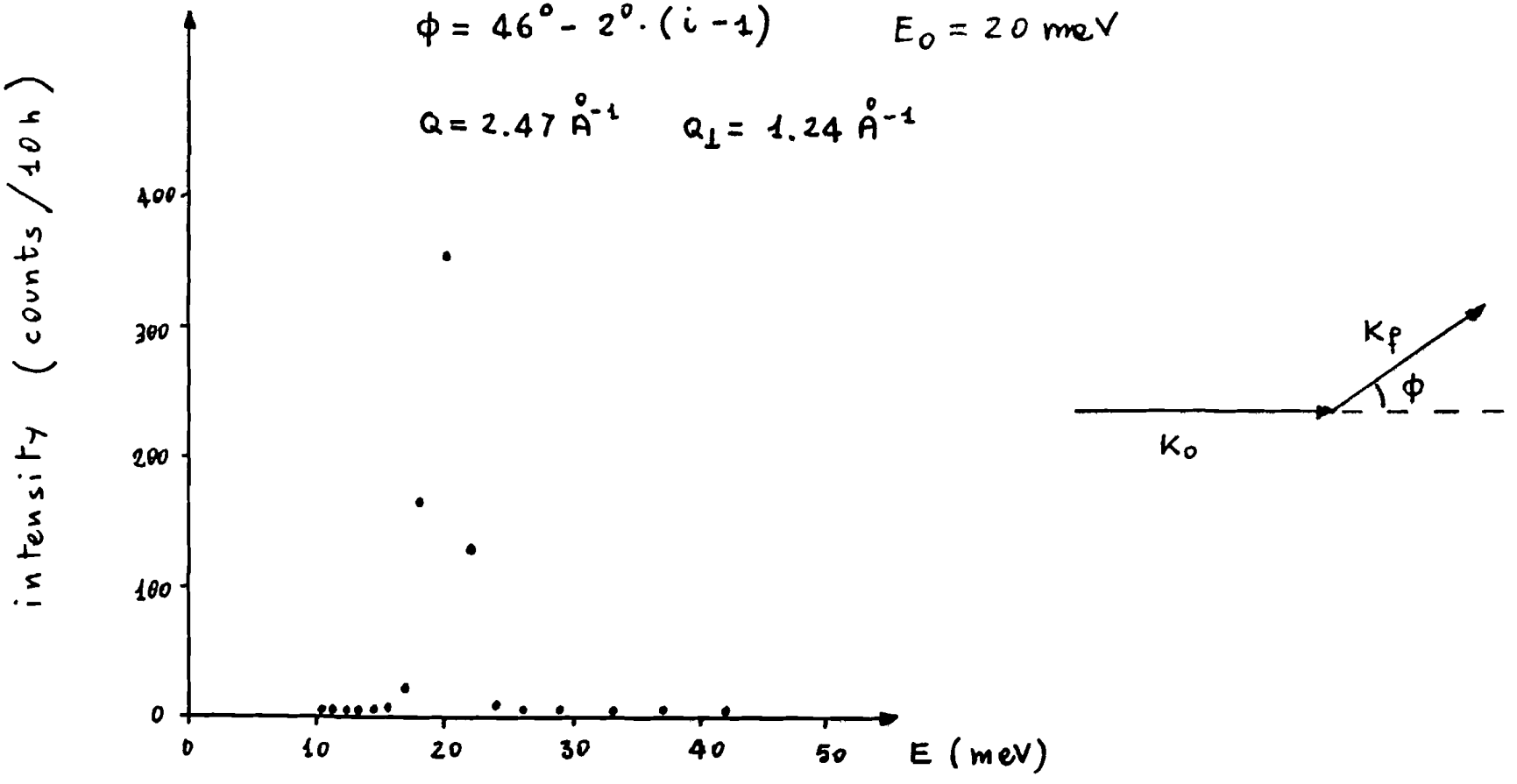
$\phi = 46^\circ - 2^\circ \cdot (i-1)$
$E_0 = 20$ meV
$Q = 2.47$ Å^{-1}
$Q_\perp = 1.24$ Å^{-1}
intensity (counts / 10 h)
400
300
200
100
0
0
10
20
30
40
50
E (meV)
K_f
ϕ
K_0

fig. 3

Proceedings of the Eighth Meeting of the International Collaboration on Advanced Neutron Sources (ICANS-VIII)
8-12 July 1985, Rutherford Appleton Laboratory Report RAL-85-110

THE LOS ALAMOS CONSTANT-Q SPECTROMETER

R. A. Robinson, R. Pynn*, J. Eckert and J. A. Goldstone

Physics Division, Los Alamos National Laboratory, Los Alamos, N.M. 87545, U.S.A.

Abstract

A constant-Q spectrometer which has been installed on the pulsed source of the Los Alamos Neutron Scattering Center, is described. It features a number of innovations that ease sample and analyser alignment and a novel composite crystal analyser which exploits the mosaic properties of plastically deformed germanium in a new way. Observations of phonon dispersion in aluminium and of incoherent scattering in ZrH_2 are reported, along with background measurements.

1. Introduction

In this paper, we report the construction and initial operation of an improved constant-Q spectrometer[1] installed at the Los Alamos Neutron Scattering Center.[2] It is shown schematically in Figure 1 and its parameters are listed in Table 1. It is quite similar to the Harwell machine,[3,4] but features a number of significant improvements. Those relating to ease of operation of the instrument are listed in Section 2. In addition, we have proposed and tested a new analyser geometry, which is described in Section 3. In Section 4, we describe measurements on phonons in aluminium and we discuss data reduction. Finally, in Section 5, we outline our plans for future improvements and make some comments on pulsed

*Permanent address: Institut Laue Langevin, 156X Centre de Tri, 38042 Grenoble CEDEX, France

source inelastic instruments in general. We have chosen to emphasise new features or ideas in a fairly concise form and the reader interested in more detail is referred to Reference 1.

2. Improvements

(a) Line-up detector

We have chosen a longer sample-line-up detector flight path. This means that the Bragg peaks used in sample or analyser rocking curves are better separated. To boost count rate while searching for the peak in the first place, we have used a bank of three detectors subtending approximately 2°. In addition, vertical and horizontal ^{10}B-coated stretched film Soller collimators[5] (of 10' divergence) can be placed in this flight path for fine adjustment of sample or analyser orientation.

(b) Variable sample-image point separation

The spectrometer was constructed in such a way that the sample-image point separation can be varied between 20 and 40 cm. This entails moving the whole detector shielding assembly, which is mounted on rails, and moving the analyser crystal correspondingly. To this end, the analyser is suspended from a translation stage.

(c) Analyser mounting

The analyser crystal is mounted on a small two-axis motorised goniometer, which is in turn suspended from a two-dimensional translation stage. The idea of this arrangement is that the analyser can be translated reproducibly to the sample position (see A' in Figure 1) and that a rocking curve can be performed on the analyser, the scattered neutrons being detected in the same line-up counter as used for the sample. The analyser is then rotated (by 45°) and translated back to its normal position and orientation. We have experienced no difficulties aligning either samples or analyser crystals in this manner.

(d) Cadmium absorber after the sample

A major source of background is due to neutrons which pass directly through the sample, but which are then scattered, by air at the image point, directly into the main detector bank. To eliminate this source, we have placed a cadmium absorber in the beam midway between the sample and image points. This has the effect of reducing the subcadmium neutron background to better than 0.1 counts per minute. A typical background run is shown in Figure 2a. For comparison purposes, we also show a ZrH_2

spectrum in Figure 2b, and this Figure shows that it is possible to reach quite high energy transfers before background becomes a problem. We have also tried adding 3.5 mm of erbium, which has low energy nuclear resonances at 460 and 584 meV,[6] and this has the effect of moving the cut-off in Figure 2 to even shorter times. One could also consider using samarium and indium, which also have low-energy nuclear resonances, to push the threshold to yet shorter times.

(e) Other shielding arrangements

The shielding in the vicinity of the sample and analyser has been kept simple and flexible in order that the analyser can be moved and so that L_2 can be changed. When L_2 is at its minimum value, we have found it necessary to place vertical collimation between the sample and the analyser to eliminate contamination by out-of-plane analyser Bragg reflections. We have also placed 0.5 m long boron-aluminium composite sheets between the detectors as shown in Figure 1. These reduce the solid angle viewed by each detector and thereby reduce the background. An aluminium box, filled with B_4C, was placed behind the detector bank. In other respects, the spectrometer shielding was conventional.

3. The Analyser

Although we initially used a small germanium analyser (as described in Table 1) in the disc geometry proposed by Windsor,[4] we have proposed and tested an alternative, the "organ-pipe" geometry. It consists of a set of cylindrical crystals of identical crystallographic orientation, as shown in Figure 3. Any reflection in the [hhk] zone can be accessed by rotating all of the elements in unison. It has the following advantages:

(a) It maintains the flexibility of the disc (i.e., one can change reflection)

(b) It is far easier to make a large analyser in this geometry - less material is required and the cost is lower. This has the consequence that L_2 can be increased to provide room for sample environment equipment and collimators.

(c) The mosaic spread and thickness can be chosen to vary in the optimum manner along the length of the analyser (i.e., as a function of ϕ).

(d) The anisotropic mosaic properties of plastically deformed germanium (or copper) can be exploited to give a large mosaic spread within the

scattering plane (horizontal) and a small vertical mosaic spread for all reflections in the [hhk] zone. This is not possible in the disc geometry.

4. Results

As a demonstration experiment, we have chosen to measure several zone-boundary phonons in aluminium. We have exploited the fact that its lattice parameter is almost (to within 2.5%) exactly double the size of the (220) d-spacing of germanium. This means that one can scan along the zone boundary direction $\langle 1+\zeta, \bar{1}, 0\rangle$ as shown in the inset to Figure 4b. The results are shown as an intensity map in Figure 4a. There is clearly an intense, almost dispersionless phonon at approximately 25 meV, with a weaker dispersive mode at higher energies. Peak positions obtained from this map are compared to the 80 K results of Stedman and Nillson[7] in Figure 4b. The general agreement is good, but there is a small systematic discrepancy in the dispersive mode. This is mainly due to the fact that our measurements were made at room temperature and that the lattice is softer. A number of constant-$\underline{Q}$ scans can be constructed from these data and we show three in Figure 5. Resolution widths calculated within the framework reported previously[8,1] are also shown. In order to produce the intensity map shown in Figure 3a, the following steps must be followed:

(a) Perform rebinning from (ϕ,t) to $(Q_{\parallel},E)$ coordinates, where t is the observed time-of-flight, $Q_{\parallel}$ is the component of the momentum transfer parallel to the incident wave vector, and E is the energy transferred to the sample. This process should also include (implicitly or explicitly) multiplication by the appropriate Jacobian.

(b) Correct for the incident spectrum (which is measured using a low efficiency beam monitor), the detector efficiency and the analyser efficiency (the product of which can be measured in a vanadium scan).

(c) Correct for the variation of resolution volume across the data set. This is the equivalent of the $k_F^3 \cot\theta_A$ factor familiar in triple-axis spectroscopy.

5. Future Improvements

(a) More detectors

We are currently increasing the number of detectors to 64. It is clear from Figure 4a that the present number is insufficient, in the sense that one does not "get down to background" on both sides of the 25 meV phonon.

(b) Copper Analyser

We do not believe that second-order contamination is a problem in most experiments,[1] and one therefore does not need to use diamond structure material like germanium. We estimate[9] that gains of approximately 70% in reflectivity can be achieved at 50 meV if copper is used. The gain will be yet greater for higher incident energies. Furthermore, copper behaves in a more ideal manner during the plastic deformation process.

(c) Sample-analyser collimation

It would be advantageous to be able to vary the secondary spectrometer resolution using a fan-type collimator[10] between the sample and analyser. Backgrounds are also likely to be reduced once such a device is employed.

(d) Support the analyser crystal from below

The present arrangement is to mount the analyser crystal from above from a translation stage and to align it using the same line-up counter as for the sample. While this system poses no problems for small analysers, it is more difficult for large analyser assemblies. In addition, the supports for the translation stage get in the way of shielding and sample environment equipment for the sample. Given that we have shown that one can fabricate a large analyser crystal and thereby increase L_2 substantially, it may be worthwhile to support such an analyser from below, by means of a conventional goniometer. As it would no longer be possible to translate this to the sample position, a second line-up counter dedicated to the analyser would be necessary. Of course, it will still be necessary to translate it into the main beam for alignment purposes.

(e) Evacuate the image point

It will clearly be advantageous to evacuate the image point, or at least fill it with an argon atmosphere.

(f) Improve the moderator

As suggested at the Shelter Island Workshop,[11] this type of spectrometer could well benefit from a tall thin (vertically defocussed) moderator and one in which the moderator pulse width could be changed by means of a variable poison depth.

References

1. R. A. Robinson, R. Pynn and J. Eckert, submitted to Nucl. Instrum. Methods (1985) (also Los Alamos Report LAUR 85-1900).
2. R. N. Silver in Proceedings of 6th meeting of ICANS, Argonne,1982, Argonne National Laboratory Report ANL-82-80 p. 51.
3. C. G. Windsor, R. K. Heenan, B. C. Boland and D. F. R. Mildner, Nucl. Instrum. Methods 151, 477 (1978).
4. C. G. Windsor "Pulsed Neutron Scattering", Taylor and Francis, London 1981, Chapter 9.
5. C. J. Carlile, J. Penfold and W. G. Williams, J. Phys. E 11, 837 (1978)
6. S. F. Mughabghab and D. I. Garber, Brookhaven National Laboratory Report BNL-325, 3rd Edition, Volume I (1973).
7. R. Stedman and G. Nillson, Phys. Rev. 145, 492 (1966).
8. R. Pynn and R. A. Robinson, in Proceedings of Workshop on "High Energy Excitations in Condensed Matter" at Los Alamos, February 1984, Los Alamos Report LA-10227-C, p. 45.
9. For the method of calculation, see A. K. Freund in Proceedings of meeting on "Fokussierende Neutronenmonochromator und -analalysatoranordnungen", Hahn Meitner Institute Report HMI-B273 (1978) or R. A. Robinson and A. K. Freund, Institut Laue Langevin Report **** (1985).
10. A. F. Wright, M. Berneron and S. P. Heathman, Nucl. Instrum. Methods 180, 655 (1981).
11. C. G. Windsor, W. J. L. Buyers, R. A. Cowley, R. A. Robinson and S. M. Shapiro in Proceedings of Workshop on "Scientific Opportunities with Advanced Facilities for Neutron Scattering", Shelter Island, October 1984, CONF-8410256, p. 25.

TABLE 1

Moderator-sample distance L_1	6.990 m
Sample-image distance L_2	0.199-0.402 m
Image-detector distance L_3	1.447 m
Sample-alignment counter distance L_4	1.050 m
Angular (ϕ) range of detectors allowed by shielding	10°-70°
Spacing between detectors	0.59°
Moderator material	water at room temperature
thickness	2.3 cm
poisoning	none
area (viewed by sample)	~10 cm x 10 cm
Beam size at sample	2.5 cm wide x 5 cm high
Detectors	25x 1.25 cm diameter, 10 cm active length ^{3}He proportional counters, mounted vertically
Analysers	1x 5 cm diameter, 1 cm thick Ge disc and 1x 22cm long 5 cm high "organ-pipe" Ge analyser
Line-up detector	3 detectors identical to main detector
Incident beam monitor	1x low efficiency BF_3 monitor

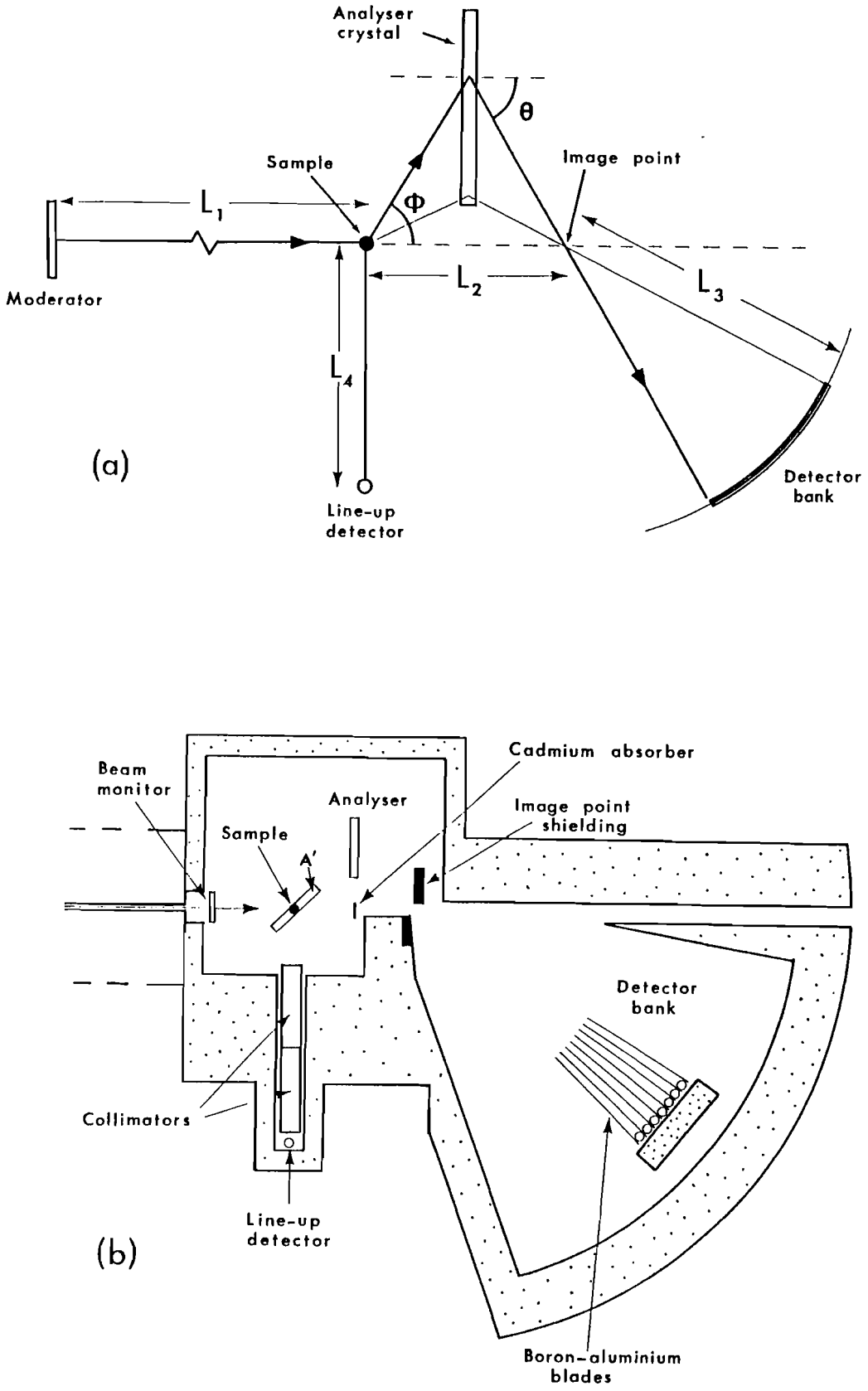

Figure 1: The schematic layout of a constant-Q spectrometer, showing (a) the symbolic conventions adopted in this work and (b) the physical details of the Los Alamos machine. A' = analyser translated to sample position for alignment purposes.

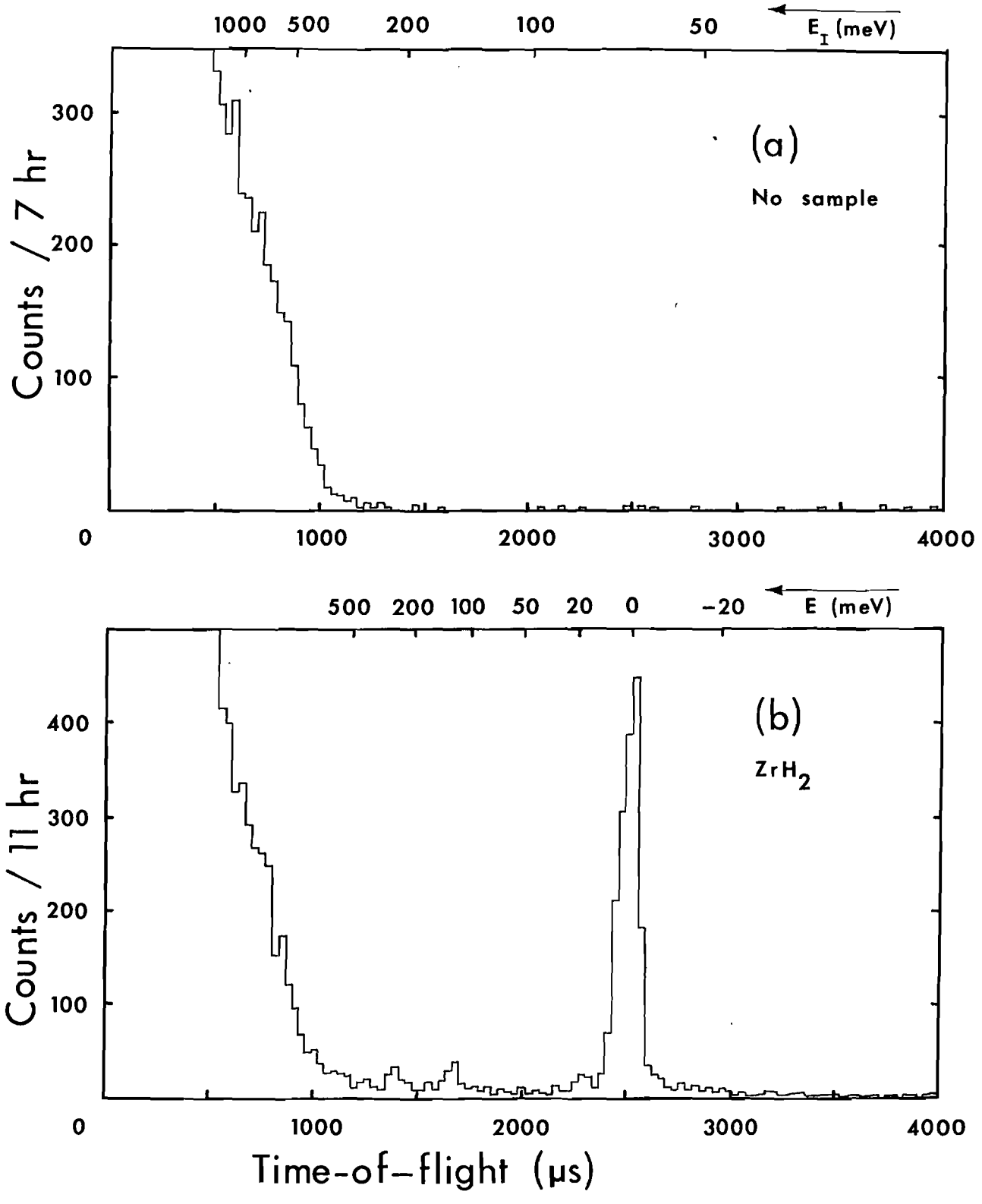

Figure 2: Time-of-flight spectra: (a) A background run. The spectrometer was set up with the "organ-pipe" analyser on the (331) reflection with no sample. ϕ = 24.5°. An energy scale, corresponding to elastic scattering at the image point is provided. (b) A ZrH_2 spectrum in the same counter as (a), with a Ge(331) analyser. An energy transfer scale is also provided. The elastic line is visible at 2500 μs and the first and second harmonics of the 140 meV excitation at 1700 and 1350 μs respectively. In both cases the data have been binned into 32 μs time channels.

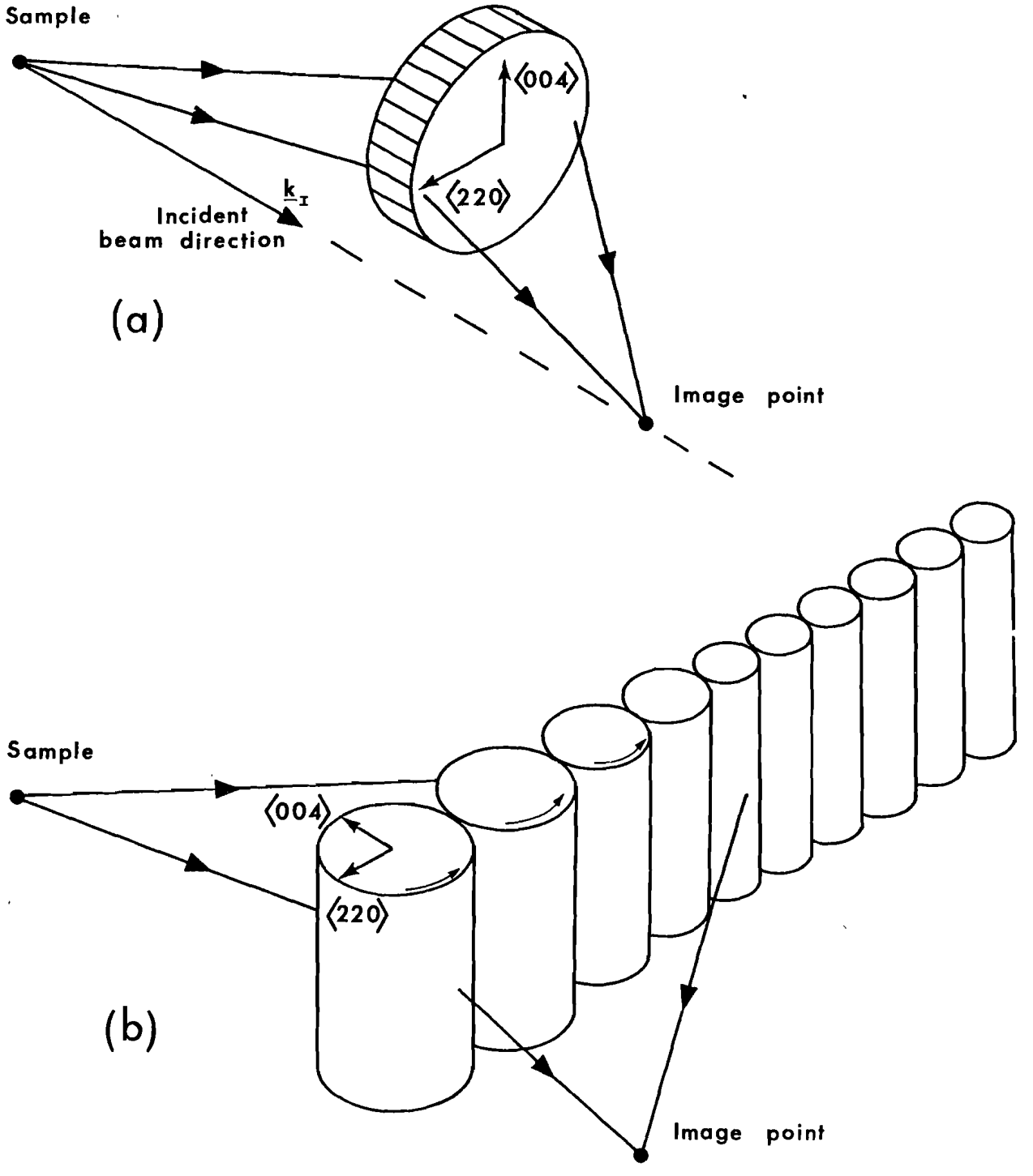

Figure 3: Possible flexible analyser geometries: (a) the disc[4] and (b) the "organ-pipe" described in detail in Reference 1.

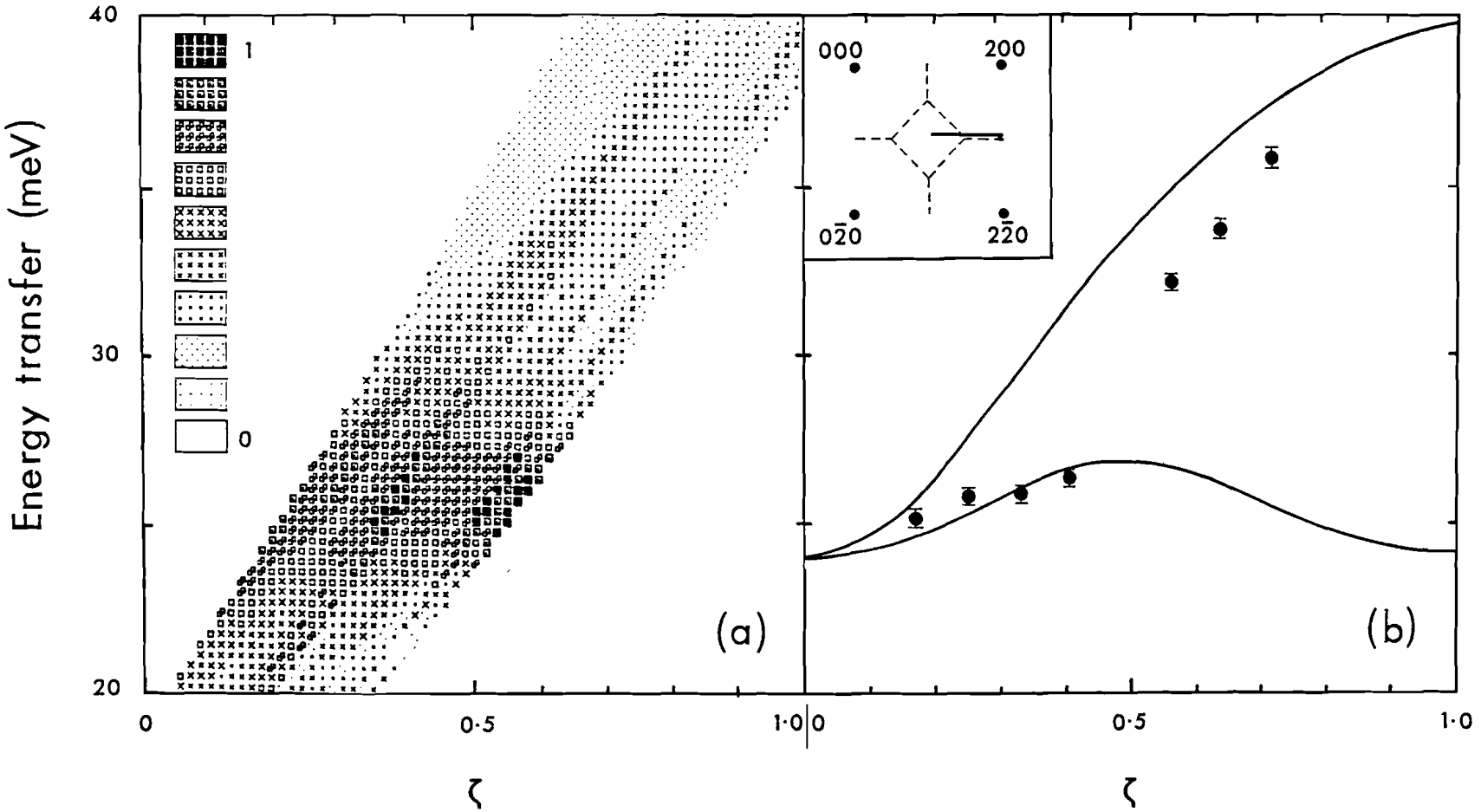

Figure 4: Aluminium phonon dispersion measured along <1+ζ,$\bar{1}$,0> with a germanium (220) analyser: (a) our results presented as an intensity map and (b) dispersion curves for the same piece of ($Q_{\parallel}$,E) space. The solid line represents the 80 K data of Stedman and Nillson[7] and the points show our results when binned into constant-Q scans. The vertical bars represent the errors in the positions of the respective constant-Q peaks. The measurements were made within the [001] zone, between (1$\bar{1}$0) and (2$\bar{1}$0) and this region of reciprocal space is shown in the inset. A quadratic intensity scale (from 0 to 1) was used, with 1 representing the intensity of the most intense ($Q_{\parallel}$,E) bin.

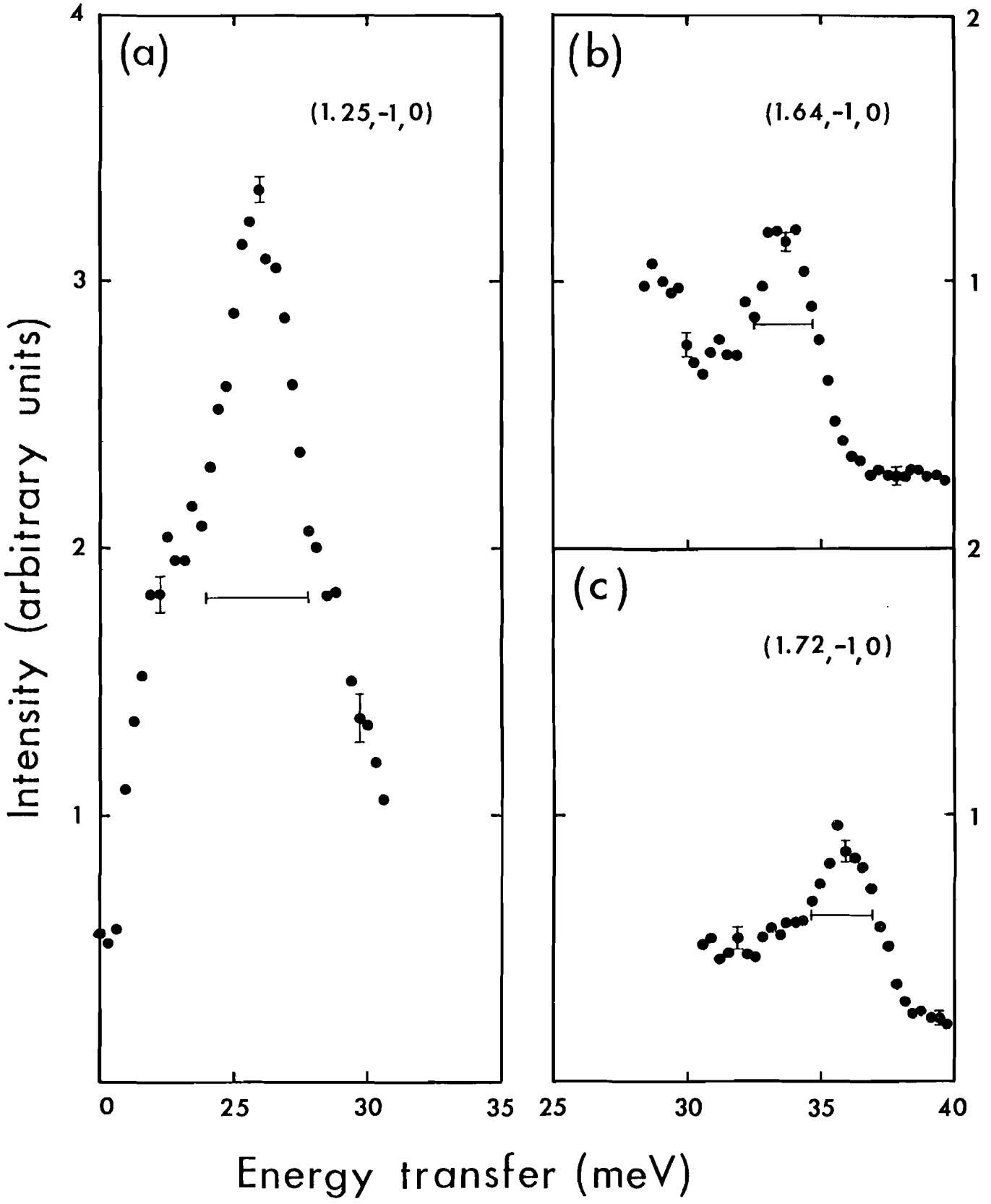

Figure 5: Constant-$\underline{Q}$ scans for (a) $\underline{Q}$ = (1.25,-1,0), (b) $\underline{Q}$ = (1.64,-1,0) and (c) $\underline{Q}$ = (1.72,-1,0) for aluminium at room temperature. Each scan was obtained by binning over 0.12Å^{-1} (0.078 reciprocal lattice units) in $Q_{\parallel}$. The horizontal bars show the calculated FWHM resolution width. The tail of the lower mode is clearly visible in (b), but there were not sufficient detectors at higher angles to cover this piece of $(Q_{\parallel},E)$ space.

Proceedings of the Eighth Meeting of the International Collaboration on Advanced Neutron Sources (ICANS-VIII)
8-12 July 1985, Rutherford Appleton Laboratory Report RAL-85-110

Development of Polarized Epithermal Neutron Spectrometer PEN at KENS

M. Ishida, Y. Ishikawa, S. Ishimoto*, M. Kohgi, A. Masaike+, Y. Masuda*, K. Morimoto* and T. Nakajima*

Physics Department, Tohoku University
Sendai 980, Japan

*National Laboratory for High Energy Physics
Oho-machi, Tsukubagun, Ibarakiken 305, Japan

+Physics Department, Kyoto University
Kyoto 606, Japan

Abstract

The recent progress of the Polarized Epithermal Neutron Spectrometer (PEN) at KENS is described. A great improvement of the quality factor of the dynamically polarized proton filter (DPPF) has been achieved by employing a ^{4}He-^{3}He heat exchanger for the cooling of the filter which realizes the complete removal of liquid ^{3}He from neutron beam path. This cooling system is considered to be the most promising one in the practical use of the DPPF for polarized neutron scattering experiments.

1. Introduction

The Polarized Epithermal Neutron Spectrometer (PEN) at KENS[1,2] is designed to utilize the polarized white epithermal neutrons for the studies of nuclear polarization dependent scattering, magnetic scattering, nuclear parity dependent scattering, etc.. The neutron polarization is achieved by passage through a dynamically polarized proton filter (DPPF).[3,4] Since 1983, after the construction of main parts of the spectrometer, our efforts have been concentrated on the improvement of its performance, especially on getting an intense polarized neutron beam. We present here the recent progress of this point.

2. Improvement of dynamically polarized proton filter

The most difficult point for production of intense polarized white neutrons by use of the dynamically polarized proton filter (DPPF) is to remove ^{3}He liquid from the neutron beam path as much as possible ensuring the enough cooling power for the filter material which is heated up by microwave absorption. This is because the ^{3}He liquid is the coolant of the cooling system which cools the filter material down to ca. 0.5k, and, on the other hand, it is the highly neutron absorbing material. In the course of the efforts to overcome this difficulty, we have developed several types of the DPPF systems so far.[2,5] In this section Two types of them, which have recently be developed, are described.

a) Type I filter

The first type of the DPPF is shown in Fig.1. The filter

material was a mixture of ethylene glycol and ethylene glycol Cr(v) complex, which was filled in four separated cells of 2.4mm width x 20mm height x 15mm thickness. The filter thickness was decided by the optimization of the produced neutron polarization and the transmitted beam intensity. The filter cells were immersed in a liquid ^{3}He container which was also a part of a microwave cavity. Spaces of 2.4mm width were left between the cells for good coolant convection around the filter material. The filter was inserted into a ^{3}He cryostat, set in the center of a superconducting magnet of 25KG, and cooled down to ca, 0.5k. By use of this filter configuration, maximum proton polarization of 67% was realized. This result is satisfactory in the condition of the magnetic field and the coolant temperature. The neutron polarization was determined by the transmission through the filter and the 200 Bragg scattering from a Fe_8Co_{92} single crystal. Neutron transmission through the filter was also used to monitor the liquid ^{3}He level in the container. If the liquid ^{3}He level is within the neutron beam path, unpolarized beam mixes with the polarized beam. The lowering of the liquid ^{3}He level ,however, causes an anomalous increase in the neutron counting for the transmission measurement, and therefore it is easily detectable. During this experiment the level was found to be always above the neutron beam path. The results of the neutron polarization are shown in Fig.2. The close circles in the figure are polarizations determined by the transmission measurement. Solid curve is a calculated value by use of the cross section data by Lushchikov et al.[3] and the proton poralization of 67%. A good agreement is seen between these results. These values are found to be the highest polarization that have ever been achieved

for epithermal white neutron beam, and are sufficient for neutron scattering experiments. The open circles are the polarization determined by the $Fe_8Co_{\frac{8}{9}2}$ Bragg scattering. They are systematically smaller than the value determined by the transmission measurement. Most of the deference is considered to come from the depolarization of neutrons in the beam path after the filter. Further tuning of the magnetic field along the neutron beam path is necessary in order to increase the neutron polarization at the sample position for the scattering experiments up to the value obtained by the transmission measurement.

b) Type II filter

Although, by use of type I filter, the high enough polarization of the epithermal white neutrons could be achieved, the effective beam size is still limited one since the layers of liquid ^{3}He obstruct partly the neutron beam path. In order to enlarge the beam size, a new type of filter, which utilizes the super liquid ^{4}He as the first stage coolant , has been developed. The configuration of this type of filter is shown schematically in Fig.3. The filter material was same as the case of type I filter, but it was formed into beads of about 1.5mm in diameter. The beads filled a Cu mesh box of 3x4x1.5cm^3 which was set in the microwave cavity filled with liquid ^{4}He. The bottom of the cavity, on both inside and outside of which Ag fine powder of about 1μm in diameter was sintered, was immersed in a liquid ^{3}He pool which was cooled to ca. 0.5K by pumping. Since the thermal resistance of the super liquid ^{4}He is negligibly small, the heat produced inside the cavity can be effectively transfered to the liquid ^{3}He pool through the heat exchanger composed of the

sintered Ag fine powder layers. By this configuration we can achieve the complete removal of liquid ^{3}He from the neutron beam path.

A test experiment to see the cooling efficiency of this type of filter system was carried out. In order to simulate the heating up by microwave, a manganine heater winded around a Cu frame of 4x1.5cm^2 was immersed in the cavity filled with liquid ^{4}He. The temperature of the liquid ^{3}He in the pool and liquid ^{4}He inside the cavity were measured with calibrated Ge thermometers. The pressure of ^{3}He gas at the surface of liquid ^{3}He pool was also measured to check the temperature of the liquid ^{3}He. The input power were monitored by the supplied current and voltage to the heater. The results are shown in Fig.4. The fact that a difference between the temperatures of the liquid ^{3}He and ^{4}He exists and increases with increasing input power indicates that there is some amount of thermal resistance of the heat exchanger between the inside and outside of the cavity, as expected. The dynamical polarization of protons using this type of filter system was performed. The amount of the filter material was about 14cc. The microwave of 20-30mW was irradiated on the filter material. The temperature of liquid ^{4}He on that time was about 0.5K. The maximum proton polarization obtained in this condition was 50%. This value is rather low than the case of type I filter, 67%. We guess that this difference mainly comes from the difference of sample amount. In fact, The sample amount of this type filter was 4.7 times as much as the case of type I (3cc). In spite of this fact, we could obtain a great improvement of the performance by this filter system. This point is discussed in the following section.

c) comparison of the performance

The quality factor of a neutron polarizing filter is defined as $Q=P^2T$, where P and T are neutron polarization and transmittance through the filter, respectively. Since the neutron counting statistics in the usual experimental condition is proportional to the incident neutron beam size, it is reasonable to define the total quality factor, which represent the performance, as $Q=AP^2T$, where A is the area of the filter. We plotted the quality factors for our typical DPPFs developed so far in Fig.5 by closed marks. The abcissa shows the years when the development was performed. The quality factors are calculated at the neutron energies of 0.1 and 1eV by using the experimentally obtained neutron polarization and transmittance. The data noted as Pre-PEN in the figure are results of a test experiment for PEN using a horizontal field cryostat[5]. The quality factors of the type II filter are estimated from the proton polarization determined by the NMR enhacement since neutron beam experiment was not available because of the long shutdown of KENS in 1984 fiscal year. We have recently started neutron beam experiments to confirm this results. It can be seen from the figure that a great improvement of the performance has been achieved step by step. The open marks in the figure show the estimated value for the type II filter supposing the proton polarization to be 80%. Since the beam size of $3x4cm^2$ obtained by this filter is large enough for usual scattering experiments, we regard these value as our goal value. From the discussion given in the preceding section, it is clear that, in order to reach the goal, we should make further efforts on the improvements of the total cooling power of the system, microwave

input power and also the efficiency of the ^{4}He-^{3}He type heat exchanger.

3. Summary

We have achieved a great improvement of the quality factor of the DPPF by employing a ^{4}He-^{3}He heat exchanger for the cooling system of the filter. It realized the complete removal of liquid ^{3}He from the neutron beam path. This cooling system is considered to be the most promising one in the practical use of the DPPF for polarized neutron scattering experiments.

references

1) M. Kohgi, Proceedings of the Sixth Meeting of the International Collaboration on Advanced Neutron Sources, ANL-82-80(1983)172.

2) M. Ishida, Y. Masuda, M. Kohgi, Y. Kanno, S. Hiramats, Y. Ishikawa, A. Masaike and K. Morimoto, KENS REPORT-V, KEK Progress Report 84-2(1984)207 ; M. Ishida, Y. Masuda, Y. Kanno, M. Kohgi, Y. Ishikawa and A. Masaike, ibid. (1984)211.

3) V. I. Lushchikov, Yu. V. Taran and F. L. Shapiro, Soviet J. Nucl. Phys. 10(1970)669.

4) S. Hiramatsu, S. Isagawa, S. Ishimoto, A. Masaike, K. Morimoto, S. Funahashi, Y. Hamaguchi, N. Minakawa and Y. Yamaguchi, J. Phys. Soc. Jpn., 45(1978)949.

5) J. M. Newsam, M. Ishida, S. Isagawa, Y. Ishikawa, S. Ishimoto, M. Kohgi, A. Masaike, Y. Masuda, K. Morimoto and T. Nakajima, KENS REPORT-III, KEK Internal 82-5(1982)123.

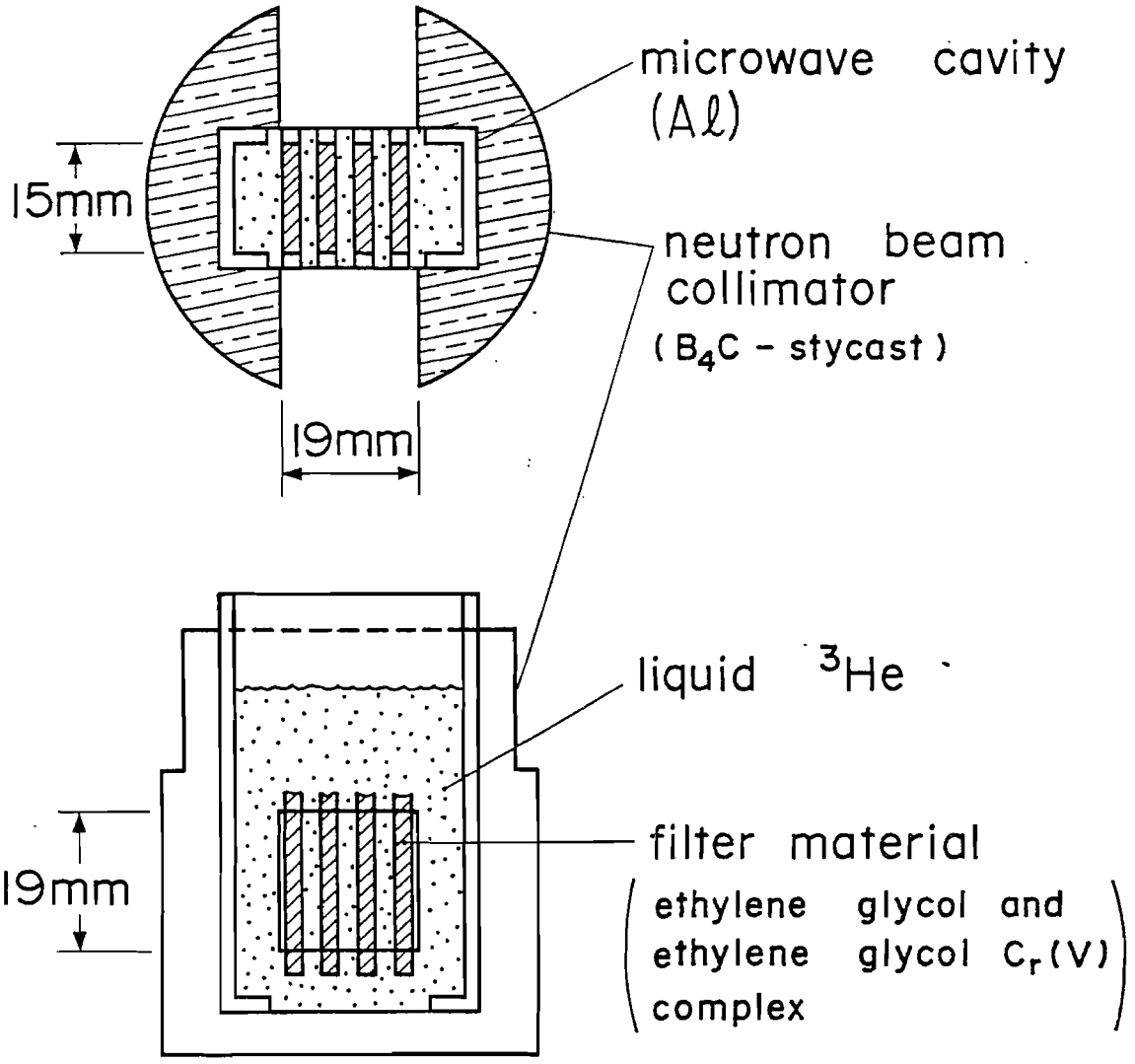

Fig.1 Type I filter. Filter cells are immersed in the liquid ^3He container which is also used as a microwave cavity. The cavity is set in the neutron beam collimator which has windows of $19 \times 19 mm^2$ in the center of the beam.

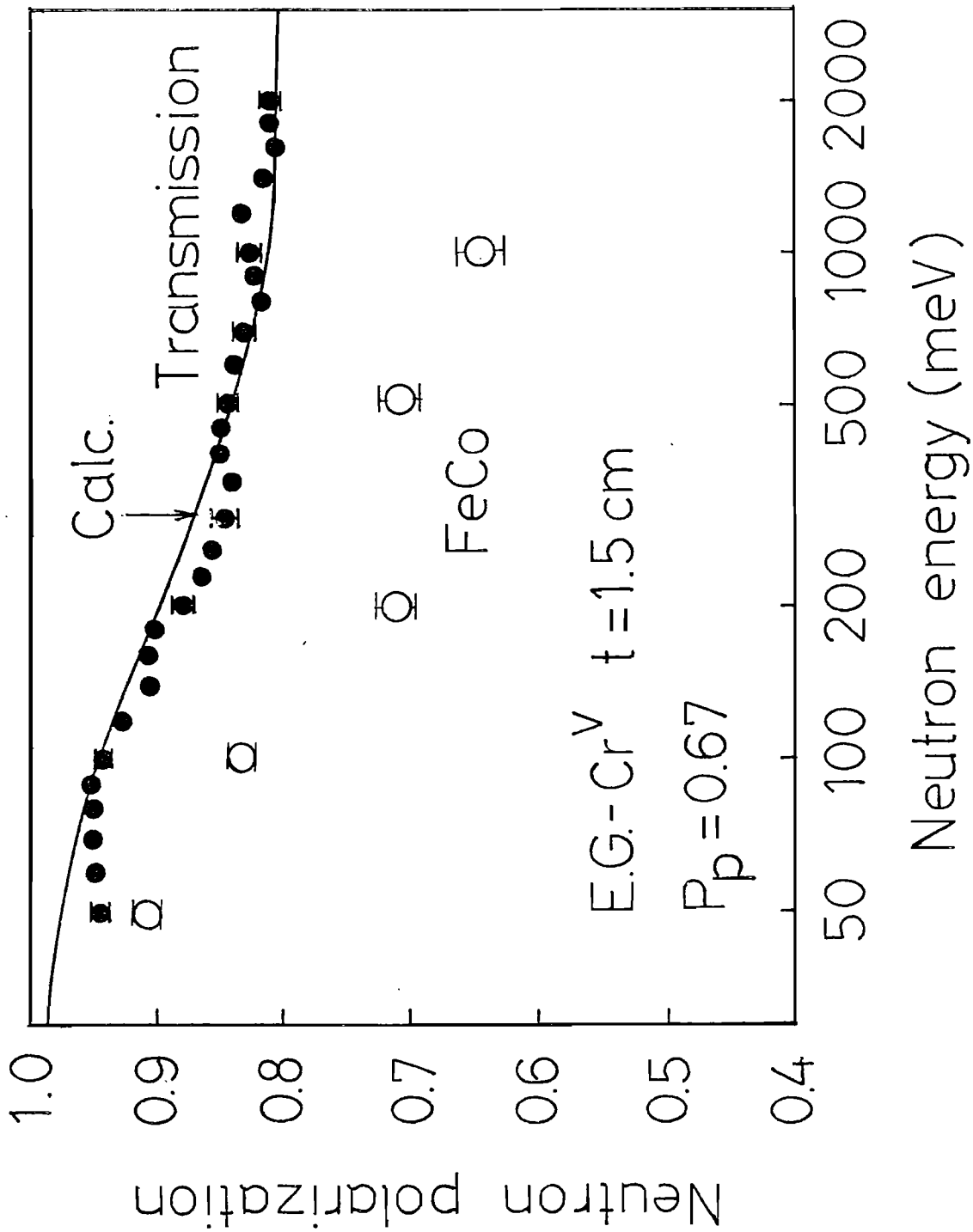

Fig.2 Polarization of the neutron beam obtained by the type I filter. Closed circles are the polarization determined from the transmission measurement. Solid line is the calculated polarization with the proton polarization of 67%. Open circles are the polarization determined by the (200) Bragg scattering from Fe_8Co_{92} single crystal.

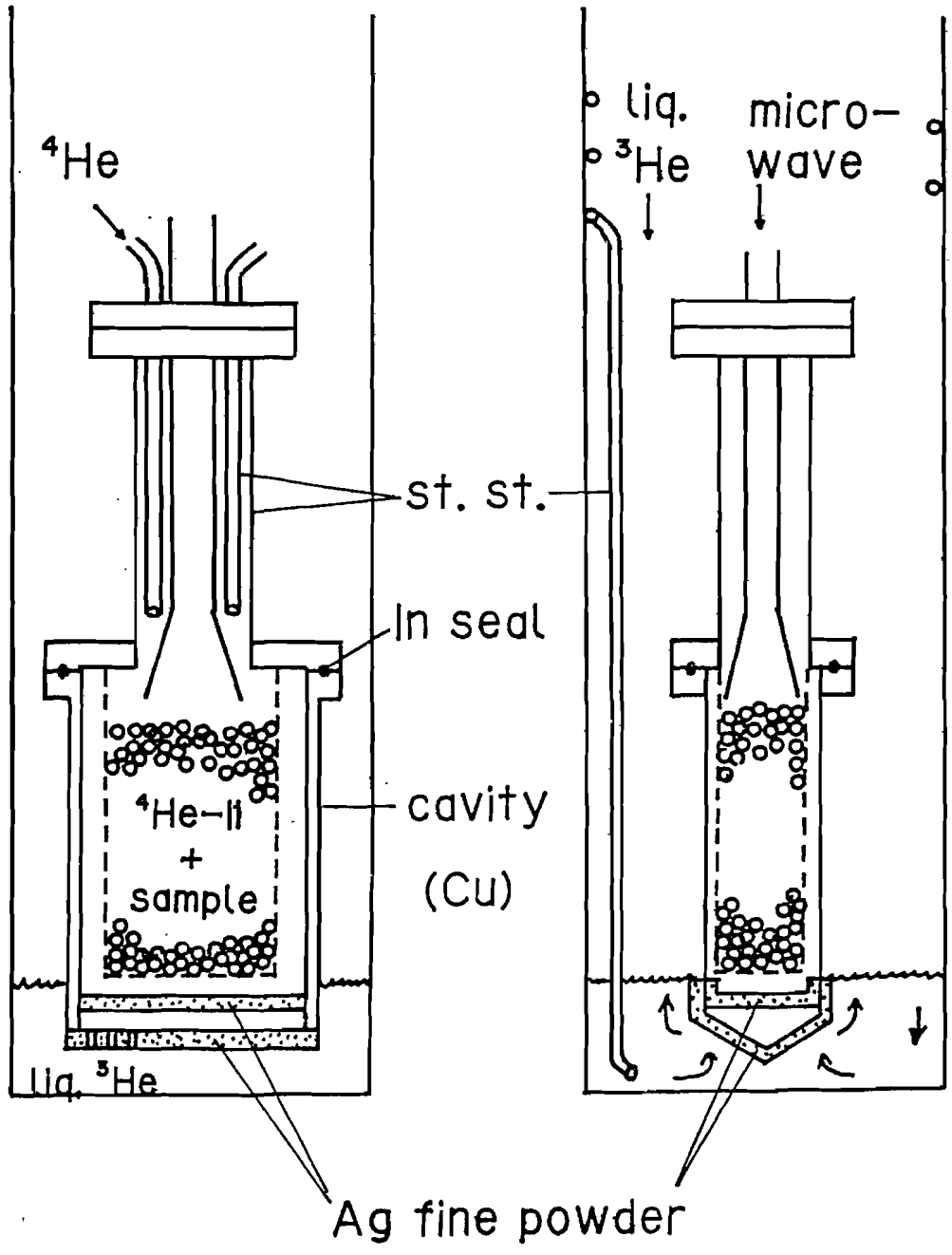

Fig.3 Type II filter. Beads of filter material fill a Cu mesh box which is set in the microwave cavity filled with liquid ^{4}He. The bottom of the cavity is immesed in the liquid ^{3}He pool. Ag fine powder is sintered on the both sides of the bottom of the cavity for the effective heat exchange.

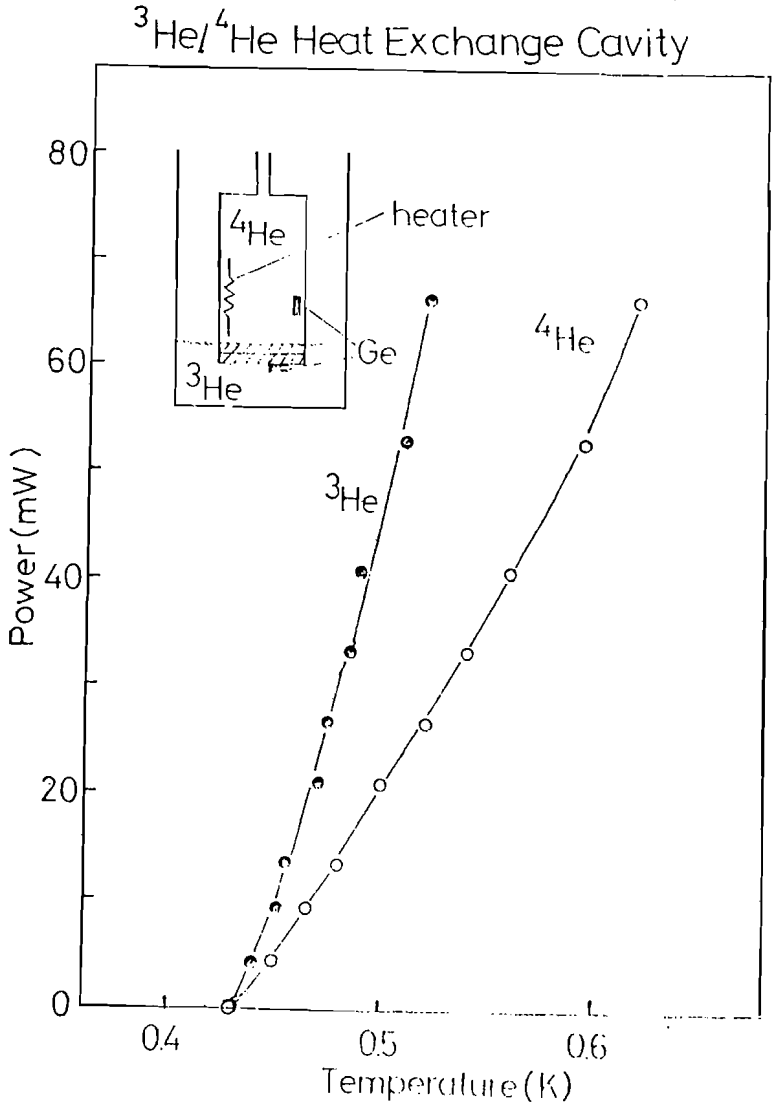

Fig.4 Cooling power of type II filter. Open circles are temperatures inside the microwave cavity. Closed circles are temperatures in the ^{3}He pool. Ordinate shows applied power.

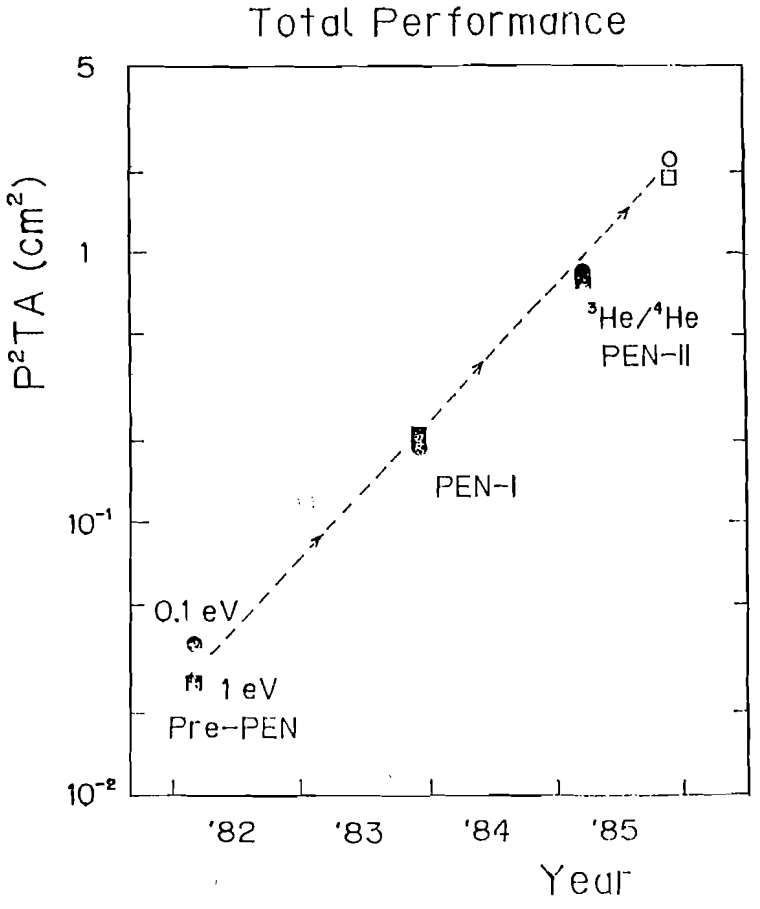

Fig.5 Performance of the dynamically polarized proton filters developed on PEN. Data noted as Pre-PEN are the results of test experiments performed prior to PEN. Data noted as PEN-I and PEN-2 show the results of experiments by using the type I and typeII filters described in the text, respectively. Open marks show the estimated quality factor by using the type II filter supposing the proton polarization to be 80%.

INDEX OF AUTHORS